



HAL
open science

Structural and functional analyses of the interaction of tetherin with the dendritic cell receptor ILT7

Nicolas Aschman

► **To cite this version:**

Nicolas Aschman. Structural and functional analyses of the interaction of tetherin with the dendritic cell receptor ILT7. Structural Biology [q-bio.BM]. Université Grenoble Alpes, 2015. English. NNT : 2015GREAV064 . tel-01682995

HAL Id: tel-01682995

<https://theses.hal.science/tel-01682995>

Submitted on 12 Jan 2018

HAL is a multi-disciplinary open access archive for the deposit and dissemination of scientific research documents, whether they are published or not. The documents may come from teaching and research institutions in France or abroad, or from public or private research centers.

L'archive ouverte pluridisciplinaire **HAL**, est destinée au dépôt et à la diffusion de documents scientifiques de niveau recherche, publiés ou non, émanant des établissements d'enseignement et de recherche français ou étrangers, des laboratoires publics ou privés.

THÈSE

Pour obtenir le grade de

DOCTEUR DE L'UNIVERSITÉ DE GRENOBLE

Spécialité : **Biologie Structurale et Nanobiologie**

Arrêté ministériel : 7 août 2006

Présentée par

Nicolas ASCHMAN

Thèse dirigée par le **Pr Winfried WEISSEHORN**

préparée au sein de l'**Unit of Virus Host Cell Interactions**
dans l'**École Doctorale Chimie et Sciences du Vivant**

Analyses structurales et fonctionnelles de l'interaction de la tétherine avec le récepteur ILT7

Thèse soutenue publiquement le **28 avril 2015**,
devant le jury composé de :

Dr Andrea CIMARELLI

(Rapporteur)

Dr Yves GAUDIN

(Rapporteur)

Pr Marc JAMIN

(Président)

Dr Andrew McCARTHY

(Examineur)

Dr Laurent TERRADOT

(Examineur)

Pr Winfried WEISSEHORN

(Membre)



Structural and functional analysis of the
interaction of tetherin with the dendritic cell
receptor ILT7

Nicolas Aschman

June 28, 2015

Abstract

Human immunodeficiency virus 1 (HIV-1) specifically infects CD4⁺ T cells, thereby preventing an appropriate activation of cytotoxic T cells and B cells in response to opportunistic pathogens. In addition, HIV-1 antagonises host restriction factors, including tetherin. In the absence of the viral protein Vpu, tetherin potently inhibits virus particle release from infected cells. Tetherin also triggers proinflammatory signaling upon sensing virus assembly, and activates the dendritic cell receptor ILT7. The principal objective of this thesis was to elucidate the structural details underlying the interaction of tetherin with ILT7. Despite difficulties in the production of recombinant ILT7, the crystal structure of the N-terminal ILT7 domain could be determined. Furthermore, binding of tetherin to full-length ILT7, but not to the N-terminal domain, could be confirmed by SPR. These results provide a solid basis for the more detailed characterisation of the interaction.

Résumé

Le virus d'immunodéficience humaine 1 (VIH-1) cible spécifiquement les cellules CD4⁺ et empêche ainsi l'activation de cellules T cytotoxiques et B lors d'une infection secondaire. Le VIH-1 antagonise également la plupart des facteurs de restriction de l'hôte, y compris la tétherine. En l'absence de la protéine virale Vpu, la tétherine inhibe le relargage de particules virales et provoque leur dégradation. La tétherine est également capable d'induire une signalisation pro-inflammatoire en réponse au bourgeonnement viral ainsi que d'activer le récepteur de cellules dendritiques ILT7. L'objectif principal de cette étude consistait à élucider les bases structurales de l'interaction entre la tétherine et ILT7. Malgré de nombreuses difficultés rencontrées dans la production recombinante de ILT7, on a pu déterminer la structure cristallographique du domaine N-terminale du récepteur. La ligation de la tétherine à l'ectodomaine entier de ILT7, mais pas au domaine N-terminal, a également été montré. Ces résultats constituent une base solide pour la caractérisation plus détaillée de l'interaction.

Acknowledgements

First and foremost, I would like to express my gratitude to my supervisor Winfried Weissenhorn for giving me the chance of joining his team at a time when my background in structural biology was limited to a few rusty memories from early morning lectures. When my project turned out to be more challenging than expected and initially had me seriously struggling, Winfried has always remained supportive and confident. Among many other things, I greatly appreciate that the door of Winfried's office was always open, that he always took time for discussion and was always available for advice.

I would like to thank the members of my jury, namely Andrea Cimarelli and Yves Gaudin, who act as *rapporteurs*, as well as Marc Jamin, Andrew McCarthy and Laurent Terradot. I am very grateful also to Carlo Petosa and Ramesh Pillai for their constructive feedback as members of my thesis advisory committee.

During the last year of my thesis I have been involved in a fruitful collaboration with the laboratory of Prof Eric Cohen (Institut de Recherches Cliniques de Montréal, Canada). In this regard, I would especially like to thank Mariana Bego for sharing her insights and providing protein samples, as well as Edouard Côté for analysing my samples by flow cytometry.

I am indebted to all of my team members for teaching me virtually everything about protein expression, purification and crystallography. I am especially thankful to Patricia Renesto for introducing me to the art of cloning, for sharing her experience of mammalian cell culture, for co-writing my first review article and generally for her helpfulness. I will miss her anecdotes and always remember the good moments shared in the lab. Special thanks also go to Miriam Hock for teaching me many techniques and helping me troubleshoot my experiments countless times ; to Jens Radzimanowski for introducing me to protein crystallisation, X-ray diffraction and data processing ; to Christophe Caillat for his help with model building and refinement, and generally useful advice ; and to Aurélien Dordor for untold scientific and less-scientific discussions. I will also fondly remember my colleagues Pauline Macheboeuf, Géraldine Mayeux and Nolwenn Miguet, as well as previous team members David Lutje Hulsik, Nicolas Martinelli and Emilie Poudevigne.

Many other people have been helpful by teaching me new techniques or providing useful advice, among them Pascal Fender whom I would like to thank for his help with cell culture and SPR, as well as for his eternal good mood and humour ; Vladimir Rybin and Piotr Gerlach for introducing me to ITC and MST analysis, respectively ; Sergiy Avilov for his help with confocal microscopy and Natasha Alexandrovna for her advice on protein expression in mammalian cell lines. Filip Yabukarski has helped me, through countless discussions, make light of some of the more obscure aspects of protein crystallography. I am also thankful to Nicolas Tarbouriech, Max Nanao and

Chloe Zubieta for their spontaneous advice on crystallographic data processing and model refinement.

In the context of the Partnership for Structural Biology (PSB, Grenoble), I have made use of several platforms and facilities, most notably the Eukaryotic Expression Facility (EEF) operated by the Berger group where all insect cell expression was carried out. I am grateful to the Berger team for providing this service, with special thanks to Alice Aubert for always providing me with healthy cells at a moment's notice. I would also like to thank Philippe Mas (thermal shift assays), Daphna Fenel and Guy Schoehn (electron microscopy) and Luca Signor (mass spectrometry).

The administrative and technical staff of my host laboratory have been extremely helpful and kind, and I would like to thank Sandrine Vignon in particular for her assistance with awkward paperwork of all kind. I would like to acknowledge the financial support of the Agence Nationale de la Recherche sur le SIDA et les hépatites virales (ANRS) and the Fonds National de la Recherche of Luxembourg (FNR).

Last but not least I would like to thank my parents for their unconditional support in all my endeavours, and my wife Corinne for her undying optimism, patience and love.

*Nick Aschman
Grenoble, March 2015*

Contents

Abstract	iii
Acknowledgements	v
Abbreviations	xi
<i>Introduction (français)</i>	15
1 Introduction	17
1.1 Molecular and structural biology of HIV	19
1.1.1 Assembly and budding	20
1.1.2 Infection and replication	22
1.2 Innate immune response to HIV	26
1.2.1 Interferon response	27
1.2.2 Restriction factors	29
1.3 Tetherin structure and function	31
1.3.1 Expression and trafficking	32
1.3.2 Topology and structure	33
1.3.3 Inhibition of virus release	35
1.3.4 Organisation of subcellular structure	41
1.3.5 Immune sensing and signaling activities	42
1.3.6 Modulation of the innate immune response	42
1.4 ILT7 and the leukocyte Ig-like receptor family	43
1.4.1 Topology, structure and signal transduction	44
1.4.2 Functional activity and role in HIV-1 infection	45
Objectives	51
2 Methods	53
2.1 Bioinformatics	53
2.1.1 Multiple sequence alignment and phylogenetics	53
2.1.2 Domain, structure and disorder prediction	54
2.1.3 Post-translational modifications and processing	54
2.1.4 <i>Ab initio</i> protein–protein docking and interface characterisation	54
2.2 Molecular cloning and mutagenesis	56

2.2.1	Molecular cloning	56
2.2.2	Site-directed mutagenesis	56
2.2.3	Bacmid cloning	57
2.3	Protein expression and purification	59
2.3.1	Preparation of tetherin ectodomain	59
2.3.2	Bacterial expression of ILT7	59
2.3.3	Insect cell expression of ILT7	61
2.3.4	Mammalian expression of ILT7	63
2.4	Biochemical and biophysical characterisation	64
2.4.1	Fluorescent labeling	64
2.4.2	Peptide mass fingerprinting	64
2.4.3	Surface plasmon resonance	65
2.4.4	Isothermal titration calorimetry	67
2.4.5	Microscale thermophoresis	67
2.5	Protein crystallography	68
2.5.1	Crystallisation and data collection	68
2.5.2	Structure determination and refinement	70
2.6	Cell biology	71
2.6.1	Cloning of tetracysteine-tagged tetherin	71
2.6.2	HIV-1 virus-like particle release assay	71
2.6.3	Fluorescent labeling and confocal microscopy	72
2.6.4	Flow cytometry analysis with fluorescent ILT7(D1)	72
3	Materials	75
3.1	Buffers and solutions	75
3.2	Reagents, media and kits	76
3.3	Enzymes and antibodies	77
3.4	Bacterial strains and cell lines	77
3.5	Equipment and consumables	78
	<i>Résultats (français)</i>	79
4	Results	83
4.1	Bioinformatic analyses of the ILT7 ectodomain	83
4.1.1	Topology and domain organisation	83
4.1.2	Secondary structure and disorder prediction	85
4.1.3	Prediction of post-translational modifications	85
4.2	Recombinant expression of the ILT7 ectodomain	87
4.2.1	Mammalian cell expression	87
4.2.2	Insect cell expression	87
4.2.3	Bacterial expression	91

4.3	Structure and ligand-binding properties of ILT7(D1)	93
4.3.1	Crystallisation and X-ray diffraction	93
4.3.2	Crystal structure at 1.55 Å resolution	95
4.3.3	Interaction with the tetherin ectodomain	99
4.3.4	Functional activity	102
4.3.5	<i>In silico</i> docking of the tetherin coiled-coil domain	102
4.4	Tertiary structure prediction and <i>in silico</i> docking of ILT7(D1-2)	108
4.4.1	Predicted tertiary structure	108
4.4.2	<i>In silico</i> docking of the tetherin coiled-coil domain	109
4.5	Characterisation of ILT7(D1-4)	111
4.5.1	Peptide mass fingerprinting	112
4.5.2	Interaction of tetherin with insect cell-expressed ILT7	113
4.6	Tetherin imaging using biarsenical fluorophores	116
	<i>Discussion (français)</i>	119
	5 Discussion	121
	Bibliography	130
	Appendix A PCR primer sequences	155
	Appendix B Review: Structural basis of tetherin function	157
	Appendix C Review: La tétherine, dernière amarre du HIV	167

Abbreviations

ADP	Atomic displacement parameter
AIDS	Acquired immunodeficiency syndrome
Amp	Ampicillin
APS	Ammonium persulfate
βME	2-mercaptoethanol
BAL	British anti-Lewisite
BSA	Bovine serum albumin
BST2	Bone marrow stromal antigen 2 (synonym for Tetherin)
CD	Circular dichroism
CD4	Cluster of differentiation 4 (cell surface receptor)
cDNA	Complementary DNA
Cam	Chloramphenicol
DC	Dendritic cell
DNA	Deoxyribonucleic acid
DLS	Dynamic light scattering
DMEM	Dulbecco's modified Eagle medium
DTT	Dithiothreiol
EDC	1-ethyl-3-(3-dimethylaminopropyl)carbodiimide hydrochloride
EDTA	Ethylenediaminetetraacetic acid
ESCRT	Endosomal sorting complexes required for transport
FBS	Foetal bovine serum

FIV	Feline immunodeficiency virus
FPLC	Fast protein liquid chromatography
FRET	Fluorescence resonance energy transfer
GDT	Global distance test
Gen	Gentamicin
GSH	Reduced glutathione
GST	Glutathione S-transferase
GPI	Glycosyl-phosphatidyl-inositol
GSSG	Oxidised glutathione
HBS	HEPES-buffered saline
HBSS	Hank's balanced salt solution
HEK293T	Human endothelial kidney 293T (cell line)
HEPES	4-(2-hydroxyethyl)-1-piperazineethanesulfonic acid
HIV	Human immunodeficiency virus
IFN	Interferon
Ig	Immunoglobulin
IgSF	Immunoglobulin superfamily
ILT	Immunoglobulin-like transcript (synonym for LILRs)
IMAC	Immobilised metal ion affinity chromatography
IPTG	Isopropyl β -D-1-thiogalactopyranoside
ISG	Interferon-stimulated gene
ITC	Isothermal titration calorimetry
Kan	Kanamycin
LILR	Leukocyte Ig-like receptor (synonym for ILTs)
MALDI-TOF	Matrix-assisted laser desorption ionisation / time-of-flight (mass spectrometer)

MALLS	Multi-angle laser light scattering
MES	2-(N-morpholino)ethanesulfonic acid
MPD	2-methyl-2,4-pentanediol
MST	Microscale thermophoresis
MWCO	Molecular weight cut-off
NHS	N-hydroxysuccinimide
NTA	Nitrilotriacetic acid
OD_x	Optical density (at wavelength <i>x</i>)
PAGE	Polyacrylamide gel electrophoresis
PBS	Phosphate-buffered saline
PCR	Polymerase chain reaction
PDB	Protein Data Bank
PEG	Polyethylene glycol
PES	Polyethersulfone
PMF	Peptide mass fingerprinting
RMSD	Root mean square deviation
RNA	Ribonucleic acid
SDS	Sodium dodecyl sulfate
SEC	Size exclusion chromatography
SIV	Simian immunodeficiency virus
SPR	Surface plasmon resonance
TBS	Tris-buffered saline
TC	Tetracysteine (sequence motif)
TEMED	Tetramethylethylenediamine
Tet	Tetracycline
TEV	Tobacco etch virus

TLR	Toll-like receptor
TMD	Transmembrane domain
Tris	Tris(hydroxymethyl)aminomethane
VdW	van der Waals (radius/interactions)
VLP	Virus-like particle

Introduction (français)

Le syndrome d'immunodéficience acquise (SIDA) est une maladie infectieuse dévastatrice qui a causé plus de 25 millions de morts depuis son apparition en 1981. Chez l'humain, le SIDA est causé par deux lentivirus appelés virus d'immunodéficience humaine 1 et 2 (VIH-1 et -2), dont le premier est responsable de la pandémie actuelle tandis que le VIH-2 est resté largement confiné à l'Afrique de l'Ouest. Le SIDA est la phase symptomatique et tardive de l'infection par le VIH, et consiste dans une réduction massive de lymphocytes CD4⁺ tels les cellules T auxiliaires essentielles pour la coordination de la réponse immunitaire.

En commun avec d'autres rétrovirus, le génome du VIH contient trois gènes structuraux nommés *gag*, *pol* et *env* encodant des polyprotéines (Figure 1.1, p. 20). Gag comprend les protéines matrice (MA), capsid (CA) et nucléocapsid (NC) ainsi que trois peptides nommés p6, SP1 et SP2. Le gène *pol*, qui encode les enzymes protéase (PR), transcriptase inverse (RT) et intégrase, est traduit par un décalage du cadre de lecture donnant lieu à une protéine Gag-Pol dans ~5% des cas. Enfin, le gène *env* encode le précurseur gp160 de la glycoprotéine de surface, qui est découpé ultérieurement dans ses sous-unités gp120 et gp41. Le génome du VIH-1 comprend également des gènes codant pour les protéines régulatrices Tat et Rev, ainsi que plusieurs protéines accessoires nommées Vpr, Vif, Vpu et Nef. La protéine Vpu est unique au VIH-1 et à quelques virus d'immunodéficience simienne (VIS), tandis que le VIH-2 ainsi que la plupart des VIS encodent une protéine accessoire nommée Vpx. Certaines protéines accessoires jouent un rôle notamment dans la neutralisation de facteurs de l'immunité innée des cellules hôtes.

Les facteurs de restriction sont des protéines exprimées suite à une stimulation par des interférons (IFNs) qui possèdent une activité antivirale précise et agissent de manière autonome. Les principaux facteurs de restriction du VIH caractérisés à ce jour sont APOBEC3G, la tétherine, TRIM5 α et SAMHD1 (Sheehy et al., 2002; Neil et al., 2008; Stremlau et al., 2004; Hrecka et al., 2011). Les modes d'action des principaux facteurs de restriction sur le cycle viral du VIH-1 sont illustrés schématiquement dans la Figure 1.3 (p. 30). Il faut noter cependant que ces gènes ont subi une pression de sélection positive massive et les protéines sont généralement inactives contre les virus de type sauvage suite à la co-évolution d'antagonistes viraux. Dans le cas du VIH-1, l'activité de la tétherine est par exemple inhibée par la protéine accessoire Vpu (Neil et al., 2008; Van Damme et al., 2008).

La tétherine est une protéine transmembranaire de type 2 dont le domaine extracellulaire adopte une structure allongée de ~17 nm modifiée par l'ajout d'une deuxième ancre membranaire de type glycosyl-phosphatidylinositol sur le bout carboxylique et comprenant deux sites de N-glycosylation (Figure 1.5, p. 34 ; Kupzig et al. (2003)). La protéine forme des homod-

imères par l'implication d'une partie de son ectodomaine dans un faisceau d'hélices stabilisé par trois ponts disulfure (Figure 1.6, p. 35) (Hinz et al., 2010). Avant la découverte de la tétherine en tant que facteur de restriction, il avait été observé que la présence de la protéine Vpu du VIH-1 était essentielle pour le relargage viral dans certains types de cellules—tels la lignée cellulaire HeLa, mais pas dans d'autres (Terwilliger et al., 1989; Strebel et al., 1989). En 2008, la tétherine a ensuite été identifiée comme facteur de restriction par sa susceptibilité à Vpu et son expression constitutive dans des cellules cancéreuses comme les cellules HeLa (Neil et al., 2008; Van Damme et al., 2008). La tétherine cause la rétention de virions naissants à la membrane plasmique, probablement en insérant une de ces paires d'ancres membranaires dans la membrane virale, et induit leur internalisation et dégradation par une voie endo-lysosomale (Figure 1.7, p. 37) (Neil et al., 2006; Perez Caballero et al., 2009; Miyakawa et al., 2009; Venkatesh and Bieniasz, 2013).

Outre son activité antivirale directe, la tétherine est également impliquée dans l'activation et la régulation immunitaire. En effet, la tétherine est capable d'induire l'expression de nombreux gènes pro-inflammatoires en activant les facteurs de transcription NF- κ B (Figure 1.8, p. 43) (Matsuda et al., 2003). Cette activité ne dépend pas de l'association avec la Vpu mais résulte directement de la rétention des particules virales, la tétherine agissant donc comme détecteur de bourgeonnement viral (Galão et al., 2012; Tokarev et al., 2013; Galão et al., 2014). La tétherine a également été identifiée comme le ligand du récepteur ILT7 (Ig-like transcript 7 ou leukocyte Ig-like receptor A4 [LILRA4]) exprimé à la surface des cellules dendritiques plasmacytoïdes (pDCs) (Cao et al., 2009). L'activation d'ILT7 résulte dans une diminution de la production d'interféron- α (IFN- α) induit par les récepteurs de type Toll (TLR) 7 et 9 suite à la détection de motifs moléculaires associés à des pathogènes (Cao et al., 2006, 2009). Suite à ces observations, les auteurs ont proposé que l'interaction de la tétherine avec ILT7 pourrait constituer un mécanisme de rétro-contrôle négative sur la production d'IFN pendant une infection virale. En effet, les pDCs sont les productrices principales d'IFN et d'autres cytokines pro-inflammatoires, et jouent donc un rôle important dans l'installation d'un état antiviral à travers l'organisme. Cependant, une production prolongée de cytokines pro-inflammatoires peut engendrer des immunopathologies et doit donc être soumis à une régulation précise.

La caractérisation structurelle et fonctionnelle de l'interaction entre la tétherine et le récepteur ILT7 permettrait de mieux comprendre le mécanisme sous-jacent, et pourrait contribuer éventuellement à la mise au point de molécules permettant la modulation de la réponse IFN.

1

Introduction

Acquired immunodeficiency syndrome (AIDS) is a devastating infectious disease that has caused more than 25 millions deaths since it was first characterised in 1981, with sub-Saharan Africa carrying the greatest burden. In humans, AIDS is caused by lentiviruses named human immunodeficiency viruses 1 and 2 (HIV-1 and -2), which are currently infecting an estimated 35 million people worldwide¹. HIV-1 is responsible for the ongoing pandemic, whereas HIV-2, which is less transmissible and pathogenic, has remained largely restricted to West Africa. The virus is primarily transmitted by sexual contact, accounting for 80 % of adult cases, but also spreads percutaneously through the re-use of hypodermic needles or contaminated blood transfusions, and perinatally during pregnancy, delivery or breastfeeding. While AIDS first came to prominence as a disease of men having sex with men in North America, the virus today mainly spreads by heterosexual contact, with young women comprising 60 % of people living with HIV in sub-Saharan Africa and 50 % globally¹. HIV is highly prevalent in many additional demographic groups, including sex workers and their clients in many Asian countries (India, China, Indonesia) and injecting drug users in ex-Soviet states as well as Iran¹. Considerable progress has been made in the development of antiretroviral therapy (ART) drugs and strategies, which typically rely on a combination of three drugs to block viral replication in infected cells. In addition, a number of recent studies have highlighted the potential of prophylactic methods such as vaginal/rectal gels based on the reverse transcriptase (RT) inhibitor tenofovir, male circumcision as well as preventive ART, which drastically reduces virus transmission rates (Cohen et al., 2011; Siegfried et al., 2009).

Although both the number of new infections and HIV-related deaths are declining worldwide, the AIDS pandemic continues to pose unprecedented challenges. Many social and ethical aspects will have to improve, such as availability of prophylaxis, access to treatment and elimination of the stigmatisation and criminalisation of seropositive people. Furthermore, in the absence of a vaccine or cure, drug regimens will be

¹UNAIDS Gap Report 2014—http://www.unaids.org/en/media/unaids/contentassets/documents/unaidspublication/2014/UNAIDS_Gap_report_en.pdf [accessed 17 Sep 2014]

prone to the development of resistance. It is worth noting that HIV causes significant non-AIDS morbidity and mortality through an increased risk of cancers, cardiovascular disease and co-infection with tuberculosis or hepatitis B and C viruses (reviewed in Maartens et al., 2014).

AIDS is the symptomatic late phase of HIV infection and is characterised by a depletion of CD4⁺ T lymphocytes, such as T helper cells, that are crucial in coordinating an immune response. The weakened immune system is thus incapable of defending the body against opportunistic infections and certain cancers such as Kaposi's sarcoma, which ultimately leads to death from these secondary diseases. The loss of CD4⁺ T cells was initially believed to mainly result from cytopathic effects of direct infection, since HIV specifically targets cells expressing the CD4 receptor on which it depends for viral entry. However, the biggest loss is caused by apoptosis of non-infected 'bystander' cells, induced by contact with HIV proteins released by infected cells, increased syncytia formation and dysregulation of cytokines towards a pro-apoptotic state (reviewed in Alimonti et al., 2003).

From the onset of the AIDS pandemic, a considerable effort has gone into understanding the origins, epidemiology and pathogenicity of HIV. It is now clear that HIV-1 arose from zoonotic transmission of simian immunodeficiency viruses (SIVs) from chimpanzees (*Pan troglodytes*) and gorillas (*Gorilla gorilla*) in central Africa, probably in the context of bushmeat hunting (reviewed in Sharp and Hahn, 2011). SIVs have been discovered in over 40 primate species, with each species generally carrying a monophyletic virus strain. The existence of mosaic strains however goes to show that cross-species transmission and recombination does occur. Given that SIVs often do not seem to cause immunodeficiency in their respective host species—with the notable exception of chimpanzees, one could hypothesise that the disease is the result of switching hosts. Interestingly, by comparing SIV-infected monkeys on the island of Bioko in Equatorial Guinea to the same genii from mainland Africa, Worobey et al. (2010) could date the emergence of SIV to at least 32 000 years ago. The most immediate predecessors of HIV-1 are simian viruses harboured by two subspecies of chimpanzees (SIV_{cpz}) as well as gorillas (SIV_{gor}). While SIV_{cpz} has probably originated quite recently through the recombination of viruses acquired from red-capped mangabeys (*Cercocebus torquatus*) and greater spot-nosed monkeys (*Cercopithecus nictitans*), SIV_{gor} has been traced to a single transmission event from chimpanzees to gorillas about 100–200 years ago (Bailes et al., 2003; Takehisa et al., 2009).

The different strains of HIV-1 are divided into four groups named M, N, O and P, which probably each correspond to a distinct transmission event of SIV to humans (reviewed in Sharp and Hahn, 2011). The M ('major') group represents the pandemic viruses with over 90% of infections, seconded by group O ('outlier'), which is largely restricted to Central Africa. Groups N and P were discovered more recently and remain extremely rare, with group P viruses having only been documented in two pa-

tients to date. All viruses closely resemble SIV_{cpz} strains, with groups M and N having been traced to individual chimpanzee communities in southern Cameroon where cross-species transmission probably occurred (Keele et al., 2006). Group P viruses cluster with SIV_{gor} strains in phylogenetic analysis and are believed to have been transmitted from gorillas, although their exact origin could not be pinpointed yet given the lack of data on strains of gorilla viruses (reviewed in Sharp and Hahn, 2011). The origin of group O is unclear.

HIV-2 is most closely related to SIVs harboured in sooty mangabeys (*Cercocebus atys*; SIV_{smm}) and it is now accepted that transmission to humans occurred on at least eight different occasions, giving rise to groups A–H. However, only groups A and B have spread significantly in humans, while groups C–H are quite rare and therefore sometimes considered as ‘dead-end’ transmissions (reviewed in Sharp and Hahn, 2011).

1.1 Molecular and structural biology of HIV

Retroviruses are characterised by a single-stranded RNA genome that features both a 5′ cap and a 3′ poly-adenylated (polyA) tail and can thus directly serve as mRNA for translation. The so-called provirus is formed when the viral RNA genome is reverse-transcribed into DNA and integrated into the host cell DNA. Depending on the provirus insertion site, the viral DNA genome is then transcribed normally by the cellular protein expression machinery.

In common with all other known retroviruses, HIV-1 contains three open reading frames (ORFs) named *gag*, *pol* and *env*. The former codes for the Gag polyprotein that comprises the structural matrix (MA), capsid (CA) and nucleocapsid (NC) proteins, the p6 protein, as well as two short “spacer” peptides called SP1 and SP2. The *pol* gene, which codes for the viral protease (PR), reverse transcriptase (RT) and integrase (IN) enzymes, is adjacent to *gag* and is translated by programmed ribosomal frameshifting at a frequency of ~5%, giving rise to Gag-Pol polyproteins. Scanning of the ribosome past the *gag* termination codon depends on the presence of several conserved pseudoknots in the RNA secondary structure that cause a –1 frameshift (Huang et al., 2014). The third gene, *env*, encodes the precursor envelope glycoprotein named gp160 or Env, which is later processed into the two subunits gp120 and gp41, also referred to as surface (SU) and transmembrane (TM) glycoproteins respectively. In addition to the structural proteins and enzymes, HIV-1 encodes further proteins mainly involved in regulation and immune evasion, namely the regulatory proteins Tat and Rev, as well as the accessory proteins Vpr, Vif, Vpu and Nef. These proteins, together with Env, are expressed from merely two transcripts with overlapping reading frames and requiring multiple splicing (Figure 1.1). The main differences regarding genome organisation between HIV-1, HIV-2 and the major SIV strains are observed in the presence or absence of the accessory genes *vpx* and *vpu*. More specifically, whereas *vpu* is found in HIV-1 as

well as a small number of closely related SIVs, *vpx* is encoded by HIV-2 and most SIV strains while it is absent from HIV-1.

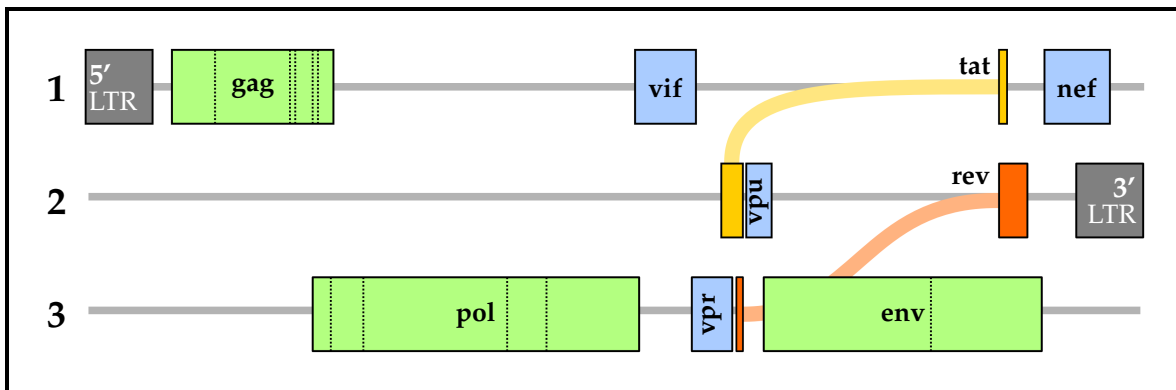


Figure 1.1 Genome organisation of HIV-1. The genes coding for the main structural polyproteins Gag, Pol and Env are coloured in green. Translation of Gag–Pol results from a -1 frameshift of the ribosome. The exons composing the essential regulatory genes *tat* and *rev* are shown in yellow and orange, respectively. Genes encoding the accessory proteins Vif, Vpu, Vpr and Nef are coloured in blue. Finally, the two long terminal repeat (LTR) regions that flank the retroviral genome are also indicated.

1.1.1 Assembly and budding

The viral life cycle begins, arguably, when a new virion starts to form within an infected cell, and in the case of HIV-1, virion assembly is initiated by oligomerisation of the Gag polyprotein at the plasma membrane (reviewed in Ganser Pornillos et al., 2008). More specifically, Gag clusters in membrane microdomains enriched in cholesterol and sphingolipids, or so-called “lipid rafts”, and interacts with the phospholipid PI(4,5)P₂ (phosphatidylinositol 4,5-bisphosphate). The amino-(N-)terminal MA domain is myristoylated and binds to the inner leaflet of the membrane, whereas the CA domain mediates lateral interaction between Gag molecules together with the adjacent SP1. In the same fashion Gag–Pol polyproteins are integrated into the nascent Gag lattice, and Gag also mediates the packaging of two copies of the viral RNA (vRNA) genome via its NC domain. The mechanism by which the viral envelope glycoprotein Env—which at this point consists in a fully glycosylated trimeric complex of its gp41 and gp120 subunits—is incorporated into budding virions is not completely understood, although it has been shown to depend on both the cytosolic tail of Env and the MA domain of Gag (Muranyi et al., 2013). Alternatively, both proteins could localise to lipid rafts and Env be incorporated in a random fashion. In either case it becomes evident that Gag is central in the assembly of HIV-1 particles.

In order to become infectious, HIV-1 virions undergo maturation, which starts during the late stages of the budding process and mainly relies on the viral protease PR (reviewed in Ganser Pornillos et al., 2008). The protease is part of the Pol polyprotein,

from which it is able to separate through autoproteolysis. It proceeds by catalysing the five-fold cleavage of Gag into its six component proteins and peptides, thus triggering the condensation of the NC-vRNA complex as well as the formation of the capsid. Similarly, the viral enzymes RT and IN are produced by PR-mediated cleavage from Gag-Pol polyproteins. The completed capsid consists of CA proteins arranged in a hexameric lattice, that together with the ribonucleoprotein (RNP) complex, enzymes and tRNA primers it contains, forms the conical core of the virus (Figures 1.2B and D).

While Gag is sufficient to induce the formation of spherical particles, their release through membrane fission depends on components of the cellular ESCRT (endosomal sorting complexes required for transport) machinery (reviewed in Sundquist and Kräusslich, 2012). The p6 domain of Gag contains two “late domain” motifs, PTAP and YPXL, which mediate this process by serving as binding sites for the ESCRT proteins TSG101 and Alix respectively (Garrus et al., 2001; Strack et al., 2003). The mechanism involving TSG101, which is part of the heterotetrameric ESCRT-I complex, is not fully understood, but both ESCRT-I and Alix essentially provide the basis for recruitment of ESCRT-III proteins from the CHMP2 and CHMP4 families (Morita et al., 2011). All CHMP proteins are capable of oligomerisation but possess a carboxy-terminal autoinhibitory domain that blocks oligomerisation (Zamborlini et al., 2006; Lata et al., 2008a; Bajorek et al., 2009). CHMP4 is recruited to budding sites and its autoinhibition is relieved, triggering polymer assembly within the membrane neck formed by the budding virion (Hanson et al., 2008; Pires et al., 2009). In turn, CHMP4 serves as a scaffold for polymers composed of CHMPs 2A, 2B or 2A/3 that are hypothesised to form a dome-like structure lining the inner membrane leaflet (Lata et al., 2008b; Morita et al., 2011; Effantin et al., 2013). Finally, CHMP2 recruits VPS4 ATPases (vacuolar protein sorting-associated proteins 4A and -B) by interacting with the enzyme’s amino-terminal MIT (microtubule interacting and transport) domain (Obita et al., 2007; Stuchell Brereton et al., 2007). Although the details underlying the fission event that separates cell and virion membranes is very poorly understood, it is currently believed that VPS4 disassembles ESCRT-III polymers using energy from ATP hydrolysis immediately prior to virion release (Fabrikant et al., 2009; Baumgärtel et al., 2011). It is thus possible that the rapid depolymerisation of a dome-shaped ESCRT-III assembly leads to sufficient constriction of the virion neck to cross the energy barrier for membrane fission.

Jouvenet et al. (2006) showed that the primary site of HIV-1 budding is at the plasma membrane, thus contradicting previous assumptions that budding could take place intracellularly. The authors suggest rather that fully assembled virions found in endosomal compartments are probably the result of endocytosis of viral particles from the plasma membrane. Astonishingly, full assembly of a single virion was recently determined to be accomplished in 5–6 min (Jouvenet et al., 2008). Interestingly, HIV budding preferentially takes place in contact zones between infected “donor” cells and

uninfected CD4⁺ “target” cells such as T helper cells, macrophages and dendritic cells (DCs) (discussed in Vasiliver Shamis et al., 2010). Termed virological synapses, such contact regions are thought to be based on the interaction between HIV-1 gp120 and the CD4 receptor as well as being mediated by host proteins that get incorporated into virions and bind to molecules on the target cell. For instance, the cell surface glycoprotein ICAM-1 (intercellular adhesion molecule 1), which is upregulated in infected cells, is commonly present in HIV-1 virions and correlates with increased infectivity. Since the interaction of ICAM-1 expressed on antigen-presenting cells (APCs) with the T cell receptor LFA-1 (lymphocyte function-associated antigen 1) is an essential component of immunological synapses, it is speculated that such adhesion molecules also underly the formation of virological synapses between CD4⁺ cells (reviewed in Vasiliver Shamis et al., 2010). It is worth noting however, that virions undergo the entire budding process outlined above independently of cell-free or cell-to-cell transmission via virological synapses.

1.1.2 Infection and replication

In order to infect a target cell, the virion’s contents need to be released into the cytosol. This is achieved by attachment of the viral envelope glycoprotein to specific receptors on the target cell surface followed by fusion of viral and cellular membranes. The principal entry receptors used by HIV are CD4, CCR5 (CC chemokine receptor 5) and CXCR4 (CXC chemokine receptor 4) whereby only one of the latter two is required as a co-receptor. The co-receptor requirement is strain-dependent and consequently, HIV strains are classified according to their X4 or R5-tropism. However, while R5 viruses represent the majority of highly transmissible strains, X4 tend to arise later during infection and probably already rely on some degree of immunosuppression (discussed in Weiss, 2013). The gp120 sub-unit of Env comprises two regions named “inner” and “outer” domains in respect to their orientation within the trimeric spike, as well as five variable loops (V1–V5) that may each adopt a variety of different conformations (Figure 1.2C). In a first docking step, CD4 is specifically recognised by the outer domain of gp120, which triggers the conformational changes required for exposure of the co-receptor binding sites (Kwong et al., 1998). A second step sees binding of the co-receptor and significant rearrangements within gp41, consisting in the folding of the heptad repeat regions HR1 and HR2 into a six-helical bundle and extension of the fusion peptide (FP) towards the target cell membrane (Buzon et al., 2010). The cell membrane and viral envelope are now sufficiently close for fusion, however the precise physics underlying this process still need to be elucidated.

Unlike influenza virus for instance, HIV-1 does not require low pH for fusion, which renders it capable of fusing directly with the plasma membrane. Nevertheless, it is clear that HIV-1 fusion can take place within endosomes after receptor-mediated

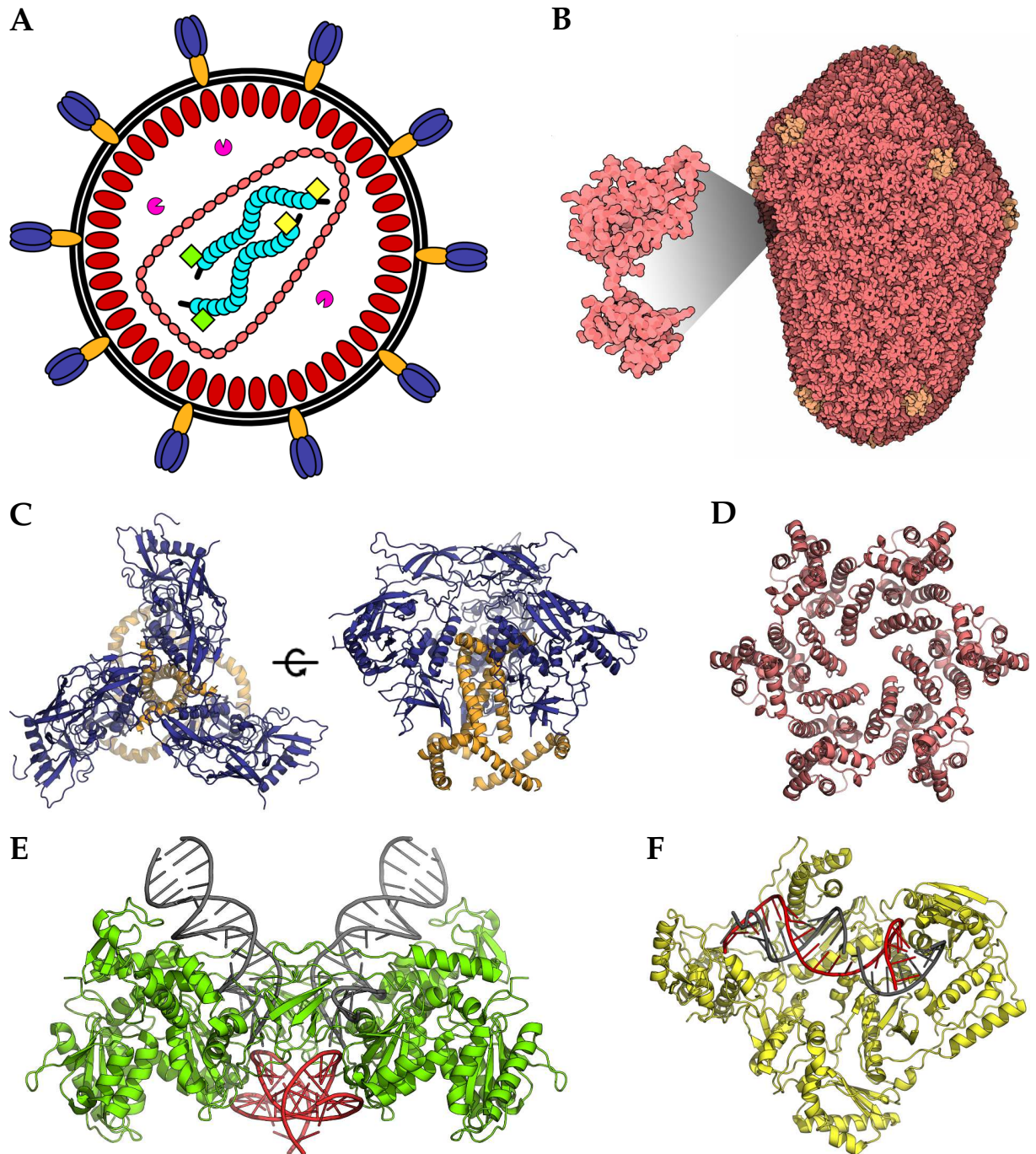


Figure 1.2 Structure of the HIV-1 virion. (A) Schematic representation of a mature HIV-1 virion. The represented proteins are gp120 (blue), gp41 (orange), MA (red), CA (salmon), NC (cyan), PR (pink), RT (yellow) and IN (green). (B) Cryo-EM model of the viral capsid composed of 216 CA hexamers and 12 CA pentamers (PDB 3J3Q ; illustration by David S. Goodsell/RCSB PDB). Crystal structures of (C) the trimeric envelope glycoprotein composed of gp41 (orange) and gp120 (blue ; 4NC0), (D) a CA hexamer (3MGE), (E) the tetrameric integrase complex from prototypic foamy virus bound to viral (black) and cellular (red) DNA (30S1), and (F) the HIV-1 reverse transcriptase bound to a hybrid RNA-DNA molecule (4B30).

endocytosis from the cell surface and that this mode of entry can lead to productive infection (Miyachi et al., 2009; Daecke et al., 2005). Notably, the endocytosis of intact virus particles in dendritic cells, mediated by C-type lectins and other receptors, is thought to play an important role in early infection with HIV founder strains and will be discussed in more detail below. Attachment of incoming virions to CXCR4 is also influenced by interactions of gp120 with heparan sulfate (reviewed in Connell and Lortat Jacob, 2013).

The fusion event releases the viral core into the cytosol where its contents will form the reverse transcription complex (RTC), followed by the pre-integration complex (PIC) once reverse transcription is complete. Since the viral genome enters the nucleus via the nuclear pore, it is likely that the capsid remains largely intact during trafficking to the nuclear envelope, thereby maintaining the integrity of the RTC and shielding viral DNA from recognition by cellular pattern recognition receptors (PRRs) that would trigger an immune response. Indeed, nuclear import of the viral genome is mediated by CA via its interaction with cellular proteins such as TNPO3, CPSF6, cyclophilin A (CypA) and Nup358, the latter being a component of the nuclear pore complex (Krishnan et al., 2010; Lee et al., 2010; Luban et al., 1993; Schaller et al., 2011). The size of the viral core exceeds the diameter of the nuclear pore, and together with the finding that PICs are devoid of CA, this suggests that uncoating of the core is taking place (Miller et al., 1997). The exact timepoint and mechanism of uncoating being the subject of fierce debates, it is however plausible to assume that reverse transcription takes place within the intact core, concomitantly with its transport to the nucleus (discussed in Arhel, 2010). In this model, the capsid would thus prevent dilution of RT away from the viral RNA during transcription, and would disassemble only after completion of the reverse transcription process. Alternatively, it has been proposed that uncoating immediately follows fusion, with partial or complete disintegration of the core being required for the formation of RTCs, however rather than discussing these quite speculative models I will refer to several reviews on the matter by Arhel (2010); Hilditch and Towers (2014).

The reverse transcriptase of HIV-1 carries out three separate enzymatic activities, namely RNA-dependent DNA synthesis, DNA-dependent DNA synthesis and hydrolytic cleavage of RNA (RNase H activity) in RNA/DNA hybrids. The enzyme is a heterodimer of p66 and p51 (Figure 1.2F), which are two alternative PR-mediated cleavage products of the Gag-Pol polyprotein (Lowe et al., 1988). While the carboxy-terminal RNase H domain is only present on the longer p66 subunit, the amino-terminal polymerase domain of both subunits can be subdivided into so-called fingers, palm, thumb and connection sub-domains. DNA binds in the cleft formed by fingers, palm and thumb, where the latter sub-domain is highly flexible and exerts a grip on the bound primer strand in order to maintain it in the correct orientation (discussed in Le Grice, 2012). The DNA polymerase active site comprises three aspartic acid residues

(Asp185, 186 and 110) located within the palm, which—in common with many other known nucleic acid polymerases—features a five-stranded β -sheet with two α -helices on one side (Kohlstaedt et al., 1992; Jacobo Molina et al., 1993). The RNase H domain folds into a five-stranded β -sheet surrounding an arrangement of three α -helices and flanked by an additional carboxy-terminal α -helix on the opposite face (Davies et al., 1991). Hydrolysis of RNA is dependent on two divalent metal cations coordinated by residues Asp443/Asp549 and Asp443/Glu478/Asp498 respectively, where the first cation coordinates a water molecule for attack on the phosphodiester bond while the second cation stabilises the 3' hydroxyl group (Le Grice, 2012). Interestingly, both enzymatic activities are mediated solely by the p66 subunit, while p51—which adopts a markedly different fold despite the identical amino acid sequence—is thought to play the role of a rigid scaffold (Le Grice, 2012). Reverse transcription of the single-stranded viral RNA genome into double-stranded DNA is initiated from a cellular tRNA hybridised to the primer binding site (PBS) located near the 5' end of the vRNA. The RT proceeds through several steps of synthesis and RNA degradation, with transfer of the nascent (–)-strand DNA from the 5' to 3' terminus in between. Synthesis of the (+)-strand DNA is initiated at two so-called poly-purine tracts (PPTs) located at the centre and 3' end respectively (reviewed in Le Grice, 2012).

After the PIC has translocated through the nuclear pore, the vDNA is inserted into chromosomal DNA through the action of IN, thus turning into a provirus. The exact location of provirus integration is variable but probably not completely random, as weak palindromic consensus sequences have been identified (Wu et al., 2005). Moreover, insertion preferentially takes place within active transcription units as well as on nucleosomal DNA (Brady et al., 2009; Pruss et al., 1994). HIV-1 integrase is composed of three domains, namely an amino-terminal α -helical bundle stabilised by a Zn^{2+} ion, a catalytic core domain and a carboxy-terminal SH3-like β -barrel (Cai et al., 1997; Eijkelenboom et al., 1995). The catalytic domain belongs to the RNase H family of polynucleotidyl transferases, with an active site motif composed of three acidic residues coordinating two divalent metal cations (Dyda et al., 1994). While structural data on each of the individual domains of HIV-1 IN have been available for 20 years, the mode of DNA interaction has remained elusive. More recently, clues as to the protein's interaction with DNA have come from the structure of prototype foamy virus (PFV) IN crystallised in complex with viral DNA (Hare et al., 2010). Notably, the protein forms a tetrameric assembly joined to both ends of the vDNA molecule, with two IN dimers held together by both protein–protein and protein–DNA interactions (Figure 1.2E). The blunt ended vDNA is first processed by removal of two nucleotides from the 3' end of each strand, which then react with a phosphodiester bond on the cellular DNA in a single-step transesterification (Engelman et al., 1991). The two integration sites are separated by five nucleotides, which results in five-nucleotide duplications of host cell DNA at either flank of the viral insert. The final integration steps are accom-

plished by the cellular DNA repair machinery, although no specific enzymes have so far been implicated with much certainty (reviewed in Craigie and Bushman, 2012).

Interestingly, our endeavours to unravel the workings of retroviruses—and especially HIV-1—have not only led to the wealth of knowledge briefly touched on above, but also provided new insights into our immune system, most notably through the discovery of restriction factors. Over the last few years, a whole new research field has developed around these factors of intrinsic immunity, based on their systematic targeting by viral proteins with which they frequently undergo co-evolution. The significance of restriction factors in the context of HIV infection will be further elaborated on in the following sections.

1.2 Innate immune response to HIV

Dendritic cells (DCs) are professional antigen-presenting cells (APCs) that often constitute the first type of immune cells to encounter incoming pathogens and play a crucial role in priming effector cells such as CD4⁺ helper and CD8⁺ cytotoxic T cells by exposing pathogen-derived antigens on class II major histocompatibility complexes (MHCs). A distinction is generally made between two major subsets, namely conventional (cDC; also termed myeloid DCs or mDCs) and plasmacytoid (pDC) DCs.

In HIV infection however, DCs can be a double-edged sword. On one hand, DCs are themselves susceptible to infection because they express CD4, CXCR4 and CCR5 on their cell surface. Although infection of DCs by HIV-1 is believed not to be productive, the question remains under debate. More importantly however, several types of DCs are also able to capture HIV particles through a range of alternative cell surface receptors, including the C-type lectin receptors (CLRs) DC-SIGN (DC-specific ICAM3-grabbing nonintegrin) and DCIR (DC immunoreceptor), as well as the heparan sulfate proteoglycan syndecan-3 (Geijtenbeek et al., 2000; Lambert et al., 2008; de Witte et al., 2007a). Contrary to the conventional route of chemokine receptor-mediated entry, binding of gp120 to these receptors does not seem to trigger membrane fusion but rather leads to the uptake of intact virions into nonlysosomal compartments (Turville et al., 2004). Following the migration of cDCs from the site of infection to lymph nodes, infectious particles can be transferred to T helper cells via virological synapses (reviewed in Piguet and Sattentau, 2004). Langerhans cells, which are specialised cDCs located in epidermal tissues, specifically express a CLR named Langerin that similarly leads to endocytosis of HIV particles albeit causing their degradation in acidic compartments named Birbeck granules (de Witte et al., 2007b). This ability to inhibit virus transmission is of particular importance in the case of HIV, as Langerhans cells are the first DCs to come into contact with HIV particles in mucosal epithelia of the cervix, vagina and foreskin.

Closer to the subject matter at hand are pDCs, which, in addition to their role as

APCs, are capable of producing considerable amounts of interferon and other proinflammatory cytokines upon sensing viral infection.

1.2.1 Interferon response

Interferons (IFNs) are a group of cytokines produced by host cells in response to microbial infection or the detection of cancer cells. They stimulate cellular defenses, activate immune effector cells such as natural killer (NK) cells, and more generally induce an inflammatory state. Three classes of IFN have been identified to date, namely type I (IFN- α , - β , - ω , - ϵ , - τ , - δ and - κ), type II (IFN- γ) and type III (IFN- λ 1, - λ 2 and - λ 3) (reviewed in Randall and Goodbourn, 2008). Of these, IFN- α/β , as well as type III IFNs, are induced directly in many different cell types upon viral infection and will thus be the main focus of this section.

IFN- α and - β interact with target cells through a heterodimeric cell surface receptor composed of the IFNAR1 and IFNAR2 gene products. Stimulation of the IFNAR1/IFNAR2 receptor, which appears to be expressed in all cell types, triggers a signaling cascade that results in the expression of a large number of genes that initiate an antiviral state in the target cell. The tasks performed by these IFN-stimulated genes (ISGs) are diverse and wide ranging, as exemplified by the restriction factors outlined above, which represent but one class of ISGs. Transcriptional activation of ISGs is mediated by components of the JAK (just another kinase) and STAT (signal transducers and activators of transcription) families, as well as IRF-9 (IFN regulatory factor 9) which, together with STAT1 and STAT2, forms a complex that binds to the IFN-stimulated response element (ISRE) found in the promoter region of most ISGs (reviewed in Platanias, 2005).

Cells recognise “foreign” pathogen-derived matter in a variety of ways through a range of so-called pattern recognition receptors (PRRs). The substrates recognised by PRRs are referred to as pathogen-associated molecular patterns (PAMPs) and include molecules such as dsRNA, ssRNA, unmethylated CpG DNA and viral proteins. Recognition of PAMPs triggers a signaling cascade that results in the induction of IFN production, where the exact pathways and transcription factors involved are complex and only partially understood. Transcription of IFN- β , for instance, is triggered by the activation of IFN regulatory factor 3 (IRF-3) and NF- κ B in the cytoplasm, which leads to their translocation to the nucleus and formation of a so-called enhanceosome (reviewed in Randall and Goodbourn, 2008).

A well-characterised PAMP encountered in many viral infections, either as part of the genome or as a replication or transcription intermediate, is dsRNA. Convergent transcription of overlapping reading frames might even give rise to dsRNA in DNA virus replication. The main PRR responsible for detection of dsRNA within endosomes, as well as extracellularly, is Toll-like receptor 3 (TLR3) (Alexopoulou et al., 2001).

Depending on cell type, TLR3 is expressed in endosomal compartments (myeloid dendritic cells—mDCs), lysosomes (macrophages) or even at the cell surface (fibroblasts) (Johnsen et al., 2006; de Bouteiller et al., 2005; Matsumoto et al., 2002). The localisation of TLR3 in endosomes notably allows detection of viral dsRNA from entering virions prior to replication, and as such ensures a rapid IFN response in the absence of established infection. Upon binding to dsRNA, TLR3 undergoes dimerisation and phosphorylation, leading to recruitment of the adaptor protein TRIF (Toll/interleukin-1 receptor domain-containing adaptor inducing IFN- β). The binding of TRIF triggers signaling and ultimately transcriptional activation of IFN- β via the NF- κ B and IRF-3 pathway mentioned above (reviewed in Randall and Goodbourn, 2008).

Retroviruses do not proceed through a dsRNA stage and are sensed instead by TLR7 and TLR8, which both detect ssRNA in endosomes resulting from internalisation of viral particles (Heil et al., 2004). Whereas TLR7 is expressed almost exclusively in pDCs, TLR8 is found in myeloid cells such as cDCs, monocytes and macrophages (reviewed in Cervantes et al., 2012). Interestingly, it was shown that cytoplasmic RNA can be taken up into endosomes through autophagy and thus be exposed to TLR7 (Iwasaki, 2007; Lee et al., 2007). Discrimination between host and pathogen-derived ssRNA is independent of nucleotide sequence, but rather seems to rely on recognition of cellular modifications such as methylation and pseudouridines, as well as the presence of several uridines in close proximity (Diebold et al., 2006; Karikó et al., 2005). In pDCs, TLR7 induces IFN transcription via NF- κ B and IRF-7 but using distinct signaling pathways from TLR3 (Beignon et al., 2005). Upon binding of ssRNA, TLR7 recruits the signaling adaptor myeloid differentiation factor 88 (MyD88) as well as interleukin-1 receptor-associated kinase 4 (IRAK-4) and IRAK-1. In turn, this complex engages with components of the NF- κ B pathway or directly with IRF-7 (reviewed in Randall and Goodbourn, 2008).

In addition to nucleic acids, IFN expression may also be induced by determinants such as viral proteins or bacterial lipopolysaccharide (LPS). Since 1992 it has been known that HIV-1 gp120 induces IFN- α production in PBMCs (Capobianchi et al., 1992). More recently, it was shown that gp120 activates TLR-2 and -4 expressed on the surface of endothelial cells of the female upper genital tract (Nazli et al., 2013). The interaction is heparan sulfate-dependent and results in the induction of NF- κ B.

In the cytoplasm, viral RNA is detected by a different class of PRRs, namely the RNA helicases RIG-I (retinoic acid-inducible gene 1), MDA5 (melanoma differentiation-associated gene 5) and LGP2 (Laboratory of Genetics and Physiology 2), which are collectively referred to as RIG-I-like receptors (RLRs). The three structurally related proteins share a central helicase and carboxy-terminal domains implicated in RNA-binding, with RIG-I and MDA5 featuring additional amino-terminal caspase activation and recruitment domains (CARDs) (reviewed in Gack, 2014; Rodriguez et al., 2014). Upon interaction with RNA featuring a 5'-triphosphate as well as double-stranded sec-

ondary structure elements, both RIG-I and MDA5 interact with the mitochondria- and peroxisome-associated adaptor protein MAVS (mitochondrial antiviral signaling). The signaling cascade results in the induction of IRF-1, IRF-3 and NF- κ B (Dixit et al., 2010). The incoming HIV-1 RNA genome activates RIG-I, probably based on the considerable secondary structure compared to cellular RNA (Solis et al., 2011; Berg et al., 2012). Interestingly however, in *de novo* infection of human macrophages, RIG-I is depleted by lysosomal degradation in a viral protease-dependent manner, thus preventing RIG-I-mediated immune signaling (Solis et al., 2011).

Perhaps more relevant to immune detection of HIV is a very recently discovered third class of cytosolic DNA sensors comprising cGAS (cyclic-di-GMP-AMP [cGAMP] synthetase) and IFI16 (IFN-inducible protein 16) (Wu et al., 2013; Sun et al., 2013; Unterholzner et al., 2010). Indeed, cGAS recognises HIV-1-derived DNA intermediates of reverse transcription, which leads to production of cGAMP and activation of an endoplasmic reticulum-associated adaptor called STING (stimulator of IFN genes ; Gao et al., 2013). Activated STING recruits TANK-binding kinase 1 (TBK1), which in turn activates IRF-3 through phosphorylation, resulting in IFN- α/β production (Ishikawa and Barber, 2008). In a similar fashion, IFI16 binds to single- and double-stranded HIV-derived DNA but not to DNA/RNA duplex intermediates, followed by activation of STING and TBK1/IRF-3-mediated IFN induction (Jakobsen et al., 2013). Over the past few years it has become clear that STING plays a central role in IFN stimulation in response to viral DNA, including direct binding to DNA and possibly, regulation of the RIG-I–MAVS pathway (Ishikawa et al., 2009; Abe et al., 2013).

Despite being subverted by HIV and contributing to the spread of infection, pDCs are nonetheless capable of detecting viral components and triggering an innate immune response (reviewed in Acchioni et al., 2014). In many cases however, the virus has evolved mechanisms to avoid detection or antagonise cellular effectors. The extent of viral countermeasures has really become clear with the recent and ongoing discovery of host restriction factors.

1.2.2 Restriction factors

In mammalian cells, restriction factors often constitute the first line of defense against viral infection, and are defined as autonomously and dominantly acting proteins many of which are induced by interferon (IFN). All of the well-described restriction factors have undergone significant positive selection and are mostly inactive against wild-type viruses infecting their natural host cells. As a result, restriction factors tightly limit a virus' range of susceptible species and cell types, thus posing a significant barrier against cross-species transmission. In a striking example of co-evolution, viruses have evolved to avoid or actively antagonise cellular restriction factors, as in the case of the HIV-1 accessory proteins Vif, Vpu and Nef. While circumstantial evidence for

factors involved in the restriction of HIV-1 has existed since the 1990s, the three most prominent restriction factors known to date—APOBEC3G, tetherin and TRIM5 α —were identified more recently using comparative transcriptomics or cDNA library screening of non-permissive cells (Sheehy et al., 2002; Neil et al., 2008; Stremlau et al., 2004). In addition to these well-studied proteins, an ever increasing number of restriction factors continue to be discovered. Tetherin, also referred to as BST2 (bone marrow stromal antigen 2), HM1.24 or CD317 (cluster of differentiation 317), was identified as a potent restriction factor of HIV-1 for its ability to inhibit virus release in the absence of the HIV-1 accessory protein Vpu (Neil et al., 2008; Van Damme et al., 2008). As the main subject of this thesis, it will be treated in depth in the following section. Figure 1.3 illustrates the impact on the viral life cycle of the major restriction factors currently known to target HIV-1.

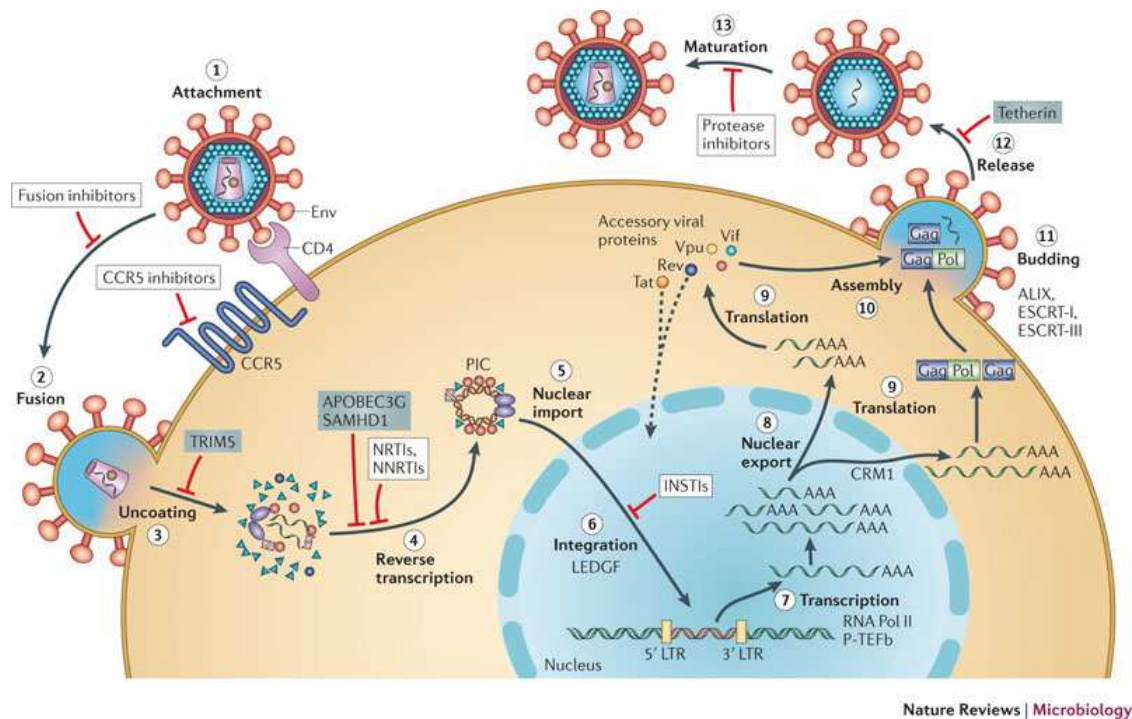


Figure 1.3 Life cycle of HIV-1 and modes of action of the major cellular restriction factors. Reprinted by permission from Macmillan Publishers Ltd: *Nature Reviews Microbiology* (Engelman and Cherepanov, 2012), copyright 2012.

Apolipoprotein B mRNA-editing enzyme catalytic polypeptide-like 3G (APOBEC3G) is characterised by its cytidine deaminase activity, which catalyses the modification of cytidine to uridine residues in both RNA and DNA. The restriction factor is efficiently antagonised by the HIV-1 accessory protein Vif (virion infectivity factor) (Sheehy et al., 2002). Two, and possibly more, other proteins of the 11-member APOBEC3 protein family, namely APOBEC3F and -H, show a similar albeit less potent effect on HIV-1 and are also regulated by Vif (reviewed by Albin and Harris, 2010). Through the RNA-dependent binding of APOBEC3G to the HIV-1 nucleocapsid (NC) domain, the pro-

tein is packaged into nascent virions in the absence of Vif (Bogerd and Cullen, 2008). In subsequently infected cells, the enzyme then deaminates up to 10% of cytidines in newly synthesised single-stranded DNA during reverse transcription (reviewed in Malim and Bieniasz, 2012). In addition to hypermutation, APOBEC3G also seems to physically block the progress of reverse transcriptase along the genomic RNA, resulting in reduced cDNA levels (Iwatani et al., 2007; Bishop et al., 2008). Vif-based counteraction depends on its direct interaction with APOBEC3G, followed by recruitment of a cellular ubiquitin ligase complex, polyubiquitination and proteasomal degradation (Yu et al., 2003; Sheehy et al., 2003).

In contrast to the two previous restriction factors, TRIM5 α (tripartite motif-containing 5 α) acts at the post-entry stage of the HIV-1 life cycle rather than post-integration (Strem-lau et al., 2004). While the net effect of TRIM5 α activity is the abolishment of reverse transcription, the precise mechanism still needs to be elucidated. TRIM5 α binds to the viral capsid, possibly forming multimeric assemblies, and causes the premature disassembly of the capsid core and associated reverse transcription complexes (reviewed by Malim and Bieniasz, 2012). Although TRIM5 α comprises a RING domain with E3 ubiquitin ligase activity, its restriction activity does not entirely depend on proteasomes since it is able to restrict HIV-1 in the presence of proteasome inhibitors (Perez Caballero et al., 2005). Given that proteasome inhibition also precludes capsid disassembly (Wu et al., 2006; Diaz Griffero et al., 2007), neither process thus seems to be solely responsible or essential for antiviral activity. These observations possibly hint at the existence of a so far unidentified alternative mechanism by which TRIM5 α is able to inhibit viral infection.

A further retroviral restriction factor worth mentioning is SAMHD1, which is named after the SAM (sterile alpha motif) and HD (histidine-aspartate) domains that characterise the protein (reviewed in Zheng et al., 2012). SAMHD1 is a dimeric nuclear protein induced by IFN- γ which inhibits HIV-1 replication by depleting cellular dNTPs through its dGTP triphosphohydrolase activity. The protein's antiviral activity is limited to non-dividing cells such as dendritic cells, monocytes, resting CD4⁺ T cells and macrophages, although the latter still display low levels of HIV-1 replication. In the case of HIV-2 and some SIV strains, SAMHD1 is targeted for proteasomal degradation via the accessory protein Vpx, while in HIV-1 no such countermeasure exists. Instead, it has been suggested that HIV-1 might profit from not infecting dendritic cells because of their intrinsic ability to sense viral infection and elicit a potent antiviral response (Manel et al., 2010).

1.3 Tetherin structure and function

Human tetherin is encoded by the gene *bst2* composed of four exons (Ishikawa et al., 1995) and was first discovered as a marker of bone marrow stromal cells from which

et al., 1995; Erikson et al., 2011). Moreover, tetherin expression is strongly induced in many additional cell types by interferons (IFN- α , - β , - ω , - γ and - λ 3) as well as IL-27 (reviewed in Sauter, 2014). Indeed, the *bst2* promoter contains binding sites for the transcription factor Stat3, a component of the Jak/Stat signaling cascade underlying many cytokine receptor systems (Ohtomo et al., 1999). In a cytokine-independent fashion, tetherin expression is also induced through activation of Toll-like receptors (TLR) 3 and 8 (Bego et al., 2012).

As a type II transmembrane protein, tetherin is co-translationally translocated into the endoplasmic reticulum (ER), with its transmembrane domain acting as a signal anchor sequence. The trafficking of tetherin from the ER to the Golgi apparatus with subsequent transport to the plasma membrane relies on N-glycosylation of two conserved residues (Kupzig et al., 2003). Rather than being an exclusive cell surface protein, studies using electron and immunofluorescence microscopy have revealed that tetherin continually cycles between the plasma membrane, the *trans*-Golgi network (TGN) and endosomal compartments (Masuyama et al., 2009; Habermann et al., 2010). Indeed, the amino-terminal cytosolic tail contains a conserved dual tyrosine motif (YxY), which enables the protein's clathrin-mediated internalisation (Rollason et al., 2007). This process depends on binding of the α -adaptin subunit of the AP2 adaptor complex to the YxY motif (Masuyama et al., 2009). An isoform lacking residues 1–12 was recently discovered that seems to be preferentially located at the plasma membrane—which could be explained by the absence of the internalisation motif (Cocka and Bates, 2012). While a functional role could so far not been attributed to the short isoform, the conservation in most mammalian species of a 'leaky' Kozak sequence causing ribosome slippage as well as the alternative AUG codon (Met13) suggests that a distinct role does exist. The short and long isoforms were found to associate in both homo- and hetero-dimers (Cocka and Bates, 2012).

1.3.2 Topology and structure

Tetherin is composed of a short cytoplasmic tail, an alpha-helical transmembrane domain and a coiled coil ectodomain (Kupzig et al., 2003). Its carboxy-terminus is modified by a glycosyl-phosphatidyl-inositol (GPI) anchor, conferring a highly unusual topology (Figure 1.5) only shared by a small number of other known proteins, including an isoform of the prion protein with an uncleaved signal sequence (Stewart et al., 2001; Sauter, 2014). The extracellular domain is further modified by N-linked glycosylation of two conserved asparagines (Asn65 and 92) and contains three cysteines (Cys53, 63 and 91) involved in the formation of disulfide-linked homodimers (Kupzig et al., 2003).

Crystal structures of the extracellular domain (Figure 1.6) reveal a parallel dimeric coiled coil motif, stabilised by the disulfide bond at position 91 as well as salt bridges

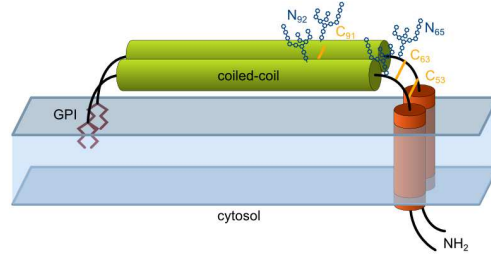


Figure 1.5 Schematic topology of human tetherin. Tetherin is a type II transmembrane protein featuring two N-linked glycosylation sites and is modified with a glycosyl-phosphatidyl-inositol (GPI) anchor at its C-terminus. The protein forms homodimers that are cross-linked by three disulfide bonds located in the extracellular domain.

between Glu105–Lys106 and Glu133–Arg138 (Hinz et al., 2010; Schubert et al., 2010; Yang et al., 2010). Under reducing conditions, the thermostability of the coiled coil domain is markedly decreased, which underlined the importance of the disulfide bonds (Hinz et al., 2010). Interestingly, the coiled coil “knobs-into-holes” interface is interrupted by several irregular residues at conserved heptad positions, including Gly109 and Ala130, resulting in an increased radius and pitch of the superhelix (Figure 1.6A). These destabilising features may allow the coiled coil to disassemble during dynamic processes, while the disulfide cross-links ensure its subsequent reassembly (Hinz et al., 2010).

An *ab initio* model of the entire ectodomain calculated from small angle X-ray scattering (SAXS) data suggests an elongated ~ 170 Å configuration with a kinked hinge separating the coiled coil core domain from the transmembrane region (Hinz et al., 2010). These results are corroborated by the SAXS model obtained from the murine tetherin ortholog, whereby it is worth noting that the murine tetherin crystal structure rather suggest a prolongation of the coiled coil fold along the entire ectodomain (Swiecki et al., 2011 ; Figure 1.6C).

Under reducing conditions, tetherin is capable of assembling into tetramers (Figure 1.6B) by forming an antiparallel four-helix bundle involving the amino-terminal third of the ectodomain (Schubert et al., 2010; Yang et al., 2010). Tetramerisation of the soluble ectodomain (residues 47–154) is disrupted by mutation of Leu70 to Asp (Schubert et al., 2010) and interestingly, as detailed below in section 1.3.5, the same residue is required for tetherin-mediated NF- κ B signaling. Nevertheless, although tetherin tetramers have been identified in solution under reducing conditions, their physiological relevance is currently uncertain, especially given the oxidising environment of extracellular space.

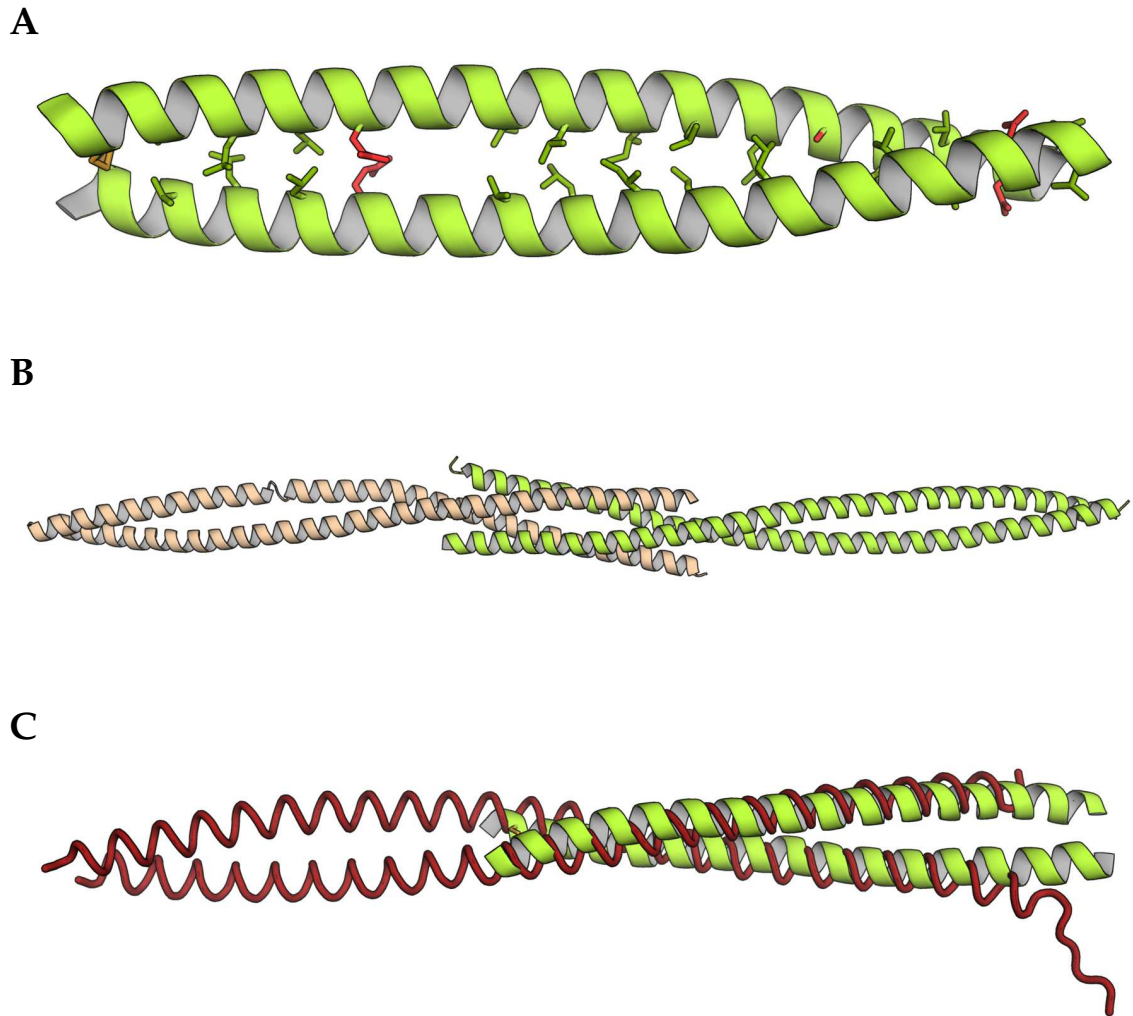


Figure 1.6 Crystal structures of the tetherin extracellular domain. (A) Coiled coil core region (residues 80–159) at 2.77 Å resolution, with regular “knobs-into-holes” contacts shown as green sticks and disruptive residues highlighted in red (Hinz et al., 2010 ; PDB 2X7A). (B) Tetherin tetramer mediated by folding of N-terminal part into antiparallel four-helix bundle (Schubert et al., 2010 ; 3NWH). (C) Crystal structure of murine tetherin (Swiecki et al., 2011 ; 3NI0), in red, superimposed on the human extracellular core region.

1.3.3 Inhibition of virus release

Prior to the discovery of tetherin as a restriction factor of HIV-1, it had been known that the viral accessory protein Vpu was essential for virus release in certain cell types while being dispensable in others (Terwilliger et al., 1989; Strebel et al., 1989). In HeLa cells for instance, fully matured Vpu deficient virus particles were shown to accumulate at the cell surface as well as in intracellular endosomal compartments (Göttlinger et al., 1993; Neil et al., 2006). These observations prompted a search for a factor capable of physically tethering nascent virions to cellular membranes that was constitutively expressed in HeLa cells but not in cells displaying no requirement on Vpu, such as

HEK293T or HT1080. Since the identification of tetherin in 2008, much effort has gone into understanding the exact mechanism behind tetherin-mediated inhibition of virus release.

Mechanism of viral particle retention

Several models for tetherin-mediated virion attachment were initially considered, including a parallel (or equatorial) configuration with one subunit of each dimer embedded in the viral and cell membrane respectively, or alternatively, a non-covalent association between two tetherin dimers each located in one of the membranes. It is now clear however, that during the budding process, virions become entrapped by tetherin dimers when one pair of membrane anchors is inserted into the nascent viral envelope while the second pair remains embedded in the plasma membrane (Figure 1.7 ; Neil et al. (2008); Van Damme et al. (2008); Perez Caballero et al. (2009); Venkatesh and Bieniasz (2013)). Moreover, Venkatesh and Bieniasz (2013) could recently show that there is a 3–5-fold preference for insertion of the GPI anchor over the transmembrane domain into the viral membrane. Electron micrographs of tetherin-expressing cells infected with HIV-1 Δ *vpu* show that in addition to being attached to the plasma membrane, virions become tethered to each other (Neil et al., 2007, 2008). This rather simplistic mechanism is thus elegantly reflected by the protein's topology.

Following inhibition of their release, viral particles are internalised through clathrin-mediated endocytosis and targeted for lysosomal degradation, as evidenced by colocalisation with markers of early (Rab5A) and late endosomes (CD63) respectively (Neil et al., 2006). This process relies on interaction of tetherin with Rabring7 (Rab7-interacting RING finger protein, also known as BCA2), possibly followed by recruitment of Rab7 (Miyakawa et al., 2009). It is worth noting, however, that Rabring7 has recently been shown to bind to the Gag MA domain, targeting it for lysosomal degradation independently of tetherin (Nityanandam and Serra Moreno, 2014). The mode of internalisation and degradation of tethered virions, including the role played by Rabring7, thus needs further clarification.

The basis of tetherin recruitment to HIV budding sites is not entirely clear, although it has been hypothesised that tetherin and HIV Gag may simply co-localise in sphingolipid- and cholesterol-rich membrane microdomains ("lipid rafts") due to the theoretical affinities of both tetherin GPI and the Gag MA domain for such membrane regions (Jouvenet et al., 2009; Hammonds et al., 2010). However, while particles of HIV and other enveloped viruses have indeed been shown to preferentially assemble within and bud from lipid rafts (Nguyen and Hildreth, 2000), the localisation of tetherin to such membrane domains remains under debate because the protein fails to co-localise with several known lipid raft markers (Lehmann et al., 2011; Grover et al., 2013). Recent observations by Grover et al. (2013) rather suggest that tetherin localisation to budding sites depends on Gag-induced membrane curvature as well as the pres-

ence of the ESCRT proteins Tsg101 and Alix. Based on super-resolution microscopy of a tetherin–mEos fluorescent protein chimera, 4–7 tetherin dimers were estimated to be present per HIV-1 budding site in the absence of Vpu (Lehmann et al., 2011). A significantly higher number of dimers (80–400) was however arrived at in an alternative approach, where tethered virions were proteolytically removed from the cell surface and the number of virion-associated tetherin dimers analysed by quantitative Western blotting (Venkatesh and Bieniasz, 2013).

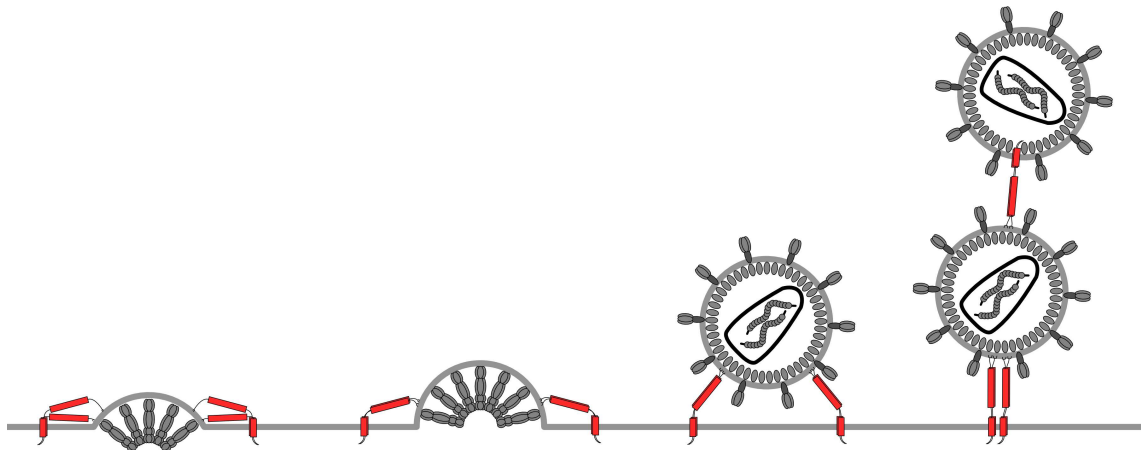


Figure 1.7 Schematic representation of the proposed mechanism of HIV particle retention by tetherin. During the budding process, the pair of GPI anchors from a tetherin homodimer is inserted into the nascent virion. The fully assembled particles are retained at the plasma membrane and are tethered to each other. The conformational flexibility conferred by the labile coiled coil domain, in conjunction with the stabilising disulfide bonds, allows the protein to remain embedded in the budding virion throughout this dynamic process.

The requirement of tetherin’s post-translational modifications for virion retention has been addressed by several studies. For instance, while each of the individual disulfide bonds is dispensable, mutation of all three cysteines (Cys53, 63 and 91) drastically reduces antiviral activity without affecting subcellular localisation (Perez Caballero et al., 2009). The mutation of both glycosylation sites (Asn65 and 92) impedes cell surface transport, and in turn almost completely abrogates antiviral activity. Mutation of Asn65 alone only slightly reduces activity, while the substitution of Asn92 with an alanine has a significant effect on virus release (Perez Caballero et al., 2009; Hinz et al., 2010). As expected, the removal of either membrane anchor completely abolishes antiviral activity (Perez Caballero et al., 2009). Similarly, the importance of the coiled coil in virus retention was assessed by mutating sets of key residues along the coiled coil interface, resulting in a loss of HIV-1 tethering activity in each case (Hinz et al., 2010). When expressed as soluble ectodomain constructs spanning residues 47–159, these mutants show a decrease in dimer formation, indicating that dimerisation and disulfide cross-linking are essential for tetherin’s antiviral activity (Hinz et al., 2010). Going one

step further, Perez Caballero et al. (2009) deleted the entire coiled coil domain, completely abolishing the protein's activity. They then re-introduced a heterologous coiled coil from dystrophin myotonia protein kinase (DPMK) which restored antiviral activity. Finally, the same authors designed an artificial protein with tetherin-like size and topology using components from various unrelated proteins. This artificial tetherin significantly inhibited the release of HIV-1 virions, thus indicating that the protein's antiviral activity is largely mediated through its topology rather than sequence. Mutation of the tetramerisation interface residue Leu70 to Asp results in an attenuated restriction of HIV-1 Δ vpu in HEK293T cells compared to wild-type tetherin, although in both cases the number of released particles is three orders of magnitude lower than in the absence of tetherin (Schubert et al., 2010). This indicates that, while not being essential, tetherin tetramerisation might enhance restriction of HIV-1.

Viral antagonism

In infections with HIV-1, and more specifically group M viruses, tetherin is potently antagonised by the viral accessory protein Vpu (Neil et al., 2008; Van Damme et al., 2008). This 15–16 kDa type I membrane protein comprises a very short extracellular tail, a single membrane-spanning α -helix and a cytoplasmic domain (Cohen et al., 1988; Strebel et al., 1988; Maldarelli et al., 1993). There are a number of indications that the transmembrane domain may mediate homo-oligomerisation of Vpu into a pentameric ion channel, reminiscent of the Influenza M2 protein (Hussain et al., 2007). The cytoplasmic domain is composed of two α -helices, termed H1 and H2, connected by a flexible loop featuring a highly conserved di-serine motif DSGxxS. The phosphorylated di-serine motif serves as a binding site for β -TrCP (β -transducin repeat-containing protein), a component of the ubiquitin-proteasome pathway (Margottin et al., 1998; Buttica et al., 2007). Before the discovery of its anti-tetherin activity, Vpu was mainly known for its ability to initiate the degradation within the endoplasmic reticulum (ER) of newly synthesised CD4, the principal host cell receptor for HIV entry (reviewed in Dubé et al., 2010a; Sauter, 2014). Upon direct binding to CD4, the di-serine motif of Vpu is phosphorylated by casein kinase II, resulting in the recruitment of the cellular SCF (Skp1/Cullin1/F-box) E3 ubiquitin ligase complex via β -TrCP1 and -2. The cytosolic tail of CD4 is then poly-ubiquitinated, targeting the protein for proteasomal degradation, which possibly relies on components of the ER-associated degradation (ERAD) pathway.

In 2008, Van Damme et al. already observed that Vpu causes a down-regulation of tetherin expression at the cell surface, however the details underlying the anti-tetherin activity of Vpu are complex and remain somewhat elusive. Mechanisms of proteasomal and/or endo-lysosomal degradation, as well as sequestration of the protein within a perinuclear compartment have all been proposed. Nonetheless, independently of the downstream pathway involved, it has become evident that both proteins directly

interact via their respective transmembrane domains, as determined by a number of studies employing mutagenesis, cysteine crosslinking and single genome analyses (Vigan and Neil, 2010; Kobayashi et al., 2011; McNatt et al., 2013; Pickering et al., 2014). Expression of Vpu results in a decreased total cellular level of tetherin, without affecting transcription. Whereas initial findings suggested a mechanism of proteasomal degradation similar to that of CD4, it is more likely that Vpu-mediated degradation of tetherin rather employs an ESCRT-dependent endo-lysosomal pathway, although the residues that become ubiquitinated on the cytoplasmic tail of tetherin have not been identified (Goffinet et al., 2009; Mangeat et al., 2009; Douglas et al., 2009; Iwabu et al., 2009; Mitchell et al., 2009). Indeed, the sequential sorting of ubiquitinated tetherin into vesicles, endosomes and eventually lysosomes depends on HRS and UBAP1, which are both components of the cellular ESCRT machinery (Janvier et al., 2011; Agromayor et al., 2012). Furthermore, the involvement of β -TrCP in tetherin internalisation is unclear, as the di-serine β -TrCP binding motif is not strictly required (Kluge et al., 2013). Rather, it has been suggested that a putative ExxxLV trafficking motif located on the cytoplasmic H2 helix of Vpu was found to be required for anti-tetherin activity (Kueck and Neil, 2012). In any case, it has become clear that for multiple reasons degradation alone cannot account for tetherin counteraction induced by Vpu (discussed in Dubé et al., 2010b), and it is now established that Vpu causes sequestration of both newly synthesised and recycled tetherin in the TGN by a direct interaction, thus inhibiting tetherin transport to the plasma membrane (Dubé et al., 2009; Hauser et al., 2010; Andrew et al., 2011; Schmidt et al., 2011).

Contrary to the pandemic M viruses, no efficient tetherin countermeasures seem to have evolved in N, O and P group viruses. Interestingly, a highly pathogenic group N isolate capable of potently counteracting tetherin was found to have acquired a DxxxLV motif, resembling the trafficking motif present in HIV-1 group M Vpu (Sauter et al., 2012). This suggests that overcoming restriction by human tetherin poses a major obstacle in widespread transmission in the human population—an obstacle that only group M viruses have overcome through the adaptation of Vpu so far. Notably, while the immediate simian HIV-1 predecessors SIV_{cpz} and SIV_{gor} both encode a Vpu homologue, the protein is inactive against tetherin in their respective hosts (Sauter et al., 2009). In common with most other SIVs that do not encode a Vpu homologue, these viruses rather rely on the accessory protein Nef as a tetherin antagonist (Jia et al., 2009; Zhang et al., 2009). Unlike Vpu, Nef does not lead to degradation of tetherin in rhesus macaques, but causes its clathrin- and AP2-mediated removal from the cell surface following a direct interaction (Serra Moreno et al., 2013). Intriguingly, the binding of Nef was mapped to a DDIWK motif on the cytoplasmic tail that is missing in the human orthologue, thus rendering human tetherin resistant against Nef-mediated endocytosis (Jia et al., 2009; Zhang et al., 2009; Sauter et al., 2009). Three further known simian viruses carry a *vpu* gene, namely those infecting greater spot-nosed (*Cercopithecus nic-*

titans ; SIV_{gsn}), Mona (*C. mona* ; SIV_{mon}) and mustached monkeys (*C. cephus* ; SIV_{mus}). In these monkey viruses, Vpu is potentially active against tetherin from their respective hosts, as well as tetherin from other monkey species (Sauter et al., 2009).

The relative success of HIV-1 group O viruses, which have infected tens of thousands of people, has remained somewhat puzzling, given their apparent lack of an effective tetherin antagonist. Interestingly, it has recently been found that group O Nef proteins successfully reduce tetherin levels at the cell surface of primary human peripheral blood mononuclear cells (PBMCs) (Kluge et al., 2014). A comparison with SIV_{gor} Nefs further revealed that this activity specifically results from adaptation to human tetherin. Finally, group O Nefs have evolved to bind to a distinct region in the cytoplasmic tail of human tetherin, directly adjacent to the deleted five amino acid motif described above (Kluge et al., 2014).

HIV-2 also lacks a *vpu* gene, and has instead evolved to neutralise tetherin via its Env protein (Le Tortorec and Neil, 2009; Hauser et al., 2010). Similar to SIV Nef, HIV-2 Env mediates the removal of tetherin from the cell surface, without however affecting total cellular levels. More likely, the restriction factor is relocalised to or retained in the TGN (Le Tortorec and Neil, 2009). The anti-tetherin activity of Env has been known for some time to depend on a highly conserved GYxxΦ endocytosis motif present on the protein's cytoplasmic tail, that serves as a binding site for AP2 (Abada et al., 2005; Noble et al., 2006). Given the presence of this motif in other HIV/SIVs, the recognition of tetherin by HIV-2 must rely on other determinants, possibly located in the extracellular domains of both proteins. Moreover, considering that in addition HIV-2 Env-mediated tetherin counteraction seems to be cell type-dependent, Le Tortorec and Neil (2009) suggest that additional cellular factors might be involved.

Restriction of other enveloped viruses

The restriction activity of tetherin was discovered in the context of HIV-1, and most research has indeed been focused on retroviral infection. Nevertheless, it is important to realise that enveloped viruses from all major families seem to be susceptible to tetherin restriction to some extent. Correspondingly, these viruses have evolved an arsenal of antagonists, some of which I will briefly introduce.

Ebola virus is a negative-stranded RNA virus of the filovirus family of which several species cause zoonotic infection in humans, characterised by severe haemorrhagic fever and high mortality. Tetherin inhibits the release of virus-like particles (VLPs) composed of the matrix protein VP40, an effect that is abolished in the presence of the Ebola glycoprotein GP (Kaletsky et al., 2009). Remarkably, while GP is able to interact with tetherin, it does not result in degradation of the restriction factor nor its down-regulation from the cell surface, although the exact mechanism remains to be elucidated (reviewed in Kühl and Pöhlmann, 2012).

Herpes simplex virus 1 (HSV-1) is an alphaherpesvirus with a double-stranded

DNA genome that assembles intracellularly rather than budding from the cell surface. The HSV-1 glycoprotein M (gM) has been shown to antagonise tetherin by causing it to accumulate in the TGN, either by preventing transport to or by mediating its removal from the cell surface (Blondeau et al., 2013). However, while gM is able to rescue restriction of HIV-1 in the absence of Vpu, it cannot entirely account for restriction in HSV-1, suggesting the existence of a second gM-independent anti-tetherin mechanism in this virus (Blondeau et al., 2013). Indeed, Zenner et al. (2013) could show that the HSV-1 protein Vhs (virion host shutoff factor), which is present in the viral tegument and thus released into the cytoplasm immediately following infection, degrades tetherin mRNA through its endoribonuclease activity.

In the case of Kaposi's sarcoma-associated herpesvirus (KSHV), a potentially oncogenic gammaherpesvirus mainly affecting immunocompromised patients, tetherin restriction is counteracted by the viral protein K5 (Bartee et al., 2006). The RING-CH domain of K5 acts as a ubiquitin ligase and has been shown to ubiquitinate tetherin at Lys18, leading to its ESCRT-dependent endosomal degradation (Pardieu et al., 2010). This pathway is independent of the mechanism employed by HIV-1 Vpu, since mutation of lysine residues ubiquitinated by Vpu has no effect on K5-mediated degradation (Pardieu et al., 2010).

1.3.4 Organisation of subcellular structure

Independently of virus infection, tetherin has been suggested to associate with lipid rafts via its GPI anchor, and loses this localisation when the anchor is enzymatically removed by treatment with phosphoinositide phospholipase C (PI-PLC) (Kupzig et al., 2003). This indicates that the transmembrane domain is probably excluded from lipid rafts, and that several tetherin molecules could thus stabilise or organise such membrane domains by delimiting them much like a picket fence (Kupzig et al., 2003). Indeed, such a notion is supported by the observations of Billcliff et al. (2013), who could show that lipid raft markers are redistributed and their diffusional mobility increased upon silencing of tetherin expression using siRNA. Moreover, tetherin indirectly associates with the apical actin network in polarised cells, and its knock-out results in the collapse of the apical actin organisation and microvilli (Rollason et al., 2009). This interaction is mediated by binding of RICH2 to the dual tyrosine motif located on the cytosolic tail of tetherin, followed by association with EBP50 and ezrin (Rollason et al., 2009 ; Figure 1.8). The presence of RICH2 also renders the dual tyrosine motif inaccessible thus precluding clathrin-mediated endocytosis of tetherin. A further consequence of tetherin knock-out are elevated levels of active Rac GTPase, a regulatory protein involved in numerous cellular processes including cytoskeletal organisation. This effect could potentially point to a regulatory role of tetherin on RICH2, which is a Rac GTPase-activating protein (GAP) and thus stimulates Rac activity (Rollason et al.,

2009).

1.3.5 Immune sensing and signaling activities

Tetherin is capable of activating NF- κ B transcription factors, which are at the heart of many cellular defense responses because they induce the expression of many proinflammatory genes (Matsuda et al., 2003). This signaling activity was found to depend on the cytosolic dual tyrosine motif YxY as well as Leu70, a highly conserved residue that mediates tetherin tetramerisation in the ectodomain (Cocka and Bates, 2012; Tokarev et al., 2013). As a consequence, the short tetherin isoform has no signaling activity, given its lack of the dual tyrosine motif (Cocka and Bates, 2012). By introducing a set of mutations known to disrupt coiled coil formation, Tokarev et al. (2013) could show that an intact ectodomain was essential both for viral restriction and induction of NF- κ B activity. In contrast, the authors found that the presence of the GPI anchor, which is required for virion retention, is entirely dispensable for NF- κ B activation, indicating that both functions are based on distinct processes. An interaction of tetherin with TAK1 (TGF- β -activated kinase 1) and its regulatory factor TAB1 (TAK1-binding protein 1) via the YxY motif was reported in co-immunoprecipitation experiments (Tokarev et al., 2013). Interestingly, the expression of Vpu-deficient HIV-1 stimulates tetherin-mediated NF- κ B activation, suggesting that tetherin may act as a sensor of virus assembly (Galão et al., 2012; Tokarev et al., 2013). More specifically, the retention of HIV-1 particles causes phosphorylation of Tyr6 and Tyr8 on the cytoplasmic tail of tetherin, which leads to recruitment of spleen tyrosine kinase (Syk) and ultimately assembly of a complex comprising TAK1 and as well as the TRAF2 and -6 signaling adapters (Galão et al., 2014 ; Figure 1.8). This mechanism is reminiscent of signaling through hemi-immunoreceptor tyrosine-based activation motifs (HemI-TAMs) found in C-type lectin receptors that is based on the association of two Yxx Φ motifs upon dimerisation of the receptor. Furthermore, Galão et al. (2014) reported that phosphorylation and thus NF- κ B activation is dependent on tetherin's association with the cortical actin cytoskeleton via RICH2. The authors could also show that a naturally occurring polymorphism (R19H) impairs binding to RICH2 and abolishes tetherin's signaling activity without affecting the retention of HIV-1 Δ vpu particles.

1.3.6 Modulation of the innate immune response

In 2009, tetherin was discovered to directly interact with a cell surface receptor of plasmacytoid dendritic cells (pDCs) called ILT7 (immunoglobulin-like transcript 7) (Rissoan et al., 2002; Cao et al., 2009). ILT7 is an immunomodulatory receptor that depends on its association with the γ chain of the high affinity Fc ϵ -receptor I (Fc ϵ RI γ) for signal transduction (Cao et al., 2006). Binding of tetherin to ILT7–Fc ϵ RI γ leads to a reduction in TLR-stimulated production of proinflammatory cytokines including type I IFN and

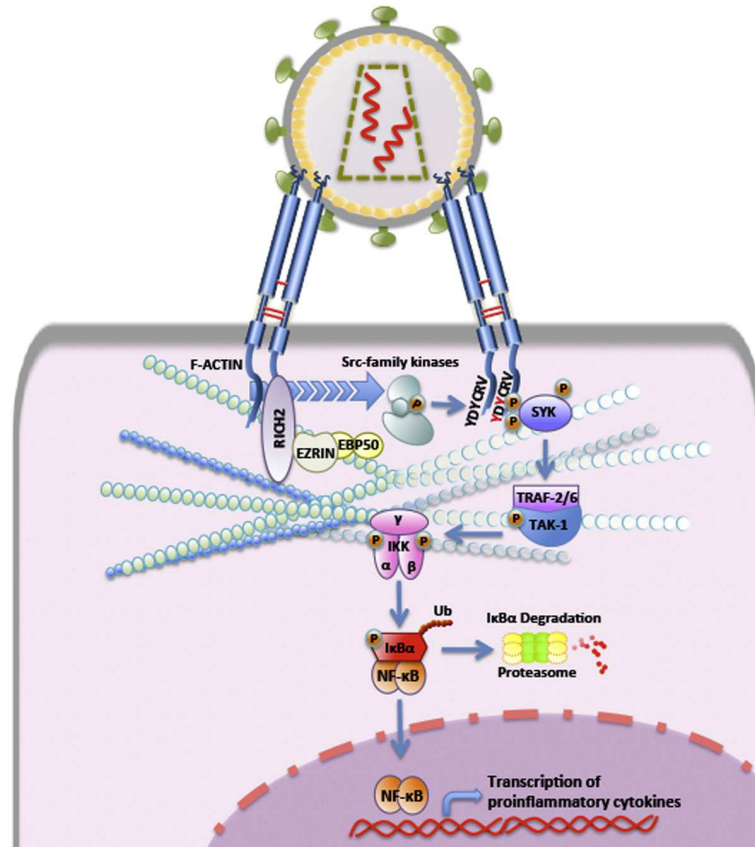


Figure 1.8 Signal transduction cascade triggered by tetherin upon sensing of HIV-1 assembly at the plasma membrane. *Reprinted from Arias and Evans (2014), by permission from Elsevier, copyright 2014.*

TNF α (Cao et al., 2006, 2009). Interestingly, the fact that expression of tetherin is itself stimulated by IFN has prompted many to interpret activation of ILT7 as a negative feedback mechanism of IFN production. The expression of tetherin on the surface of IFN-stimulated cells would thus allow pDCs to sense the extent of immune activation and modulate cytokine production to guarantee an optimal response.

As my doctoral thesis revolves around the interaction between tetherin and ILT7, I shall introduce the subject in more detail over the following pages.

1.4 ILT7 and the leukocyte Ig-like receptor family

Immunoglobulin-like transcript 7 (ILT7 ; also LILRA4, CD85g) is part of the leukocyte immunoglobulin-like receptor (LILR) family, which comprises 11 protein-coding genes as well as two pseudo-genes located on chromosome 19 (Young et al., 2001). The LILR genes belong to a chromosomal region referred to as the leukocyte receptor complex (LRC), which harbours a large range of immunoglobulin (Ig) superfamily genes, including killer Ig-like receptors (KIRs) expressed in natural killer (NK) cells, leukocyte-

associated Ig-like receptors (LAIRs) and sialic acid-binding Ig-like lectins (SIGLECs), to name but a few (reviewed in Barrow and Trowsdale, 2008).

LILRs are mostly expressed on myeloid cells such as granulocytes, macrophages and cDCs, but some members are also found on cells of the lymphoid lineage. Such is the case for instance of ILT2, which is expressed on B cells, NK cells and T cells as well as myeloid cells (reviewed in Brown et al., 2004). Interestingly, expression of ILT7 seems to be restricted to pDCs and was furthermore found to decrease upon maturation of pDCs (Rissoan et al., 2002; Ju et al., 2004; Cho et al., 2008; Tavano et al., 2013). This suggests that ILT7 expression is limited to circulating undifferentiated pDCs. Although LILR receptors vary little in their overall architecture, the diversity of molecules they recognise and the high degree of interplay are only starting to be elucidated. Here I will give a brief introduction to LILRs, while focusing primarily on ILT7.

Multiple nomenclatures for these proteins are currently in use, and most but not all LILRs carry alternative designations with non-matching indices. For example, LILRB1 is also known as ILT2, LIR-1 (leukocyte Ig-like receptor 1) and MIR-7 (monocyte Ig-like receptor). The LILR nomenclature is the only one to cover the entire gene cluster, and will thus be used in this document. To avoid confusion, I will however include the ILT designation where available, since it is used exclusively in some parts of the literature.

1.4.1 Topology, structure and signal transduction

The N-terminal extracellular region of all LILRs is composed of either two or four immunoglobulin(Ig)-like domains (termed D1–D4) that are anchored to the membrane by a single α -helix—with the notable exception of ILT6, which is soluble. The ectodomain amino acid sequences are highly conserved among LILRs and contain several potential N-linked glycosylation sites (Figure 1.11, p. 49). Based on their mode of signaling, LILRs can be divided into two sub-families (Figure 1.9). While subfamily ‘B’ receptors possess a long cytoplasmic tail featuring multiple immunoreceptor tyrosine-based inhibition motifs (ITIMs) and transduce signals directly, members of subfamily ‘A’ lack a cytoplasmic domain and associate with adapters to signal through immunoreceptor tyrosine-based activation motifs (ITAMs). Notably, subfamily ‘A’ receptors feature a conserved positively charged residue in their transmembrane region that mediates binding to signaling adapters. As briefly mentioned above, ILT7 associates with the γ chain of Fc ϵ -receptor I, which features an ITAM on its cytoplasmic domain but possesses no ligand-binding capabilities of its own, given its lack of an ectodomain.

The ILT7–Fc ϵ RI γ signaling cascade—in common with those of other ITAM-bearing receptors—is initiated when ligand-binding induces the phosphorylation of both ITAM tyrosines by Src-family kinases, which leads to the recruitment of Syk kinase via its Src homology 2 (SH2) domain (Cao et al., 2006). In turn, Syk causes the phosphorylation of downstream components which results in a considerable calcium influx into the

cell (Cao et al., 2006; Cho et al., 2008). The subsequent events in ILT7 signaling, as well as the factors causing interference with TLR-mediated activation of IFN transcription, remain still to be uncovered. It is worth mentioning that in some cases ITAM-mediated signaling involves ligand-induced clustering of multiple receptors (Brown et al., 2004). In addition, as part of the Fc receptor complex, the γ chain forms a disulfide-linked homodimer, which could hint at a possible dimerisation of ILT7, although no such observations have been made to date.

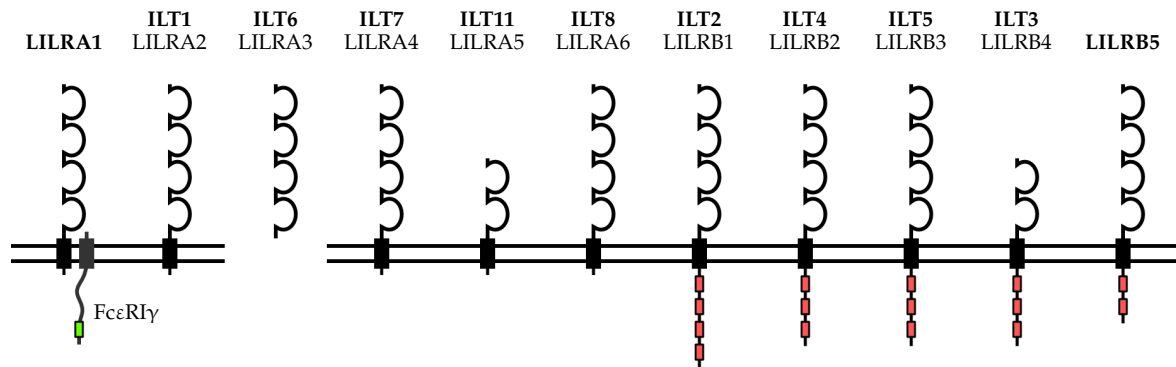


Figure 1.9 Overview of the leukocyte immunoglobulin-like receptor (LILR) family. Subfamily ‘A’ LILRs associate with immunoreceptor tyrosine-based activation motif (ITAM)-bearing adapters such as the γ chain of the high affinity Fc ϵ receptor whereas subfamily ‘B’ receptors feature multiple immunoreceptor tyrosine-based inhibition motifs (ITIMs) on their cytoplasmic tails. ITAM and ITIMs are represented by green and red boxes, respectively.

1.4.2 Functional activity and role in HIV-1 infection

LILRs primarily appear to regulate the activity of other immune receptors in a cell-type dependent manner. Several LILRs, including ILT1, ILT2, ILT4, ILT6 and LILRA1, recognise MHC class I complexes and are referred to as group I receptors. In particular, ILT2 and ILT4 have been shown to bind to multiple classical and non-classical human leukocyte antigens (HLAs), suggesting that the interaction is not allele-specific (Colonna et al., 1999; Shiroishi et al., 2003). This is corroborated by crystal structures of ILT2 and ILT4 in complex with soluble HLA-G and HLA-A2, respectively (Figure 1.10A), that reveal an interaction with the α 3 domain, and—in the case of ILT2—additionally with the β 2 microglobulin chain (Willcox et al., 2003; Shiroishi et al., 2006). Continuous crosslinking of ILT2 was shown to inhibit T cell receptor (TCR) activation in cytotoxic T cells and to induce regulatory T cells, thus promoting immunosuppression (Dietrich et al., 2001; Young et al., 2008). These studies further revealed that primary monocytes did not differentiate into DCs under ILT2 activation, and were unresponsive to TLR stimuli such as LPS (Young et al., 2008). Similar tolerogenic effects on DCs have been

observed for ILT3 and ILT4 in the context of organ transplantation, where upregulation of these receptors on donor APCs resulted in functional inactivation of helper T cells and was linked with increased allograft acceptance (Chang et al., 2002). Moreover, the interaction with ILT2/4 was shown to competitively inhibit binding to CD8, which could hint at a LILR-mediated mechanism of cytotoxic T cell inhibition beyond interference with antigen presentation and TLR signaling pathways (Shiroishi et al., 2003).

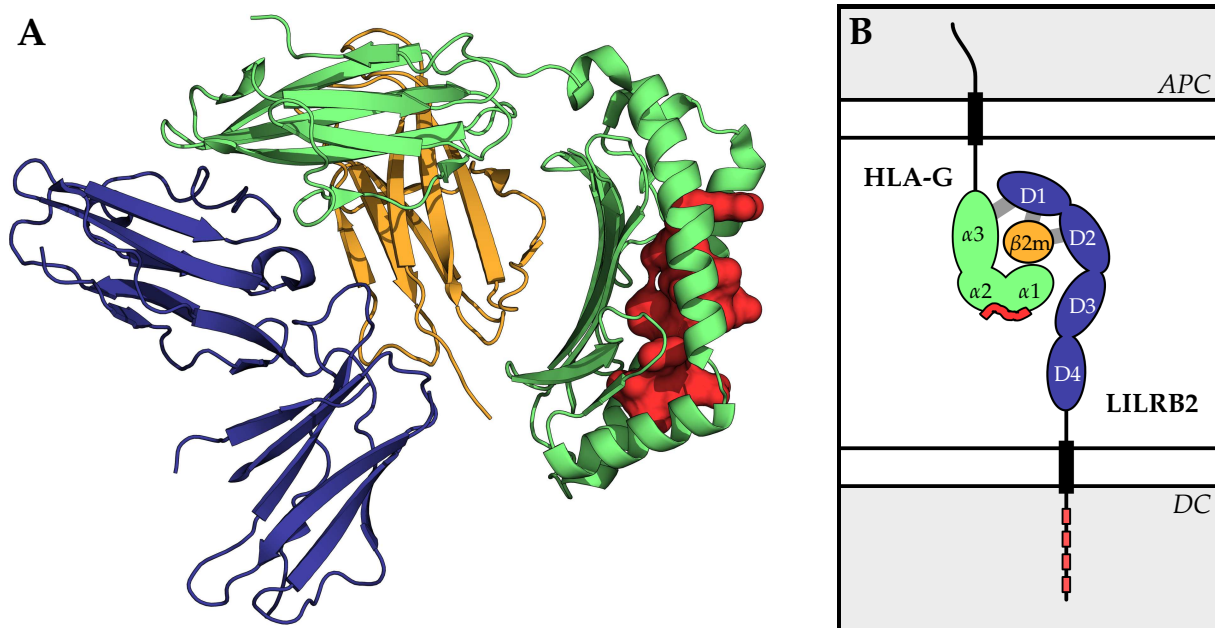


Figure 1.10 Structural basis of ILT4 binding to HLA-G. (A) Crystal structure (PDB 2DYP) of the two N-terminal ILT4 domains (D1–D2 ; blue) in complex with soluble HLA-G (green), β 2 microglobulin (β 2m ; orange) and an antigen-derived peptide (red). (B) Schematic representation of the interaction between an HLA complex and LILR expressed on an antigen-presenting (APC) or dendritic cell (DC), respectively. The proposed LILR configuration would allow for recognition of HLA allele-specific regions by membrane-proximal LILR domains. *Diagram inspired by Lichterfeld and Yu (2012).*

In the case of HIV-1, various HLA alleles have been linked to an accelerated progression to AIDS, and some indications suggest this to be partially caused by differences in LILR binding specificity and/or affinity (reviewed in Lichterfeld and Yu, 2012). A well characterised example concerns HLA-B*35 alleles, which can be divided into two subclasses based on their amino acid preference for a single position in the antigenic peptide (Gao et al., 2001). The more common ‘PY’ subtypes specifically bind peptides with a proline in position 2 and a tyrosine in position 9 and seem not to impact on disease progression. On the contrary, ‘Px’ subtypes, which are less restrictive for position 9, are invariably associated with accelerated progression to AIDS (Gao et al., 2001). Although initially attributed to a decreased induction of cytotoxic T cells, it has now been shown that the ‘Px’-associated effects are primarily caused by an en-

hanced binding to ILT4 expressed on DCs, resulting in impaired antigen-presenting and cytokine-producing activities (Gao et al., 2005; Huang et al., 2009). Interestingly, the 'PY' and 'Px' alleles compared by Huang et al. differ by a single amino acid and were tested with identical HIV-1-derived peptides. These results thus seem to contradict the broad specificity of HLA recognition by LILRs and—as proposed by Lichterfeld and Yu—could point to a possible involvement of the D3–D4 domains in binding to the more polymorphic $\alpha 1$ and $\alpha 2$ HLA regions (Figure 1.10B).

LILRs that share < 60% sequence similarity with ILT2/4 are attributed to group II, and do not seem to have conserved MHC-binding interfaces. However, ligands for all but one of these receptors have yet to be identified. Prior to the discovery of tetherin as a ligand, the role of ILT7 in suppressing type I IFN production in pDCs had already been established through antibody-crosslinking of the receptor. The principal PRRs expressed in pDCs are the endosomal TLR7 and -9, which sense pathogen-derived ssRNA and CpG-rich DNA, respectively. In the presence of ILT7 crosslinking, the stimulation of pDCs with either CpG-rich oligonucleotides or inactivate influenza virus results in a marked decrease of IFN α , IFN β and TNF α transcription (Cao et al., 2006). In a separate study, Cho et al. (2008) could confirm these results, but also made the observation that cytokine production *increased* upon CpG-stimulation if ILT7 was crosslinked with an antibody directed against a different epitope. However, in the absence of known ILT7 ligands, the physiological relevance of this contradicting effect could not be evaluated. In the search for a natural ligand, Cao et al. (2009) identified a number of cancer cell lines that could trigger ILT7–Fc ϵ RI γ signaling in a co-cultured reporter cell line. The most potent activators were breast carcinoma T47D cells, which were then used to generate hybridomas from immunised mice. After screening of hybridoma clones, two monoclonal antibodies were selected and matched against a human cDNA library. Both antibodies recognised two separate epitopes on cells transfected with tetherin cDNA. Recombinant tetherin was shown to co-precipitate with recombinant ILT7 ectodomain, and to inhibit IFN production in pDCs stimulated with inactivated influenza virus or CpG oligonucleotides as before. By surface plasmon resonance (SPR), both proteins were furthermore found to interact with micromolar affinity. Based on these results, the authors propose a model whereby tetherin-mediated activation of ILT7 constitutes a negative feedback mechanism of pDC activation, allowing for a finetuned production of proinflammatory cytokines.

However, the role of tetherin in such a regulatory mechanism was recently challenged. Tavano et al. (2013) employed human peripheral blood mononuclear cells (PBMCs) to study the effect of antibody-mediated inhibition of tetherin or ILT7 on IFN production. Briefly, the cells were stimulated with TLR9 substrate (CpG oligonucleotides) or HIV after preincubation with ILT7- or tetherin-specific antibody. As expected, crosslinking of ILT7 suppressed IFN production, whereas blocking tetherin to prevent ILT7 activation had no effects on IFN levels despite a marked upregula-

tion of tetherin expression in all PBMCs. Moreover, the same authors could show that crosslinking of ILT7 on pDCs inhibits the upregulation of the chemokine receptor CCR7 following TLR7/9 stimulation, without negatively affecting other APC markers (Tavano and Boasso, 2014). Since the expression of CCR7 on the cell surface of lymphocytes induces their migration to lymph nodes, these results suggest that ILT7 could regulate pDC tissue distribution upon maturation. In light of these observations, Tavano and Boasso hypothesise that rather than providing negative feedback regulation in the context of viral infection, the stimulation of ILT7 may constitute a homeostatic mechanism in immature circulating pDCs, capable of influencing their differentiation towards an APC phenotype.

All things considered, results on the interaction of tetherin with ILT7 are few and many questions remain to be addressed in order to decipher the role of the interaction in IFN regulation in more detail. More specifically, a deeper understanding of the interaction could be gained by elucidating its structural basis.

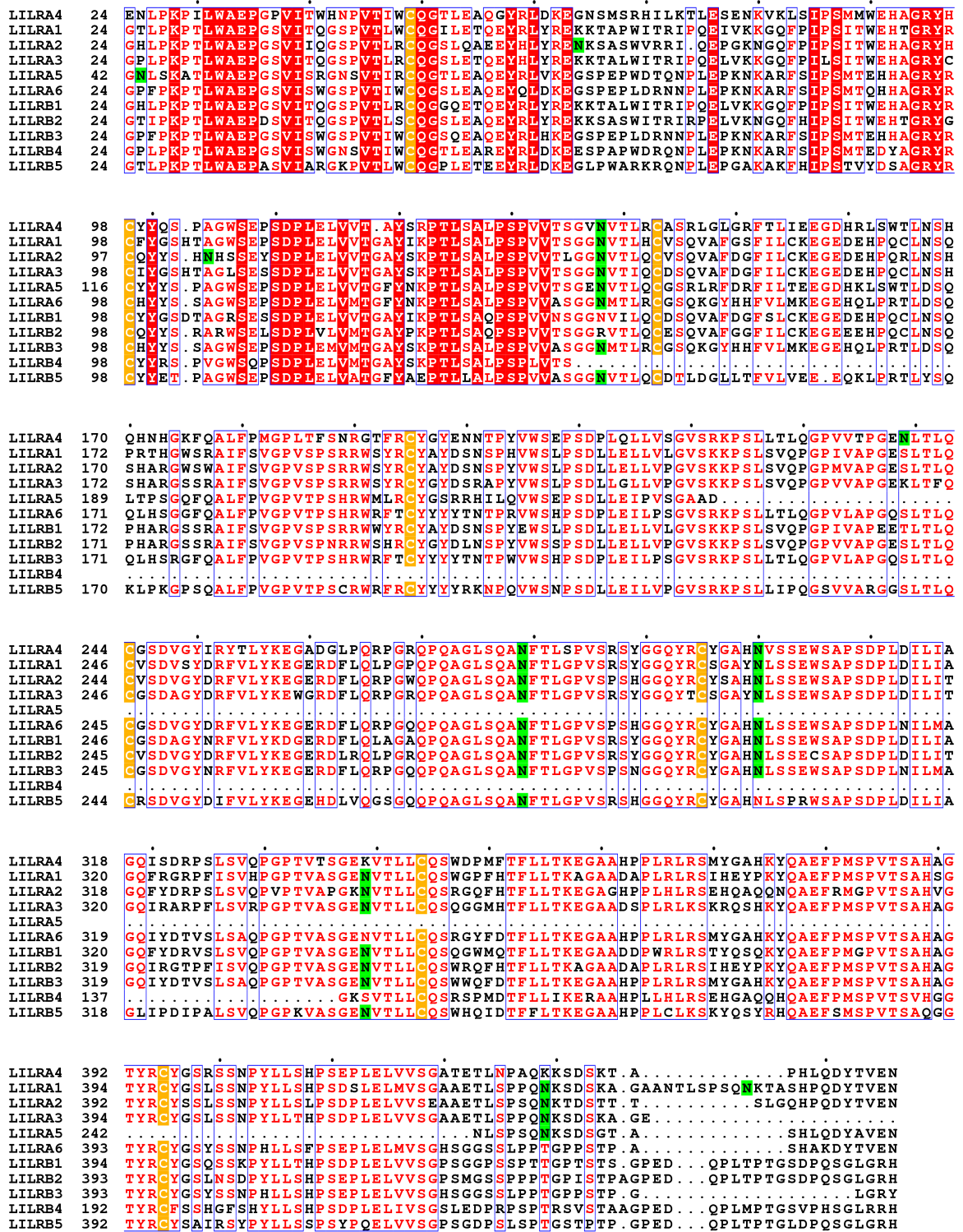


Figure 1.11 Multiple sequence alignment of human leukocyte Ig-like receptors (LILRs). Conserved disulfide-forming cysteines and predicted N-linked glycosylation sites are highlighted in orange and green, respectively.

Objectives

The principal objective of this thesis was to elucidate the structural details underlying the interaction of tetherin with the immunomodulatory receptor ILT7 (Ig-like transcript 7). As the production of the tetherin ectodomain had been previously established, the major focus of this project was the recombinant expression and purification of the ILT7 ectodomain. In order to determine optimal conditions for complex formation, the interaction between both proteins had to be characterised using various biophysical and biochemical techniques. Due to substantial difficulties encountered in the production of the entire ILT7 ectodomain, the crystallisation and functional characterisation of the N-terminal Ig-like domain alone became a major objective of this thesis.

A secondary aim was to investigate the possible oligomerisation of tetherin at HIV-1 budding sites. Indeed, since a small number of tetherin molecules are incorporated into budding HIV-1 particles despite interference of the viral antagonist Vpu, we hypothesised that a critical local concentration rather than the mere presence of tetherin is required for efficient restriction. The antiviral activity of tetherin might thus depend on self-organisation of homodimers into higher-order assemblies. We proposed to test this hypothesis by labeling cell surface-expressed tetherin with the small fluorescent molecules FLAsH/ReAsH and measuring the interaction between adjacent homodimers by combined fluorescence resonance energy transfer (FRET) and total internal reflection (TIRF) microscopy.

2

Methods

2.1 Bioinformatics

A number of public web-based programs and databases were utilised in this work and, where available, the appropriate scientific publications are cited. In addition, the associated unified resource locator (URL), software version and/or date of access are given in each case. For increased readability, this information is reproduced separately in Table 2.1 (page 55).

2.1.1 Multiple sequence alignment and phylogenetics

Protein sequences of tetherin orthologues and members of the leukocyte Ig-like receptor (LILR) family were retrieved from the UniProtKB database and aligned using the T-Coffee web service (Notredame et al., 2000) with default parameters. Multiple sequence alignments were formatted using the TeXshade package (Beitz, 2000). UniProt accession numbers for sequences of tetherin orthologues shown on page 32 are: Q10589 (human), D7RVC2 (chimpanzee), D2JNR5 (gorilla), D3GCW0 (orangutan), C3W5K8 (rhesus macaque), F8R0X8 (cat), Q8R2Q8 (mouse), Q811A2 (rat), C4NF76 (pig) and W8E3X2 (horse). Accession numbers for human LILRs shown on page 49 are: 075019 (LILRA1), Q8N149 (ILT1/A2), Q8N6C8 (ILT6/A3), P59901 (ILT7/A4), A6NI73 (ILT11/A5), Q6PI73 (ILT8/A6), Q8NHL6 (ILT2/B1), Q8N423 (ILT4/B2), 075022 (ILT5/B3), Q8NHJ6 (ILT3/B4) and 075023 (B5).

For the phylogenetic analysis of individual LILR Ig-like domains, protein sequences were obtained from a protein–protein BLAST (Basic Local Alignment Search Tool) search by querying the ILT7 D1-domain sequence against the UniProtKB/SwissProt database. The sequences were aligned with the Clustal Omega web service (Sievers et al., 2011), which also produces a phylogenetic tree in Newick syntax. Cladograms were rendered using the TreeVector tool.

2.1.2 Domain, structure and disorder prediction

In order to identify conserved domains and their boundaries, the ILT7 sequence was queried against the Pfam and CATH databases (Finn et al., 2014; Sillitoe et al., 2013). The domain boundaries were taken as the extremities of the hidden Markov model (HMM) alignment produced by Pfam. The presence and location of a transmembrane domain was predicted using the Tmpred server (Hofmann and Stoffel, 1993), which compares a query sequence against a large database of known transmembrane proteins, as well as the Phobius server based on HMMs that differentiate between signal peptide and transmembrane sequences (Käll et al., 2004).

Prediction of ILT7 secondary structure and disordered regions was performed using the Psipred and Disopred programs, respectively (Buchan et al., 2013). Psipred produces a three-class prediction (helix, strand and loop), using a neural network trained on evolutionary related sequence profiles obtained from PSI-BLAST (Position-Specific Iterated BLAST), with an ~80 % accuracy (Jones, 1999). Disopred is a neural network-based algorithm trained on disordered residues missing from crystal structures and achieved a precision of ~75 % in the latest CASP (Critical Assessment of protein Structure Prediction) experiments (Jones and Cozzetto, 2014).

Tertiary structure prediction of the ILT7 ectodomain (residues 24–446) was performed using the RaptorX server, which utilises a template-based fold recognition algorithm (Källberg et al., 2012). RaptorX also predicts secondary structure, as well as disorder and solvent accessibility. In particular, secondary structure prediction is based on a conditional neural field-based algorithm that distinguishes all eight classes recognised by the DSSP algorithm by taking into account relationships between the secondary structure of adjacent residues (Wang et al., 2011).

2.1.3 Post-translational modifications and processing

As a type I transmembrane protein, ILT7 features an N-terminal signal peptide for targeting towards the secretory pathway. The position of the signal peptidase cleavage site was predicted using the SignalP server with default settings for eukaryotes with a TM region (Petersen et al., 2011). The presence of N- and O-linked glycosylation sites on the ILT7 ectodomain was predicted using the NetNGlyc and NetOGlyc servers, respectively (Gupta et al., 2004; Steentoft et al., 2013).

2.1.4 *Ab initio* protein–protein docking and interface characterisation

Protein–protein docking using the crystal structures of ILT7(D1) and tetherin(80–147), as well as the predicted tertiary structure of ILT7(D1-2), was performed using the ClusPro 2.0 server. For the docking *per se*, the server relies on the program PIPER, which

conducts rigid-body docking using a scoring function based on a pairwise interaction potential (Kozakov et al., 2006). The potential comprises weighted energy terms for the contribution of van der Waals force, electrostatics and desolvation. Based on the relative weights used in the docking step, four different classes of models are produced by the ClusPro server, namely balanced, electrostatic-favoured, hydrophobic-favoured and van der Waals/electrostatics-favoured. For each class, the top 1000 models are then clustered based on the root mean square deviation (RMSD) between the structures, with large clusters being more likely to include the “real” conformations. Finally, the algorithm generates a consensus model for each of the ten largest clusters per class. The docking solutions were analysed using the PISA program, which identifies residues that are part of the buried interface within the complex, and estimates the change in free solvation energy upon formation of the complex (Krissinel and Henrick, 2007).

Name	Version	URL
Databases		
PDB		http://www.rcsb.org/pdb/
UniProtKB		http://www.uniprot.org/
Bioinformatics software		
BLAST		http://blast.ncbi.nlm.nih.gov/
ClusPro	2.0	http://cluspro.bu.edu/
Clustal Omega	1.2.1	http://www.ebi.ac.uk/Tools/msa/clustalo/
DisEMBL	1.5	http://dis.embl.de/
Disopred	3	http://bioinf.cs.ucl.ac.uk/psipred/
FindMod		http://web.expasy.org/findmod/
GlycoMod		http://web.expasy.org/glycomod/
Mascot		http://www.matrixscience.com/
NetNGlyc		http://www.cbs.dtu.dk/services/NetNGlyc/
NetOGlyc		http://www.cbs.dtu.dk/services/NetOGlyc/
Phobius		http://phobius.sbc.su.se/
PISA		http://www.ebi.ac.uk/pdbe/pisa/
Psipred	3.2	http://bioinf.cs.ucl.ac.uk/psipred/
RaptorX		http://raptorx.uchicago.edu/
SignalP		http://www.cbs.dtu.dk/services/SignalP/
T-Coffee		http://www.t-coffee.org/
TeXshade		http://www.ctan.org/pkg/texshade
TMpred		http://embnet.vital-it.ch/software/TMPRED_form.html
TreeVector		http://supfam.cs.bris.ac.uk/TreeVector/
Crystallography software		
CCP4		http://www.ccp4.ac.uk/
MATTPROB		http://www.ruppweb.org/mattprob/
Phenix		http://www.phenix-online.org/
XDS		http://xds.mpimf-heidelberg.mpg.de/

Table 2.1 List of software and databases used in this work. Version numbers and/or access dates are indicated where relevant.

2.2 Molecular cloning and mutagenesis

All the DNA constructs referred to in this manuscript are summarised in Table 2.2 (page 58). In order to avoid confusion and increase readability, the different ILT7 expression constructs have been numbered #1–19.

2.2.1 Molecular cloning

Classic protocols were used for cloning all expression constructs. Briefly, the target DNA sequence was amplified by PCR using a high fidelity polymerase kit (KAPA Biosystems) according to the manufacturers' instructions. Oligonucleotide primers were order from Eurofins Genomics and were designed to contain appropriate restriction sites, stop codons, as well as any protein features such as affinity tags, epitope tags, protease cleavage sites and signal sequences. A list of all primer sequences used in this work is given in Appendix A. PCR products were purified, verified on agarose gel and double-digested with restriction enzymes (New England Biolabs [NEB]) for 3–5 h at 37 °C. Plasmid DNA was double-digested, followed by treatment with alkaline phosphatase (Promega) for 1 h at 37 °C. Both insert and vector DNA were then separated by agarose gel electrophoresis, extracted and purified. Insert and vector DNA were mixed at a 4:1 mass ratio, diluted in ligation buffer and supplemented with T4 ligase (NEB). After incubation at room temperature for 1–2 h, the ligation mix were transformed into competent *E. coli* TOP10 (Life Technologies) by heat shock for 2 min at 42 °C and diluted into pre-warmed medium. After growth for 1 h in the absence of antibiotics, the cells were collected by centrifugation and spread on agar plates containing appropriate antibiotics. The following day, multiple colonies were picked to inoculate small overnight cultures. Plasmid minipreps were performed using a kit (Qiagen) and following the manufacturer's protocol. Finally, plasmid clones were verified by restriction digestion and validated by DNA sequencing (Eurofins Genomics).

2.2.2 Site-directed mutagenesis

Site-directed mutagenesis was performed using overlap-extension PCR (OE-PCR) based on a pair of reverse-complementary oligonucleotides carrying the desired mutation(s). Two contiguous fragments were amplified in separate reactions each containing one of the mutated primers in addition to a flanking primer. The two PCR products were mixed at a 1:1 ratio and extended in a third reaction, the overlaps created during the first step serving as primers. Finally, the flanking primer pair was added during the last 10–15 cycles to further amplify the full-length mutated DNA fragment.

2.2.3 Bacmid cloning

All baculovirus-based protein expression was performed using the MultiBac system developed by the Berger group at EMBL Grenoble (Trowitzsch et al., 2010). In order to generate recombinant baculovirus, the gene of interest was first cloned into the transfer plasmid pFL using the regular protocol described above. In a second step, *E. coli* DH10 cells carrying the EMBacY bacmid (Figure 2.1) were transformed with the plasmid DNA by heat shock for 45 s at 42 °C and outgrown in lysogeny broth (LB) overnight at 37 °C in the absence of antibiotics. Positive clones, in which the target gene was successfully transferred into the bacmid by Tn7-based transposition, were then selected by blue-white screening. Briefly, transformed cells were serially diluted and spread out on agar plates containing 10 µg mL⁻¹ tetracycline, 10 µg mL⁻¹ gentamicin, 50 µg mL⁻¹ kanamycin and supplemented with 200 µg mL⁻¹ X-Gal and 1 mM isopropyl β-D-1-thiogalactopyranoside (IPTG). After 24–48 h, positive (white) colonies were streaked out on a fresh set of agar plates. From the second screening plates, positive clones were picked for standard plasmid minipreps. The purified bacmid DNA was precipitated in ethanol immediately prior to transfection of insect cells.

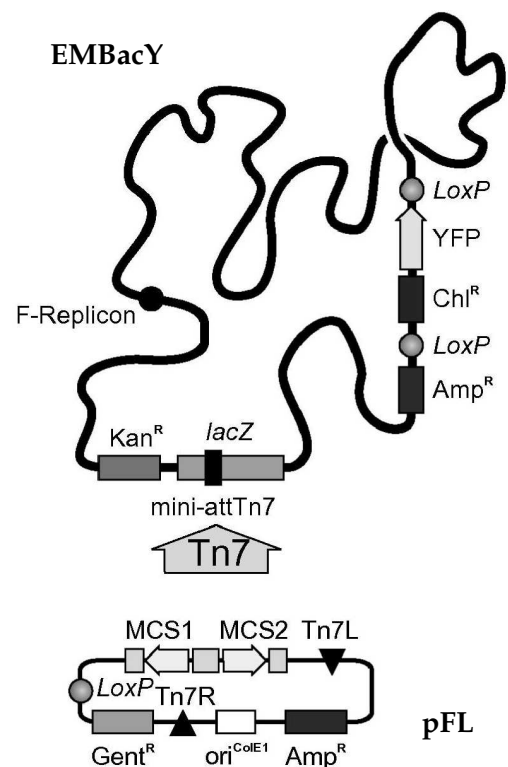


Figure 2.1 Map of the EMBacY bacmid and pFL transfer plasmid. The gene of interest is cloned into the transfer plasmid by conventional restriction/ligation cloning and transformed into DH10 cells carrying the bacmid. The transfer plasmid is then inserted into the bacmid by Tn7-based transposition. Transposases are encoded by a separate helper plasmid. *Modified from Trowitzsch et al. (2010), by permission from Elsevier, copyright 2010.*

Name	Features	Strain	Backbone	Res.	Opt. ¹	Cloning sites
Bacterial						
Tetherin(47–159)	6×His – TEV CS – Tetherin(47–159)	Rosetta™ 2	pETM11	Kan	N	NcoI, EcoRI
Tetherin(80–147)	6×His – TEV CS – Tetherin(80–147)	<i>id.</i>	pETM11	Kan	N	NcoI, EcoRI
GST-Tetherin	6×His – GST – TEV CS – Tetherin(47–159)	<i>id.</i>	pBADM30	Amp	N	NcoI, XhoI
ILT7#16	ILT7(24–118)	BL21 RIL	pET22b	Amp	Y	NdeI, XhoI
ILT7#17	ILT7(24–118) – 6×His	<i>id.</i>	pET22b	Amp	Y	NdeI, XhoI
ILT7#18	6×His – TEV CS – ILT7(24–118)	<i>id.</i>	pProEx-HTb	Amp	Y	NcoI, HindIII
ILT7#10	6×His – TEV CS – ILT7(17–223)	<i>id.</i>	pProEx-HTb	Amp	Y	NcoI, HindIII
ILT7#12	6×His – TEV CS – ILT7(17–223) ; I165C ; T175C	<i>id.</i>	pProEx-HTb	Amp	Y	NcoI, HindIII
ILT7#13	ILT7(24–219)	<i>id.</i>	pET22b	Amp	Y	NdeI, XhoI
ILT7#14	ILT7(24–219) – 6×His	<i>id.</i>	pET22b	Amp	Y	NdeI, XhoI
ILT7#15	ILT7(24–219) – 6×His ; I165C ; T175C	<i>id.</i>	pET22b	Amp	Y	NdeI, XhoI
ILT7#9	pelB SP – ILT7(24–223) – 6×His	<i>id.</i>	pMEK219	Amp	N	SfiI, EcoRI
ILT7#11	pelB SP – ILT7(24–223) – 6×His	<i>id.</i>	pMEK219	Amp	Y	SfiI, EcoRI
Baculovirus						
ILT7#7	Melittin SP – ILT7(24–223) – TEV CS – FLAG – 6×His	High Five™	pFL	Amp	N	EcoRI, XbaI
ILT7#8	Melittin SP – 10×His – TEV CS – ILT7(24–430)	<i>id.</i>	pFL	Amp	Y	EcoRI, XbaI
ILT7#19	Melittin SP – 10×His – TEV CS – ILT7(24–435)	Sf21	pFL	Amp	Y	EcoRI, XbaI
Mammalian						
Tetherin(wt)	Tetherin(1–161)	HEK293T	pcDNA3.1	Amp	N	NheI, BamHI
Tetherin-TC155	Tetherin(1–161) ; 155 <i>ins</i> (CCPGCC)	<i>id.</i>	pcDNA3.1	Amp	N	NheI, BamHI
Tetherin-FLN155	Tetherin(1–161) ; 155 <i>ins</i> (FLNCCPGCCMEP)	<i>id.</i>	pcDNA3.1	Amp	N	NheI, BamHI
ILT7#1	VWF SP – ILT7(24–430) – thrombin CS – 6×His	<i>id.</i>	pABC264	Amp	N	BamHI, NotI
ILT7#2	VWF SP – ILT7(24–223) – thrombin CS – 6×His	<i>id.</i>	pABC264	Amp	N	BamHI, NotI
ILT7#3	VWF SP – 6×His – TEV CS – ILT7(24–430)	<i>id.</i>	pABC345	Amp	N	BamHI, NotI
ILT7#4	VWF SP – 6×His – TEV CS – ILT7(24–223)	<i>id.</i>	pABC345	Amp	N	BamHI, NotI
ILT7#5	ILT7(1–223) – TEV CS – FLAG – 6×His	<i>id.</i>	pcDNA3.1	Amp	N	BamHI, XbaI
ILT7#6	ILT7(1–430) – TEV CS – FLAG – 6×His	<i>id.</i>	pcDNA3.1	Amp	N	BamHI, XbaI

Table 2.2 List of expression constructs. ¹DNA sequence was codon-optimised for *E. coli* or *S. frugiperda* respectively. *SP*: signal peptide, *CS*: protease cleavage site, *TEV*: tobacco etch virus, *pelB*: pectate lyase B, *VWF*: Von Willebrand factor.

2.3 Protein expression and purification

2.3.1 Preparation of tetherin ectodomain

Both the native and GST-fused tetherin ectodomain (residues 47–159) constructs were highly over-expressed in a soluble form. Expression plasmids were transformed into *E. coli* Rosetta2(DE3) cells (Novagen), from which starter cultures were grown in LB supplemented with 50 mg mL⁻¹ kanamycin and 34 mg mL⁻¹ chloramphenicol. For expression, cultures were grown in baffled conical flasks at 37 °C under agitation until the optical density at 600 nm wavelength (OD₆₀₀) reached 0.8. Protein expression was then induced by addition of IPTG to a final concentration of 1 mM and incubation was continued overnight at 18 °C.

Bacterial cells were collected by centrifugation for 20 min at 4500 × *g* and resuspended in lysis buffer (20 mM Tris, (100 mM NaCl, (10 mM imidazole, pH 7.5). The cells were lysed by sonication on ice and cleared by centrifugation for 45 min at 40000 × *g* (4 °C). Supernatants were carefully decanted, sterile filtered and loaded onto a nickel affinity column equilibrated in buffer A (20 mM Tris, 100 mM NaCl, 10 mM imidazole, pH 7.5). The column was washed extensively with buffers A, B (buffer A containing 1 M NaCl and 1 M KCl) and C (buffer A containing 50 mM imidazole). Finally, bound protein was eluted in 2 mL-fractions with buffer D (buffer A containing 300 mM imidazole).

If required, proteolytic removal of the affinity tag was initiated by adding 1 mM DTT, 0.5 mM EDTA and TEV protease at a mass ratio of 1:100 (protease:tetherin). After mixing, the sample was incubated for 1 h at room temperature, then transferred into dialysis tubing with a 10 kDa cut-off and dialysed against buffer E (20 mM Tris, 100 mM NaCl, pH 7.5) overnight at 4 °C. Digested tetherin was separated from undigested protein and TEV protease on a nickel affinity column equilibrated in buffer A, followed by concentration of the protein to 500 µL using spin concentrators with a 3.5 kDa molecular weight cut-off (MWCO ; Amicon).

The sample was further purified by size exclusion chromatography on a Superdex 75 column (GE Healthcare) using a fast liquid protein chromatography (FPLC) system (GE Healthcare) equilibrated in buffer F (20 mM HEPES, 100 mM NaCl, 5 mM EDTA, pH 7.5).

2.3.2 Bacterial expression of ILT7

Soluble cytoplasmic expression Immunoglobulin-like domains are generally not expressed in a soluble form in the bacterial cytoplasm due to the disulfide bond necessary for correct folding. The recombinant expression of ILT7 constructs comprising D1 (#17) or D1-2 (#14) was however attempted in the *E. coli* strains Origami(DE3) pLysS or *trx*⁻AD494(DE3) (Novagen) which lack components of the glutathione and thioredoxin

disulfide-reducing pathways. For expression trials, plasmid DNA was transformed into competent Origami B or AD494 cells and spread on agar plates. Single colonies were used to inoculate 5 mL LB containing $100 \mu\text{g mL}^{-1}$ ampicillin and $34 \mu\text{g mL}^{-1}$ kanamycin, and bacteria were grown at 37°C under agitation until $\text{OD}_{600} \sim 0.6$. Protein expression was induced with 1 mM IPTG (final) and incubation was continued for 3 h at 37°C or overnight at 20°C . Cells were collected by centrifugation for 10 min at $5000 \times g$, resuspended in 1 mL lysis buffer (50 mM Tris, 100 mM NaCl, pH 8) and lysed by sonication for 2 min on ice. The lysate was then cleared by centrifugation for 20 min at $20000 \times g$ to obtain the soluble fraction. Non-induced, total and soluble lysate fractions were then analysed for protein expression by SDS-PAGE.

Periplasmic expression ILT7 constructs featuring the *pelB* signal sequence for periplasmic localisation (#9 and #11) were transformed into competent *E. coli* BL21(DE3) RIL cells (Stratagene), from which pre-cultures were grown in LB containing $100 \mu\text{g mL}^{-1}$ ampicillin and $34 \mu\text{g mL}^{-1}$ chloramphenicol for 12–16 h at 37°C . Main cultures were grown to $\text{OD}_{500} \sim 0.8$ in 1 L flasks at 37°C . Protein expression was induced by addition of 1 mM IPTG (final) and incubation was continued overnight at 18°C . Cells were collected by centrifugation for 15 min at $5000 \times g$, resuspended in ice-cold 50 mL buffer A (25 mM Tris, 20 % sucrose, 1 mM EDTA, pH 7.5) and supplemented with 50 mg lysozyme. The cell suspension was incubated for 45 min at 4°C with slow stirring, then cleared by centrifugation for 15 min at $5000 \times g$. The supernatant was diluted two-fold with buffer B (25 mM Tris, 100 mM NaCl, pH 7.5) and loaded on a nickel-affinity column equilibrated with buffer B. After washing the column successively with buffer B containing 10, 30, 50 and 70 mM imidazole, bound protein was eluted in 2 mL-fractions using buffer B containing 250 mM imidazole. Protein expression and purification were assessed by Coomassie-stained SDS-PAGE and anti-His-tag Western blot.

Inclusion body expression A range of ILT7 constructs (#10 and #12–18) were expressed in bacterial inclusion bodies to be subsequently refolded *in vitro*. Cultures were prepared as above and protein expression was induced at $\text{OD}_{600} \sim 0.6$ with 1 mM IPTG for 3 h at 37°C . Cells were collected by centrifugation for 20 min at $5000 \times g$ and lysed by sonication in extraction buffer (50 mM Tris, 50 mM EDTA, 10 mM DTT, 1 % Triton X-100, pH 8). The insoluble inclusion body fraction was collected by centrifugation of the cell lysate for 30 min at $15000 \times g$. In order to solubilise and remove cell debris, pellets were resuspended in 10 mL extraction buffer using a Potter homogeniser. After incubation on a rotator for 1 h at room temperature, the suspension was centrifuged for 30 min at $15000 \times g$. This step was repeated with extraction buffer containing 1 M NaCl and finally with extraction buffer without Triton X-100. Inclusion bodies were divided into 2 mL-aliqouts and centrifuged. After discarding the supernatants, the pellets were stored at -20°C .

Prior to refolding, inclusion body pellets were thawed at room temperature, re-suspended in 1 mL 8 M guanidium chloride (GndCl) and incubated 1 h in a 37 °C-waterbath. The solution of denatured protein was diluted to 2 mL with 8 M GndCl, thoroughly vortexed, then cleared by centrifugation for 30 min at $20000 \times g$ ($> 10^\circ\text{C}$). Supernatants containing solubilised inclusion body protein were carefully transferred into a fresh tube and used on the same day. In the case of His-tagged ILT7 constructs, the extracted protein was purified by nickel affinity chromatography under denaturing conditions. Briefly, the column was equilibrated in buffer A (100 mM NaH_2PO_4 , 10 mM Tris, 8 M urea, pH 8). After loading the denatured protein sample, the column was washed with buffers A and B (100 mM NaH_2PO_4 , 10 mM Tris, 8 M urea, pH 6.3). Bound protein was eluted with buffer C (100 mM NaH_2PO_4 , 10 mM Tris, 8 M urea, pH 4.5) in 2 mL-fractions. Urea-containing buffers were prepared freshly to prevent carbamylation of primary amines.

***In vitro* refolding and purification of ILT7** For *in vitro* refolding, denatured ILT7 was first prepared as described above. The denatured protein was then rapidly diluted to a final concentration of 1–2 μM by dropwise addition into a large volume of refolding buffer (50 mM Tris, 400 mM L-arginine, 100 mM NaCl, 5 mM reduced glutathione [GSH], 0.5 mM oxidised glutathione [GSSG], pH 8). Incubation was continued overnight at 4 °C under slow stirring. The refolding solution was concentrated to ~ 50 mL in a stirred cell (Amicon) using a 10 kDa MWCO membrane (Sartorius) and cleared by centrifugation for 30 min at $40000 \times g$. The sample was dialysed against buffer A (50 mM Tris, 100 mM NaCl, pH 8) overnight at 4 °C, and cleared by centrifugation as before. In the case of the N-terminally tagged construct, removal of the affinity tag was performed by adding TEV protease at a mass ratio of 1:100 (protease:ILT7), 1 mM DTT and 0.5 mM EDTA, followed by incubation for 3 h at room temperature. The sample was passed on a nickel affinity column equilibrated with buffer A containing 10 mM imidazole. The flow-through fraction, containing cleaved ILT7, was concentrated to 500 μL using spin concentrators with a 3.5 kDa MWCO (Amicon) and loaded onto a Superdex 75 size exclusion chromatography column equilibrated in buffer B (20 mM Tris, 100 mM NaCl, pH 8).

It is worth noting that this protocol promotes disulfide bond formation through several factors, namely (i) a favourable pH for thiol deprotonation ($pK_a \sim 8.3$) on cysteines, (ii) a low concentration and thus a reduced risk of inter-chain crosslinking and (iii) the presence of glutathione redox partners to facilitate disulfide shuffling as illustrated in Figure 2.2.

2.3.3 Insect cell expression of ILT7

Insect cell expression was carried out at the Eukaryotic Expression Facility (EEF) at the EMBL Grenoble. Suspension cultures were grown in conical flasks under agitation at a

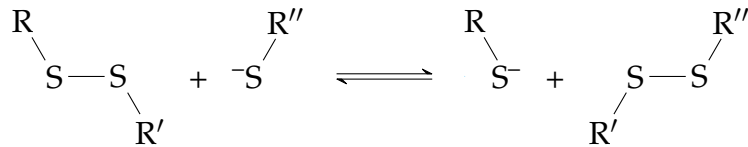


Figure 2.2 Diagram showing disulfide bond shuffling between the thiol groups of three cysteine residues, R, R' and R''. The cysteines may be part of the same protein chain, different protein chains, or glutathione molecules. This illustrates how the likelihood of aberrant disulfide formation can be decreased by adding glutathione redox partners to the refolding solution.

controlled room temperature of 27 °C and passaged 3–4 times per week. Two different insect cell lines were used, namely Sf21 and High Five™ cells (Life Technologies), derived from *Spodoptera frugiperda* and *Trichopulsia ni*, respectively. Sf21 cells were maintained at a cell density of $0.5\text{--}2 \times 10^6$ cells/mL in Sf-900 II serum-free medium (Life Technologies) without supplements. High Five cells were maintained at a cell density of $0.5\text{--}1 \times 10^6$ cells/mL in Express Five® medium (Life Technologies) supplemented with 16 mM L-glutamine.

Baculovirus production For the production of first generation (V_0) baculovirus, Sf21 cells were seeded into six-well plates at a density of $0.5\text{--}1.0 \times 10^6$ cells per well and left to settle for 15 min. The ethanol-precipitated bacmid DNA was air-dried, resuspended in 20 μ L sterile H₂O and diluted with 200 μ L cell culture medium. In parallel, 10 μ L Fugene HD transfection reagent (Promega) was diluted in 200 μ L medium and added to the DNA suspension. Per bacmid clone, 150 μ L of the transfection mixture was then added to each of two wells. After 48 h, the supernatants were removed, pooling duplicates to obtain ± 6 mL V_0 virus per clone. In order to assess protein expression, the cells were covered with fresh medium and incubated for 48 h. Culture supernatant and cell lysates were then analysed by anti-His-tag Western blot. For virus amplification, 25 mL Sf21 cell culture at 5×10^5 cells/mL were infected with 3 mL V_0 and counted at 24 h intervals. If necessary, the cultures were diluted with medium to maintain cell density at or below 1.0×10^6 cells/mL. Following cell proliferation arrest incubation was continued for 48 h, after which the cultures were cleared by centrifugation for 3 min at $800 \times g$. Supernatants containing the V_1 virus stock were transferred into sterile tubes and stored at 4 °C.

Small-scale expression Prior to large-scale expression for protein production, the optimal viral dose and duration of expression were determined by infecting multiple 25 mL cultures (5×10^5 cells/mL) with different titres of V_1 . Typically 0.1, 0.2, 0.5 and 1 mL of V_1 were used per flask. As for virus amplification, cells were counted every 24 h and samples were removed for analysis by SDS-PAGE or Western blot. The optimal viral dose was determined as the volume causing proliferation arrest after a single

cell doubling or one day in the case of Sf21 cells.

Large-scale expression and purification For large-scale expression, Sf21 or High Five cells were expanded into multiple 500 mL cultures and infected with V_1 at a density of 1×10^6 cells/mL. Incubation was continued for 72–96 h at 27 °C. Since all ILT7 constructs comprised a signal sequence, secreted protein had to be purified from culture supernatants. After clearing the cultures by centrifugation for 30 min at $330 \times g$, the supernatants were dialysed for 12–16 h against buffer A (20 mM Tris, 150 mM NaCl, pH 7.2) at room temperature with 2–3 changes of the dialysis bath. The dialysed sample was concentrated two-fold in a stirred cell with a 10 kDa MWCO membrane and filtered using a bottle-top vacuum filter. The protein was then loaded onto a nickel affinity column equilibrated with buffer B (20 mM Tris, 150 mM NaCl, 10 mM imidazole, pH 7.2) and washed successively with buffer B containing 30, 50 and 70 mM imidazole. The bound protein fraction was eluted in 2 mL-fractions with buffer B containing 300 mM imidazole and analysed by Coomassie-stained SDS-PAGE and anti-His-tag Western blot. The peak fractions were pooled, extensively dialysed against buffer C (20 mM Tris, 150 mM NaCl, 10 % glycerol, pH 7.2) at room temperature and concentrated ten-fold in a 10 kDa MWCO spin concentrator. Samples were subjected to analytical size exclusion chromatography on a Superdex 200 column (GE Healthcare) and analysed by Coomassie-stained SDS-PAGE and Western blot.

2.3.4 Mammalian expression of ILT7

Mammalian protein expression was carried out in the HEK 293T cell line derived from human embryonic kidney cells and expressing the Simian Vacuolating Virus 40 (SV40) large T-antigen. The presence of the T-antigen allows for episomal replication of plasmids encoding the SV40 origin of replication and consequently results in increased protein expression. Adherent HEK 293T cells were maintained in Dulbecco's modified Eagle's medium (DMEM) supplemented with PenStrep (Gibco) and 10 % foetal bovine serum (FBS). Cells were incubated in a CO₂ incubator at 37 °C and passaged twice weekly using TrypLE Express (Gibco) for detachment. At 10–16 h prior to transfection, confluent cells were resuspended and seeded into six-well plates at a density of $4\text{--}5 \times 10^5$ cells per well. For transient transfection, 3–5 µg DNA was diluted in DMEM to a final volume of 100 µL and augmented with 4.5–7.5 µL Fugene HD (Roche) transfection reagent. After replacing the culture medium with fresh minimal DMEM, the transfection mixture was added dropwise to each well. The medium was changed to complete DMEM containing 3 % FBS after 24 h and protein expression was assayed by Western blot after 24–72 h. Transfection-grade plasmid DNA was prepared using endotoxin-free kits (Qiagen).

2.4 Biochemical and biophysical characterisation

2.4.1 Fluorescent labeling

Fluorescent labeling of recombinant ILT7 and tetherin was necessary for microscale thermophoresis (MST ; see below) as well as flow cytometry-based experiments. In both cases, succinimidyl esters of Alexa Fluor® (Life Technologies) dyes were used to label primary amines on the target protein. In a first step, the sample buffer was exchanged to labeling buffer (100 mM NaHCO₃, 100 mM NaCl, pH 8.3) by size exclusion chromatography on a Superdex 75 column. The reactive dye was dissolved in anhydrous dimethylsulfoxide (DMSO) to a concentration of 10 mg mL⁻¹ and added to the protein sample at a 5-fold molar excess. The sample was incubated for 1 h on a rotator in the dark, and cleared by centrifugation for 15 min at 20000 × g. The sample was then purified on a Superdex 75 size exclusion column in Tris buffer (20 mM Tris, 100 mM NaCl, pH 8) which stopped the labeling reaction and removed unreacted dye. In order to calculate the degree of labeling, the protein absorbance was first corrected for contribution of the dye at the 280 nm wavelength:

$$A_{\text{corr}} = A_{280} - A_{\text{dye}} \times CF$$

where A_{dye} is the absorbance of the dye at its excitation maximum (λ_{dye}) and CF is a correction factor. The degree of labeling then equals:

$$\text{degree of labeling} = \frac{A_{\text{dye}} \times \epsilon_{\text{prot}}}{A_{\text{prot}} \times \epsilon_{\text{dye}}}$$

The parameter values used in the calculation are:

	AF488	AF633	AF647
λ_{dye} (nm)	495	632	650
ϵ_{dye} (cm ⁻¹ M ⁻¹)	71000	100000	239000
CF	0.11	0.55	0.03

2.4.2 Peptide mass fingerprinting

For validation purposes, the identification of recombinantly expressed protein was done by peptide mass fingerprinting performed at the mass spectrometry platform of the Institut de Biologie Structurale (IBS, Grenoble). Bands of interest were excised from Coomassie-stained SDS-PAGE gels after extensive rinsing with HPLC-grade water and cut into ~1 mm³ pieces. The samples were then sequentially washed for 30 min with 50 µL buffer alone (25 mM sodium bicarbonate pH 8), 2×30 min with buffer containing 50 % acetonitrile and finally for 5 min with 100 % acetonitrile. Cysteines were

then reduced with buffer containing 25 mM DTT for 30 min at 56 °C, and alkylated with buffer supplemented with 20 mM iodoacetamide for 45 min in the dark. Wash steps were repeated as above. Trypsin was diluted to 19 $\mu\text{g mL}^{-1}$ in buffer and added to the gel pieces for overnight digestion at 37 °C. After the peptide-containing liquid was transferred to a fresh tube, the gel pieces were washed for 2 \times 20 min with a 5 % acetonitrile/0.1 % TFA solution, 2 \times 20 min with 50 % acetonitrile/0.1 % TFA, and finally 5 min with 100 % acetonitrile. Each 50 μL -wash fraction was added to the peptide solution, which was then concentrated to \sim 10 μL using a SpeedVac centrifugal evaporator (Savant). Finally, the sample was applied to a reverse-phase C18 desalting spin tip (Pierce) and eluted directly onto the target using 2 μL of the matrix (10 mg mL^{-1} α -cyano-4-hydroxycinnamic acid in 50 % acetonitrile, 0.1 % TFA). Analysis was performed on a MALDI-TOF mass spectrometer (Autoflex, Bruker Daltonics) operated in reflectron-positive mode.

The list of peptide masses was queried against the SwissProt database using the Mascot search engine (Matrix Science), allowing for one missed cleavage site. Acceptable amino acid modifications were methionine oxidation and cysteine carbamidomethylation, the latter resulting from iodoacetamide treatment. In addition, because of the suspected presence of N-linked glycans, the unmatched peptide masses were analysed with the GlycoMod tool (Cooper et al., 2001). As insect cells produce high mannose-type N-glycans only, sialic acids were excluded from the search. Possible post-translational modifications were also identified using the FindMod tool (Wilkins et al., 1999). All mass values cited in the text refer to monoisotopic and mono-protonated (MH^+) peptide masses.

2.4.3 Surface plasmon resonance

All surface plasmon resonance (SPR) experiments were performed on a Biacore 3000 system (GE Healthcare) using CM5 dextran-coated sensor chips (GE Healthcare). Ligands of interest were either immobilised directly by amine-coupling, or indirectly through capture by covalently attached antibodies or streptavidin. The running buffer used in all experiments (HBS-PE) was composed of 10 mM HEPES pH 7.5, 150 mM NaCl, 3 mM EDTA and 0.005 % Surfactant P20. Covalent attachment of proteins by amine-coupling was carried out according to the kit manufacturer's instructions (GE Healthcare). Briefly, both reference (FcR) and sample (FcS) flow cells were activated with a freshly prepared 1:1 mixture of EDC (1-ethyl-3-[3-dimethylaminopropyl]carbodiimide hydrochloride) and NHS (N-hydroxysuccinimide) for 10 min at a flow rate of 5 $\mu\text{L min}^{-1}$. The sample to be immobilised was diluted in sodium acetate buffer and applied to the flow cell in short increments until the desired response level was reached. Both flow cells were then deactivated by a 10 min-injection of 1 M ethanolamine (pH 8.5). The amount of immobilised ligand was recorded as the difference between initial and final

response (R_{ligand}), and was empirically targeted to be 2500–5000 response units (RUs). Analyte samples were dialysed against running buffer and cleared by centrifugation at $20000 \times g$ for 20 min (4 °C). A serial dilution was then performed into running buffer, and individual sample concentrations measured on a NanoVue spectrophotometer (GE Healthcare). After equilibration of the sensor surface and stabilisation of the baseline response, analyte was injected using the 'KInject' mode with contact and dissociation times individually determined for each experiment. Relative response data was obtained by subtracting FcR from the FcS response. Sensorgrams were processed using BIAevaluation software (GE Healthcare).

Analysis of ILT7(D1-4) binding to GST-tetherin Purified GST-Tetherin (5.8 mg mL^{-1}) was diluted 1000-fold in 50 mM sodium acetate pH 4 for amine coupling. The protein was applied to the activated FcS for 5 min, resulting in an $R_{\text{ligand}} = 4900 \text{ RU}$ after deactivation. FcR was activated and deactivated to produce a signal corresponding to the non-specific interaction of analyte with the dextran matrix.

Nickel-affinity purified ILT7 (construct #19) was serially diluted from a $5.6 \mu\text{M}$ stock solution to yield samples at 2.8, 1.4, 0.7, 0.35 and $0.175 \mu\text{M}$. One sample was concentrated to $9.6 \mu\text{M}$ in a 3.5 kDa MWCO spin concentrator. The three highest analyte concentrations were used to record a first sensorgram at a flow rate of $10 \mu\text{L min}^{-1}$ with 3 min contact time and allowing for a 3 min dissociation phase per injection. The surface was regenerated by applying 10 mM HCl for 1 min. A second sensorgram was recorded with a 90 s contact time, 3 min dissociation phase, and identical flow rate and regeneration conditions. Only concentrations of $2.8 \mu\text{M}$ and below were tested in the second experiment. As a control experiment, purified GST was immobilised in a separate flow cell ($R_{\text{ligand}} = 3900 \text{ RU}$) and ILT7 samples at $0.35\text{--}2.8 \mu\text{M}$ were injected under identical experimental conditions. In order for the responses caused by non-specific binding of ILT7 to GST to be comparable between experiment and control surfaces, the amount of immobilised GST needed to be equal to that of GST-tetherin. Assuming the same rate of attachment, the theoretical R_{ligand} to achieve for GST was calculated as follows:

$$\begin{aligned} R_{\text{ligand}}(\text{GST}) &= R_{\text{ligand}}(\text{GST-tetherin}) \times \frac{M_r(\text{GST})}{M_r(\text{GST-tetherin})} \\ &= 4900 \times \frac{28860}{41832} \\ &= 3381 \text{ RU} \end{aligned}$$

We can thus expect that interaction of ILT7 with GST on the control or experimental surfaces would result in a similar response, although a quantitative evaluation of the contribution to the response is not possible.

Analysis of tetherin binding to ILT7(D1) In a first experiment, purified tetherin(47–159) was immobilised on a CM5 sensor surface by amine coupling as described above, resulting in an $R_{\text{ligand}} = 1306$ RU after deactivation. Purified ILT7#17 was diluted to 4 and 40 μM in HBS-PE and applied to the sensor surface for 7 min at a flow rate of 10 $\mu\text{L min}^{-1}$. Alternatively, ILT7 was immobilised by amine coupling on a separate sensor chip ($R_{\text{ligand}} = 1250$ RU) and tetherin was injected at concentrations of 1.2, 40 and 120 μM for 5 min at a flow rate of 10 $\mu\text{L min}^{-1}$.

2.4.4 Isothermal titration calorimetry

For ITC measurements, ILT7(D1) and tetherin(47–159) were purified as before, extensively dialysed against sample buffer (20 mM Tris, 100 mM NaCl, 5 mM EDTA, pH 8) and degassed under vacuum. The experiment was performed on a VP-ITC system (MicroCal) at 26 °C by injecting 12 μL aliquots of tetherin (555 μM) into a cell containing 1.4 mL of ILT7 at a concentration of 32 μM . The data were corrected for the heat of dilution and analysed using Origin software (MicroCal).

2.4.5 Microscale thermophoresis

The interaction of ILT7(D1) with tetherin(47–159) was measured by microscale thermophoresis (MST) using a Monolith NT.115 instrument (NanoTemper) with blue and red detection channels. MST is based on the Soret effect, which derives from the differential diffusion of different molecules in a mixture along a temperature gradient. In an MST experiment, large particles typically diffuse from a hot to a cold zone, while smaller particles display the opposite effect. However, the thermophoretic behaviour is affected by factors other than size and is therefore not entirely predictable. The method as applied here requires one of the interaction partner to be fluorescently labeled and kept at constant concentration. A measurement consists in recording the change in fluorescence while a temperature gradient is applied to the sample using an infrared laser diode. The relative fluorescence signal thus represents the degree of thermophoresis taking place in the sample. A dataset in turn is provided by a titration series of reaction mixtures that have been allowed to reach equilibrium. Finally, a kinetic model can be fitted to the data points linking concentration of the titrant to relative fluorescence.

ILT7(D1) was fluorescently labeled with NT647 and its concentration adjusted to 200 nM. A two-fold serial dilution of tetherin in sample buffer (20 mM Tris, 100 mM NaCl, 5 mM EDTA, pH 8) was prepared in PCR strip tubes and ILT7 was added to result in a final concentration of 100 nM. LED power was set at 80 % to achieve optimal fluorescence counts (800–1000) and standard treated capillaries were chosen for the experiment as no difference could be observed with hydrophilic or hydrophobic coating. In a first experiment, the optimal laser power was determined by acquiring one data series each at 20, 40 and 80 % settings with tetherin concentrations of 1.53–50 000 nM

and ~15 min equilibration time before the start of the experiment. In a second experiment, triplicate readings were acquired at 80 % laser power after an equilibration time of ~2.5 h. In the third experiment, tetherin was used at a higher concentration range of 6.1–200 000 nM, with otherwise identical experimental parameters.

2.5 Protein crystallography

This section summarises the general protocols used for the crystallisation, X-ray diffraction and structure solution of ILT7. The experimental procedures leading to the crystal structure of the ILT7#19 construct are outlined in more detail. The web addresses and version numbers of crystallographic software mentioned below can be found in Table 2.1 on page 55.

2.5.1 Crystallisation and data collection

High throughput screening Initial crystallisation screening was performed at the high-throughput crystallisation (HTX) platform of the European Molecular Biology Laboratory (EMBL, Grenoble). Crystallisation drops containing 100 nL sample and 100 nL precipitant were set up in a sitting drop vapour diffusion format in an imaging robot (RockImager, Formulatrix) at 20 °C. Screens comprised a range of commercially available sparse matrix and grid screens by manufacturers Qiagen and Hampton Research. Screening of ILT7#19 at a concentration of 7.5 mg mL⁻¹ produced trapezoidal prism-shaped crystals in conditions containing 100 mM MES pH 6 and 30 % (w/v) PEG-6000. Spherulites and large clustered crystals were obtained under numerous other conditions.

Hanging drop vapour diffusion Positive hits from the HTX screen were reproduced and refined by hand in hanging drop vapour diffusion plates. Briefly, 500 µL reservoir solutions were individually prepared within the plates from freshly made stock solutions. Drops were set on siliconised glass coverslips by adding 1–3 µL protein sample to 1 µL reservoir solution. Plates were stored at 20 °C and inspected regularly on a stereo microscope. The best crystals of ILT#19 were obtained under conditions containing 30 % (w/v) PEG-6000 and 8 % (v/v) glycerol, the latter being added to reduce the nucleation rate and improve crystal size.

Streak- and microseeding To prepare a seed stock, a small number of crystals were briefly washed in fresh reservoir solution and transferred into a microtube containing 50 µL reservoir solution. After adding a plastic bead (Hampton Research), the crystals were crushed by extensive vortexing until no visible fragments remained when inspected on a microscope. Immediately prior to use, a 1000-fold dilution series was pre-

pared from the seed stock in reservoir solution. For microseeding, 0.5 μL of each seeding solution were added to crystallisation drops set up as above. For streak-seeding, a seeding tool made from natural fibre (Hampton Research) was briefly dipped into the seeding solution and streaked in a straight line across a freshly setup crystallisation drop. In both cases, multiple drops were setup for each seed dilution.

Additive screening Crystallisation trials in the presence of additives were carried out using reagents from a commercial kit (Additive ScreenTM, Hampton Research). Briefly, after hanging drops were setup as above with 2 μL protein sample and 1 μL crystallisation solution, 0.3 μL of additive were mixed into the drop by rapid pipetting. In the case of volatile compounds, 50 μL of the additive solution was added to the reservoir.

Crystal harvesting, cryoprotection and storage Before crystal harvesting, a range of cryoprotectant solutions were freshly prepared for each condition and contained 10–20 % glycerol or 10–20 % ethylene glycol. Using a cryo- (Hampton Research) or litholoop (Molecular Dimensions), crystals were transferred from the crystallisation drop into a drop of cryoprotectant on a separate coverslip. If necessary, crystal bundles were broken apart and individual crystals transferred into a second drop of cryoprotectant. The loop was then frozen by plunging it into liquid nitrogen. Vials of harvested crystals were stored in canes or directly in ESRF sample-changer baskets, which reduces the risk of ice formation during transfer.

For the co-crystallisation trial of ILT7 with tetherin, crystals were harvested directly from HTX crystallisation plates using the automated CrystalDirectTM harvester developed by the Marquez and Cipriani groups at the EMBL Grenoble (Cipriani et al., 2012; Márquez and Cipriani, 2014). Briefly, HTX screening is carried out on specially-designed plates in which crystals grow on a very thin film. The harvesting robot is capable of excising any area of interest from the film through laser-induced photoablation, mounting it on a pin for data collection and transferring the sample into liquid nitrogen. In addition, crystallisation drops can be automatically injected with cryoprotectant or dehydrated through aspiration prior to excision.

X-ray diffraction Data collection took place at the European Synchrotron Radiation Facility (ESRF, Grenoble). A range of beamlines were used, including the bending magnet beamline BM14, the ID14-4, ID23-1 and ID29 beamlines as well as the ID23-2 microfocus beamline. These beamlines were all equipped with the automatic SC3 sample changer developed at the ESRF. Both the original and 2.0 versions of the MxCuBE software were used for data acquisition (Gabadinho et al., 2010). ILT7#19 data were recorded at an X-ray wavelength of 0.978 57 Å under cryogenic conditions on beamline ID23-1, which is equipped with a Pilatus 6M-F detector (Dectris).

Controlled dehydration The dehydration of crystals at room temperature can sometimes induce rearrangements within the lattice that, by changing symmetry or increasing order, may improve X-ray diffraction. The ESRF BM14 beamline can be equipped with a remote-controlled humidifier that provides a vapour-stream directed onto the mounted crystal. The relative humidity can be adjusted from the control hutch, and the changes in drop size can be monitored in real time. ILT7 crystals were harvested from the crystallisation plates and manually mounted on the diffractometer. Relative humidity was then progressively decreased from 98–80% and single diffraction patterns recorded to assess diffraction quality. For data collection, the vapour-nozzle was remotely switched with a cryostream, thereby freezing the crystal.

2.5.2 Structure determination and refinement

Data reduction Automatic indexing and integration of the data were performed with the XDS software using detector-specific parameter files (Kabsch, 2010). The CCP4 tool Aimless was then used for scaling, assessment of data quality and determination of a reasonable high resolution cutoff (Winn et al., 2011; Evans and Murshudov, 2013). The main criteria for cutoff definition were the degree of completeness and the value of $CC_{1/2}$, which is the correlation coefficient calculated between random half datasets, and represents a statistically more robust estimation of data quality than previously used R values (Karplus and Diederichs, 2012). In addition, the diffraction anisotropy was checked using the Diffraction Anisotropy Server at UCLA (Strong et al., 2006), without however applying ellipsoidal truncation to the data as no significant anisotropy was observed.

Molecular replacement Phases for the ILT7 data were obtained by molecular replacement using the Phaser-MR program as part of the Phenix suite (Adams et al., 2010). The crystal structures of several other leukocyte Ig-like receptors (LILRs) were used as search models, notably ILT4/B2 (PDB 2GW5), ILT6/A3 (3Q2C) and ILT3/B4 (3P2T). The search models were edited with Sculptor to (i) match a sequence alignment with ILT7(D1), (ii) prune sidechains according to Schwarzenbacher et al. (2004) and (iii) rename/renumber residues to facilitate model building. The composition and number of search model copies were adjusted based on the most probable Matthews coefficient, as calculated with MATTPROB (Kantardjieff and Rupp, 2003). In the case of ILT7#19, residues 2–95 of the pruned ILT3/B4 crystal structure were used as a search model, and led to a single solution with a log-likelihood gain of 827 and translation function Z-score of 30.4.

Model building and refinement Models were refined in several cycles of manual model building with Coot (Emsley et al., 2010), followed by restrained refinement with

phenix.refine. Per-residue TLS parameters were refined during the last cycles, and water molecules were placed prior to the final refinement run. Diffraction data and refinement statistics for ILT7#19 are summarised in Table 4.1 (p. 96).

2.6 Cell biology

2.6.1 Cloning of tetracysteine-tagged tetherin

For the visualisation of tetherin in transiently transfected cells, we employed a fluorescent labeling technique based on the biarsenical small-molecule reagents FAsH and ReAsH (Griffin et al., 1998; Adams et al., 2002). These molecules, which are derivatives of fluorescein and resorufin, respectively, contain two arsenic atoms that each covalently bind to a pair of thiols. The consensus tetracysteine motif CCPGCC was identified as a polypeptide binding site for FAsH/ReAsH, and several flanking sequences have since been discovered that increase binding affinity. Importantly, the reagents become fluorescent only when bound to the tetracysteine motif, which allows the selective labeling of recombinant proteins fused with a tetracysteine tag in many different situations. The plasma membrane is permeable to FAsH, which can thus also be used for intracellular labeling. Moreover, FAsH and ReAsH can be used in fluorescence resonance energy transfer (FRET) experiments, given their overlapping excitation/emission spectra. Here, the minimal tetracysteine sequence (CCPGCC) or a high-affinity version (FLNCCPGCCMEP) described by Martin et al. (2005) were inserted after Tyr155 near the C-terminus of tetherin by OE-PCR. The two constructs, which were ligated into a pcDNA3.1 backbone (Life Technologies), will subsequently be referred to as tetherin-TC155 (minimal tag) and tetherin-FLN155 (high-affinity tag).

2.6.2 HIV-1 virus-like particle release assay

The HIV-1 restriction activity of tetherin mutants was assessed in a virus-like particle (VLP) release assay in HEK 293T cells, which do not constitutively express tetherin. The cells were co-transfected with tetherin and a plasmid encoding the HIV-1 Gag polyprotein (pCG-Gag). Indeed, the expression of Gag is sufficient to produce non-infectious VLPs that undergo the entire budding process and are susceptible to restriction by tetherin. Cell culture and transient transfection of HEK 293T cells were performed as for small-scale protein production (see page 63). For co-transfection in six-well plates, 3 µg of tetherin DNA was mixed with 0.3 µg pCG-Gag or empty pcDNA3.1 as a negative control. The culture supernatant was removed 24 h post-transfection and filtered at 0.22 µm. A 500 µL sample was deposited on top of 3 mL sucrose solution (20%) and centrifuged at $120000 \times g$ for 3 h at 4 °C. The supernatant was discarded and the VLP-containing pellet was resuspended in SDS loading buffer. For cell lysate

samples, monolayers were washed twice with PBS, resuspended in 500 μ L PBS and mixed with 4 \times SDS loading buffer. The samples were separated by SDS-PAGE and analysed by Western blot using anti-p24 antibody.

2.6.3 Fluorescent labeling and confocal microscopy

For the imaging of fixed or living HEK 293T cells by fluorescence microscopy, cells were seeded onto multi-chambered coverslips (μ -Slide, Ibidi) or imaging dishes (μ -Dish, Ibidi) 12–16 h before transfection with tetracysteine-tagged tetherin constructs. At 24–48 h post-transfection, supernatants were discarded, cell monolayers were washed twice with PBS, and fixed with paraformaldehyde (4 % in PBS) for 20 min at room temperature. The FLAsH labeling solution was prepared by diluting 1 μ L FLAsH-EDT₂ (2 mM) and 12 μ L DTT (1 M) in a final volume of 800 μ L HBSS buffer. The FLAsH washing solution was prepared by diluting 20 μ L BAL buffer in 2 mL HBSS. After several wash steps, the cells were incubated with the labeling solution for 5–60 min in the dark at room temperature, followed by washing with BAL solution for 2 \times 5 min. Alternatively, the cells were fixed after labeling for 1–4 min or living cells were labeled for 15–60 min in a 37 °C CO₂ incubator.

For immunofluorescent staining, the fixed cells were blocked with normal goat serum for 1 h at room temperature. The blocking solution was discarded and the cells were incubated with primary antibody solution (rabbit anti-tetherin serum, 1:1000 in PBS) for 1 h at room temperature. After washing for 3 \times 5 min with PBS, the cells were incubated with secondary antibody solution (Alexa Fluor 594-conjugated goat anti-rabbit IgG, 1:1000 in PBS) for 30 min in the dark at room temperature. The cells were again washed for 3 \times 5 min with PBS, followed by incubation with PBS supplemented with nuclear counterstain (NucBlue, Life Technologies) for 20 min. The staining solution was replaced with PBS prior to imaging.

Images were acquired on a Leica TCS SP2 laser-scanning confocal microscope equipped with an acousto-optical beam splitter (AOBS) and helium-neon, argon and 405 nm diode laser lines. However, in order to avoid bleed-through from the Hoechst 33342 nucleic acid stain, images were acquired sequentially and averaged over three frames. Live cell imaging was performed in an environmental chamber at a controlled 37 °C temperature but without the 5 % CO₂ atmosphere required for optimal pH buffering.

2.6.4 Flow cytometry analysis with fluorescent ILT7(D1)

The binding of purified ILT7 to tetherin under native conditions was tested by flow cytometry using fluorescently labeled ILT7(D1) to stain tetherin-expressing cells. ILT7(D1) construct #17 was prepared and labeled with AF488 as detailed above, and its concentration adjusted to 25 or 50 μ g mL⁻¹ for low- and high-dose labeling respectively. HEK 293T cells were transfected with lentiviral plasmids encoding wild-type tetherin 2 d

before the experiment and incubated with ILT7-AF488 for 1 h at 4 °C prior to analysis. Control experiments were performed with non-transfected cells as well as with cells labeled with anti-Tetherin polyclonal rabbit serum or normal rabbit serum followed by AF488-conjugated anti-rabbit IgG. The labeled cells were then analysed on a CyAn flow cytometer (Beckman Coulter) running FlowJo software (Treestar). This experiment was carried out in collaboration with the laboratory of Prof Eric Cohen (Institut de Recherches Cliniques de Montréal, Montréal, Canada), who performed the analyses using fluorescently labeled protein provided by us.

3

Materials

3.1 Buffers and solutions

HEPES-buffered saline (HBS)

10 mM HEPES

150 mM NaCl

Adjust pH to 7.4

1.92 mM glycine

1 % (w/v) SDS

Adjust pH to 8.3

10×Phosphate-buffered saline (PBS)

100 mM Na₂HPO₄

18 mM KH₂PO₄

1.37 M NaCl

27 mM KCl

Adjust pH to 7.4

SDS-PAGE resolving gel (12 %)

3.2 mL 30 % Acrylamide/0.8 % Bis

2 mL 1.5 M Tris (pH 8.8)

80 μL 10 % SDS

80 μL 10 % APS

8 μL TEMED

2.6 mL H₂O

10×Tris-buffered saline (TBS)

500 mM Tris

1.5 M NaCl

Adjust pH to 7.4

SDS-PAGE stacking gel (4 %)

0.67 mL 30 % Acrylamide/0.8 % Bis

1.25 mL 0.5 M Tris (pH 6.8)

50 μL 10 % SDS

50 μL 10 % APS

5 μL TEMED

3 mL H₂O

Towbin transfer buffer

25 mM Tris

192 mM glycine

20 % (v/v) methanol

SDS-PAGE sample buffer (4×)

240 mM Tris (pH 6.8)

8 % (w/v) SDS

40 % (v/v) glycerol

0.04 % (w/v) bromophenol blue

SDS-PAGE running buffer (10×)

250 mM Tris

3.2 Reagents, media and kits

Name	Cat.#	Vendor
Streptavidin (<i>Streptomyces avidinii</i>)	S4762	Sigma-Aldrich, St. Louis, MO, USA
EZ-Link Sulfo-NHS-LC-Biotin (no-weigh)		Pierce Protein Biology, Rockford, IL, USA
Red NHS Protein Labeling Kit	L001	NanoTemper, Munich, Germany
Alexa Fluor® NHS Ester	A-20000	Life Technologies, Carlsbad, CA, USA
DMSO, anhydrous	D12345	Life Technologies
TC-FIAsh™ II detection kit	T34561	Life Technologies
Biacore Amine Coupling kit	BR100050	GE Healthcare, Little Chalfont, UK
Surfactant P-20	BR100054	GE Healthcare
Western ECL substrate	170-5061	Bio-Rad, Hercules, CA, USA

Table 3.1 List of biochemistry reagents

Name	Cat.#	Vendor
Ni-NTA Superflow resin	30430	Qiagen, Hilden, Germany
HisTrap excel, 5 mL	17-3712-06	GE Healthcare
rProtein A Sepharose Fast Flow medium	17-1279-01	GE Healthcare
Superdex 75 10/300 GL column	17-5174-01	GE Healthcare
Superdex 200 10/300 GL column	17-5175-01	GE Healthcare

Table 3.2 List of chromatography media and columns

Name	Cat.#	Vendor
DMEM GlutaMAX™, high glucose	10566-016	Life Technologies
Sf-900™ II SFM	10902-088	Life Technologies
Express Five® SFM	10486-025	Life Technologies
Fetal Bovine Serum, South America origin	10270-106	Life Technologies
HBSS, 1X, calcium, magnesium	14025092	Life Technologies
L-Glutamine, 200 mM	25030-081	Life Technologies
Penicillin-Streptomycin, 10 000 U/mL	15140-122	Life Technologies
TrypLE™ Express Enzyme, phenol red	12605-010	Life Technologies
Nutridoma-SP, 100X	11011375001	Roche, Basel, Switzerland
NucBlue® Live	R37605	Life Technologies
FuGENE® HD	E2311	Promega,

Table 3.3 List of cell culture media and reagents

Name	Cat.#	Vendor
QIAprep Spin Miniprep Kit	27104	Qiagen
EndoFree Plasmid Mega Kit	12381	Qiagen
QIAquick PCR Purification Kit	28104	Qiagen
QIAquick Gel Extraction Kit	28704	Qiagen

Table 3.4 List of molecular biology kits

3.3 Enzymes and antibodies

Name	Cat.#	Vendor
KAPA HiFi DNA Polymerase		Kapa Biosystems, <i>Wilmington, MA, USA</i>
T4 DNA Ligase	M0202T	New England Biolabs, <i>Ipswich, MA, USA</i>
Antarctic Phosphatase <i>Restriction enzymes</i>	M0289S	New England Biolabs New England Biolabs

Table 3.5 List of enzymes

Name	Cat.#	Vendor
Mouse anti-His-tag, peroxidase conjugate	A7058	Sigma-Aldrich
Anti-HA.11 Clone 16B12	MMS-101P	Covance, <i>Princeton, NJ, USA</i>
Rabbit anti-Tetherin serum	11721	NIH AIDS Reagents Program
Goat anti-Rabbit IgG, Alexa Fluor® 594 conjugate	A-11037	Life Technologies
Normal goat serum, 10 %	50-197Z	Life Technologies

Table 3.6 List of antibodies and sera

3.4 Bacterial strains and cell lines

Name	Cat.#	Vendor
BL21-CodonPlus™ (DE3) RIL	230245	Agilent Technologies, <i>Santa Clara, CA, USA</i>
AD494(DE3)		Novagen
Rosetta™2 (DE3)	71397	Merck Millipore, <i>Darmstadt, Germany</i>
Origami™ (DE3) pLysS	70618	Merck Millipore

Name	Cat.#	Vendor
OneShot® TOP10	C4040-03	Life Technologies

Table 3.7 List of *E. coli* strains

Name	Cat.#	Vendor
HEK 293T	CRL-3216	ATCC
Sf21 cells	11497-013	Life Technologies
High Five™ cells	B855-02	Life Technologies

Table 3.8 List of eukaryotic cell lines

3.5 Equipment and consumables

Name	Cat.#	Vendor
Standard Treated Capillaries	K002	NanoTemper
μ-Slide, 8-well, ibiTreat	80826	ibidi, München, Germany
μ-Dish, 35 mm low, ibiTreat	80136	ibidi
HyBond ECL blotting membrane	RPN82D	GE Healthcare
Amersham Hyperfilm ECL	28-9068-35	GE Healthcare
Biacore Sensor Chip CM5	BR100012	GE Healthcare

Table 3.9 List of consumables

Name	Cat.#	Vendor
Biacore 3000	BR110045	GE Healthcare
MicroCal VP-ITC		Malvern Instruments, Malvern, UK
Leica TCS SP2 confocal microscope		Leica Microsystems, Wetzlar, Germany
ÄKTAprime Plus FPLC system	11-0013-13	GE Healthcare
TransBlot Turbo transfer system	170-4155	Bio-Rad
Stirred cell, 400 mL	5124	Merck Millipore

Table 3.10 List of equipment

Résultats (français)

L'objectif principal de cette thèse était d'élucider les détails structuraux gouvernant l'interaction entre la tétherine et le récepteur immuno-modulateur ILT7. Comme la production du domaine extracellulaire de la tétherine avait été préalablement établie au laboratoire, nous nous sommes concentrés sur l'expression recombinante et la purification de l'ectodomaine d'ILT7.

Le domaine extracellulaire de ILT7 étant composé de quatre domaines de type Ig, il était essentiel de choisir un système d'expression permettant l'oxydation des ponts disulfure. En effet, la formation des ponts disulfure conservés au sein de domaines Ig est essentielle pour le repliement correct du motif structural β -sandwich. Une glycosylation correcte pourrait également être importante pour garantir la solubilité et la stabilité de la protéine. Comme les systèmes d'expression bactériens conventionnels ne permettent pas ces modifications post-traductionnelles, on a eu recours, dans un premier temps, à l'expression dans des lignées de cellules humaines ou d'insectes. Pour l'expression en cellules HEK 293T, des constructions comprenant les domaines D1–D2 (résidus 24–223) ou D1–D4 (24–435) ont été clonées dans des plasmides contenant une séquence signal pour l'adressage de la protéine vers voie de sécrétion, ainsi qu'une étiquette polyhistidine carboxy-(C-) ou amino-(N)-terminale. Cependant, après de nombreux essais, aucune expression a pu être détectée par Western blot, en utilisant un anticorps anti-polyhistidine (Figure 4.4, p. 88). Dans une deuxième approche, on a généré des baculovirus recombinants pour l'expression des domaines D1–D2 et D1–D4 en cellules d'insecte. Dans les deux cas, la protéine a été détectée dans la fraction cellulaire mais pas dans le surnageant de culture, ce qui suggère un blocage au niveau de la voie de sécrétion (Figure 4.5A–B, p. 89). Finalement, un troisième baculovirus a été créé, basé sur une construction mise au point par l'équipe du Prof Eric Cohen (Institut de Recherches Cliniques de Montréal, Canada), dont le bout carboxylique a été allongé de cinq résidus supplémentaires (24–435). Cette protéine est sécrétée dans le surnageant de culture 72–96 h après infection (Figure 4.5C–D, p. 89). La protéine a pu être purifiée en quantité limitée, et son interaction avec la tétherine a pu être validée par résonance de plasmon en surface (Figure 4.22, p. 115).

En parallèle avec les essais d'expression en cellules eukaryotes, on a tenté de produire les domaines D1–D2 ou le domaine D1 seul d'ILT7 en *Escherichia coli*. Afin de garantir la formation de ponts disulfure, on a généré des constructions comprenant une séquence signal pour l'adressage de la protéine au périplasma. En effet, l'espace périplasmique des bactéries Gram-négatives constitue un environnement favorable pour l'oxydation des cystéines par la présence d'enzymes de la famille Dsb. De manière alternative, on a eu recours à deux souches *E. coli* déficientes des enzymes réducteurs thiorédoxine réductase (*trxB*) et/ou glutathion réductase (*gor*), qui permettent potentiellement l'expression cytoplasmique de protéines contenant des

ponts disulfure. Les deux approches n'ont cependant pas permis d'obtenir de la protéine soluble (Figure 4.7, p. 91). Sous des conditions normales, l'expression bactérienne d'ILT7 résulte dans l'accumulation de la protéine dans des corps d'inclusion sous une forme insoluble. Après de nombreux essais, on a réussi de reconstituer le domaine N-terminal d'ILT7 (résidus 24–118) par repliement *in vitro* et de purifier la protéine ainsi obtenue (Figure 4.8, p. 93). En revanche, le repliement *in vitro* de plusieurs constructions comprenant les domaines D1–D2 n'a pas été réussi.

Des cristaux obtenus avec la protéine ILT7(D1) nous ont permis de résoudre la structure du domaine à une résolution de 1.55 Å par remplacement moléculaire basé sur la structure d'ILT3 (Figure 4.10, p. 98). La structure consiste en un motif de type immunoglobuline (Ig) classique, caractérisée par un sandwich de deux feuillets beta anti-parallèles, reliés par un pont disulfure. Les deux extrémités du brin C' sont mal définies dans la densité électronique, suggérant la présence de boucles flexibles étendues. En effet, une comparaison avec les structures de domaines D1 d'autres membres de la famille ILT/LILR montre que l'organisation de la région C' permet de distinguer entre récepteurs reconnaissant des molécules du complexe majeur d'histocompatibilité (CMH) et ceux reconnaissant des ligands non-CMH (Figure 4.11, p. 100).

Malgré l'absence d'informations sur les résidus impliqués dans l'interaction entre ILT7 et la tétherine, on peut spéculer que le domaine D1—distal de la membrane—contribue probablement à la reconnaissance de la tétherine, vu son exposition ainsi que la présence de nombreux polymorphismes. Toutefois, en ayant recours à de multiples techniques de biophysique tels la résonance de plasmon en surface (SPR), la titration calorimétrique isotherme (ITC) et la microthermophorèse (MST), il ne nous a pas été possible de mesurer une interaction significative avec l'ectodomaine de la tétherine (Figures 4.13, p. 101 et 4.14, p. 103). De plus, l'analyse par cytométrie en flux de cellules exprimant la tétherine (type sauvage) et pré-traitées avec ILT7(D1) conjugué à un fluorophore n'a également pas montré d'interaction (Figures 4.15, p. 104). La co-cristallisation de ILT7(D1) avec la tétherine (résidus 47–159) a été tenté sans succès.

En dépit de l'absence d'interaction du domaine N-terminal avec la tétherine, on a réalisé du docking *in silico* basé sur les structures cristallographiques de la tétherine(80–147) et ILT7(D1) afin d'identifier une interface partielle à faible affinité. Deux classes d'interfaces potentielles ont été retenues, impliquant une interaction du bout N-terminal du coiled-coil de la tétherine avec la boucle latérale C' ou la face C-terminale d'ILT7 (Figures 4.16 et 4.17, pp. 105 et 107). Une expérience de docking a également été réalisé à partir d'une structure prédite des domaines D1–2 d'ILT7 avec la tétherine(80–147). De manière intéressante, les meilleurs modèles obtenus sont compatibles avec l'interface la plus probable identifiée précédemment et suggèrent une contribution majeure du domaine D2 dans l'interaction (Figures 4.19 et 4.20, pp. 111 et 112).

Un objectif secondaire de cette thèse était de déterminer l'état d'oligomérisation de la tétherine aux sites de bourgeonnement du VIH-1. En effet, il a été observé que même en présence de l'antagoniste viral Vpu, des molécules de tétherine sont incorporées dans les virions naissants. Ceci suggère qu'une réduction de la concentration locale de la tétherine est suffisante pour inhiber l'activité anti-virale de la protéine, et que sa capacité de restriction pourrait donc dépendre d'une auto-organisation en assemblages multimériques. On a tenté de vérifier cette hypothèse en co-exprimant de la tétherine comprenant le motif tétracystéine CCPGCC et la polypro-

téine Gag du VIH-1 dans des cellules HEK 293T. La tétherine-tétracystéine peut être rendue fluorescente par l'ajout de la molécule FAsH (fluorescein biarsenical hairpin binder) et visualisée à la surface cellulaire par microscopie de fluorescence par réflexion totale interne (TIRF). Une éventuelle interaction entre plusieurs dimères de la tétherine pourrait alors être quantifiée en mesurant le degré de transfert d'énergie entre molécules fluorescentes (FRET). Après de nombreux essais de mise au point, on n'a pas été en mesure de tirer des conclusions à cause d'un bruit de fond excessif et d'un taux considérable marquage non-spécifique (Figures 4.23 et 4.24, pp. 117 et 118).

4

Results

4.1 Bioinformatic analyses of the ILT7 ectodomain

4.1.1 Topology and domain organisation

In order to define regions of ILT7 likely to be recombinantly expressed in a soluble form, the target protein was characterised using a range of publicly available bioinformatics tools and databases. Pairwise alignment of ILT7/LILRA4 with all eight four-domain containing human LILRs shows sequence identities $> 59\%$, with ILT8/A6 sharing the highest identity of 72% . A Pfam database search identified four Ig domains (D1-D4) belonging to two families that are designated Ig₂ (D1 and D3) and Ig₃ (D2 and D4), respectively. This alternating arrangement of domains is shared between all two- and four-domain containing LILR paralogues and orthologues. The four ILT7 domain boundaries determined by HMM-alignment with Pfam are: 28–117 (D1), 122–197 (D2), 227–315 (D3) and 323–398 (D4). Pairwise alignment of all the separate LILR Ig-like domains (Figure 4.1) shows in addition that the two-domain receptors ILT11/A5 and ILT3/B4 most closely resemble the D1-D2 and D1/D4 domains of ILT7/A4, respectively. Based on these observations, it can be assumed that the domain organisation and overall structure of ILT7/A4 matches that of ILT1/A2, ILT2/B1, ILT3/B4, ILT4/B2, ILT6/A3 and ILT11/A5, for which partial crystal structures are available. It is worth noting that none of the LILR structures determined so far comprises more than two contiguous domains, and that only D1-D2 or D3-D4 have been crystallised. This is consistent with the above observation that pairs of Ig domains might form larger structural units in LILRs.

Immunoglobulin-like domains are commonly classified into several subsets according to their similarity to antibody variable (V-set) or constant domains (C1-set). Domains that structurally resemble constant domains, yet share a high sequence similarity with variable domains belong to the C2-set. Finally, the remaining domains are considered to be intermediate and are referred to as I-set domains. In terms of this classification, all LILR domains most closely resemble C2-set Ig domains.

As a type I transmembrane protein, ILT7 is expected to feature both a single transmembrane domain as well as an N-terminal signal sequence targeting its translation into the endoplasmic reticulum (ER). Using different algorithms, the transmembrane α -helix and signal peptide were predicted to span residues 447–465 and 1–23, respectively. The output from the SignalP server indicated the presence of a potential alternative signal peptide cleavage site after Gly16, albeit with a lower score than for position Ala23.

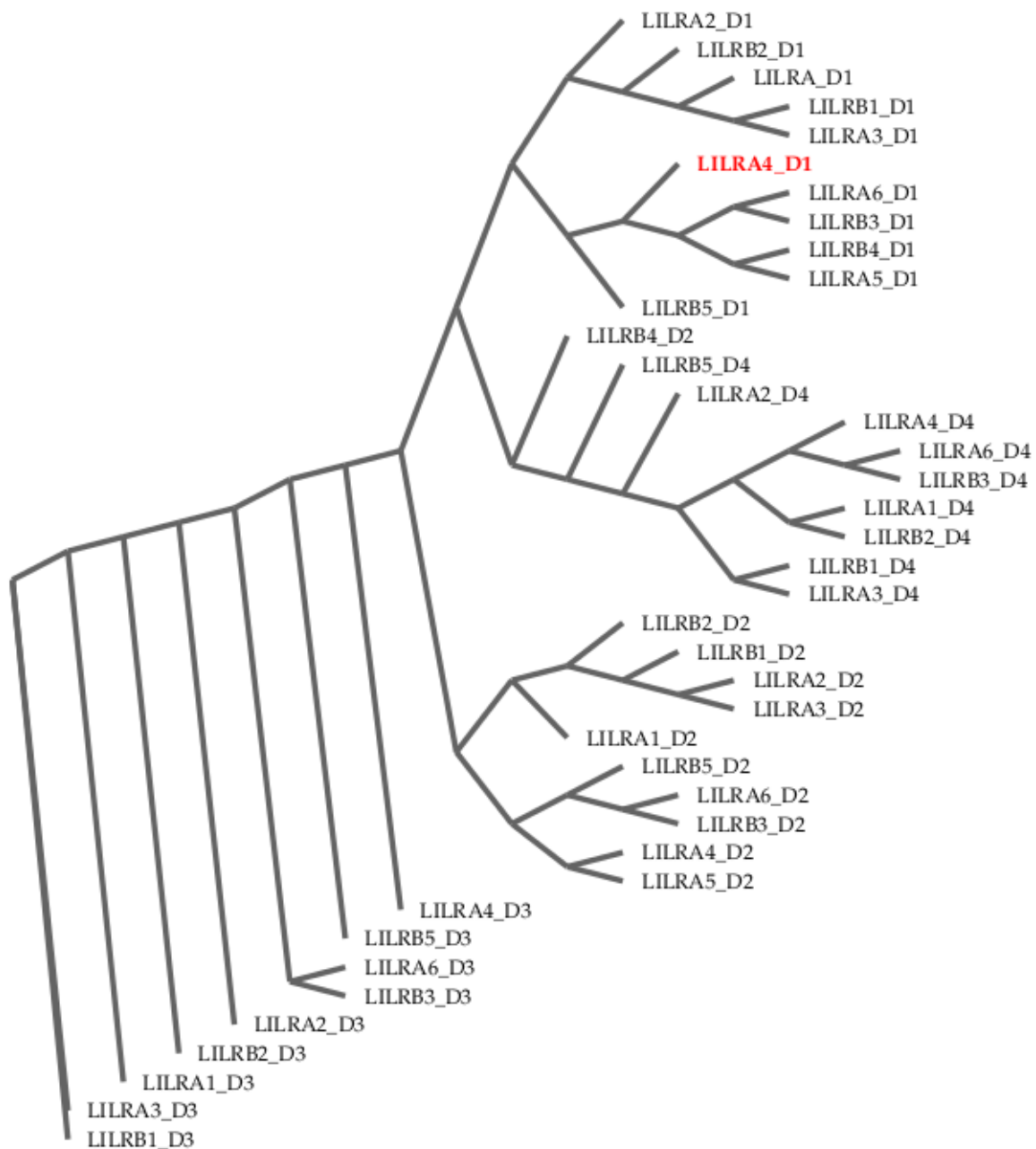


Figure 4.1 Phylogenetic tree (cladogram) of individual LILR domains. The D1 domain of ILT7/LILRA4 – which will be the subject of further investigation below – is highlighted in red.

4.1.2 Secondary structure and disorder prediction

The structural diversity among Ig superfamily proteins is extremely low compared to their sequence diversity, as illustrated by the superposition of 454 representative domains from the CATH database shown in Figure 4.2. Secondary structure prediction based on the ILT7 ectodomain sequence (residues 24–446) thus unsurprisingly identified β -strands as well as the major loop regions. Eight-class prediction by the RaptorX server also indicates short stretches of 3_{10} helices, as well as hydrogen-bonded (β -)turns, in some connecting regions (Figure 4.3). A 12-residue stretch (425–436) in the stalk region linking domain D4 to the transmembrane domain was predicted by several methods to be disordered (Figure 4.3). In addition, the region linking domains D3/D4 also scored above threshold according to the REMARK-465 criterion used by the DisEMBL server. These results hint at a certain degree of flexibility in both the stalk and D3/D4 inter-domain regions.

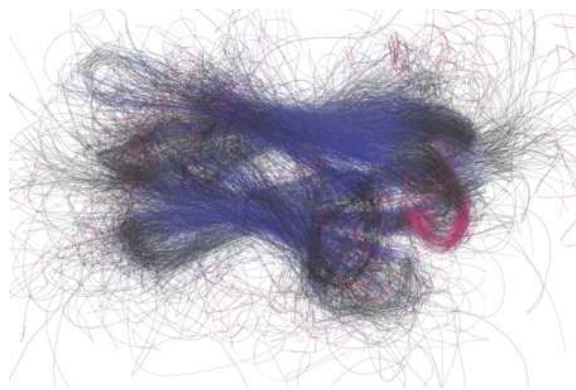


Figure 4.2 Superposition of representative Ig superfamily domains from the CATH database. The backbone structures are coloured by secondary structure, with β -strands and helical elements coloured in blue and red, respectively. *Image downloaded from the CATH Immunoglobulin superfamily page (ID 2.60.40.10).*

4.1.3 Prediction of post-translational modifications

Disulfide bonds linking the two β -sheets of Ig-like domains are a well conserved feature of this structural motif. From the multiple alignment of LILR sequences (page 49), it can be seen that in each predicted domain a pair of cysteines are conserved across the protein family (Cys49, -98, -143, -195, -244, -295, -344 and -395). On the other hand, another pair of cysteines that is conserved among LILRA1, ILT2/B1, ILT4/B2 and ILT6/A3, is absent in ILT7 where the substituted residues are Ile155 and Thr165. Potential glycosylation of the ILT7 ectodomain was evaluated using neural network-based algorithms. N-linked glycosylation was predicted to occur on four residues located in domains D2 (Asn138), D3 (Asn279 and -300) as well as in the D2/3 linker region (Asn239). While the three former asparagines are well conserved among all LILRs, Asn239 is only found in ILT7. Conversely, the conserved asparagines in position 339 (all LILRs) and 429 (subfamily 'A') are lacking in ILT7. Based on the presence of consensus sequence motifs and conservation, it can thus be assumed that ILT7 features at least three, and possibly four N-linked glycans. In addition, seven potential

O-linked glycosylation sites were predicted on threonines 134 and 333, and on serines 221, 225, 325, 431 and 433, of which the latter two achieved confidence scores exceeding 70 %.

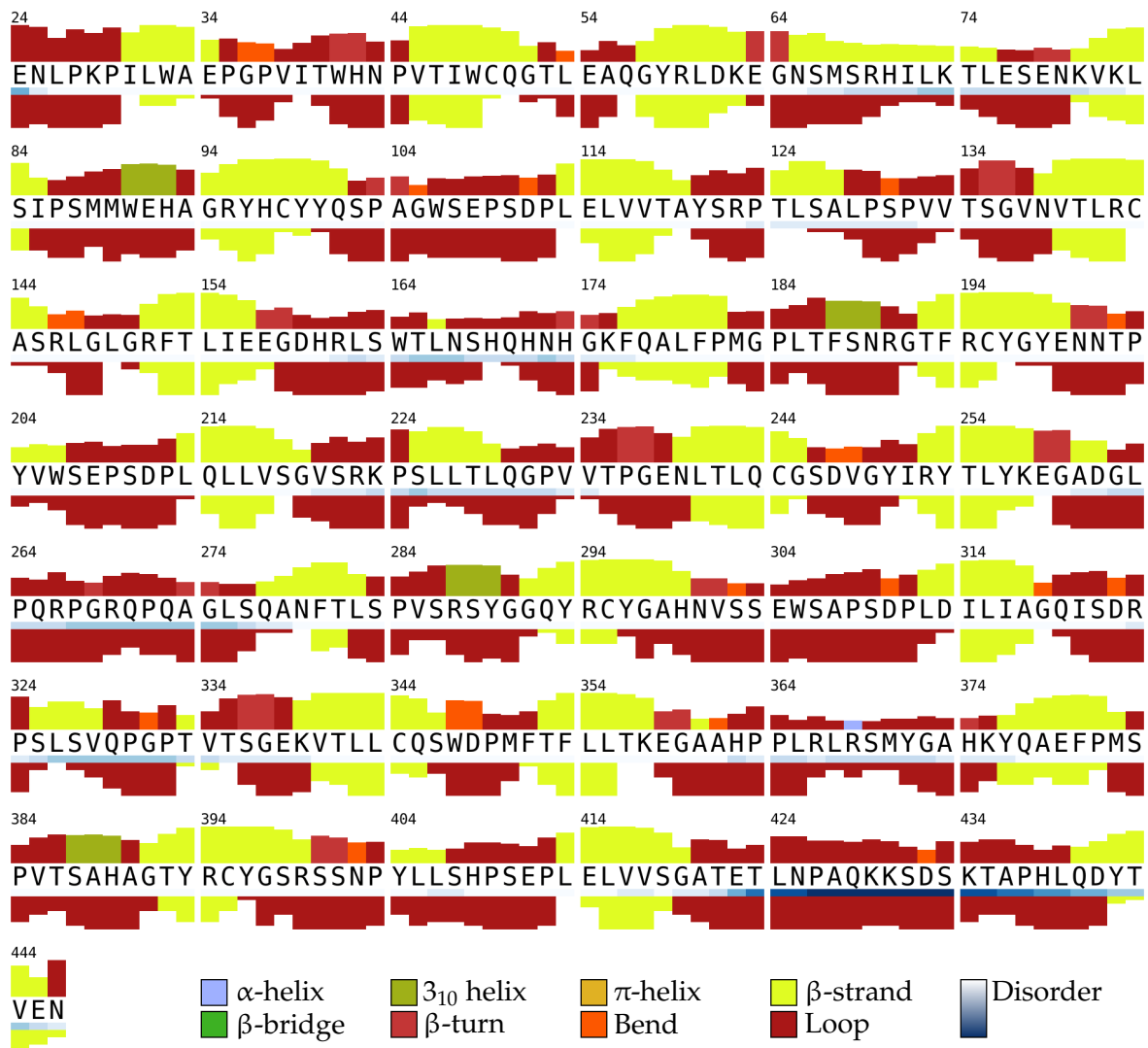


Figure 4.3 Predicted secondary structure and disordered regions of ILT7. Secondary structure types predicted by the RaptorX or PsiPred programs are represented as colour-coded bars above and below the sequence, respectively. Bar heights correspond to the confidence score for the predictions. The probability of disorder, as predicted by the DisoPred program, is indicated by blue boxes below the sequence.

4.2 Recombinant expression of the ILT7 ectodomain

The extracellular region of ILT7 being composed of four C2-type Ig-like domains, it was essential to choose an expression system allowing the formation of disulfide bonds. Indeed, formation of the conserved disulfide bonds found in Ig-like domains is crucial for the correct folding of the β -sandwich structural motif. In addition, the predicted glycosylation of the protein might be fundamental for the stability of the protein and contribute to its solubility. As conventional bacterial expression can provide none of these modifications, we resorted to eukaryotic expression systems in a first instance. An overview of all expression constructs discussed below can be found on page 58.

4.2.1 Mammalian cell expression

In an initial attempt, four constructs were created for expression in the human-derived HEK 293T cell line. The constructs comprised domains D1-2 (residues 24–223) or all four domains (24–430), an heterologous signal sequence for targeting to the secretion pathway as well as an N- or C-terminal cleavable polyhistidine(His)-tag. Small-scale expression trials were performed by transient transfection of adherent HEK 293T cells and protein expression was assessed 24–96 h post-transfection by anti-His-tag Western blot of cell lysates and culture supernatants (Figure 4.4). After initial results failed to indicate protein expression of the protein, several steps were taken to optimise experimental conditions, despite expression and detection of the positive control. Plasmid transfection can be inhibited by the presence of endotoxin, however the use of endotoxin-free kits for plasmid preparation, including for preparation of the control plasmid, had no effect. Alternative transfection methods were tried, including polyethylenimine (PEI), calcium phosphate, Lipofectamine® and FuGENE® reagents, but again did not affect the outcome. Similarly, the use of fresh cell stocks and culture reagents, as well as varying the number of passages prior to transfection did not lead to expression of recombinant ILT7. A range of additional constructs were designed to comprise the endogenous ILT7 signal peptide in conjunction with C-terminal His- and FLAG-epitope tags. Again, no protein expression could be detected in small-scale expression trials.

4.2.2 Insect cell expression

Following the failure of mammalian cell expression, recombinant baculoviruses were generated for protein expression in insect cells. Manipulation of insect cells is carried out in a level 1 laboratory and the cells are grown as suspension cultures in conical shaker flasks. The baculovirus/insect cell expression system thus combines the ease and potential high yield of bacterial expression with the benefits of an eukaryotic machinery for secretion and post-translational modification. Although glycosylation

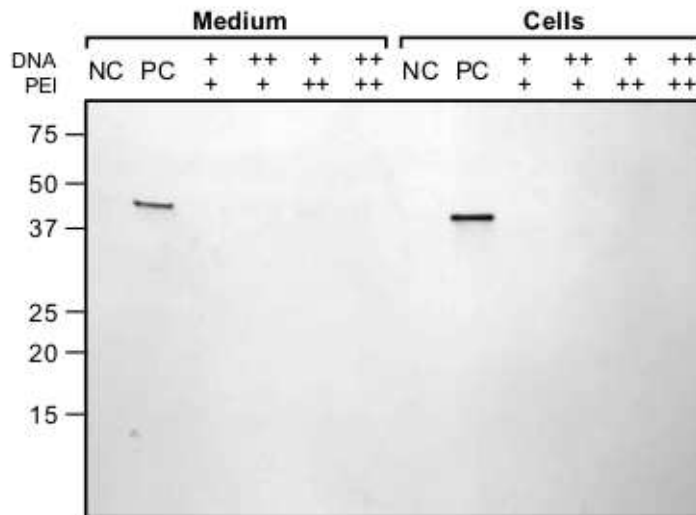


Figure 4.4 Western blot of small-scale ILT7(D1-2) expression test in HEK 293T cells. Cells were transiently transfected either with 3 (+) or 5 μ g (++) DNA per 35 mm-dish, using a PEI-to-DNA ratio of 2 (+) or 3 (++) . Lysates and culture supernatants of non-transfected cells (NC) or cells transfected with a plasmid expressing His-tagged PG9 as a positive control (PC) were also included. Stained with anti-His-tag antibody.

is different and less complex than in mammalian cells, the glycosylation of ILT7 is likely to contribute to the protein's stability. In order to direct the protein to the secretion pathway, the highly active signal sequence from the honey bee melittin gene was prepended to the ILT7 ectodomain sequence. Overall, three different constructs were cloned using the MultiBac technology developed by the Berger group at EMBL Grenoble (Trowitzsch et al., 2010).

An initial construct comprised domains D1-2 (residues 24–223 ; construct #7) and C-terminal cleavable His- and FLAG-tags. Protein expression was assayed at 48, 72 and 96 h post-infection by Western blot using anti-His-tag or anti-FLAG antibodies. While protein could be detected in cell lysates at all three timepoints, no signal was obtained from culture supernatants (Figure 4.5A). This suggests that the protein was entirely translated, given detection via C-terminal tags, but was not correctly processed through the secretion pathway. Alternatively, expression levels were below the limit of detection. A second construct (ILT7#8) spanned all four domains (24–430) and featured an N-terminal cleavable His-tag, separated from the signal peptide by an DR-linker. The design of this construct was based on the assumptions that (i) the presence of a longer unstructured region at the N-terminus would prevent any incompatibility of the ILT7 N-terminus in signal peptide removal, and (ii) all four Ig-like domains might be required for proper folding. Furthermore, the nucleotide sequence of this construct was optimised for *S. frugiperda* codon usage. Nonetheless, small-scale expression trials again indicated that the protein was translated but not secreted into the culture supernatant (Figure 4.5B).

Finally, a third baculovirus (ILT7#19) was generated based on a mammalian ILT7 expression construct designed in the laboratory of Prof Eric Cohen (Institut de Recherches Cliniques de Montréal, Montréal, Canada). The sole difference from the previous construct was the inclusion of five more residues (SDSKT) at the C-terminus, resulting in a mature protein comprising residues 24–435. Again, the DNA sequence was codon-optimised for the expression host cells. Small-scale expression tests were conducted as before, and protein expression assessed by anti-His-tag Western blot in both cell lysates and culture supernatants. Surprisingly however, ILT7#19 could be detected in culture supernatants as well as intracellularly (Figure 4.5C).

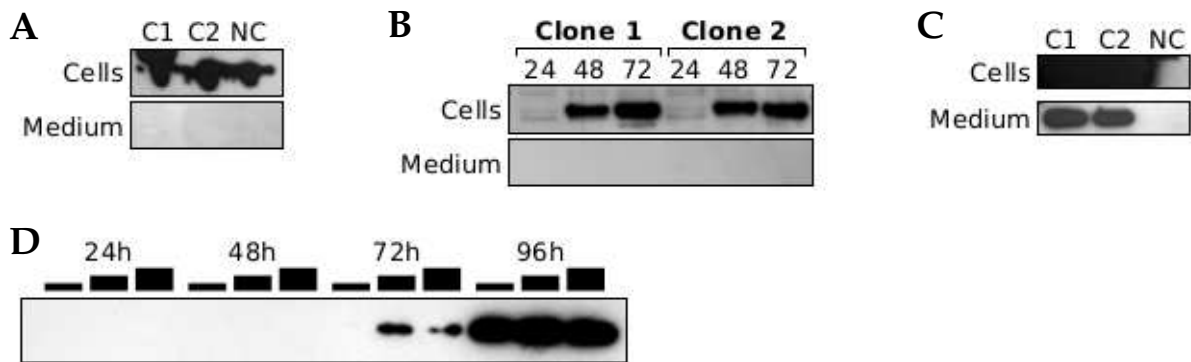


Figure 4.5 Western blots (anti-His-tag) of small-scale ILT7 expression tests in baculovirus-infected insect cells. Expression levels of (A) ILT7#7 at 72 h post-infection (hpi), (B) ILT7#8 at 48, 72 and 96 hpi and (C) ILT7#19 at 72 hpi. Two different baculovirus clones (C1 and C2) were tested in each experiment, and are compared to non-infected cells (NC). (D) Time series of ILT7#19 secretion into the culture medium of cells infected with three different viral doses.

Optimisation of ILT7(D1-4) expression Prior to large-scale protein production, infection and expression conditions were optimised to maximise the recombinant protein yield. The optimal viral dose required to arrest cell proliferation within 24 h was determined through regular cell counts of several cultures infected with different volumes of virus stock. Similarly, the optimal duration of incubation following cell proliferation arrest was assessed by Western blot analysis of samples taken at regular intervals post-infection (Figure 4.5D).

Purification of ILT7(D1-4) from cell culture supernatants Media formulations used for insect cell culture are not compatible with conventional immobilised metal affinity chromatography (IMAC) resins, as they contain chelating and/or reducing agents that strip metal ions from the column. During initial trials we resorted to an alternative nickel resin (HisTrap™ Excel, GE Healthcare) that is resistant to reducing and chelating agents. In addition, as insect cell cultures are slightly acidic (pH~6), for optimal

binding of the His-tagged protein to the affinity column the pH needs to be raised to promote deprotonation of imidazole groups ($pK_a \sim 6$). Prior to affinity purification, the culture supernatants were thus cleared by centrifugation and adjusted to pH 7 by titration of 10-fold PBS (pH 7.5). However, no significant amount of ILT7 could be obtained by this method, due in part to the substantial amount of protein precipitation on the affinity column. Nevertheless, through incremental adjustments to the purification protocol, better results could be achieved. Briefly, culture supernatants were cleared by centrifugation, concentrated 2-fold using a stirred cell, and extensively dialysed against buffer solution. Affinity purification was then carried out using a conventional nickel nitrilotriacetic acid (NTA) medium. The purity achieved through affinity chromatography alone was quite high, and protein could be concentrated to 0.4 mg mL^{-1} (Figure 4.6A). The uncleaved protein has a calculated molecular mass (M_r) of 47.9 kDa and migrates as a single band between 50–55 kDa, which is consistent with the presence of 2–4 high mannose glycans. Analytical size exclusion chromatography of a small sample on a Superdex 200 column revealed at least two separate species, retained at 8.9 and 13 mL respectively (Figure 4.6B). Based on the molecular mass, the expected elution volume of the protein would be $\sim 15 \text{ mL}$. The first peak thus represents a much higher molecular species, and possibly aggregated protein, given its proximity to the void volume ($\sim 7.5 \text{ mL}$). The earlier-than-expected elution of the second peak could be explained by the elongated structure of the protein, or alternatively by the complete dimerisation of the protein as well as an increased bulkiness caused by glycan moieties.

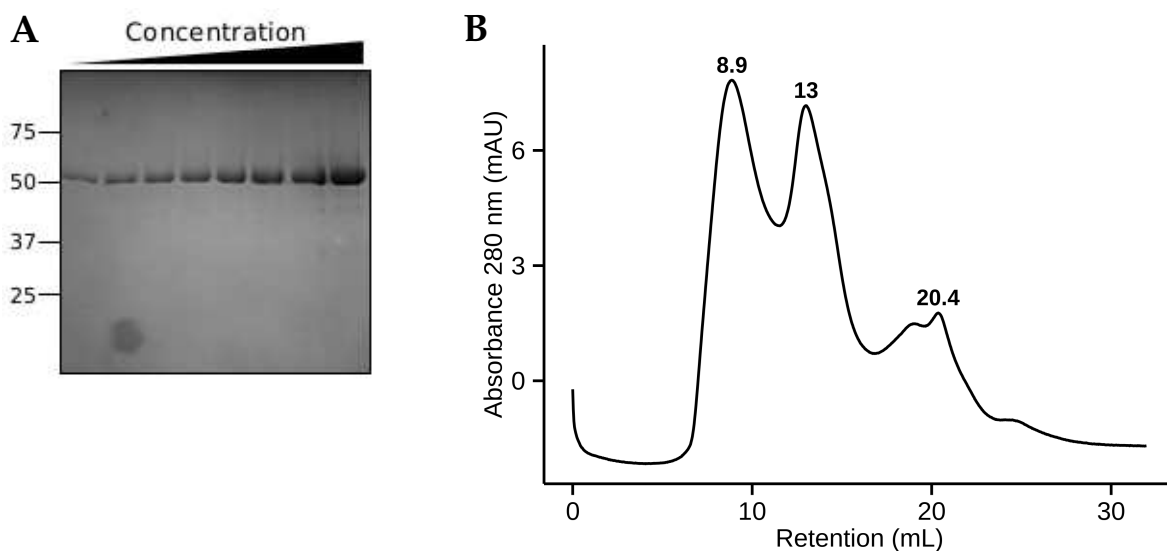


Figure 4.6 Purification of ILT7(D1-4). (A) SDS-PAGE of ILT7(D1-4) samples taken at regular intervals during concentration after nickel affinity purification. (B) Chromatogram from a Superdex 200 (10/300 GL) column.

4.2.3 Bacterial expression

In parallel to expression trials in insect cells, we attempted expression of one- or two-domain ILT7 constructs in *Escherichia coli* using three different approaches that theoretically allow the production of disulfide-containing protein. Notably, the periplasm of Gram-negative bacteria is an oxidative environment harbouring the Dsb (disulfide bond)-family of enzymes involved in disulfide oxidation and isomerisation in secreted unfolded proteins. Similarly to the eukaryotic secretion pathway, proteins are targeted for co-translational secretion into periplasmic space by an N-terminal signal sequence. For periplasmic expression of ILT7, a construct spanning domains D1 and D2 (residues 24–223) was cloned into a plasmid containing the *pelB* signal sequence and a C-terminal polyhistidine tag (construct #9). Due to very low expression levels expected from this method, protein expression in *E. coli* BL21(DE3) cells was assessed by Western blot after separation of cytoplasmic and periplasmic fractions. Large-scale expression followed by nickel-affinity purification was also attempted, however, in neither case could any recombinant protein be detected. Moreover, optimisation of the DNA sequence for *E. coli* codon usage did not change the outcome (#11).

A second approach to the production of soluble disulfide-containing protein in *E. coli* is the use of bacterial strains carrying mutant thioredoxin reductase (*trxB*) and/or glutathione reductase (*gor*) genes, which are components of two major disulfide reduction pathways. Small-scale expression trials of ILT7 constructs comprising one (ILT7#17) or two domains (#14) were conducted using *trx⁻gor⁻* Origami B™ or *trx⁻* AD494 (Novagen) cells, however no soluble protein could be obtained (Figure 4.7).

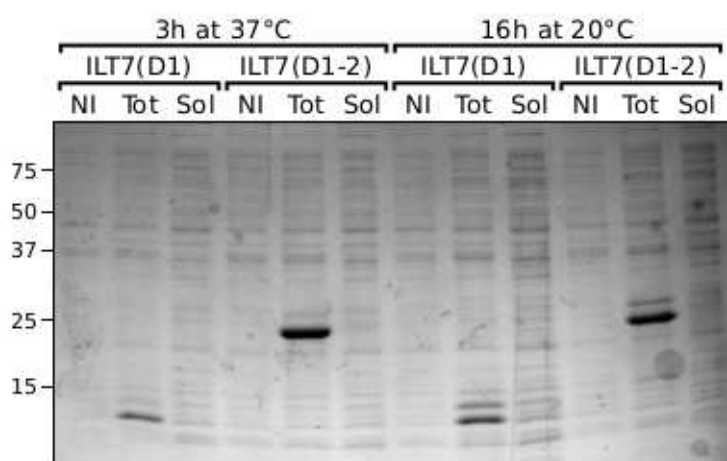


Figure 4.7 Expression trial of ILT7#14 and #17 constructs in AD494 *trx⁻* cells. After induction with 1 mM IPTG, cells were incubated for 3 h at 37 °C or overnight at 20 °C before lysis. Samples correspond to total cell lysates before (NI) or after (Tot) induction, as well as the soluble fraction (Sol) obtained after centrifugation. Bands of insoluble protein can be seen for both constructs at ~23 kDa and ~12 kDa, respectively.

Crystal structures of other members of the LILR family comprising up to two Ig-like domains have been obtained from recombinant protein expressed in bacterial inclusion bodies. After extraction and denaturation of inclusion bodies, the protein can be refolded *in vitro* by several methods, including rapid dilution into a large volume of buffer solution or stepwise dialysis against decreasing concentrations of a chaotropic agent such as guanidinium chloride or urea. In the case of disulfide-containing proteins, refolding solutions need to be buffered at a pH favourable to the oxidation of thiol groups ($pK_a \sim 8.3$) and are ideally supplemented with a redox agent such as glutathione to reduce the likelihood of non-specific disulfide cross-linking.

Bacterial expression of ILT7(D1-2) in BL21(DE3) RIL cells resulted in a massive accumulation of the protein in inclusion bodies. Inclusion body protein was readily extracted from cell lysates through several detergent wash steps. Refolding of the denatured protein was attempted using both approaches mentioned above, however after many efforts to optimise the protocol, no soluble protein could be obtained (ILT7#14). Expression was also attempted using an untagged construct (#13), because affinity purification is not required in the case of inclusion bodies that are almost exclusively composed of the target protein. The result remained unchanged. Interestingly, Cheng et al. (2011) encountered similar difficulties for the refolding of ILT3, but could stabilise the protein by introducing an additional pair of cysteines in an otherwise probably flexible loop region. The authors were hinted by the presence of two conserved cysteines in some LILRs (as mentioned in section 4.1.3). As this cysteine pair is also lacking in ILT7, we substituted the corresponding amino acids (I155C and T165C) by site-directed mutagenesis, and prepared inclusion bodies as before. However, in this case the additional disulfide bond did not improve the outcome (#15). Finally, based on the possibility of an alternative signal peptide cleavage site after Gly16, we designed two more constructs (#10 and #12) spanning residues 17–223, one of which also featured the additional cysteine pair. Again, no significant amount of soluble protein could be obtained by *in vitro* refolding.

In contrast, expression of the N-terminal domain alone (residues 24–118) with or without C-terminal affinity tag, resulted in a large amount of soluble protein after refolding by rapid dilution (ILT7#16 and #17). Since the purity achieved with the untagged protein was insufficient for crystallisation trials, our efforts were focused on the His-tagged ILT7. Purification of this protein required a first nickel affinity chromatography step under denaturing conditions prior to refolding, followed only by a polishing size exclusion chromatography column of the refolded protein (Figure 4.8A–B). Due to problems encountered during crystallisation, a further construct (#18) was cloned with a removable N-terminal His-tag, which is cleaved off by TEV protease digestion after refolding, followed by a second nickel affinity column (Figure 4.8C–D).

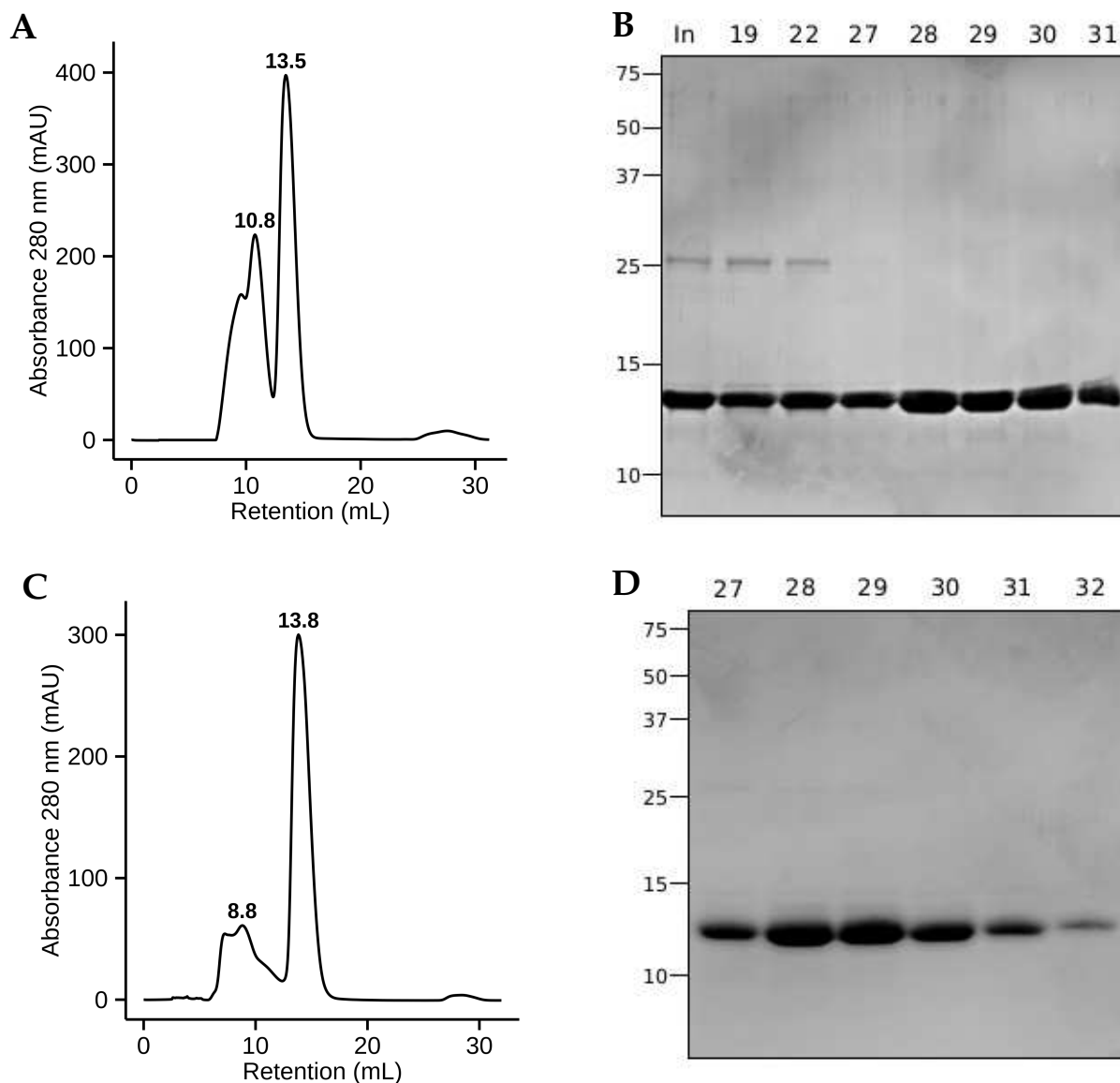


Figure 4.8 Size exclusion chromatography of ILT7(D1) on a Superdex 75 10/300 GL column. (A) Chromatogram showing the purification of C-terminally tagged ILT7#17 and (B) SDS-PAGE of samples corresponding to the void volume peak (fraction 19) or the peaks at 10.8 mL (22) and 13.5 mL (27–31). (C–D) Chromatogram and SDS-PAGE of the N-terminally tagged ILT7#18 after removal of the His-tag. Fractions 27–32 correspond to the principal peak at 13.9 mL.

4.3 Structure and ligand-binding properties of ILT7(D1)

4.3.1 Crystallisation and X-ray diffraction

Initial crystallisation conditions for the C-terminally tagged ILT7(D1) were obtained from a high-throughput screen at a protein concentration of 4.6 mg mL^{-1} . After less than 24 h, bundles of needle-shaped crystals were observed in two similar conditions containing 100 mM MES pH 6, 30 % PEG 6000 and 100 mM MES pH 6, 20 % PEG MME

5000, respectively (Figure 4.9A). Crystals could be readily reproduced by hand in hanging drop vapour diffusion plates, and the nucleation rate could be slightly reduced by doubling the precipitant-to-protein ratio. However, the crystals remained very small and initial diffraction patterns presented many badly resolved “streaky” reflections (Figure 4.9D). Indexing of the data using two major data reduction packages either failed (Mosflm) or led to indexation in the *R32* spacegroup (XDS) with too small a unit cell to accommodate a single molecule. Further refinement of the crystallisation conditions, notably through the addition of glycerol or ethylene glycol, led to larger crystals and a reduced nucleation rate (Figure 4.9B). A considerable number of crystals were tested following each reiteration of crystallisation conditions, but the quality of diffraction data could not be improved (Figure 4.9E). From data analysis with several programs, including Xtrriage, the crystals did not appear to be twinned. We thus concluded that processing failed due to irregularities inherent to crystal packing.

We attempted by several methods to obtain alternative crystal forms, including by micro-seeding and streak-seeding of crushed crystals into freshly prepared crystallisation drops, as well as by screening a range of commonly used additives. However, all crystals that resulted from these experiments were identical to the previous crystals and presented the same diffraction artifacts. A number of crystals were also subjected to controlled dehydration with the aim of inducing protein rearrangements and obtaining a more regular packing at room temperature prior to diffraction under cryo conditions. While all crystals diffracted down to 81 % relative humidity, the resolution progressively decreased and streaky reflections persisted. After vitrification of the sample, a single dataset was collected with diffraction to 3.8 Å but processing was aborted since both point group and unit cell parameters were identical to those obtained for previous crystals.

For co-crystallisation of C-terminally tagged ILT7(D1) and tetherin(47–159), both proteins were mixed to a total final concentration of 9.5 mg mL⁻¹ with a 1.5-fold molar excess of tetherin. The protein sample was submitted to high-throughput crystallisation screening and produced four positive hits within 24–72 h, all of which however resembled the needle-shaped crystals obtained from ILT7 alone. In addition, the crystals grew under conditions of pH 5.5–6 with PEGs as a sole precipitant. Nevertheless, the crystals were harvested directly from the screening plates using the robotic harvester developed at the EMBL Grenoble and tested by members of the Marquez lab. Due to overlapping diffraction from multiple crystals, none of the diffraction datasets could however be processed. We estimated that, given the observed crystal shapes and growth conditions, no co-crystallisation had occurred.

Finally, after generating an untagged ILT7(D1) protein as mentioned above, crystals presenting a trapezoidal prism morphology were obtained under many different conditions in a high-throughput screen, including with 100 mM MES pH 6, 30 % PEG 6000 as before (Figure 4.9C). The precipitant concentration was refined by hand,

and larger crystals could be obtained through the addition of 1–8% glycerol. Several datasets were recorded from different crystals at the ID23-1 beamline (Figure 4.9F), all of which diffracted to 1.5–1.8 Å and indexed in a primitive monoclinic lattice with cell parameters suggesting a *P2* spacegroup with two molecules per asymmetric unit (Table 4.1).

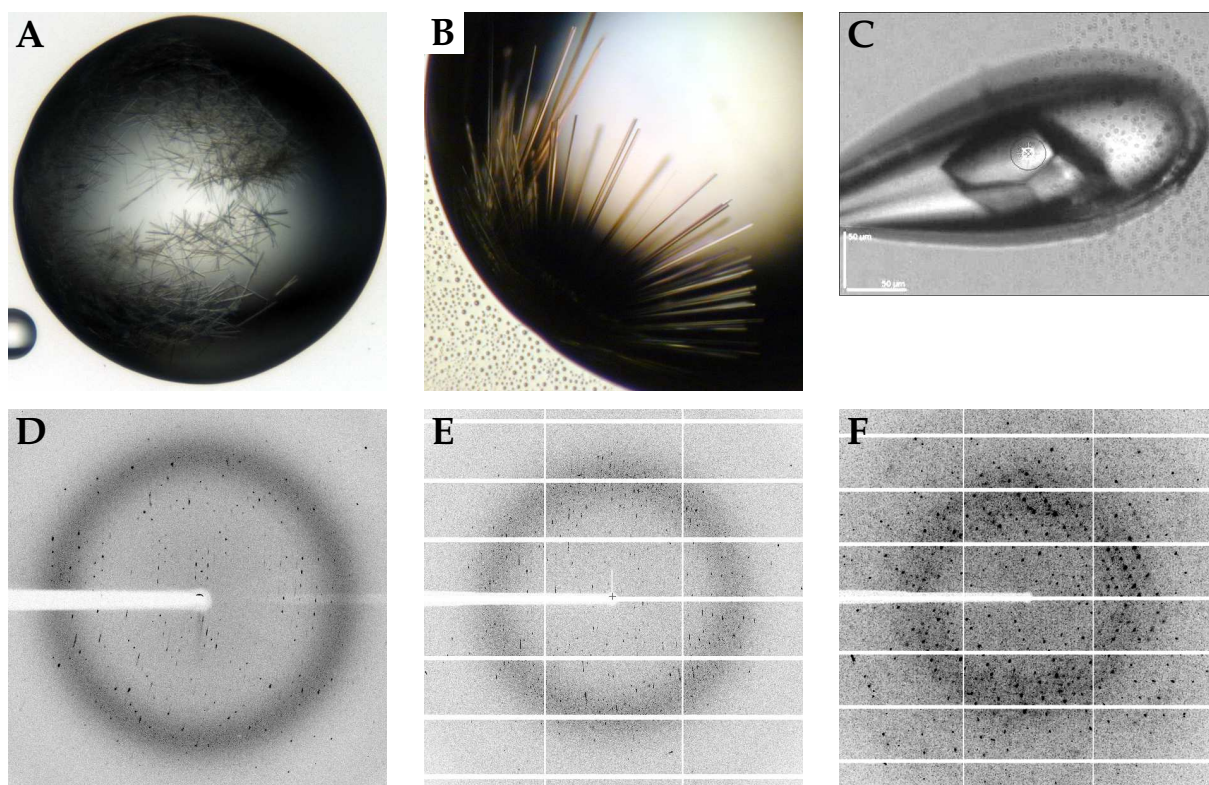


Figure 4.9 Crystals and X-ray diffraction patterns of C-terminally His-tagged ILT7(D1). (A) Initial needle-shaped crystals and (D) ‘streaky’ diffraction pattern. (B+E) While the crystals could be improved in size, diffraction quality remained poor and the data could not be phased. (C+F) Large trapezoidal prism-shaped crystal and diffraction pattern of N-terminally tagged ILT7#18 after removal of the His-tag.

4.3.2 Crystal structure at 1.55 Å resolution

The crystal structure of the N-terminal ILT7 domain was solved by molecular replacement using the crystal structure of ILT3/B4 (PDB 3P2T) as a search model. The model was completed by hand, and refined to $R_{\text{work}}/R_{\text{free}} = 0.21/0.24$. Detailed data reduction and refinement statistics are shown in Table 4.1 (page 96). The two molecules in the asymmetric unit are related by rotational symmetry, resulting in a head-to-tail dimer. The electron density is well defined apart from three residues missing at the N-terminus, as well as a most likely flexible region spanning residues 65–75. Due to more extensive crystal contacts, this region is marginally better defined in one of the molecules, where only residues 65–67 and 75–77 are missing from the electron density.

Data collection	
Space group	<i>P2</i>
Unit cell constants	
<i>a, b, c</i> (Å)	26.67, 52.96, 54.34
α, β, γ (°)	90.00, 95.91, 90.00
Resolution (Å)	37.83–1.55 (1.58–1.55)
R_{merge}	0.034 (0.294)
R_{meas}	0.044 (0.385)
Mean($I/\sigma I$)	20.1 (4.0)
Completeness (%)	98.2 (96.7)
Multiplicity	4.1 (4.0)
Refinement	
Resolution (Å)	37.83–1.55
Number of reflections (work/test)	20368/1103
$R_{\text{work}} / R_{\text{free}}$	0.21/0.24
Average B-factor	31.65
RMS deviations	
Bond lengths (Å)	0.008
Bond angles (°)	1.484
Ramachandran plot	
% favoured	96.5
% outliers	0.0
Molprobit	
Clashscore	5.34

Table 4.1 Diffraction data and refinement statistics for ILT7(D1). Numbers in brackets refer to the highest resolution shell.

The overall structure reveals a classical Ig-like fold that belongs to the constant C2-set of Ig-like domains (Figure 4.10A). The structure is characterised by two antiparallel β -sheets folded into a greek key sandwich-like motif with a stabilising disulfide bond between the two sheets. The first sheet is composed of three strands termed, by convention, A, B and E, whereas the second sheet comprises five strands named C', C, F, G and A' (Figure 4.10B). In common with other types of Ig and Ig-like domains, the core of the structural motif is formed by B, E, F and G with the disulfide bridge linking strands B and F. The C-terminal end of strand A, which is generally termed A', forms a small stretch of parallel hydrogen bonds with strand G on the opposite sheet, thereby disrupting the greek key motif. Two short helical elements are observed, namely a 3_{10} helix located between strands E–F and a type II polyproline (PPII) helix preceding strand G. The left-handed PPII helix spans residues 107–112 and is characterised by backbone torsion angles (φ and ψ) of $-66.1 \pm 6.9^\circ$ and $156.7 \pm 7.2^\circ$, respectively. The N-terminus of the structure (residues 26–29) adopts a similar albeit even shorter PPII-like twist. Strands F–G are connected by a proline-containing β -turn that, in con-

junction with the loop regions connecting B–C (residues 51–55) and C′–E (73–79), forms a potential membrane-distal interface reminiscent of the three complementarity determining regions (CDRs) of variable Ig domains. On the C-terminal end of the protein, the sidechains of residues Trp41, His42 and Trp90 possibly interact by π -stacking (Figure 4.10C).

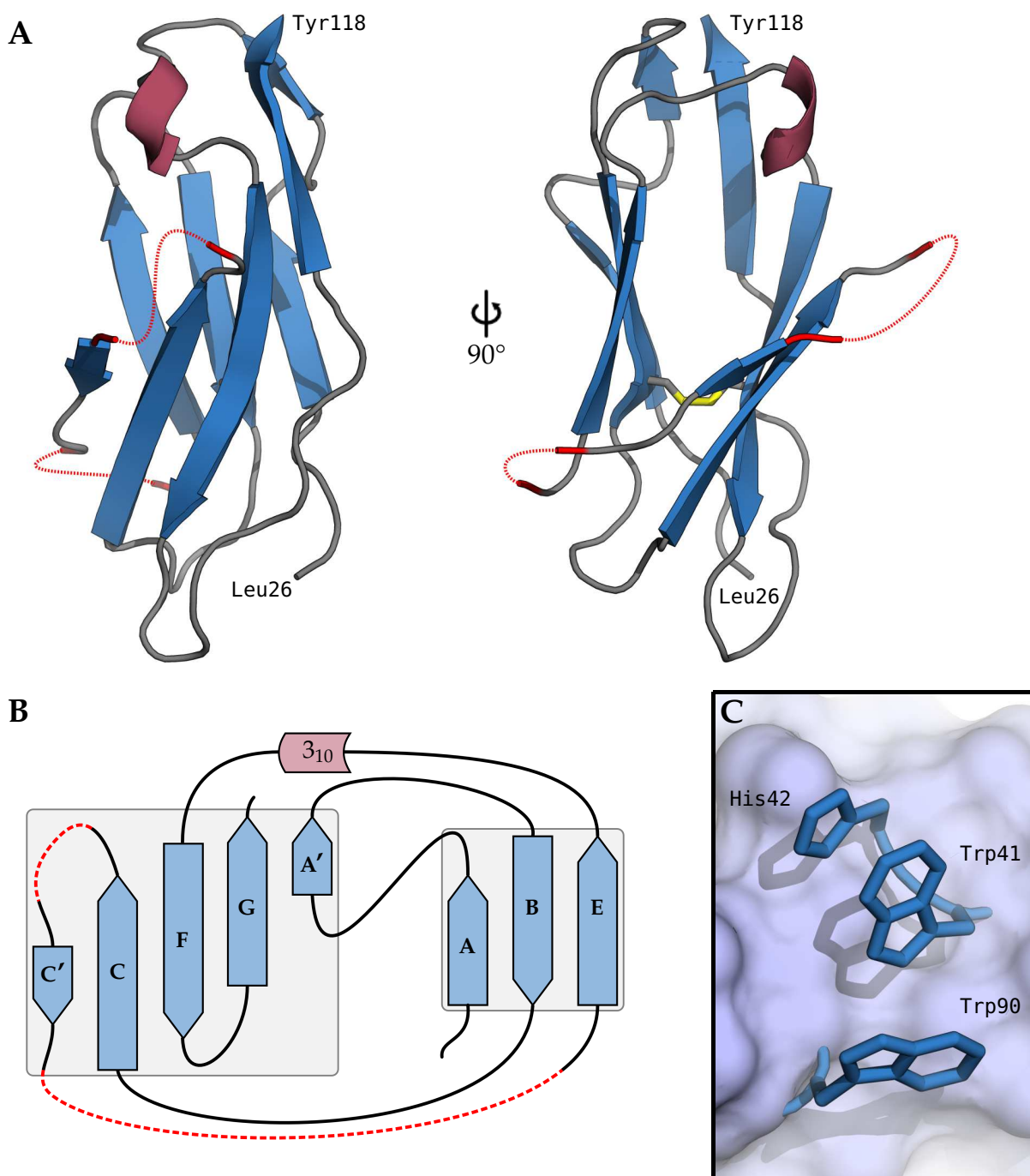


Figure 4.10 Crystal structure at 1.55 Å resolution and topology of ILT7(D1). (A) Cartoon representation of the structure showing the disulfide-linked β -sandwich fold characteristic of Ig-like domains. The 3_{10} helix connecting strands E–F is shown in pale red and the extremities of missing fragments are highlighted in light red. (B) Topology of the two β -sheets mirroring the structural features highlighted above (not to scale). (C) Possible interaction by π -stacking between the sidechains of Trp41, His42 and Trp90 at the C-terminal end of the protein.

The C' strand is located in the more poorly defined part of the electron density map, and the two extended loop regions connecting it to either side are entirely missing. Interestingly, this “lateral loop” region (residues 64–79) harbours the highest level of sequence variability among LILRs. A closer look at the sequence alignment reveals, however, that sequences cluster into two sets corresponding to the MHC- and non-MHC-binding receptors, respectively. Furthermore, by comparing the structures of the D1 domains of currently available LILRs from the two subgroups, it becomes evident that a clear distinction can be made between the lateral loop structures of both subgroups (Figure 4.11). Notably, the C' strand seems to be conserved among group 2 receptors, while in MHC-binding LILRs it is replaced by a partially α -helical loop. The crystal structures of ILT2/B1 and ILT4/B2 in complex with MHC molecules (PDB 4N00 and 2DYP) show that in both cases the helical lateral loops interact with the α 3 region of the HLA heavy chain as well as with the β 2-microglobulin subunit. However, since no interactions of group 2 LILRs have so far been characterised in depth, it is impossible to hypothesise that the lateral loop similarly acts a binding interface in these receptors.

4.3.3 Interaction with the tetherin ectodomain

Despite the lack of information on the residues involved in the interaction between ILT7 and tetherin we speculate that, given the elongated arrangement of other Ig-like proteins such as CD4 (PDB 1WI0), the D1 domain of ILT7, being the most distal from the membrane, is likely to be involved in binding to tetherin on the surface of a neighbouring cell or virus particle. We therefore assessed the interaction of tetherin with recombinant ILT7(D1) using different biophysical techniques. The production of recombinant tetherin ectodomain (residues 47–159) had been established in our laboratory prior to the start of this project. The protein is highly overexpressed in bacteria and is easily purified by nickel affinity and size exclusion chromatography (Figure 4.12).

In a first approach, we used surface plasmon resonance (SPR), which measures the interaction of a soluble analyte to a ligand that has been immobilised on an inert surface. In a first experiment, tetherin was covalently coupled to an SPR sensor chip by amine-coupling, followed by injection of purified ILT7(D1) at several concentrations (Figure 4.13A). The reverse experiment was conducted with ILT7(D1) immobilised to the sensor surface and tetherin applied as an analyte (Figure 4.13B). However, in neither case could any specific binding be detected. A possible explanation for the lack of interaction in the second experiment could be that the binding interface on the immobilised ligand was made inaccessible by the primary amine-mediated attachment to the sensor surface. In the case of ILT7, four out of five lysines are indeed found in or immediately adjacent to the lateral loop region. Given the compact dimensions of the protein, even immobilisation via the N-terminal amine or Lys8 could lead to the protein being attached in a unique orientation with a hidden binding interface. We also

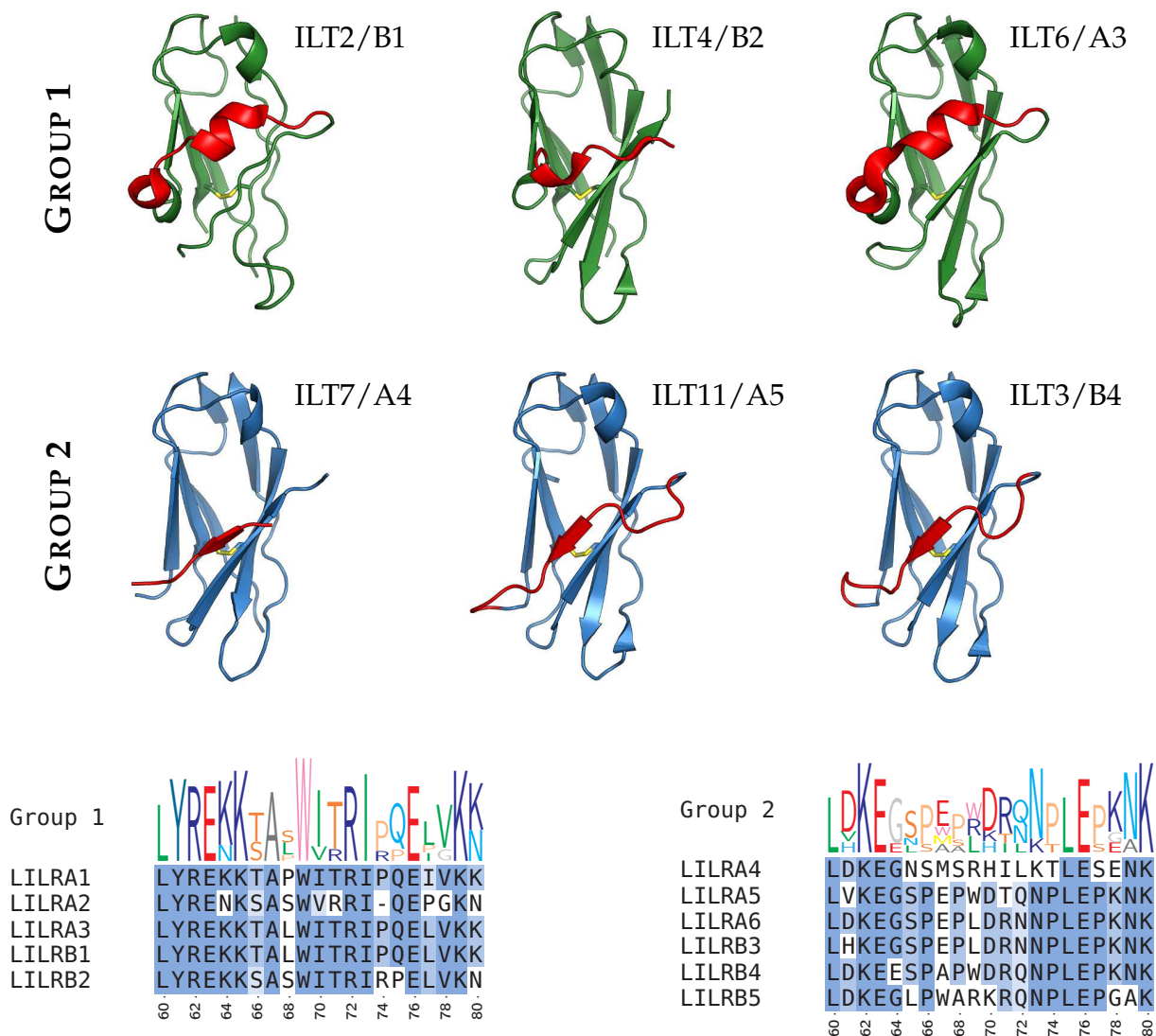


Figure 4.11 Comparison of LILR D1 domain structures. **(top)** Structures of LILRs belonging to subgroups 1 (MHC-binding) and 2 (non-MHC-binding) are shown in green and blue, respectively. PDB identifiers for the represented structures are: 1G0X (B1), 2GW5 (B2), 3Q2C (A3), 2D3V (A5) and 3P2T (B4). The “lateral loop” region is highlighted in red. **(bottom)** Multiple sequence alignments and sequence logos showing different conserved features within the “lateral loop” regions of two subgroups.

studied the interaction by isothermal titration calorimetry (ITC), using tetherin(47–159) as a titrant (Figure 4.13C). In contrast to SPR, no covalent modification of either binding partner is required for ITC and all binding interfaces should be exposed. Nonetheless, no interaction could be measured over a titration range of 4.7–88.1 μ M tetherin, corresponding to molar ratios of 0.1–3.3 tetherin over ILT7.

Microscale thermophoresis (MST) is a technique based on the differential diffusion of molecules in a temperature gradient. The degree of thermophoresis of a molecule

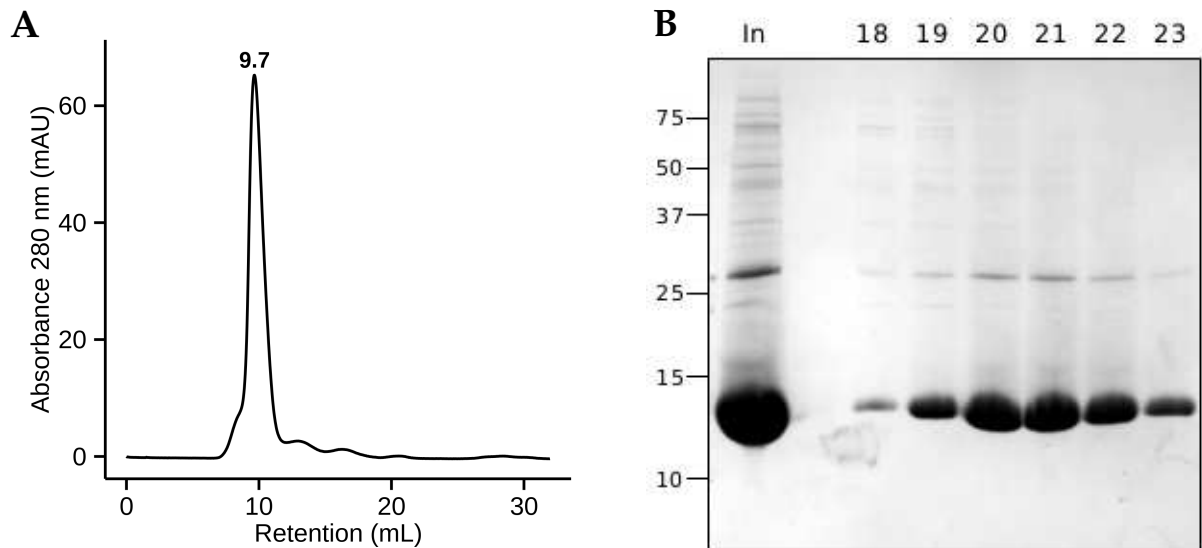


Figure 4.12 Purification of tetherin(47–159). (A) Size exclusion chromatography on a Superdex 75 column and (B) SDS-PAGE showing sample before injection (In) and fractions 18–23 corresponding to the chromatogram peak at 9.7 mL.

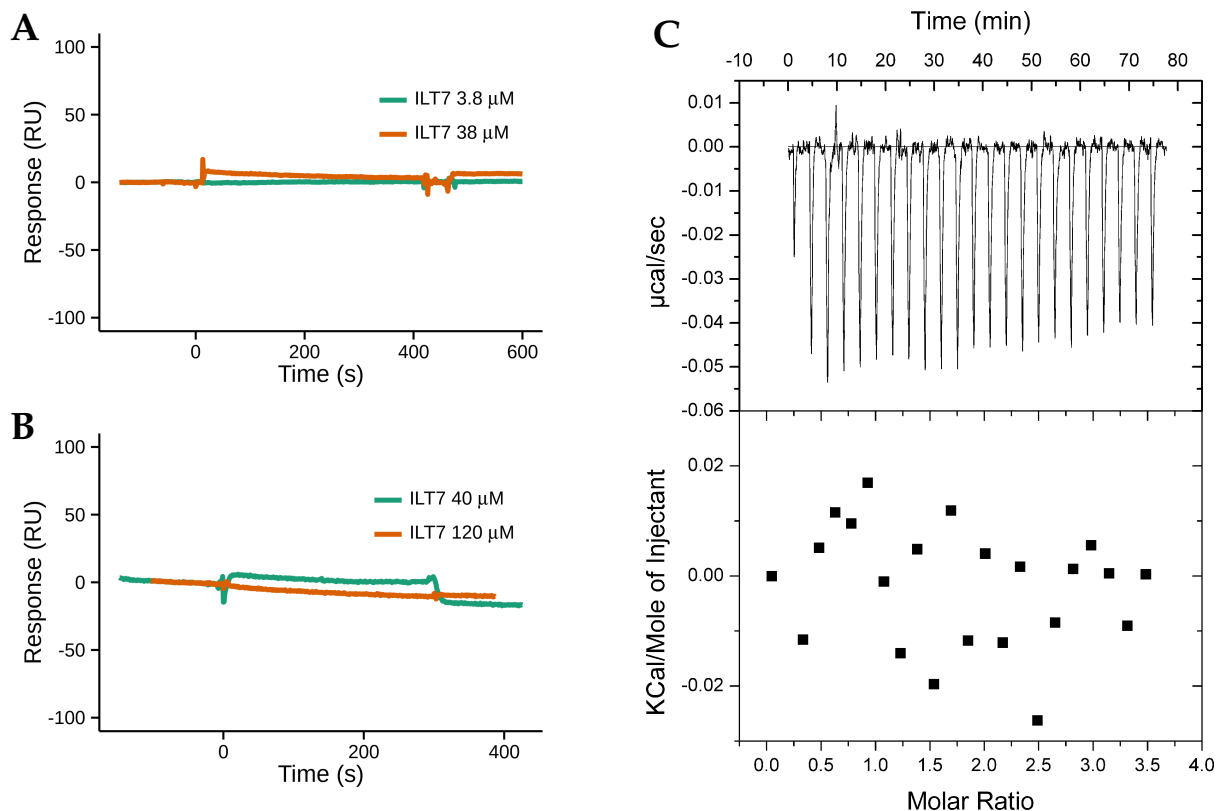


Figure 4.13 Analysis of ILT7(D1) interaction with tetherin (47–159) by SPR and ITC. SPR sensorgrams of (A) ILT7 interaction with immobilised tetherin and (B) tetherin interaction with immobilised ILT7. (C) ITC analysis using tetherin as a titrant. Raw (top) and integrated (bottom) data are shown representing a single experiment.

depends on its size, charge and solvation entropy. The effects of desolvation, size increase and changes in charge caused by complex formation are thus reflected by a change in thermophoresis. Binding kinetics and affinity are determined by labeling one of the potential interaction partners with a fluorescent dye, against which the second molecule is titrated. Thermophoresis is then measured for each sample and binding parameters can be derived from the resulting titration curve. The experimental setup consists in pre-mixing a constant amount of the fluorescent interaction partner with the serially diluted second molecule, and allowing equilibrium to be reached. In a first step, ILT7(D1) was labeled using an amine-reactive fluorescent dye and purified by size exclusion chromatography (Figure 4.14A). After optimisation of the experimental parameters, two experiments were conducted using tetherin(47–159) as a titrant at concentrations of 6–200 000 nM and ILT7(D1) at a constant concentration of 200 nM. Representative data from one experiment, with triplicate measurements for each concentration point, are shown in Figure 4.14B–D. The data fail to show a change in thermophoresis with increasing ligand concentrations, suggesting that no interaction is taking place. Interpretation of the observed increase in cold fluorescence is difficult, although it could theoretically result from complex formation and thermodiffusion in the absence of heating. More likely, however, it reflects a non-specific interaction of the titrant with the capillary surface or aggregation.

4.3.4 Functional activity

In the absence of binding in the *in vitro* assays outlined above, we addressed the interaction of purified ILT7(D1) with cell surface-expressed tetherin in collaboration with the laboratory of Prof Eric Cohen at the Institut de Recherches Cliniques de Montréal (Montréal, Canada). As tetherin dimers form clusters on the cell surface, and are suspected to assemble into higher order multimeric structures, it is indeed possible that high avidity is required for a strong interaction. Purified ILT7(D1) was fluorescently labeled as before, and used by our collaborators to probe tetherin-expressing HEK 293T cells for analysis by flow cytometry (Figure 4.15). However, as in our previous experiments, no binding activity could be observed for ILT7(D1).

4.3.5 *In silico* docking of the tetherin coiled-coil domain

Our combined results on the tetherin-binding activity of recombinant ILT7 suggest that the D1 domain might not be involved in the interaction, or might participate only weakly. To identify any potential partial binding interfaces on the D1 domain, we performed *in silico* docking based on the crystal structures of ILT7(D1) and tetherin(80–147) obtained in our laboratory (PDB 2X7A). Although more complete crystal structures of the tetherin ectodomain are available, all of them were obtained under reducing conditions and do thus likely not correspond to the native conformation found on the

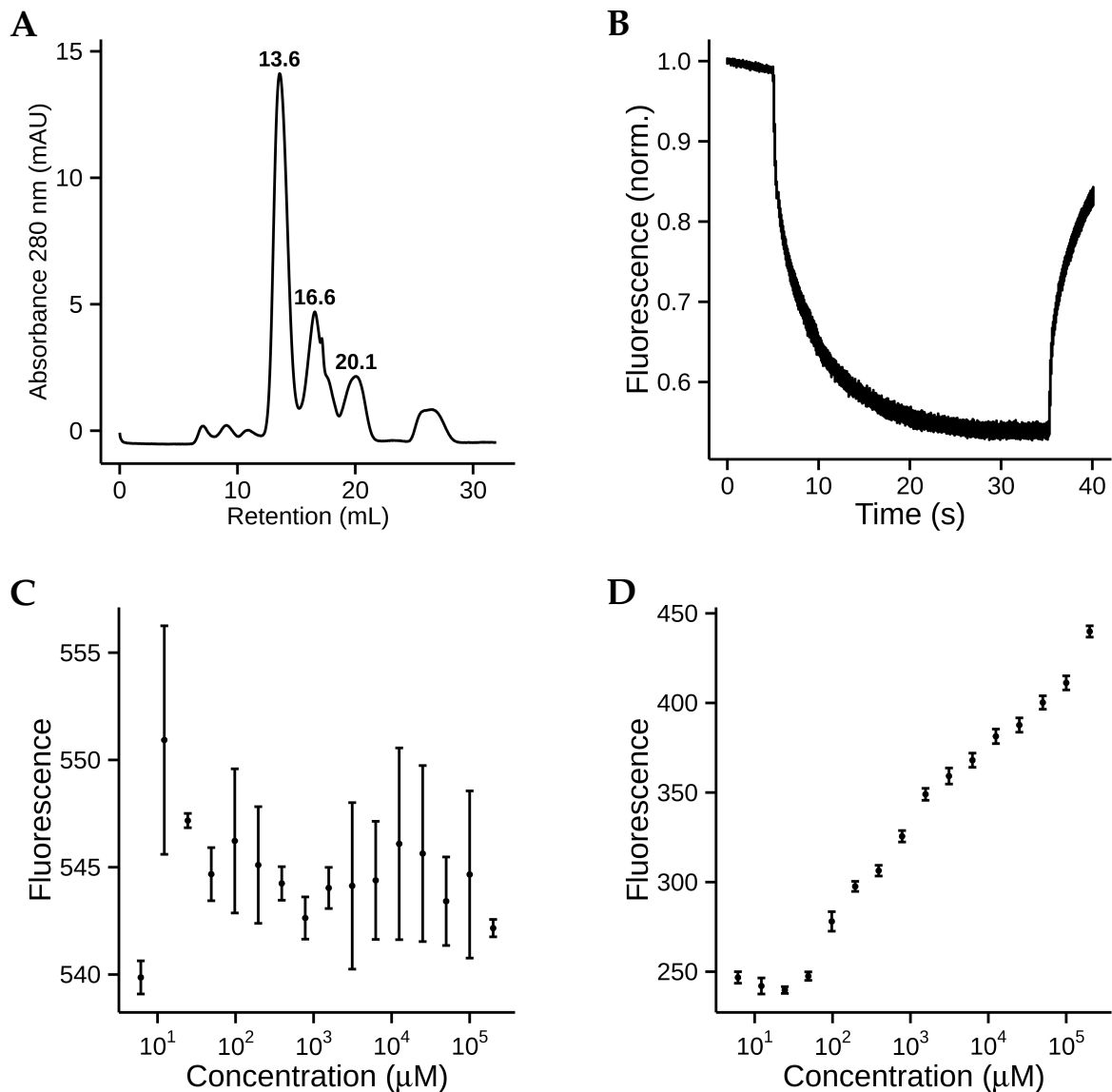


Figure 4.14 Analysis of tetherin(47–159) binding to ILT7(D1) by microscale thermophoresis (MST). (A) Size exclusion chromatography of fluorescently-labeled ILT7(D1) on a Superdex 75 column. (B) Normalised fluorescence curves from a representative MST titration series. Titration curves showing (C) thermophoresis with no evident trend relative to tetherin concentration, and (D) cold fluorescence levels following a linear or sigmoidal trend. Error bars represent the standard deviation around the mean from three measurements, after removal of outliers.

cell surface. The ClusPro docking server scores rigid body docking solutions using four different parameter sets, namely hydrophobic-favoured, electrostatic-favoured, combined van der Waals (VdW) and electrostatic interactions, as well as a balanced option combining equal contributions from all types of interaction. The top 1000 results for each parameter set are then clustered based on their root mean square deviation (RMSD) and a consensus model is calculated for each of the ten largest clusters, all of

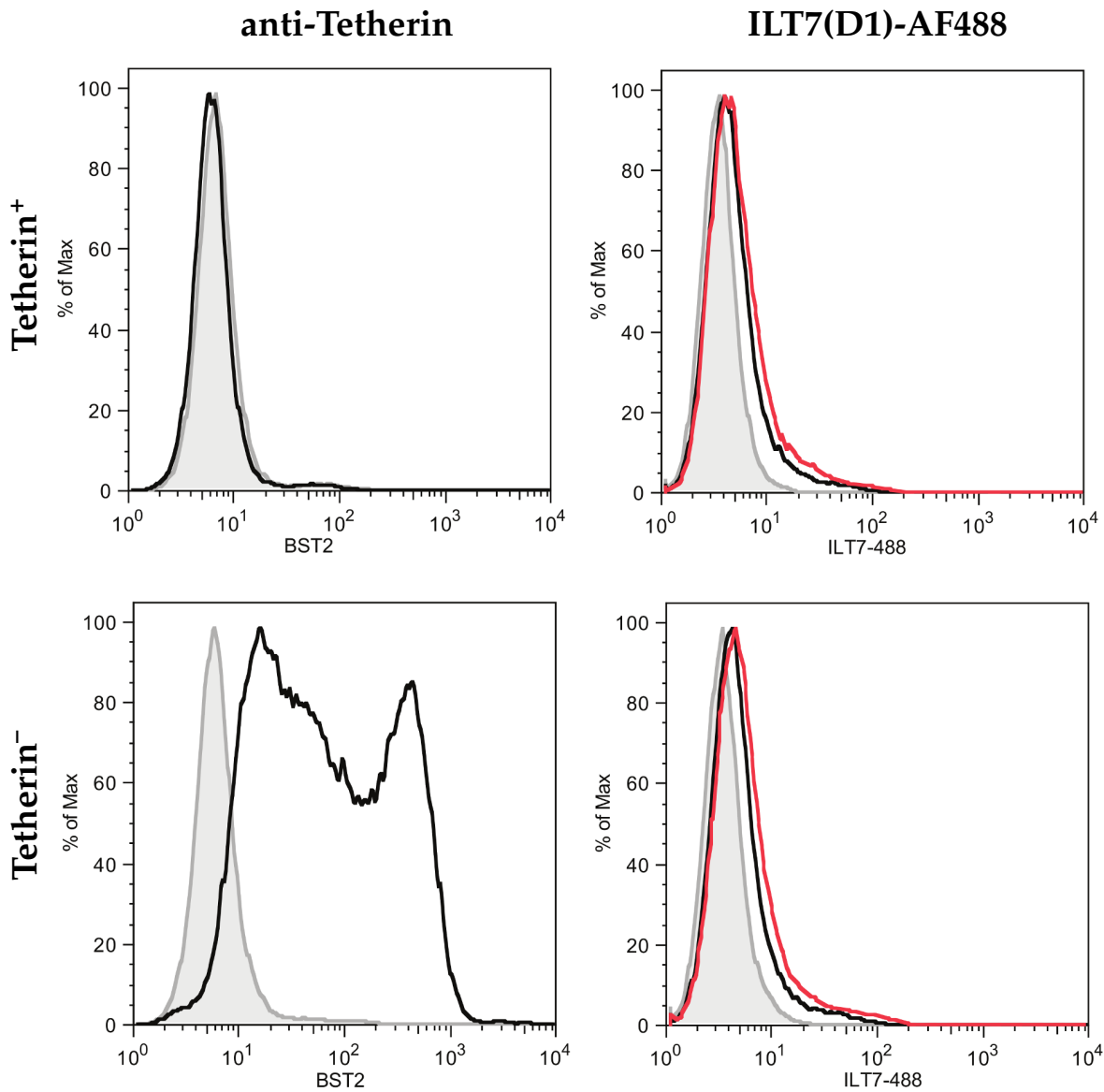


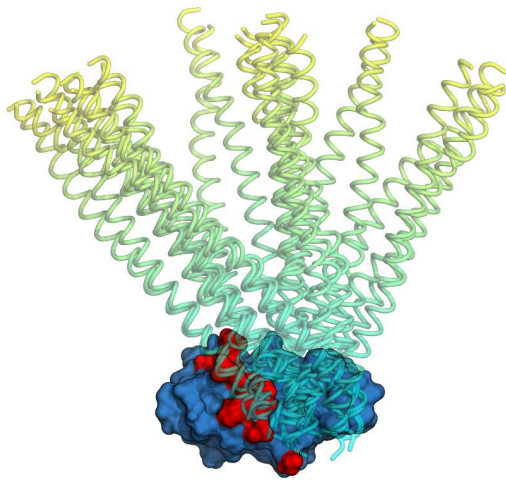
Figure 4.15 Flow cytometry analysis of ILT7(D1) binding to tetherin-expressing cells. Cell surface levels of tetherin (**left**) or tetherin–ILT7(D1) (**right**) as revealed by staining with anti-Tetherin polyclonal serum or fluorescently-labeled ILT7(D1), respectively. (**top**) Non-transfected tetherin⁻ HEK 293T cells and (**bottom**) cells transiently transfected with wild-type tetherin. Also shown are the signals from staining with isotype-matched control antibody (light grey). *Figures kindly provided by Dr Mariana Bego.*

which are then ranked by cluster size.

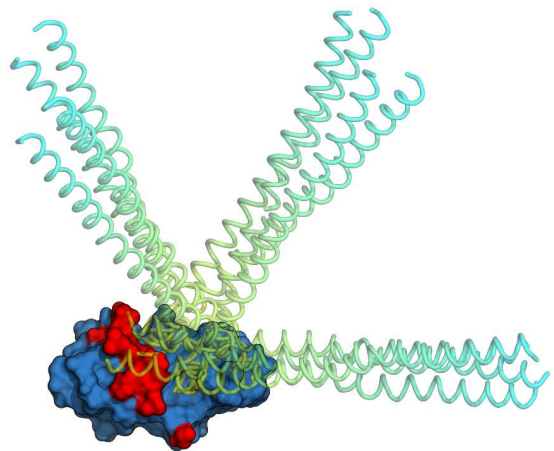
We analysed the ten most highly ranked clusters for each of the balanced, electrostatic and hydrophobic coefficients, and found that the results could be divided into four sets, based on the respective binding interfaces (Figure 4.16A–D). Set-1 contains 12 unique models that are characterised by an interaction near the N-terminal end of the tetherin coiled-coil, whereas set-2 contains 6 models where binding involves the C-terminus of tetherin. However, given the lack of residues 148–159 in the tetherin crystal

structure, set-2 models were considered artifactual because they would be physically incompatible with wild-type tetherin. Interestingly, all of the set-1 and -2 complexes returned by the server involve the “lateral loop” region of ILT7. The third set of docked structures contains 6 unique models, all of which were ranked based on hydrophobic interaction criteria and involve binding of the tetherin N-terminus to the C-terminal end of the ILT7 domain. Finally, set-4 comprises all ten models ranked according to the VdW coefficient and are based on the interaction between a central region of the tetherin coiled-coil with the lateral loop of ILT7(D1).

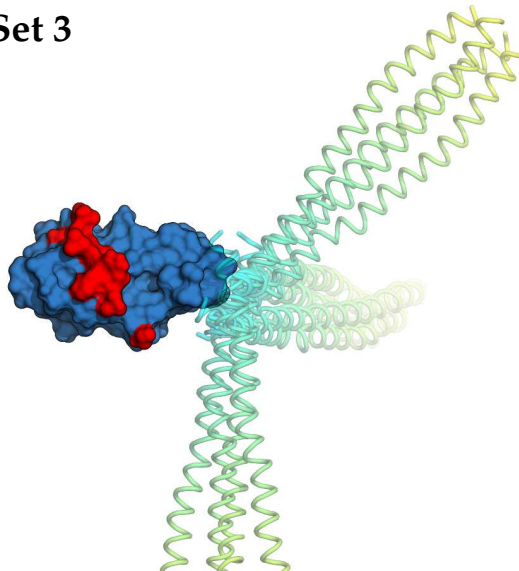
Set 1



Set 2



Set 3



Set 4

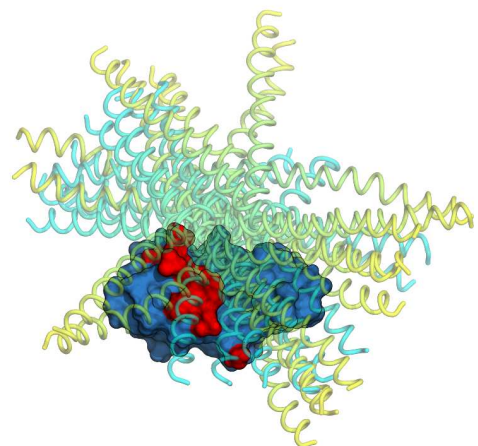


Figure 4.16 *In silico* docking of ILT7(D1) to the tetherin coiled-coil domain. The different interaction models are overlaid according to the four pairs of recurring binding interfaces that could be identified. Surface-rendered ILT7 is shown in blue with the “lateral loop” region highlighted in red. Tetherin ectodomain coiled-coils are represented as tubes with spectral colouring from N- (blue) to C-terminus (yellow).

In order to characterise the predicted interfaces in more detail, the two most highly ranked models from set-1 and -3 were used to identify interfacing residues and determine physico-chemical properties underlying the interaction. We found that in the set-1 complex, several residues located in the ILT7 lateral loop region may form possible hydrogen bonds with one tetherin monomer (tetherin-A), including Ser68, Arg69 and His70. A potential salt bridge may also exist between ILT7_Lys82 and tetherin-A_Asp103 (Figure 4.17A). Contacts with the second tetherin monomer (tetherin-B) are more difficult to interpret, but the ILT7 interface features a number of buried hydrophobic residues, as well as several charged (Asp61 and Lys62) and polar (Ser87, His92 and Tyr96) sidechains. The involvement of these latter residues is questionable however, since all of them are highly conserved among LILRs. On the other hand, the potential tetherinA contacts are part of the highly polymorphic region ${}_{65}\text{NSMSRHILKT}_{74}$, and might thus be relevant for ligand-binding. Using the PISA server, the combined surface area between ILT7 and the tetherin dimer was calculated to be 772.2 \AA^2 , with solvation free energies (ΔG) of $-2.5 \text{ kcal mol}^{-1}$ ($p = 0.534$) and $-8.7 \text{ kcal mol}^{-1}$ ($p = 0.436$) for the binding of tetherin-A and -B subunits, respectively. In comparison with the properties calculated for the interaction between tetherin monomers ($A = 1362.7 \text{ \AA}^2$; $\Delta G = -25.0 \text{ kcal mol}^{-1}$), these figures appear rather low and might hint at a likely involvement of a further interface on the D2 domain, in a similar fashion to ILT4/B2 binding to HLA-G (Figure 1.10, p. 46). The p -value associated with the free energy gain upon solvation of the first tetherin subunit also suggests a non-specific interaction ($p > 0.5$). In the case of the set-3 model, a single pair of potential hydrogen bonds was found between Glu91 and the backbone of the tetherin-B monomer (Figure 4.17B). The interface mainly consists of hydrophobic residues, including Trp41, Met89, Trp90, Ala93 and Val117 as well as the polar sidechains of His42 and Thr118. It is worth noting, however, that all of these residues except His42 and Met89 are well conserved among LILRs. The estimated gains in solvation free energy for binding to tetherin-A and -B, respectively, are $-5.6 \text{ kcal mol}^{-1}$ ($p = 0.325$) and $-3.3 \text{ kcal mol}^{-1}$ ($p = 0.481$), with an interface area of 394.8 \AA^2 . Based on these observations, the set-3 docking solutions appear to represent a more specific interaction, but might again reflect only a partial tetherin binding site.

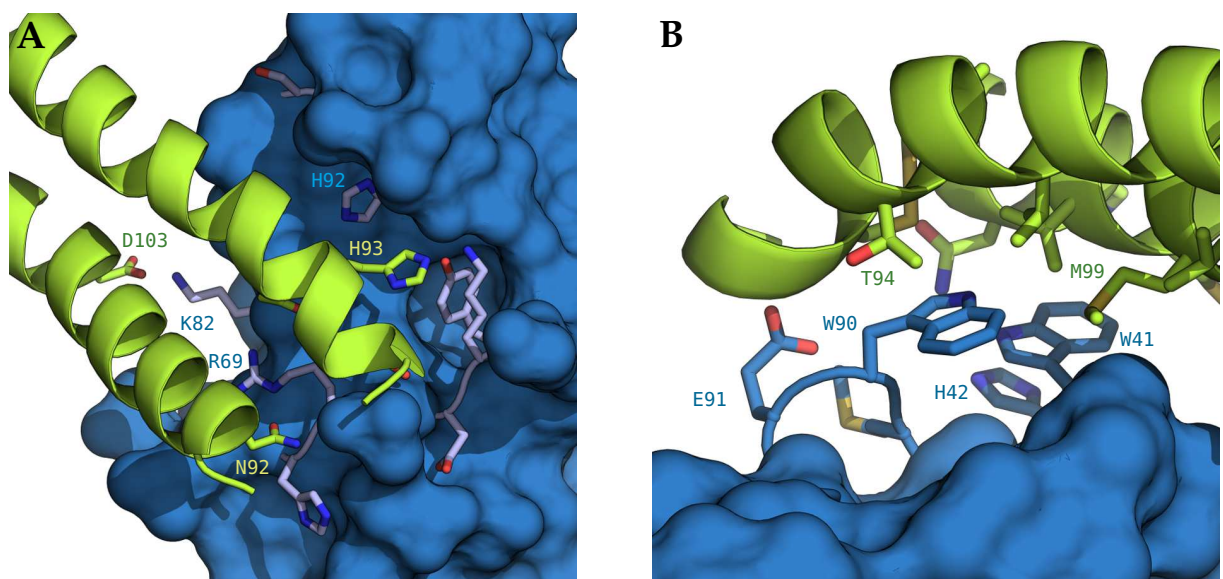


Figure 4.17 Tetherin–ILT7(D1) binding interfaces predicted by *in silico* docking. Models of the complexes formed between the N-terminal tetherin coiled-coil domain and (A) the “lateral” loop region of ILT7(D1), or (B) the C-terminal end of the ILT7 D1 domain. The shown interactions are representative of set-1 and set-3 models, respectively.

4.4 Tertiary structure prediction and *in silico* docking of ILT7(D1-2)

In the absence of a more complete ILT7 crystal structure, we performed a computational prediction of the ILT7(D1-2) tertiary structure using the multiple-template fold recognition software RaptorX. While a prediction is not expected to have the accuracy of an experimentally determined structure, given the apparent high level of sequence and structure conservation among LILRs, such a model might nevertheless provide hints for the characterisation of the interaction with tetherin.

4.4.1 Predicted tertiary structure

The predicted structure was calculated using the crystal structures of ILT3/LILRB4 and ILT11/A5 as templates (PDB 3P2T and 2D3V) and comprises residues 24–215. The generated alignment had a score of 144, with 55 % sequence identity for a target sequence length of 192 residues. The absolute quality of the resulting model is very high, as judged by a global distance test (GDT) score of 83 (unnormalised GDT=160) and a p -value of 2.1×10^{-11} . Furthermore, structural alignment between the experimental and predicted D1 domains results in an RMSD of 0.413 Å for C α atoms ($n = 74$) and 0.5 Å for all atoms ($n = 497$). Hence, the predicted structure of the D1 domain is quite accurate.

The overall structure and topology of the D2 domain is nearly identical to that of D1, with the difference of having an additional short β -strand (C'') forming a β -hairpin motif with the N-terminal end of strand E, as well as lacking strand A' (Figure 4.18A). Interestingly, the two domains are arranged at a right angle relative to each other and this conformation appears to be stabilised by two extended loop regions on the D2 domain. Potential contacts along the D1/D2 interface were identified by searching for pairs of residues in either domains with C α atoms located within a 8 Å distance (Figure 4.18B). In addition to several possible polar contacts between backbone atoms and the sidechains of Glu114 and Tyr204, the interface comprises a large number of hydrophobic residues. Overall, the sequence of the D2 domain is more conserved among LILRs, and based on the multiple sequence alignment (p. 49) and in contrast with D1, the lateral loop region comprising the C'–C'' strands features very few polymorphisms. On the other hand, variable patches of less conserved residues are found on the C-terminal face of the domain and together with the C' region of D1, forms a broad exposed surface (Figure 4.18C).

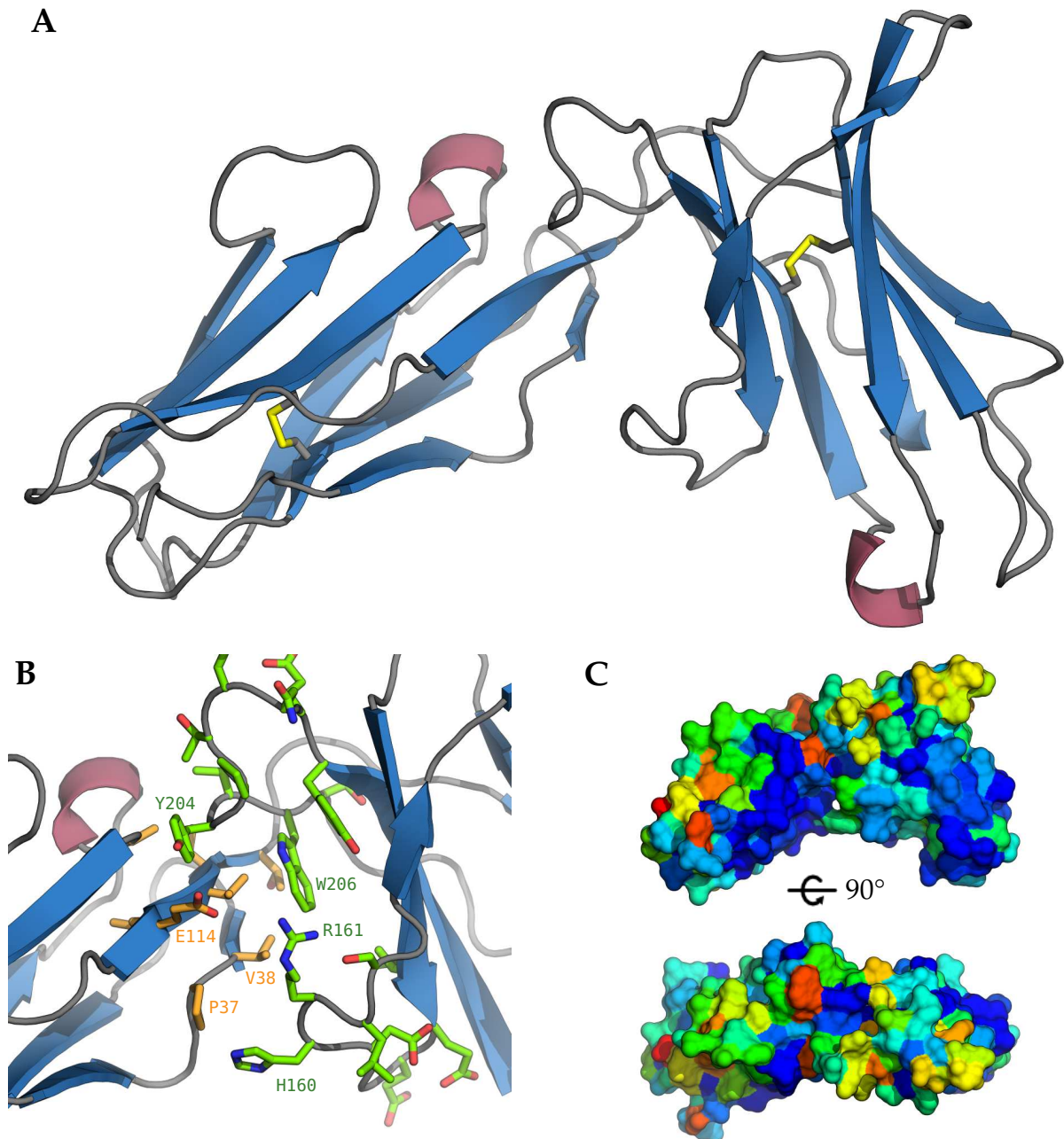


Figure 4.18 Predicted tertiary structure of ILT7(D1-2). **(A)** Structure of domains D1 (left) and D2 (right) coloured by secondary structure elements. **(B)** Detailed view of the D1/D2 interface, with potentially contacting residues ($C\alpha$ at $< 8 \text{ \AA}$) represented as sticks. Sidechains coloured in orange and green are part of the D1 and D2 domains, respectively. **(C)** Surface-rendered structure with colour scheme based on sequence conservation, from high (blue) to low (red).

4.4.2 *In silico* docking of the tetherin coiled-coil domain

In a next step, we repeated the *in silico* docking experiment using the predicted two-domain structure of ILT7. If both domains are indeed required for efficient binding and the interaction involves the coiled-coil domain of tetherin, we would expect results

with increased gains in solvation free energy ($\Delta G \ll 0$). We proceeded as before and could again split the resulting models into five sets, based purely on the topology of the interacting regions (Figure 4.19). Set-1 complexes were based on the interaction with the C-terminus of the tetherin coiled-coil and were thus not further considered because of their biological irrelevance. Set-2 contained the largest number of unique solutions (20 out of 79), including the most highly ranked results based on balanced, electrostatic and hydrophobic criteria. The set-2 complexes notably involve the external side of the D1/D2-linking region of ILT7, as well as the N-terminal end of the tetherin coiled-coil. Based on the relative orientation of tetherin, three subsets of complexes can be distinguished (a–c), of which set-2a represents all of the most highly ranked clusters returned by the docking algorithm. Sets 3 and 4 contain a small number of models that, respectively, show binding of the tetherin N-terminus to the inner side of the D1/D2-linking region and binding of the C-terminal half of the coiled-coil to the ABE β -sheet of the D2 domain. Finally, a number of diverse solutions were obtained with the fourth ranking coefficient, which favours weak VdW interactions. These models share a common interface between the central region of the tetherin coiled-coil with the ABE β -sheet of the D2 domain, but were not further analysed because of the large variability within the set.

As before, we attempted to characterise the interfaces of the best docking models in more detail in order to identify potential ILT7 residues or regions involved in the interaction with tetherin. For the set-2a model, we found a 554.7 \AA^2 interface with a solvation free energy gain of $-9.6 \text{ kcal mol}^{-1}$ ($p = 0.256$) and $-2.2 \text{ kcal mol}^{-1}$ ($p = 0.461$) upon binding of each of the two tetherin monomers, respectively. Based on the analysis of atomic distances and buried surface area, merely one potential hydrogen bond was found between the sidechains of the ubiquitously conserved ILT7_Tyr120 and tetherinA_Asn92, suggesting that the interaction is mainly mediated by a number of buried hydrophobic residues (Figures 4.20A). In the case of the most highly ranked model from set-3, the interface features three potential hydrogen bonds and one salt bridge between ILT7_Glu34 and tetherinA_Lys106, in addition to a number of hydrophobic and polar residues found within contact distance (Figure 4.20B). However, the estimated gain in solvation free energy of $-7.8 \text{ kcal mol}^{-1}$ ($p = 0.588$) and $-6.0 \text{ kcal mol}^{-1}$ ($p = 0.446$) for a combined surface area of 888 \AA^2 suggests a less-specific interaction than that observed for set-2a. Similarly, results obtained for the best model from set-4 indicate a probably non-specific interaction, as assessed by free energy calculations.

Interestingly, visual comparison of the docking results obtained with experimental and predicted structures of ILT7 reveals similar regions involved in set3 (D1) and set2a (D1-2) complexes. Indeed, a number of potential contacts are found in both models, notably between ILT7 residues Trp41, Trp90, Val117, and tetherin residues ${}_{90}\text{TCNHTVM}_{96}$, Leu98 and Met99. Nonetheless, given the relatively low contribution of these residues in terms of solvation energy, the bulk of the interaction seems to be mediated by con-

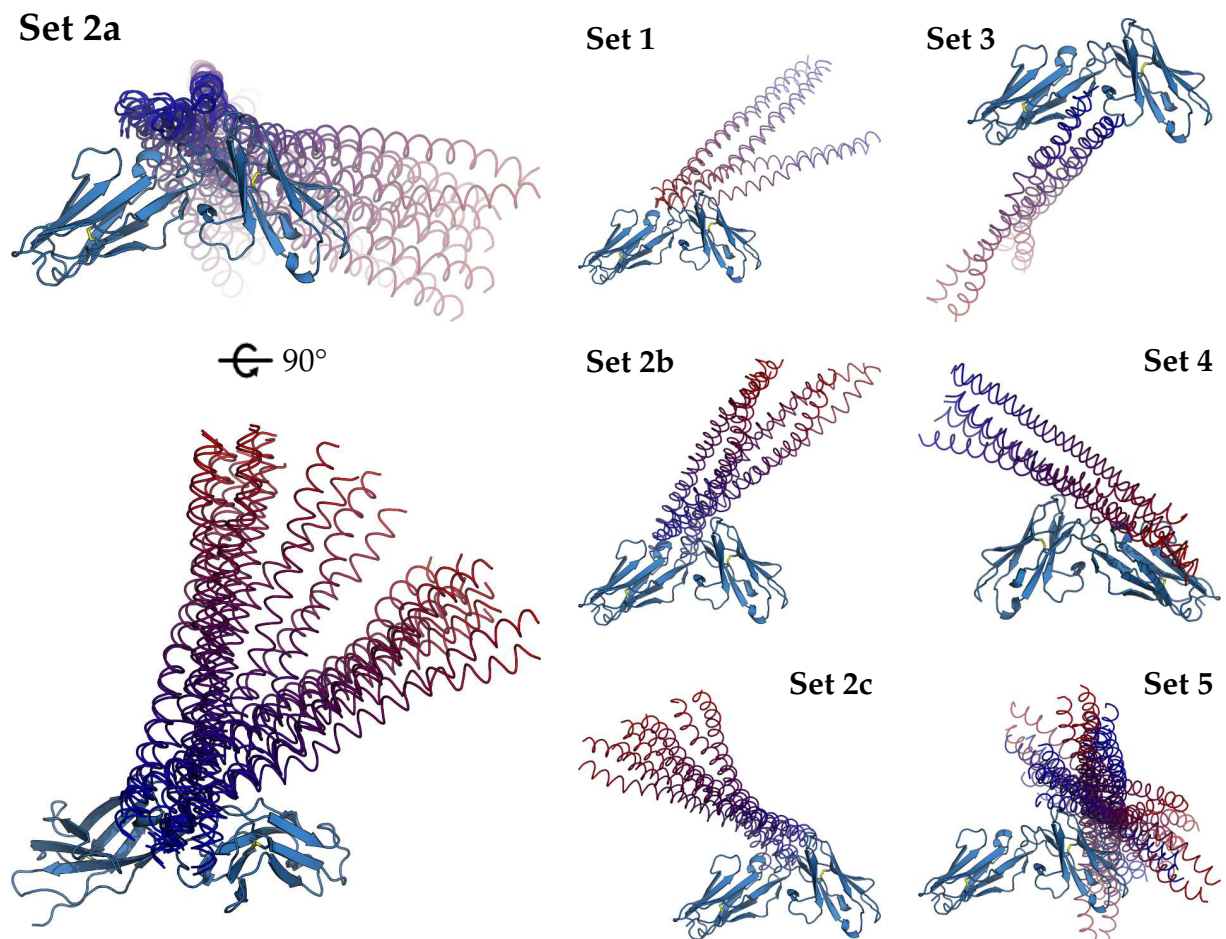


Figure 4.19 *In silico* docking of ILT7(D1-2) to the tetherin coiled-coil domain. The models corresponding to each set of docking solutions are overlaid, with tetherin chains represented as tubes coloured from N- (blue) to C-terminus (red). The predicted structure of ILT7(D1-2) is oriented with the D1 domain (N-terminus) on the left.

tacts with the D2 domain.

4.5 Characterisation of ILT7(D1-4)

The ILT7 extracellular region comprising all four Ig-like domains (residues 24–435) was expressed in baculovirus-infected insect cells and purified from cell culture supernatants as detailed in section 4.2.2. Nevertheless, optimisation of the purification protocol is still ongoing at the time of writing. In this regard, characterisation of ILT7(D1-4) in the context of this thesis has consisted in validating the identity of the protein by peptide mass fingerprinting and testing its ligand-binding properties by SPR.

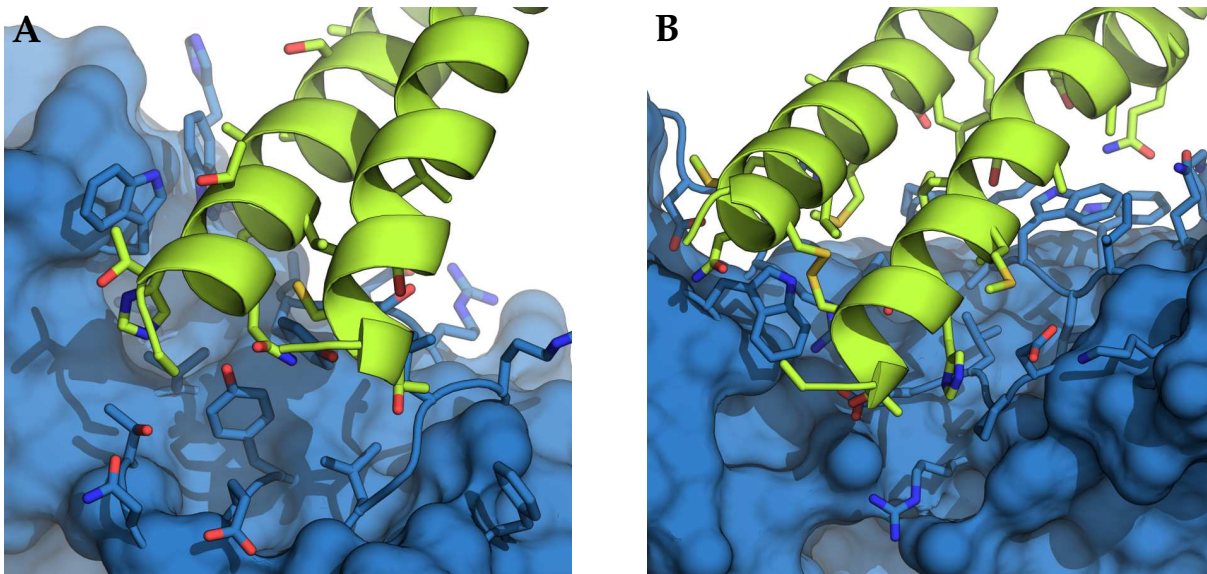


Figure 4.20 Tetherin–ILT7(D1-2) binding interfaces predicted by *in silico* docking. Detailed view of the interfaces representative of set-2a (**A**) and set-3 (**B**) complexes, with potential contact-forming residues represented as sticks.

4.5.1 Peptide mass fingerprinting

Under the experimental conditions and within the mass detection range used, trypsin digestion of the recombinant protein theoretically yields 23 different peptides, or 69 peptides when allowing for one missed cleavage site. The corresponding sequence coverage within the detection range (500–4000 Da) is 60.5% and 65.3%, respectively. The mass spectrometry experiment provided 33 peptide masses of 947.50–3381.48 Da, and a Mascot search against the SwissProt database resulted in 14 matches for ILT7 (Table 4.2A). Although this confirmed the identity of the protein, we next analysed the unmatched peptide masses for the possible presence of amino acid modifications. Merely two of the four peptides containing the putative N-linked glycosylation sites fell within the detection range, having masses of 1899.98 and 3154.67 Da, respectively. A search for N-linked glycoforms that could explain the unmatched peptide masses in conjunction with these two peptides led to a number of compatible glycan structures for the light peptide (Table 4.2B). Considering an average glycan mass of 1–1.5 kDa, it is likely that glycosylated forms of the heavy peptide were not detected in the experiment. The results are consistent with the high-mannose glycosylation expected to be found on insect cell-expressed proteins, which are composed of a minimum of two N-acetylglucosamine (GlcNAc) molecules followed by three mannose molecules from which further mannose units may branch out. It is thus possible that glycosylation may explain some of the unmatched peptide masses, although experimental evidence will be required. Similarly, one further unmatched peptide mass was found to be compatible with serine/threonine phosphorylation (Table 4.2C), although again,

Range	Mass _{obs}	MC	Sequence	Modifications
A—Matched peptides with known modifications				
83–95	1514.6730	0	LSIPSMWEHAGR	
83–95	1530.6690	0	LSIPSMWEHAGR	Oxidation (1×)
83–95	1546.6580	0	LSIPSMWEHAGR	Oxidation (2×)
152–161	1216.5430	0	FTLIEEGDHR	
162–175	1658.7530	0	LSWTLNSHQHNHGK	
162–190	3381.4790	1	LSWTLNSHQHNHGK FQALFPMGPLTFSNR	Oxidation
176–190	1725.8220	0	FQALFPMGPLTFSNR	
176–190	1741.8170	0	FQALFPMGPLTFSNR	Oxidation
195–222	3230.4780	0	CYGYENNTPYVWSEPSDPLQLLVSGVSR	Carbamidomethyl
258–269	1252.6050	0	EGADGLPQRPR	
358–366	947.4970	0	EGAAHPPLR	
376–394	2112.9130	0	YQAEFPMSPVTSAHAGTYR	
376–394	2128.9130	0	YQAEFPMSPVTSAHAGTYR	Oxidation
400–429	3178.6840	0	SSNPYLLSHPSEPLELVSGATETLNPAQK	
B—Unmatched peptides with potential glycosylation				
270–287	2793.2490	0	QPQAGLSQANFTLSPVSR	(Hex) ₃ (HexNAc) ₂
270–287	2939.3330	0	QPQAGLSQANFTLSPVSR	(Hex) ₃ (HexNAc) ₂ (Dhex) ₁
270–287	3046.5000	0	QPQAGLSQANFTLSPVSR	(Hex) ₅ (HexNAc) ₁ (Pent) ₁
270–287	3110.3590	0	QPQAGLSQANFTLSPVSR	(Hex) ₁ (HexNAc) ₃ (Dhex) ₃
270–287	3167.3700	0	QPQAGLSQANFTLSPVSR	(Hex) ₄ (HexNAc) ₂ (Pent) ₁ (Phos) ₁
C—Unmatched peptide with potential phosphorylation				
340–357	2239.0440	0	VTLLCQSWDPMTFLLTK	Oxid., Phosphorylation (1×)

Table 4.2 List of experimental peptide masses obtained by mass spectrometry and known or potential amino acid modifications. *MC*: number of missed cleavage sites, *Hex*: hexose, *Dhex*: deoxyhexose, *Pent*: pentose, *Phos*: phosphate, *HexNAc*: N-acetylhexosamine.

this observation will have to be confirmed experimentally.

4.5.2 Interaction of tetherin with insect cell-expressed ILT7

In order to assess the activity of insect cell-expressed ILT7, we performed SPR analyses using the tetherin ectodomain as a ligand. Tetherin was expressed as a glutathione S-transferase (GST) fusion protein and purified as before (Figure 4.21). Notably, the presence of GST reduces the risk of masking the binding site by direct coupling to the sensor surface, and alternatively allows coating of the sensor by antibody capture, resulting in a fully exposed tetherin ectodomain.

The GST-Tetherin fusion protein was immobilised on a dextran-coated CM5 sensor chip by amine-coupling. Purified insect cell-expressed ILT7(D1-4) was then applied in different concentrations ranging from 0.08 to 9.6 μM. For each analyte concentration, a relative response curve was recorded after subtraction of the signal from a non-coated reference surface (Figures 4.22A and B). The data show characteristic binding curves

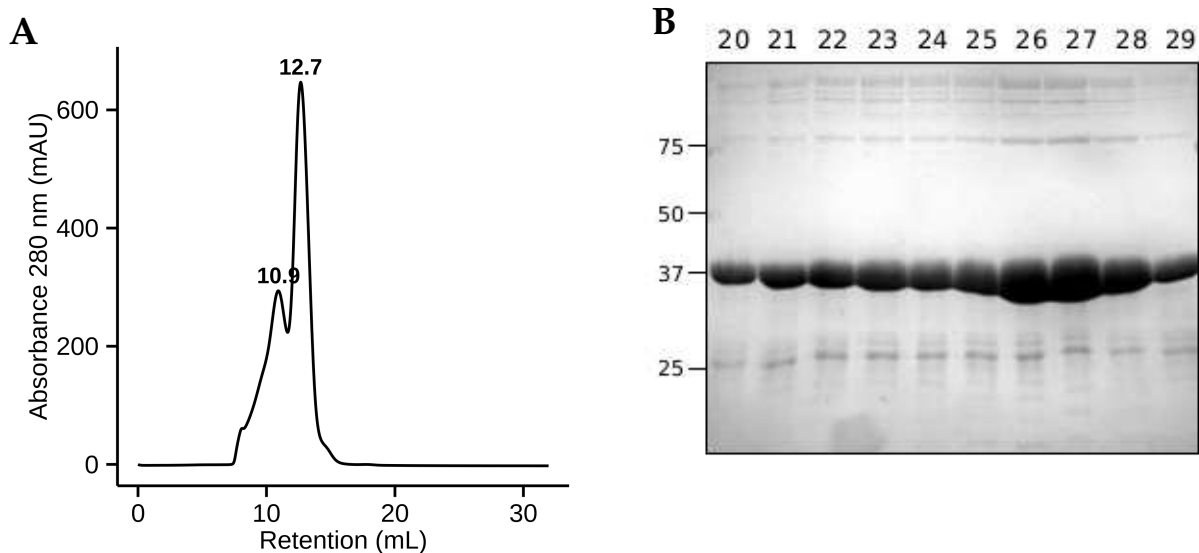


Figure 4.21 Purification of tetherin-GST. **(A)** Size exclusion chromatography on a Superdex 200 column and **(B)** SDS-PAGE of fractions corresponding to the two peaks at 10.0 mL (20–24) and 12.7 mL (25–29), respectively.

with fast on- and off-rates, suggesting a weak but specific interaction. As a negative control for possible non-specific binding of ILT7 to GST, purified GST was coupled to a separate sensor surface under identical conditions and data was recorded using the same analyte samples (Figure 4.22C). These results indicate that although ILT7 does not specifically bind to GST, a small degree of interaction is observed and thus likely contributes to the measured binding response to tetherin-GST. For this reason, description of a binding model and estimation of kinetic parameters was not possible. Moreover, because of the seemingly low affinity, a wider range of analyte concentrations would have to be measured in order to derive an accurate statistical model. Thus, while qualitative interpretation of this dataset validates the interaction between recombinant ILT7(D1-4) and tetherin, fitting of a kinetic binding model has not been attempted because of the narrow concentration range used, as well as the minor contribution of GST to the SPR signal.

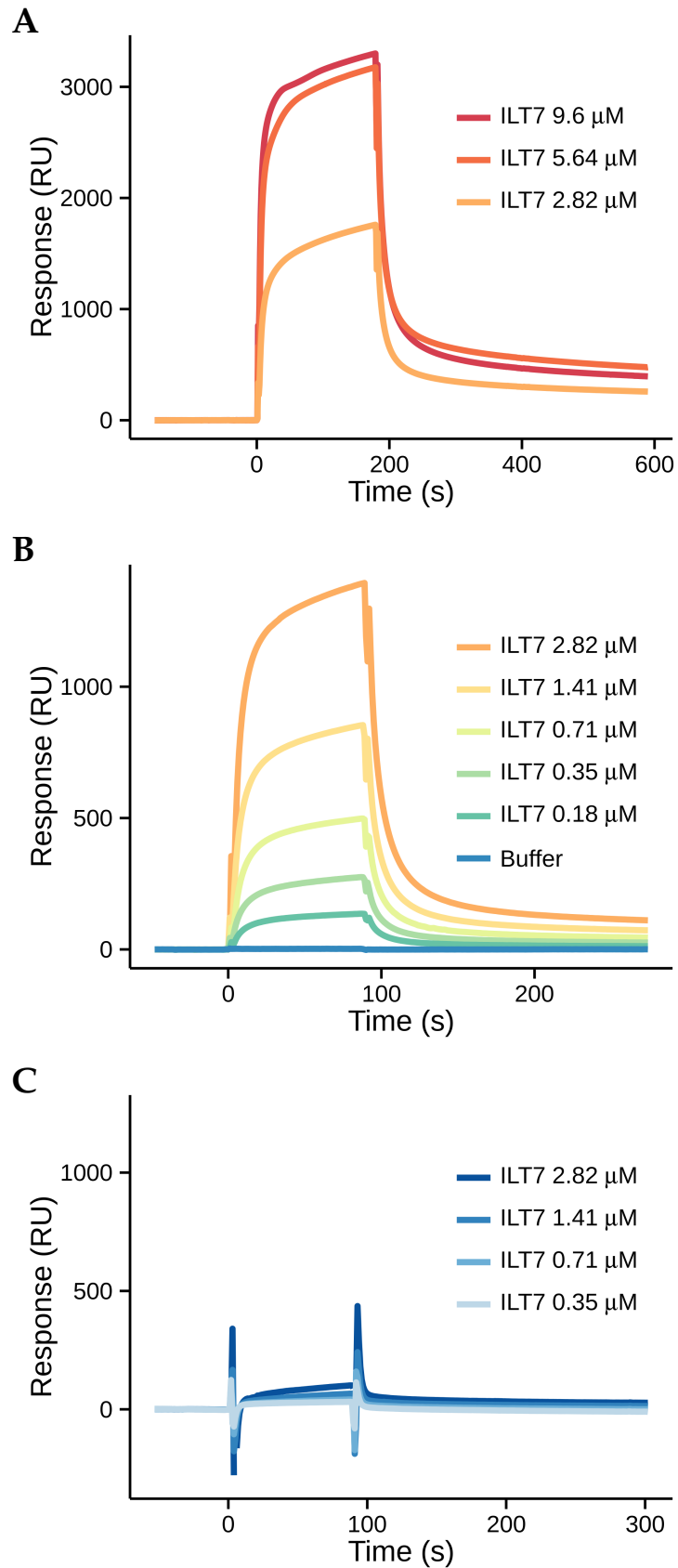


Figure 4.22 SPR sensograms of ILT7(D1-4) interaction with immobilised tetherin-GST. (A) Binding curves obtained with analyte concentrations above or (B) below the expected K_D ($\sim 1 \mu\text{M}$). (C) Negative control experiment showing the interaction of ILT7 with GST.

4.6 Tetherin imaging using biarsenical fluorophores

Immunofluorescent staining of tetherin expressed on the cell surface has shown that the protein is grouped into patches rather than being uniformly distributed across the plasma membrane. Similarly, in the context of HIV-1 particle release, multiple tetherin molecules are found at each viral budding site although the precise number currently remains unclear, having been estimated to range anywhere between 4–400 dimers per budding site. During budding, tetherin molecules also become incorporated into nascent HIV-1 virions, as the protein is readily detected in cell-free viral particles. Interestingly, this occurs despite in the presence of the tetherin antagonist Vpu, suggesting that isolated tetherin molecules, though located at the budding site, are incapable of restricting virus release. We thus hypothesise that a critical local tetherin concentration is necessary for efficient restriction, and that viral particle retention might depend on self-organisation of multiple tetherin dimers into higher order assemblies.

In order to verify the existence of such multimeric assemblies, we proposed to perform fluorescence resonance energy transfer (FRET) measurements on cell surface-expressed tetherin, differentially labeled with the small molecule biarsenical hairpin fluorophores FAsH and ReAsH. FRET can be measured if donor and acceptor are located within 1–10 nm and is generally indicative of a direct interaction in the case of macromolecules. Labeling with biarsenical fluorophores is based on the specific covalent binding of these molecules to a clonable polypeptide tag comprising the tetracysteine (TC) sequence motif CCPGCC. The binding affinity to the TC motif is influenced by the choice of flanking residues, with the sequence FLNCCPGCCMEP for instance resulting in a significantly higher affinity compared to the minimal motif. The differential labeling of low- and high-affinity tags with FAsH and ReAsH, respectively, would be achieved by application of the first fluorophore, followed by treatment with a chelating agent such as British anti-Lewisite (BAL) or ethanedithiol (EDT) to cause its targeted removal from low-affinity tags. The second fluorophore could then selectively be applied to the unoccupied tags. Alternatively, given the high stability of tetracysteine-labeling, recombinant protein could be pulse-labeled, allowing for partial recycling of tetherin from the cell surface between applications of FAsH and ReAsH, respectively.

We generated two different full-length tetherin constructs with the minimal or high-affinity tetracysteine-tag inserted after Tyr155 (tetherin-TC155 and tetherin-FLN155). In a first instance, we verified the functional activity of the recombinant proteins by assessing their ability to restrict the release of HIV-1 Gag virus-like particles (VLPs) from co-transfected HEK 293T cells. We found that both versions of TC-tagged tetherin were able to prevent the release of VLPs into cell culture supernatants, as shown by anti-p24 Western blot of supernatants purified by ultracentrifugation on a sucrose cushion (Figure 4.23B). In a next step, we validated the correct subcellular localisation

of TC-tagged tetherin at the plasma membrane by immunofluorescent staining and confocal microscopy of transiently transfected fixed HEK 293T cells (Figure 4.23A). The images confirm the presence of tetherin at the plasma membrane, and show a strong intracellular signal probably corresponding to the trans-Golgi network.

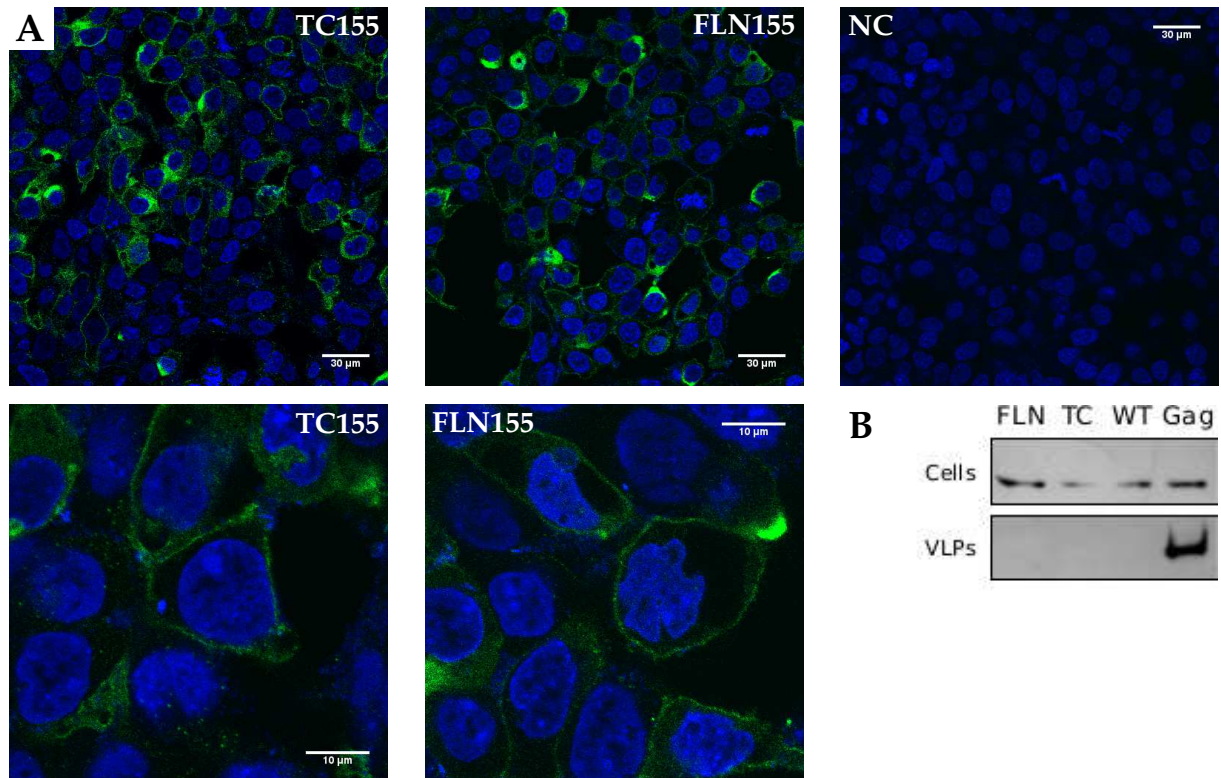


Figure 4.23 Restriction activity and subcellular localisation of TC-tagged tetherin. **(A)** Immunofluorescent staining of TC-tagged tetherin constructs expressed on the cell surface of transfected HEK 293T cells or non-transfected cells (NC). **(B)** Anti-p24 Western blot showing HIV-1 Gag in cell lysates or virus-like particles (VLPs) purified from culture supernatants of HEK 293T cells co-transfected with TC-tagged tetherin (TC155 and FLN155), wild-type tetherin (WT) or transfected with Gag alone (Gag).

For FLAsH labeling, fixed cells were initially treated with the reagent for 30–60 min at room temperature, according to the manufacturer’s instructions (Figure 4.24A). However, due to elevated levels of background fluorescence the labeling conditions needed to be optimised. Shorter labeling times of 1–30 min, as well as treatment before or after paraformaldehyde fixation were attempted, and the specificity of tetracysteine labeling was assessed by immunofluorescent staining of tetherin following labeling with FLAsH (Figure 4.24B–D). Nonetheless, while background levels could be reduced, we continued to observe non-specific staining as well as a failure of the FLAsH signal to significantly co-localise with antibody fluorescence. Given the homodimerisation of tetherin, tetracysteine-mediated labeling may be impeded by disulfide bond formation between some or all of the cysteines within each dimer. Although labeling had been performed in the presence of a reducing agent, we addressed this potential prob-

lem by co-transfecting TC-tagged and wild-type tetherin at different ratios, with the aim of obtaining a population of tetherin heterodimers. As before, we failed however to see a correlation between FIASH and antibody fluorescence (Figure 4.24E).

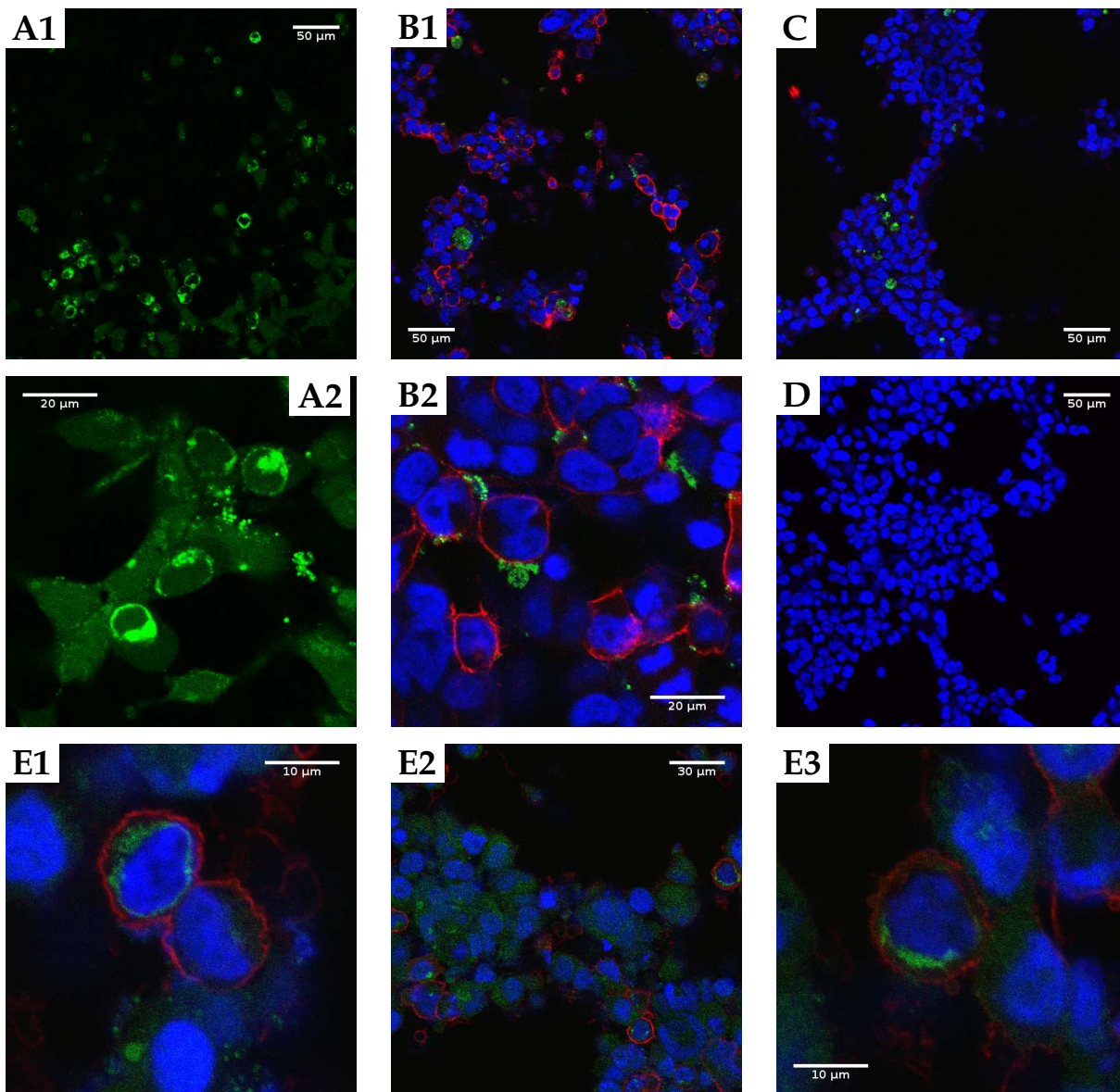


Figure 4.24 FIASH-labeling of tetherin. (A) FIASH-staining of tetherin for 30–60 min shows patchy cell surface as well as intracellular localisation, albeit with elevated levels of background fluorescence. (B) A shorter labeling time of 2 min results in lower background levels, but immunofluorescent staining reveals that FIASH-labeling does not significantly correlate with tetherin expression pattern. Co-transfection of TC-tagged and wild-type tetherin at 1:2 (E1) or 1:5 ratios (E2–3) equally does not improve FIASH specificity. (C) FIASH- and immunofluorescent staining of non-transfected cells and (D) secondary antibody control of tetherin-transfected cells. Colours correspond to signals from anti-Tetherin/anti-rabbit-AF633 immunofluorescence (red), FIASH (green) and the nuclear stain NucBlue (blue).

Discussion (français)

L'objectif principal de ce projet était la détermination de la structure du complexe formé par le récepteur ILT7 avec son ligand, la tétherine. On a rencontré des difficultés majeures pour la production recombinante de l'ectodomaine d'ILT7 dans différents systèmes d'expression, y compris en cellules HEK 293T, cellules d'insecte et *Escherichia coli*. Après de nombreux essais, aucune expression a pu être détectée en cellules 293T, et l'expression de deux ou quatre domaines Ig en cellules d'insecte a également échoué initialement. A cause de la présence de ponts disulfures essentiels au coeur des motifs structuraux de type immunoglobuline (Ig) dont est composé ILT7, l'expression bactérielle n'a pas permis d'obtenir de la protéine soluble. On a cependant réussi à renaturer *in vitro* le domaine N-terminal de la protéine (résidus 24–118) à partir de corps d'inclusion et de résoudre sa structure par cristallographie aux rayons X à une résolution de 1.55 Å.

Finalement, l'ectodomaine entier d'ILT7 (résidus 24–435) a également pu être produit, en ayant recours à l'expression en cellules d'insecte infectées par un baculovirus recombinant. Une quantité limitée de protéine a ainsi été purifiée et soumise à des expériences de résonance de plasmon en surface (SPR) avec l'ectodomaine de la tétherine, afin de confirmer l'interaction. En effet, une interaction directe entre les deux protéines n'a pas été confirmée depuis la publication originale en 2009 (Cao et al., 2009). Au vu des observations récentes par Tavano et al. (2013), contredisant le modèle proposé d'une régulation de l'interféron dans un état inflammatoire, une validation de cette interaction semble essentielle.

De manière surprenante, le domaine D1 seul n'est pas suffisant pour interagir avec le domaine extracellulaire de la tétherine (résidus 47–159) dans nos expériences *in vitro*, ni reconnaît-il la tétherine de type sauvage exprimée à la surface de cellules 293T. Le domaine D1 comprend le plus grand nombre de polymorphismes et est probablement au mieux exposé pour se lier à un ligand associé à une autre cellule. Une explication possible pour les résultats négatifs obtenus serait donc que le domaine D1 ne constitue qu'une interface partielle et de faible affinité et que d'autres régions d'ILT7 sont impliquées dans l'interaction. Des expériences de docking *in silico* réalisées sur un modèle de structure prédite des domaines ILT7 D1–D2 avec la région coiled-coil de la tétherine (résidus 80–147) semblent indiquer effectivement qu'une interface probable d'interaction se situe sur la face exposée de la jonction entre les domaines D1 et D2. Des expériences de mutagenèse ciblée de résidus clés dans cette région seraient néanmoins nécessaires pour valider ces observations.

En conclusion, les méthodes développées pour la purification d'ILT7 en cellules d'insecte et les résultats obtenus dans le cadre de ce travail, ont préparé la piste pour une caractérisation plus approfondie de l'interaction entre les deux protéines. La production d'ILT7 peut

certainement être optimisée afin d'obtenir un échantillon pur et en quantité suffisante pour entamer des essais de co-cristallisation avec la tétherine. Les interfaces d'interaction respectives des deux partenaires pourront être cartographiées plus précisément par mutagenèse et SPR à l'aide des résultats préliminaires obtenus par docking *in silico*. Alternativement, des résidus de la tétherine impliqués dans la reconnaissance d'ILT7 pourraient être identifiés par résonance magnétique nucléaire (RMN). Ces expériences, construites sur base du présent travail, vont en fin de compte contribuer au décryptage du rôle exact de la tétherine et d'ILT7 dans la régulation d'interférons.

5

Discussion

The prime objective of this thesis was to determine the structural details underlying activation of the ILT7 receptor by its protein ligand tetherin. The expression and purification of the tetherin ectodomain (residues 47–159) was already established in our laboratory, and the first crystal structure of the core coiled-coil domain (80–147) of human tetherin was determined by our group in 2010 (Hinz et al., 2010). Hence, the first task in obtaining the tetherin–ILT7 complex was the recombinant expression and purification of the ILT7 ectodomain under a soluble form.

A major obstacle in producing Ig-like proteins is the presence of a disulfide bond linking the two β -sheets forming the characteristic sandwich-like structural motif. Formation of the disulfide is not only essential for protein stability but is also a prerequisite for correct folding. In the eukaryotic cell, folding of antibodies and Ig-like proteins takes place in the endoplasmic reticulum (ER) and Golgi apparatus, whereas in Gram-negative bacteria, disulfide bond-containing proteins fold exclusively in the oxidative environment of the periplasm. Our initial efforts in ILT7 expression were focusing on eukaryotic expression systems, namely the human HEK 293T cell line and baculovirus-infected insect cells. In both cases, the protein was targeted to the secretion pathway using heterologous signal sequences optimised for protein production in the respective host species. In addition to attempting the expression of the entire ectodomain (domains D1-4), we generated several constructs comprising the first two domains (D1-2) only. Indeed, available crystal structures of other LILR family proteins are limited to D1 (ILT1/LILRA2, ILT6/A3, ILT11/A5), D1-2 (ILT2/B1, ILT3/B4, ILT4/B2), or the more recently determined D3-4 domains of ILT2/B1 and ILT4/B2, with no structure comprising all four domains existing to date. However, despite numerous trials and testing of a variety of procedures, no recombinant protein expression could be detected in 293T cells and no soluble protein could be obtained in insect cells. It is worth underlining that in 293T cells, the single-chain variable fragment (scFv) of the broadly neutralising anti-gp41 antibody PG9, cloned into the same plasmid backbone as ILT7, was used as a positive control and was consistently expressed, secreted and detected in our assays. In pDCs, cell surface expression of ILT7 notably depends

on its association with its signaling adapter, the γ -chain of the high-affinity Fc ϵ receptor (Fc ϵ RI γ) (Cao et al., 2006). However, given that this interaction is mediated by the respective transmembrane domains of both proteins, the presence or absence of the signaling adapter is unlikely to influence the trafficking of the soluble ILT7 ectodomain (residues 24–430). Even considering the possible involvement of the six residue-long extracellular tail of Fc ϵ RI γ , the absence of the ILT7 stalk region that links D4 to the transmembrane domain (431–446) precludes any interaction between our recombinantly expressed protein and the signaling adapter. Finally, a slightly longer ectodomain construct (residues 24–435) was successfully produced, first by the team of Prof Eric Cohen as a h emagglutinin-tagged protein in 293T cells, and later by ourselves as a His-tagged version in baculovirus-infected insect cells. These results also seem to corroborate the thought that the signaling adapter is not required for secretion of the ILT7 ectodomain. In retrospect, a likely explanation for our initial failure to express the protein terminating at K430 may come from the results of secondary structure and disorder prediction (page 86) performed on the ILT7 ectodomain. Notably, the region spanning residues 420–439 is predicted to adopt a random coil conformation, with residues 426–434 further predicted to be disordered, and may thus serve as a flexible stalk to the structured ectodomain. Untypical of flexible linker regions however, is the presence of four charged residues (K429, K430, D432 and K434) and the notable absence of glycines, which may hint at a possible induced folding of this region upon interaction with the D4 domain. In such a case, it could be speculated that the partial lack of the linker region could destabilise the C-terminal end of the D4 domain or cause its misfolding. Alternatively, based on the conservation of the charged residues among subfamily “A” receptors, in stark contrast with the glycine- and proline-rich composition found in subfamily “B”, this region might be involved in signal transduction by potentially mediating receptor homodimerisation or binding of an as yet unidentified interaction partner. Intriguingly, residues 422–435 achieved a high score (98–100% confidence) for disordered residues being involved in protein–protein interactions, as estimated by the DisoPred algorithm. However, in the absence of a full-length crystal structure and other experimental evidence, these observations remain highly speculative. Regarding crystallisation, it is worth noting that the recently solved crystal structures of the D3-4 domains of ILT2 and ILT4 were obtained with protein truncated after the equivalent positions 415 and 418, respectively. Although belonging to a different subfamily with a markedly differing stalk amino acid sequence, this is consistent with the idea of a linker region that forms a structural unit rather than purely serving as a flexible linker.

Our negative results obtained for the expression of two-domain constructs are more difficult to explain. All the one- and two-domain LILR crystal structures that have been solved to date were obtained using *in vitro* refolded protein. In the case of ILT1 and ILT3, the production of stable and crystallisable protein required stability-engineering

by introducing a pair of cysteines into an otherwise flexible loop region (Chen et al., 2007; Cheng et al., 2011). After failing to express ILT7(D1-2) in eukaryotic systems, we conducted extensive *in vitro* refolding and periplasmic expression trials in *E. coli*. However, neither wild-type nor mutated ILT7(D1-2) could be produced in a stable and soluble form by bacterial expression. Based on the predicted tertiary structure of two-domain ILT7, which shows an interaction between the C–C' and F–G loops of D2 with the D1 domain, one could assume that correct folding of the D2 domain depends on a completely folded D1 domain. During refolding, such a dependency might be severely rate-limiting compared to aggregation or misfolding.

The crystal structure of the D1 domain closely resembles other LILRs, as expected from the significant sequence identity. Notable differences in the amino acid sequence are located in the C' region, which is unfortunately partly missing from our electron density maps. The bad quality of diffraction data obtained with our initial crystals can be readily explained by the interference of the C-terminal polyhistidine tag in regular crystal packing, as its proteolytic removal in a second construct immediately led to an alternative well-diffracting crystal form. The protein forms non-crystallographic dimers related by a pure rotation symmetry. However, given the head-to-tail arrangement, the biological relevance of such an interaction is difficult to imagine, thus rather suggests an artifact of crystallisation. In addition, dimeric protein is also observed in size exclusion chromatography, where a minor fraction of ILT7(D1) elutes before the main peak (page 93). Nevertheless, the soluble dimers are disulfide-linked, as shown by SDS-PAGE under non-reducing conditions, and might thus be attributed to the artifactual assembly of matching β -sheets of two different protein chains during refolding.

The predicted tertiary structure of ILT7(D1-2) is relatively accurate when compared to the crystal structure over the first domain, with an RMSD of 0.413 Å for C α atoms. Expectedly, larger distances of 0.8–3.04 Å are observed between residues 68–74 of both structures, which constitute the more poorly resolved C' strand. The relative arrangement of the D1-D2 domains at a right angle appears to be shared by killer cell Ig-like receptors (KIRs), which represent the second major protein family in the leukocyte receptor complex (LRC) (Saulquin et al., 2003; Vivian et al., 2011). Like LILRs, the two N-terminal domains of KIRs belong to the C2-set and are more specifically attributed to the Ig_2 and Ig_3 families in the Pfam database, respectively. Based on the predicted ILT7 structure, the D1/D2 interface involves an interaction of two extended D2 loops with the D1 domain, probably mediated by hydrogen bonding in addition to hydrophobicity. Domains D3-4 may form a similar structural unit, possibly disposed at an even more acute angle between each other, as the crystal structures of ILT2 and ILT4 suggest. The arrangement of the entire ILT7 ectodomain is impossible to predict in the absence of a full-length LILR crystal structure. Nonetheless, a comparison can be made with other Ig-like receptors such as CD4 and ICAM-5 (intracellular adhesion molecule 5), which adopt an extended conformation, and the more closely related

three-domain KIRs (KIR3Ds) that seem to arrange into a more compact zigzag structure (Figure 5.1). It is therefore likely that, by analogy, the ILT7 ectodomain adopts a zigzag arrangement similar to KIRs rather than a fully extended conformation—or even an horseshoe-shape, with the D1-D2 domains folding back towards the plasma membrane.

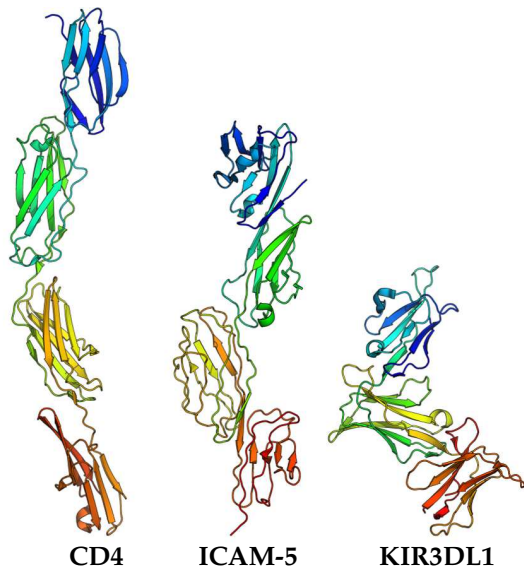


Figure 5.1 Conformations of Ig superfamily receptor ectodomains. Represented are, from left to right, the crystal structures of the D1-4 domains of CD4 (PDB 3T0E), domains D1-4 of ICAM-5 (40IB) and domains D1-3 of KIR3DL1 (3VH8). The protein chains are coloured from N- to C-terminus using a rainbow spectrum.

Surprisingly, in our *in vitro* assays the N-terminal domain of ILT7 did not interact with the tetherin ectodomain nor did it bind to cell surface-expressed wild-type tetherin in flow cytometry experiments performed by our collaborators. As the multiple sequence alignment of LILR ectodomains (page 49) shows, the region spanning residues 60–80 is the single most variable sequence patch found in ILT7 and thus more than likely involved in the specific recognition of a ligand. In addition, based on the reasoning above, the D1 domain is probably located at the membrane-distal end of the receptor resulting in its optimal exposure for ligand-binding. In some instances, the lack of binding observed in our assays could be explained by aspects of the experimental conditions used. The SPR, MST and flow cytometry experiments all relied on covalent modification of primary amines, which are found on lysine sidechains and the protein N-terminus. Lysines are typically exposed on the protein surface and are likely to participate in interaction through their charged amine group. In addition, four out of the five lysines present in the D1 domain are located in the highly variable C' region (K62, K73, K80 and K82). It is therefore possible that the tetherin binding site on D1 was inaccessible under the conditions used. The same explanation could theoretically apply to the SPR assay using tetherin as an immobilised ligand, although the tetherin ectodomain features 12 evenly spread lysines per homodimer that are unlikely to have all reacted with the dextran matrix. The negative results obtained by ITC analysis of the unmodified proteins in solution suggest that the D1 domain does not bind tetherin at the concentration used.

There are currently no data suggesting dimerisation of ILT7 nor of any other LILR,

but the possibility can not be excluded. A large number of cell surface receptors form homodimers upon ligand-binding, thereby triggering downstream signaling via cross-phosphorylation of residues located on the cytosolic tail. In the case of ILT7, signal transduction is mediated by the ITAM-bearing Fc ϵ RI γ , which forms disulfide-linked homodimers in the context of the Fc receptor. One could thus imagine that recognition of tetherin relies on avidity effects from binding of two ILT7 molecules, and that the low affinity interaction with an isolated D1 domain would defy detection by the techniques used.

Moreover, another potential explanation for the lack of binding observed *in vitro* comes from the results obtained from *in silico* docking of the predicted two-domain structure of ILT7 to the tetherin coiled-coil domain. Several of the possible interfaces identified by the docking algorithm, and specifically in “set-2” models (see page 111), are located on the outer side of the D1/D2 domain junction. Again, this could suggest that D1 merely provides a partial interface with a very low affinity, or that tetherin recognition depends on conformational rearrangements that require the hinge region linking the two domains. Interestingly, binding of ILT2/B1 and ILT4/B2 to MHC complexes is mediated by interaction of the outer D1/D2 domain junction with the β 2 microglobulin chain and HLA α 3 domain (see page 46). In addition, the five loops that constitute this region of ILT7(D1-2) harbour a relatively high proportion of amino acid polymorphisms when compared to other LILRs, and are thus likely to be involved in the recognition of a specific ligand. Nevertheless, with respect to the predicted quaternary structures of the tetherin–ILT7 complex obtained by docking, it is important to underline that only the coiled-coil domain of tetherin was included in the experiment, and an implication of the N-terminal linker region of the tetherin ectodomain can therefore not be ruled out.

Using the full-length ILT7 ectodomain produced in baculovirus-infected insect cells, we could confirm the protein’s binding to the tetherin ectodomain by SPR. Since the original publication of the interaction between the two proteins (Cao et al., 2009), there has been no further evidence of direct binding in the literature. In addition, the proposed model of negative regulation of interferon production has recently been challenged by Tavano et al. (2013), who failed to see an effect of tetherin-blockade on ILT7-induced interferon downregulation in PBMCs. Given the exclusive expression of ILT7 in circulating pDCs, the authors propose that the interaction with tetherin may represent a homeostatic mechanism on immature pDCs rather than play a role during viral infection. The SPR binding curves are characteristic of a low affinity interaction, showing fast dissociation of the complex, although reliable kinetic parameters could not be estimated in this experiment due to limited range of concentrations tested. However, based on our limited dataset we predict a dissociation constant (K_D) of 1–10 μ M. Interestingly, our SPR data do not entirely agree with the results published by Cao et al. (2009). While these authors propose a similar binding affinity in the micromolar

range, in contrast, their sensorgrams reflect both a slow association and a slow dissociation of the complex. A slower flow rate used in our experiment ($10 \mu\text{L min}^{-1}$ versus $20 \mu\text{L min}^{-1}$) might have contributed to a minor extent to increased mass transfer effects, although identical buffer conditions were used in both cases. Alternatively, the differential behaviour in the original experiment might have been caused by the expression of both interaction partners as Fc-fusion proteins, with the possible result of homodimerisation. Finally, Cao et al. used considerably lower analyte concentrations and did not provide a value for R_{ligand} , thus the kinetics of both experiments might not be comparable.

Of interest in both cases is the potential artificially induced multimerisation of tetherin through the fusion to the Fc fragment and GST, respectively. Both fusion tags have the ability to form homodimers, and could indeed have promoted the cross-linking of multiple tetherin dimers in both experiments (Figure 5.2). Considering the clustering of tetherin into foci on the cell surface, as well as our hypothesis that virus restriction depends on self-organisation of tetherin into higher-order assemblies, it is possible that binding of ILT7 likewise requires tetherin to be in a multimeric state.

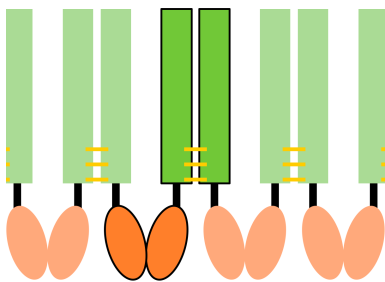


Figure 5.2 Diagram showing the potential multimerisation of the tetherin ectodomain, artificially induced by the fusion to naturally dimeric Fc-fragment or GST. Disulfide-linked tetherin ectodomains are represented in green and GST/Fc fusion partners are shown in orange, with respective interacting proteins highlighted in brighter colours.

The increased molecular mass of recombinant ILT7(D1-4) on SDS-PAGE, as well as the absence of potentially glycosylated peptides from the MALDI-TOF spectrum, both hint at the protein being glycosylated. Most secreted and cell surface-expressed proteins are glycosylated in the ER to some extent and for different purposes, followed by processing of the glycan moieties in the Golgi apparatus. Glycans may promote correct folding, increase protein stability, or be involved in interactions within the extracellular matrix or between cells. Furthermore, glycans serve as specific ligands to lectins, and as such play a fundamental role in the recognition of pathogen-derived glycoproteins, for example. The role of ILT7 glycosylation remains to be elucidated, but a potential lead may come from an interesting insight into ILT6/LILRA3, which is the only LILR family member expressed as a soluble rather than membrane-bound receptor. Indeed, the binding of recombinant ILT6 to the cell surface of monocytes was recently found to depend on N-linked glycosylation and could be blocked by preincubation with β -lactose (Lee et al., 2013). Moreover, LPS-induced cytokine production in PBMCs could be suppressed by glycosylated mammalian-expressed but not by

unglycosylated bacterial-expressed ILT6. These findings suggest that glycosylation of LILRs might not merely serve protein stability but may play a functional role, perhaps in the activation of lectin co-receptors.

Finally, our endeavour to assess tetherin-oligomerisation at HIV-1 budding sites using fluorescence microscopy techniques has led to mixed results. The fusion of tetherin to fluorescent protein is known to impede the protein's restriction activity (personal communication from Dr Nolwenn Jouvenet), and thus we resorted to a labeling technique that relies on small fluorophores in conjunction with a short clonable peptide tag. We could confirm the trafficking of TC-tetherin mutants to the cell surface, as well as their antiviral activity against HIV-1 VLPs. However, the treatment of transiently transfected cells with the labeling reagent FAsH resulted in high levels of background fluorescence as well as in a low apparent specificity for tetherin, as assessed by immunofluorescent staining. While there is a distinct possibility that the presence of FAsH could have prevented antibody recognition, the use of a polyclonal anti-tetherin serum reduces the likelihood. Background fluorescence could be remediated by drastically reducing the labeling time, although this resulted in extremely low overall fluorescence levels. We also considered the possible oxidation of some or all of the cysteines that form the TC motif, as tetherin dimerisation might place them within bonding distance. However, neither pre-treatment with reducing agents, nor co-transfection of wild-type tetherin resulted in an increased labeling specificity.

Perspectives

These results pave the road for further investigation, and most notably for structural studies using the insect cell-expressed ILT7 ectodomain. The yield of ILT7 ectodomain production can certainly be increased by further developing the purification protocol. While a small amount of pure protein could be recovered after affinity purification alone and be used for SPR analyses, more substantial amounts of protein will be required for more extensive biophysical characterisation and crystallisation trials. This implies optimal conditions of buffer, pH and ionic strength during the entire purification process, all of which will have to be determined, for instance, by thermal shift assays.

In case only limited quantities of material can be produced, or co-crystallisation with tetherin fails, the respective interfaces of tetherin and ILT7 involved in the interaction will have to be mapped in more detail. In a first instance, the differential binding of ILT7 to full-length tetherin ectodomain (47–159) compared to the coiled-coil domain alone (80–147) could be assessed by SPR. To map the tetherin interface more precisely, the complex could be analysed by ^{15}N heteronuclear single quantum coherence (HSQC) nuclear magnetic resonance (NMR), using isotopically-labeled tetherin. Site-directed mutagenesis within the D1/D2 domain junction of ILT7 could corroborate the

involvement of residue sets that were identified by *in silico* docking. This would for example consist in replacing negatively- with positively-charged residues and hydrophobic residues with polar residues. Sidechains potentially involved in hydrogen-bonding or salt bridges could also be selectively replaced. Similarly, the importance of an intact D1/D2 interdomain interface could be assessed by its disruption through site-directed mutagenesis based on the predicted tertiary structure of ILT7(D1-2).

It would be interesting to gain a better understanding of the role of ILT7 glycosylation. The total glycan mass could be determined by multi-angle laser light scattering (MALLS) after deglycosylation with endoglycosidase H, which selectively removes N-linked high-mannose glycans such as found on insect cell-expressed protein. The deglycosylated protein could further be subjected to peptide mass fingerprinting by MALDI-TOF, in order to identify peptides containing putative glycosylation sites. The possible contribution to binding affinity or specificity could be measured by SPR using deglycosylated ILT7. Finally, mutation of N-glycosylation sites or enzymatic deglycosylation might be necessary for crystallisation, as the flexible sugar structures can prevent the formation of crystal contacts.

Regarding tetracysteine-based imaging of cell surface-expressed tetherin, we could so far not verify the specificity of FAsH-labeling by immunofluorescent co-staining. When following the manufacturer-recommended labeling procedure we observe high levels of intracellular background fluorescence, as well as punctuate staining likely resulting from proteins with some degree of natural affinity for the FAsH molecule. In order to better assess the specificity of cell surface labeling, the cells could therefore be visualised on a total internal reflection fluorescence (TIRF) microscope. This technique consists in excitation of fluorophores with an evanescent wave that is generated at the glass–water boundary by illumination at a specific angle, and allows the selective visualisation of a shallow (~ 100 nm) section of the sample. In the TIRF context, TC-tetherin could be co-transfected with fluorescent HIV-1 Gag and the degree of co-localisation on the plasma membrane could be determined, even in the absence of a complete overlap with immunofluorescent staining, as the reduced fluorescent noise would allow for a more selective imaging. Finally, additional TC-tetherin constructs could be generated with the TC motif inserted in the N-terminal linker region of the ectodomain. Although the tertiary structure adopted by this region is uncertain, epitope tags have previously been inserted after Q82 for instance, without affecting trafficking or antiviral activity (Hinz et al., 2010).

Conclusion

The structural details underlying the activation of the pDC receptor ILT7 by its ligand, tetherin, remain elusive. Although I have been able to determine the crystal structure of the D1 domain of ILT7, this fragment does not appear to be sufficient for interaction

and complex formation with the tetherin ectodomain. The D1 domain structure has, however, permitted to assess the accuracy of a predicted structural model comprising the D1-D2 domains of ILT7. Docking of the tetherin coiled-coil domain to the ILT7(D1-2) model highlighted a potential binding interface on the exposed face of the D1/D2 domain junction. The involvement of this potential interface, which consists of several exposed loops, could be verified by site-directed mutagenesis of the full-length ILT7 ectodomain, followed by SPR analyses with the full-length tetherin ectodomain or the coiled-coil domain alone.

The direct interaction between ILT7 and tetherin was independently confirmed for the first time since its original publication in 2009. Moreover, the development of recombinant ILT7 production in insect cells will provide a basis for further investigation, including crystallisation of ILT7 alone or in complex with tetherin, which will provide structural details of the interaction. This will ultimately help to decipher the exact role of tetherin and ILT7 in the regulation of interferon.

Bibliography

Abada, P., Noble, B., and Cannon, P. M. (2005). Functional domains within the human immunodeficiency virus type 2 envelope protein required to enhance virus production. *J Virol*, 79(6):3627–3638.

Abe, T., Harashima, A., Xia, T., Konno, H., Konno, K., Morales, A., Ahn, J., Gutman, D., and Barber, G. N. (2013). STING recognition of cytoplasmic DNA instigates cellular defense. *Mol Cell*, 50(1):5–15.

Acchioni, C., Marsili, G., Perrotti, E., Remoli, A. L., Sgarbanti, M., and Battistini, A. (2014). Type I IFN - A blunt spear in fighting HIV-1 infection. *Cytokine Growth Factor Rev*.

Adams, P. D., Afonine, P. V., Bunkóczi, G., Chen, V. B., Davis, I. W., Echols, N., Headd, J. J., Hung, L.-W., Kapral, G. J., Grosse Kunstleve, R. W., McCoy, A. J., Moriarty, N. W., Oeffner, R., Read, R. J., Richardson, D. C., Richardson, J. S., Terwilliger, T. C., and Zwart, P. H. (2010). PHENIX: a comprehensive Python-based system for macromolecular structure solution. *Acta Crystallogr D Biol Crystallogr*, 66(Pt 2):213–221.

Adams, S. R., Campbell, R. E., Gross, L. A., Martin, B. R., Walkup, G. K., Yao, Y., Llopis, J., and Tsien, R. Y. (2002). New biarsenical ligands and tetracysteine motifs for protein labeling in vitro and in vivo: synthesis and biological applications. *J Am Chem Soc*, 124(21):6063–6076.

Agromayor, M., Soler, N., Caballe, A., Kueck, T., Freund, S. M., Allen, M. D., Bycroft, M., Perisic, O., Ye, Y., McDonald, B., Scheel, H., Hofmann, K., Neil, S. J. D., Martin Serrano, J., and Williams, R. L. (2012). The UBAP1 subunit of ESCRT-I interacts with ubiquitin via a SOUBA domain. *Structure*, 20(3):414–428.

Albin, J. S. and Harris, R. S. (2010). Interactions of host APOBEC3 restriction factors with HIV-1 in vivo: implications for therapeutics. *Expert Rev Mol Med*, 12:e4.

Alexopoulou, L., Holt, A. C., Medzhitov, R., and Flavell, R. A. (2001). Recognition of double-stranded RNA and activation of NF-kappaB by Toll-like receptor 3. *Nature*, 413(6857):732–738.

Alimonti, J. B., Ball, T. B., and Fowke, K. R. (2003). Mechanisms of CD4+ T lymphocyte cell death in human immunodeficiency virus infection and AIDS. *J Gen Virol*, 84(Pt 7):1649–1661.

Andrew, A. J., Miyagi, E., and Strebel, K. (2011). Differential effects of human immunodeficiency virus type 1 Vpu on the stability of BST-2/tetherin. *J Virol*, 85(6):2611–2619.

Arhel, N. (2010). Revisiting HIV-1 uncoating. *Retrovirology*, 7:96.

Arias, J. F. and Evans, D. T. (2014). Tethering viral restriction to signal transduction. *Cell Host Microbe*, 16(3):267–269.

Bailes, E., Gao, F., Bibollet Ruche, F., Courgnaud, V., Peeters, M., Marx, P. A., Hahn, B. H., and Sharp, P. M. (2003). Hybrid origin of SIV in chimpanzees. *Science*, 300(5626):1713.

Bajorek, M., Schubert, H. L., McCullough, J., Langelier, C., Eckert, D. M., Stubblefield, W.-M. B., Uter, N. T., Myszkka, D. G., Hill, C. P., and Sundquist, W. I. (2009). Structural basis for ESCRT-III protein autoinhibition. *Nat Struct Mol Biol*, 16(7):754–762.

Barrow, A. D. and Trowsdale, J. (2008). The extended human leukocyte receptor complex: diverse ways of modulating immune responses. *Immunol Rev*, 224:98–123.

Bartee, E., McCormack, A., and Früh, K. (2006). Quantitative membrane proteomics reveals new cellular targets of viral immune modulators. *PLoS Pathog*, 2(10):e107.

Baumgärtel, V., Ivanchenko, S., Dupont, A., Sergeev, M., Wiseman, P. W., Kräusslich, H.-G., Bräuchle, C., Müller, B., and Lamb, D. C. (2011). Live-cell visualization of dynamics of HIV budding site interactions with an ESCRT component. *Nat Cell Biol*, 13(4):469–474.

Bego, M. G., Mercier, J., and Cohen, E. A. (2012). Virus-activated interferon regulatory factor 7 upregulates expression of the interferon-regulated BST2 gene independently of interferon signaling. *J Virol*, 86(7):3513–3527.

Beignon, A.-S., McKenna, K., Skoberne, M., Manches, O., DaSilva, I., Kavanagh, D. G., Larsson, M., Gorelick, R. J., Lifson, J. D., and Bhardwaj, N. (2005). Endocytosis of HIV-1 activates plasmacytoid dendritic cells via Toll-like receptor-viral RNA interactions. *J Clin Invest*, 115(11):3265–3275.

Beitz, E. (2000). TEXshade: shading and labeling of multiple sequence alignments using LATEX2 epsilon. *Bioinformatics*, 16(2):135–139.

Berg, R. K., Melchjorsen, J., Rintahaka, J., Diget, E., Søbystad, S., Horan, K. A., Gorelick, R. J., Matikainen, S., Larsen, C. S., Ostergaard, L., Paludan, S. R., and Mogensen, T. H. (2012).

Genomic HIV RNA induces innate immune responses through RIG-I-dependent sensing of secondary-structured RNA. *PLoS One*, 7(1):e29291.

Billcliff, P. G., Rollason, R., Prior, I., Owen, D. M., Gaus, K., and Banting, G. (2013). CD317/tetherin is an organiser of membrane microdomains. *J Cell Sci*, 126(Pt 7):1553–1564.

Bishop, K. N., Verma, M., Kim, E.-Y., Wolinsky, S. M., and Malim, M. H. (2008). APOBEC3G inhibits elongation of HIV-1 reverse transcripts. *PLoS Pathog*, 4(12):e1000231.

Blondeau, C., Pelchen Matthews, A., Mlcochova, P., Marsh, M., Milne, R. S. B., and Towers, G. J. (2013). Tetherin restricts herpes simplex virus 1 and is antagonized by glycoprotein M. *J Virol*, 87(24):13124–13133.

Bogerd, H. P. and Cullen, B. R. (2008). Single-stranded RNA facilitates nucleocapsid: APOBEC3G complex formation. *RNA*, 14(6):1228–1236.

Brady, T., Agosto, L. M., Malani, N., Berry, C. C., O'Doherty, U., and Bushman, F. (2009). HIV integration site distributions in resting and activated CD4+ T cells infected in culture. *AIDS*, 23(12):1461–1471.

Brown, D., Trowsdale, J., and Allen, R. (2004). The LILR family: modulators of innate and adaptive immune pathways in health and disease. *Tissue Antigens*, 64(3):215–225.

Buchan, D. W. A., Minneci, F., Nugent, T. C. O., Bryson, K., and Jones, D. T. (2013). Scalable web services for the PSIPRED Protein Analysis Workbench. *Nucleic Acids Res*, 41(Web Server issue):W349–W357.

Butticaz, C., Michielin, O., Wyniger, J., Telenti, A., and Rothenberger, S. (2007). Silencing of both beta-TrCP1 and HOS (beta-TrCP2) is required to suppress human immunodeficiency virus type 1 Vpu-mediated CD4 down-modulation. *J Virol*, 81(3):1502–1505.

Buzon, V., Natrajan, G., Schibli, D., Campelo, F., Kozlov, M. M., and Weissenhorn, W. (2010). Crystal structure of HIV-1 gp41 including both fusion peptide and membrane proximal external regions. *PLoS Pathog*, 6(5):e1000880.

Cai, M., Zheng, R., Caffrey, M., Craigie, R., Clore, G. M., and Gronenborn, A. M. (1997). Solution structure of the N-terminal zinc binding domain of HIV-1 integrase. *Nat Struct Biol*, 4(7):567–577.

Cao, W., Bover, L., Cho, M., Wen, X., Hanabuchi, S., Bao, M., Rosen, D. B., Wang, Y.-H., Shaw, J. L., Du, Q., Li, C., Arai, N., Yao, Z., Lanier, L. L., and Liu, Y.-J. (2009). Regulation of TLR7/9 responses in plasmacytoid dendritic cells by BST2 and ILT7 receptor interaction. *J Exp Med*, 206(7):1603–1614.

Cao, W., Rosen, D. B., Ito, T., Bover, L., Bao, M., Watanabe, G., Yao, Z., Zhang, L., Lanier, L. L., and Liu, Y.-J. (2006). Plasmacytoid dendritic cell-specific receptor ILT7-Fc epsilonRI gamma inhibits Toll-like receptor-induced interferon production. *J Exp Med*, 203(6):1399–1405.

Capobianchi, M. R., Ankel, H., Ameglio, F., Paganelli, R., Pizzoli, P. M., and Dianzani, F. (1992). Recombinant glycoprotein 120 of human immunodeficiency virus is a potent interferon inducer. *AIDS Res Hum Retroviruses*, 8(5):575–579.

Cervantes, J. L., Weinerman, B., Basole, C., and Salazar, J. C. (2012). TLR8: the forgotten relative revindicated. *Cell Mol Immunol*, 9(6):434–438.

Chang, C. C., Ciubotariu, R., Manavalan, J. S., Yuan, J., Colovai, A. I., Piazza, F., Lederman, S., Colonna, M., Cortesini, R., Dalla Favera, R., and Suciuc Foca, N. (2002). Tolerization of dendritic cells by T(S) cells: the crucial role of inhibitory receptors ILT3 and ILT4. *Nat Immunol*, 3(3):237–243.

Chen, Y., Chu, F., Gao, F., Zhou, B., and Gao, G. F. (2007). Stability engineering, biophysical, and biological characterization of the myeloid activating receptor immunoglobulin-like transcript 1 (ILT1/LIR-7/LILRA2). *Protein Expr Purif*, 56(2):253–260.

Cheng, H., Mohammed, F., Nam, G., Chen, Y., Qi, J., Garner, L. I., Allen, R. L., Yan, J., Willcox, B. E., and Gao, G. F. (2011). Crystal structure of leukocyte Ig-like receptor LILRB4 (ILT3/LIR-5/CD85k): a myeloid inhibitory receptor involved in immune tolerance. *J Biol Chem*, 286(20):18013–18025.

Cho, M., Ishida, K., Chen, J., Ohkawa, J., Chen, W., Namiki, S., Kotaki, A., Arai, N., Arai, K.-i., and Kamogawa Schifter, Y. (2008). SAGE library screening reveals ILT7 as a specific plasmacytoid dendritic cell marker that regulates type I IFN production. *Int Immunol*, 20(1):155–164.

Cipriani, F., Röwer, M., Landret, C., Zander, U., Felisaz, F., and Márquez, J. A. (2012). CrystalDirect: a new method for automated crystal harvesting based on laser-induced photoablation of thin films. *Acta Crystallogr D Biol Crystallogr*, 68(Pt 10):1393–1399.

Cocka, L. J. and Bates, P. (2012). Identification of alternatively translated Tetherin isoforms with differing antiviral and signaling activities. *PLoS Pathog*, 8(9):e1002931.

Cohen, E. A., Terwilliger, E. F., Sodroski, J. G., and Haseltine, W. A. (1988). Identification of a protein encoded by the vpu gene of HIV-1. *Nature*, 334(6182):532–534.

Cohen, M. S., Chen, Y. Q., McCauley, M., Gamble, T., Hosseinipour, M. C., Kumarasamy, N., Hakim, J. G., Kumwenda, J., Grinsztejn, B., Pilotto, J. H. S., Godbole,

S. V., Mehendale, S., Chariyalertsak, S., Santos, B. R., Mayer, K. H., Hoffman, I. F., Eshleman, S. H., Piwowar Manning, E., Wang, L., Makhema, J., Mills, L. A., de Bruyn, G., Sanne, I., Eron, J., Gallant, J., Havlir, D., Swindells, S., Ribaldo, H., Elharrar, V., Burns, D., Taha, T. E., Nielsen Saines, K., Celentano, D., Essex, M., Fleming, T. R., and , H. P. T. N. . S. T. (2011). Prevention of HIV-1 infection with early antiretroviral therapy. *N Engl J Med*, 365(6):493–505.

Colonna, M., Nakajima, H., Navarro, F., and López Botet, M. (1999). A novel family of Ig-like receptors for HLA class I molecules that modulate function of lymphoid and myeloid cells. *J Leukoc Biol*, 66(3):375–381.

Connell, B. J. and Lortat Jacob, H. (2013). Human immunodeficiency virus and heparan sulfate: from attachment to entry inhibition. *Front Immunol*, 4:385.

Cooper, C. A., Gasteiger, E., and Packer, N. H. (2001). GlycoMod—a software tool for determining glycosylation compositions from mass spectrometric data. *Proteomics*, 1(2):340–349.

Craigie, R. and Bushman, F. D. (2012). HIV DNA integration. *Cold Spring Harb Perspect Med*, 2(7):a006890.

Daecke, J., Fackler, O. T., Dittmar, M. T., and Kräusslich, H.-G. (2005). Involvement of clathrin-mediated endocytosis in human immunodeficiency virus type 1 entry. *J Virol*, 79(3):1581–1594.

Davies, 2nd, J., Hostomska, Z., Hostomsky, Z., Jordan, S. R., and Matthews, D. A. (1991). Crystal structure of the ribonuclease H domain of HIV-1 reverse transcriptase. *Science*, 252(5002):88–95.

de Bouteiller, O., Merck, E., Hasan, U. A., Hubac, S., Benguigui, B., Trinchieri, G., Bates, E. E. M., and Caux, C. (2005). Recognition of double-stranded RNA by human toll-like receptor 3 and downstream receptor signaling requires multimerization and an acidic pH. *J Biol Chem*, 280(46):38133–38145.

de Witte, L., Bobardt, M., Chatterji, U., Degeest, G., David, G., Geijtenbeek, T. B. H., and Gally, P. (2007a). Syndecan-3 is a dendritic cell-specific attachment receptor for HIV-1. *Proc Natl Acad Sci U S A*, 104(49):19464–19469.

de Witte, L., Nabatov, A., Pion, M., Fluitsma, D., de Jong, M. A. W. P., de Gruijl, T., Piguet, V., van Kooyk, Y., and Geijtenbeek, T. B. H. (2007b). Langerin is a natural barrier to HIV-1 transmission by Langerhans cells. *Nat Med*, 13(3):367–371.

Diaz Griffero, F., Kar, A., Perron, M., Xiang, S.-H., Javanbakht, H., Li, X., and Sodroski, J. (2007). Modulation of retroviral restriction and proteasome inhibitor-resistant turnover by changes in the TRIM5alpha B-box 2 domain. *J Virol*, 81(19):10362–10378.

Diebold, S. S., Massacrier, C., Akira, S., Patrel, C., Morel, Y., and Reis e Sousa, C. (2006). Nucleic acid agonists for Toll-like receptor 7 are defined by the presence of uridine ribonucleotides. *Eur J Immunol*, 36(12):3256–3267.

Dietrich, J., Cella, M., and Colonna, M. (2001). Ig-like transcript 2 (ILT2)/leukocyte Ig-like receptor 1 (LIR1) inhibits TCR signaling and actin cytoskeleton reorganization. *J Immunol*, 166(4):2514–2521.

Dixit, E., Boulant, S., Zhang, Y., Lee, A. S. Y., Odendall, C., Shum, B., Hacohen, N., Chen, Z. J., Whelan, S. P., Fransen, M., Nibert, M. L., Superti Furga, G., and Kagan, J. C. (2010). Peroxisomes are signaling platforms for antiviral innate immunity. *Cell*, 141(4):668–681.

Douglas, J. L., Viswanathan, K., McCarroll, M. N., Gustin, J. K., Früh, K., and Moses, A. V. (2009). Vpu directs the degradation of the human immunodeficiency virus restriction factor BST-2/Tetherin via a betaTrCP-dependent mechanism. *J Virol*, 83(16):7931–7947.

Dubé, M., Bego, M. G., Paquay, C., and Cohen, É. A. (2010a). Modulation of HIV-1-host interaction: role of the Vpu accessory protein. *Retrovirology*, 7:114.

Dubé, M., Roy, B. B., Guiot Guillain, P., Binette, J., Mercier, J., Chiasson, A., and Cohen, E. A. (2010b). Antagonism of tetherin restriction of HIV-1 release by Vpu involves binding and sequestration of the restriction factor in a perinuclear compartment. *PLoS Pathog*, 6(4):e1000856.

Dubé, M., Roy, B. B., Guiot Guillain, P., Mercier, J., Binette, J., Leung, G., and Cohen, E. A. (2009). Suppression of Tetherin-restricting activity upon human immunodeficiency virus type 1 particle release correlates with localization of Vpu in the trans-Golgi network. *J Virol*, 83(9):4574–4590.

Dyda, F., Hickman, A. B., Jenkins, T. M., Engelman, A., Craigie, R., and Davies, D. R. (1994). Crystal structure of the catalytic domain of HIV-1 integrase: similarity to other polynucleotidyl transferases. *Science*, 266(5193):1981–1986.

Effantin, G., Dordor, A., Sandrin, V., Martinelli, N., Sundquist, W. I., Schoehn, G., and Weissenhorn, W. (2013). ESCRT-III CHMP2A and CHMP3 form variable helical polymers in vitro and act synergistically during HIV-1 budding. *Cell Microbiol*, 15(2):213–226.

Eijkelenboom, A. P., Lutzke, R. A., Boelens, R., Plasterk, R. H., Kaptein, R., and Hård, K. (1995). The DNA-binding domain of HIV-1 integrase has an SH3-like fold. *Nat Struct Biol*, 2(9):807–810.

- Emsley, P., Lohkamp, B., Scott, W. G., and Cowtan, K. (2010). Features and development of Coot. *Acta Crystallogr D Biol Crystallogr*, 66(Pt 4):486–501.
- Engelman, A. and Cherepanov, P. (2012). The structural biology of HIV-1: mechanistic and therapeutic insights. *Nat Rev Microbiol*, 10(4):279–290.
- Engelman, A., Mizuuchi, K., and Craigie, R. (1991). HIV-1 DNA integration: mechanism of viral DNA cleavage and DNA strand transfer. *Cell*, 67(6):1211–1221.
- Erikson, E., Adam, T., Schmidt, S., Lehmann Koch, J., Over, B., Goffinet, C., Harter, C., Bekeredjian Ding, I., Sertel, S., Lasitschka, F., and Keppler, O. T. (2011). In vivo expression profile of the antiviral restriction factor and tumor-targeting antigen CD317/BST-2/HM1.24/tetherin in humans. *Proc Natl Acad Sci U S A*, 108(33):13688–13693.
- Evans, P. R. and Murshudov, G. N. (2013). How good are my data and what is the resolution? *Acta Crystallogr D Biol Crystallogr*, 69(Pt 7):1204–1214.
- Fabrikant, G., Lata, S., Riches, J. D., Briggs, J. A. G., Weissenhorn, W., and Kozlov, M. M. (2009). Computational model of membrane fission catalyzed by ESCRT-III. *PLoS Comput Biol*, 5(11):e1000575.
- Finn, R. D., Bateman, A., Clements, J., Coggill, P., Eberhardt, R. Y., Eddy, S. R., Heger, A., Hetherington, K., Holm, L., Mistry, J., Sonnhammer, E. L. L., Tate, J., and Punta, M. (2014). Pfam: the protein families database. *Nucleic Acids Res*, 42(Database issue):D222–D230.
- Gabadinho, J., Beteva, A., Guijarro, M., Rey Bakaikoa, V., Spruce, D., Bowler, M. W., Brockhauser, S., Flot, D., Gordon, E. J., Hall, D. R., Lavault, B., McCarthy, A. A., McCarthy, J., Mitchell, E., Monaco, S., Mueller Dieckmann, C., Nurizzo, D., Ravelli, R. B. G., Thibault, X., Walsh, M. A., Leonard, G. A., and McSweeney, S. M. (2010). Mx-CuBE: a synchrotron beamline control environment customized for macromolecular crystallography experiments. *J Synchrotron Radiat*, 17(5):700–707.
- Gack, M. U. (2014). Mechanisms of RIG-I-like receptor activation and manipulation by viral pathogens. *J Virol*, 88(10):5213–5216.
- Galão, R. P., Le Tortorec, A., Pickering, S., Kueck, T., and Neil, S. J. D. (2012). Innate sensing of HIV-1 assembly by Tetherin induces NF κ B-dependent proinflammatory responses. *Cell Host Microbe*, 12(5):633–644.
- Galão, R. P., Pickering, S., Curnock, R., and Neil, S. J. D. (2014). Retroviral Retention Activates a Syk-Dependent HemITAM in Human Tetherin. *Cell Host Microbe*, 16(3):291–303.
- Ganser Pornillos, B. K., Yeager, M., and Sundquist, W. I. (2008). The structural biology of HIV assembly. *Curr Opin Struct Biol*, 18(2):203–217.

Gao, D., Wu, J., Wu, Y.-T., Du, F., Aroh, C., Yan, N., Sun, L., and Chen, Z. J. (2013). Cyclic GMP-AMP synthase is an innate immune sensor of HIV and other retroviruses. *Science*, 341(6148):903–906.

Gao, X., Bashirova, A., Iversen, A. K. N., Phair, J., Goedert, J. J., Buchbinder, S., Hoots, K., Vlahov, D., Altfeld, M., O'Brien, S. J., and Carrington, M. (2005). AIDS restriction HLA allotypes target distinct intervals of HIV-1 pathogenesis. *Nat Med*, 11(12):1290–1292.

Gao, X., Nelson, G. W., Karacki, P., Martin, M. P., Phair, J., Kaslow, R., Goedert, J. J., Buchbinder, S., Hoots, K., Vlahov, D., O'Brien, S. J., and Carrington, M. (2001). Effect of a single amino acid change in MHC class I molecules on the rate of progression to AIDS. *N Engl J Med*, 344(22):1668–1675.

Garrus, J. E., von Schwedler, U. K., Pornillos, O. W., Morham, S. G., Zavitz, K. H., Wang, H. E., Wettstein, D. A., Stray, K. M., Côté, M., Rich, R. L., Myszka, D. G., and Sundquist, W. I. (2001). Tsg101 and the vacuolar protein sorting pathway are essential for HIV-1 budding. *Cell*, 107(1):55–65.

Geijtenbeek, T. B., Kwon, D. S., Torensma, R., van Vliet, S. J., van Duijnhoven, G. C., Middel, J., Cornelissen, I. L., Nottet, H. S., KewalRamani, V. N., Littman, D. R., Figdor, C. G., and van Kooyk, Y. (2000). DC-SIGN, a dendritic cell-specific HIV-1-binding protein that enhances trans-infection of T cells. *Cell*, 100(5):587–597.

Goffinet, C., Allespach, I., Homann, S., Tervo, H.-M., Habermann, A., Rupp, D., Oberbremer, L., Kern, C., Tibroni, N., Welsch, S., Krijnse Locker, J., Banting, G., Kräusslich, H.-G., Fackler, O. T., and Keppler, O. T. (2009). HIV-1 antagonism of CD317 is species specific and involves Vpu-mediated proteasomal degradation of the restriction factor. *Cell Host Microbe*, 5(3):285–297.

Goto, T., Kennel, S. J., Abe, M., Takishita, M., Kosaka, M., Solomon, A., and Saito, S. (1994). A novel membrane antigen selectively expressed on terminally differentiated human B cells. *Blood*, 84(6):1922–1930.

Göttlinger, H. G., Dorfman, T., Cohen, E. A., and Haseltine, W. A. (1993). Vpu protein of human immunodeficiency virus type 1 enhances the release of capsids produced by gag gene constructs of widely divergent retroviruses. *Proc Natl Acad Sci U S A*, 90(15):7381–7385.

Griffin, B. A., Adams, S. R., and Tsien, R. Y. (1998). Specific covalent labeling of recombinant protein molecules inside live cells. *Science*, 281(5374):269–272.

Grover, J. R., Llewellyn, G. N., Soheilian, F., Nagashima, K., Veatch, S. L., and Ono, A. (2013). Roles played by capsid-dependent induction of membrane curvature and Gag-

- ESCRT interactions in tetherin recruitment to HIV-1 assembly sites. *J Virol*, 87(8):4650–4664.
- Gupta, R., Jung, E., and Brunak, S. (2004). Prediction of N-glycosylation sites in human proteins. In preparation.
- Habermann, A., Krijnse Locker, J., Oberwinkler, H., Eckhardt, M., Homann, S., Andrew, A., Strebel, K., and Kräusslich, H.-G. (2010). CD317/tetherin is enriched in the HIV-1 envelope and downregulated from the plasma membrane upon virus infection. *J Virol*, 84(9):4646–4658.
- Hammonds, J., Wang, J.-J., Yi, H., and Spearman, P. (2010). Immunoelectron microscopic evidence for Tetherin/BST2 as the physical bridge between HIV-1 virions and the plasma membrane. *PLoS Pathog*, 6(2):e1000749.
- Hanson, P. I., Roth, R., Lin, Y., and Heuser, J. E. (2008). Plasma membrane deformation by circular arrays of ESCRT-III protein filaments. *J Cell Biol*, 180(2):389–402.
- Hare, S., Vos, A. M., Clayton, R. F., Thuring, J. W., Cummings, M. D., and Cherepanov, P. (2010). Molecular mechanisms of retroviral integrase inhibition and the evolution of viral resistance. *Proc Natl Acad Sci U S A*, 107(46):20057–20062.
- Hauser, H., Lopez, L. A., Yang, S. J., Oldenburg, J. E., Exline, C. M., Guatelli, J. C., and Cannon, P. M. (2010). HIV-1 Vpu and HIV-2 Env counteract BST-2/tetherin by sequestration in a perinuclear compartment. *Retrovirology*, 7:51.
- Heil, F., Hemmi, H., Hochrein, H., Ampenberger, F., Kirschning, C., Akira, S., Lipford, G., Wagner, H., and Bauer, S. (2004). Species-specific recognition of single-stranded RNA via toll-like receptor 7 and 8. *Science*, 303(5663):1526–1529.
- Hilditch, L. and Towers, G. J. (2014). A model for cofactor use during HIV-1 reverse transcription and nuclear entry. *Curr Opin Virol*, 4:32–36.
- Hinz, A., Miguët, N., Natrajan, G., Usami, Y., Yamanaka, H., Renesto, P., Hartlieb, B., McCarthy, A. A., Simorre, J.-P., Göttlinger, H., and Weissenhorn, W. (2010). Structural basis of HIV-1 tethering to membranes by the BST-2/tetherin ectodomain. *Cell Host Microbe*, 7(4):314–323.
- Hofmann, K. and Stoffel, W. (1993). TMbase - A database of membrane spanning proteins segments.
- Hrecka, K., Hao, C., Gierszewska, M., Swanson, S. K., Kesik Brodacka, M., Srivastava, S., Florens, L., Washburn, M. P., and Skowronski, J. (2011). Vpx relieves inhibition of HIV-1 infection of macrophages mediated by the SAMHD1 protein. *Nature*, 474(7353):658–661.

Huang, J., Goedert, J. J., Sundberg, E. J., Cung, T. D. H., Burke, P. S., Martin, M. P., Preiss, L., Lifson, J., Lichterfeld, M., Carrington, M., and Yu, X. G. (2009). HLA-B*35-Px-mediated acceleration of HIV-1 infection by increased inhibitory immunoregulatory impulses. *J Exp Med*, 206(13):2959–2966.

Huang, X., Yang, Y., Wang, G., Cheng, Q., and Du, Z. (2014). Highly conserved RNA pseudoknots at the Gag-Pol junction of HIV-1 suggest a novel mechanism of -1 ribosomal frameshifting. *RNA*, 20(5):587–593.

Hussain, A., Das, S. R., Tanwar, C., and Jameel, S. (2007). Oligomerization of the human immunodeficiency virus type 1 (HIV-1) Vpu protein—a genetic, biochemical and biophysical analysis. *Virology*, 4:81.

Ishikawa, H. and Barber, G. N. (2008). STING is an endoplasmic reticulum adaptor that facilitates innate immune signalling. *Nature*, 455(7213):674–678.

Ishikawa, H., Ma, Z., and Barber, G. N. (2009). STING regulates intracellular DNA-mediated, type I interferon-dependent innate immunity. *Nature*, 461(7265):788–792.

Ishikawa, J., Kaisho, T., Tomizawa, H., Lee, B. O., Kobune, Y., Inazawa, J., Oritani, K., Itoh, M., Ochi, T., and Ishihara, K. (1995). Molecular cloning and chromosomal mapping of a bone marrow stromal cell surface gene, BST2, that may be involved in pre-B-cell growth. *Genomics*, 26(3):527–534.

Iwabuchi, Y., Fujita, H., Kinomoto, M., Kaneko, K., Ishizaka, Y., Tanaka, Y., Sata, T., and Tokunaga, K. (2009). HIV-1 accessory protein Vpu internalizes cell-surface BST-2/tetherin through transmembrane interactions leading to lysosomes. *J Biol Chem*, 284(50):35060–35072.

Iwasaki, A. (2007). Role of autophagy in innate viral recognition. *Autophagy*, 3(4):354–356.

Iwatani, Y., Chan, D. S. B., Wang, F., Maynard, K. S., Sugiura, W., Gronenborn, A. M., Rouzina, I., Williams, M. C., Musier Forsyth, K., and Levin, J. G. (2007). Deaminase-independent inhibition of HIV-1 reverse transcription by APOBEC3G. *Nucleic Acids Res*, 35(21):7096–7108.

Jacobo Molina, A., Ding, J., Nanni, R. G., Clark, Jr, A., Lu, X., Tantillo, C., Williams, R. L., Kamer, G., Ferris, A. L., and Clark, P. (1993). Crystal structure of human immunodeficiency virus type 1 reverse transcriptase complexed with double-stranded DNA at 3.0 Å resolution shows bent DNA. *Proc Natl Acad Sci U S A*, 90(13):6320–6324.

Jakobsen, M. R., Bak, R. O., Andersen, A., Berg, R. K., Jensen, S. B., Tengchuan, J., Jin, T., Laustsen, A., Hansen, K., Ostergaard, L., Fitzgerald, K. A., Xiao, T. S., Mikkelsen, J. G., Mogensen, T. H., and Paludan, S. R. (2013). IFI16 senses DNA forms of the

- lentiviral replication cycle and controls HIV-1 replication. *Proc Natl Acad Sci U S A*, 110(48):E4571–E4580.
- Janvier, K., Pelchen Matthews, A., Renaud, J.-B., Caillet, M., Marsh, M., and Berlioz Torrent, C. (2011). The ESCRT-0 component HRS is required for HIV-1 Vpu-mediated BST-2/tetherin down-regulation. *PLoS Pathog*, 7(2):e1001265.
- Jia, B., Serra Moreno, R., Neidermyer, W., Rahmberg, A., Mackey, J., Fofana, I. B., Johnson, W. E., Westmoreland, S., and Evans, D. T. (2009). Species-specific activity of SIV Nef and HIV-1 Vpu in overcoming restriction by tetherin/BST2. *PLoS Pathog*, 5(5):e1000429.
- Johnsen, I. B., Nguyen, T. T., Ringdal, M., Tryggestad, A. M., Bakke, O., Lien, E., Espevik, T., and Anthonsen, M. W. (2006). Toll-like receptor 3 associates with c-Src tyrosine kinase on endosomes to initiate antiviral signaling. *EMBO J*, 25(14):3335–3346.
- Jones, D. T. (1999). Protein secondary structure prediction based on position-specific scoring matrices. *J Mol Biol*, 292(2):195–202.
- Jones, D. T. and Cozzetto, D. (2014). DISOPRED3: precise disordered region predictions with annotated protein-binding activity. *Bioinformatics*.
- Jouvenet, N., Bieniasz, P. D., and Simon, S. M. (2008). Imaging the biogenesis of individual HIV-1 virions in live cells. *Nature*, 454(7201):236–240.
- Jouvenet, N., Neil, S. J. D., Bess, C., Johnson, M. C., Virgen, C. A., Simon, S. M., and Bieniasz, P. D. (2006). Plasma membrane is the site of productive HIV-1 particle assembly. *PLoS Biol*, 4(12):e435.
- Jouvenet, N., Neil, S. J. D., Zhadina, M., Zang, T., Kratovac, Z., Lee, Y., McNatt, M., Hatziioannou, T., and Bieniasz, P. D. (2009). Broad-spectrum inhibition of retroviral and filoviral particle release by tetherin. *J Virol*, 83(4):1837–1844.
- Ju, X.-S., Hacker, C., Scherer, B., Redecke, V., Berger, T., Schuler, G., Wagner, H., Lipford, G. B., and Zenke, M. (2004). Immunoglobulin-like transcripts ILT2, ILT3 and ILT7 are expressed by human dendritic cells and down-regulated following activation. *Gene*, 331:159–164.
- Kabsch, W. (2010). XDS. *Acta Crystallogr D Biol Crystallogr*, 66(Pt 2):125–132.
- Kaletsky, R. L., Francica, J. R., Agrawal Gamse, C., and Bates, P. (2009). Tetherin-mediated restriction of filovirus budding is antagonized by the Ebola glycoprotein. *Proc Natl Acad Sci U S A*, 106(8):2886–2891.
- Käll, L., Krogh, A., and Sonnhammer, E. L. L. (2004). A combined transmembrane topology and signal peptide prediction method. *J Mol Biol*, 338(5):1027–1036.

- Källberg, M., Wang, H., Wang, S., Peng, J., Wang, Z., Lu, H., and Xu, J. (2012). Template-based protein structure modeling using the RaptorX web server. *Nat Protoc*, 7(8):1511–1522.
- Kantardjieff, K. A. and Rupp, B. (2003). Matthews coefficient probabilities: Improved estimates for unit cell contents of proteins, DNA, and protein-nucleic acid complex crystals. *Protein Sci*, 12(9):1865–1871.
- Karikó, K., Buckstein, M., Ni, H., and Weissman, D. (2005). Suppression of RNA recognition by Toll-like receptors: the impact of nucleoside modification and the evolutionary origin of RNA. *Immunity*, 23(2):165–175.
- Karplus, P. A. and Diederichs, K. (2012). Linking crystallographic model and data quality. *Science*, 336(6084):1030–1033.
- Keele, B. F., Van Heuverswyn, F., Li, Y., Bailes, E., Takehisa, J., Santiago, M. L., Bibollet Ruche, F., Chen, Y., Wain, L. V., Liegeois, F., Loul, S., Ngole, E. M., Bienvenue, Y., Delaporte, E., Brookfield, J. F. Y., Sharp, P. M., Shaw, G. M., Peeters, M., and Hahn, B. H. (2006). Chimpanzee reservoirs of pandemic and nonpandemic HIV-1. *Science*, 313(5786):523–526.
- Kluge, S. F., Mack, K., Iyer, S. S., Pujol, F. M., Heigle, A., Learn, G. H., Usmani, S. M., Sauter, D., Joas, S., Hotter, D., Bibollet Ruche, F., Plenderleith, L. J., Peeters, M., Geyer, M., Sharp, P. M., Fackler, O. T., Hahn, B. H., and Kirchhoff, F. (2014). Nef Proteins of Epidemic HIV-1 Group O Strains Antagonize Human Tetherin. *Cell Host Microbe*, 16(5):639–650.
- Kluge, S. F., Sauter, D., Vogl, M., Peeters, M., Li, Y., Bibollet Ruche, F., Hahn, B. H., and Kirchhoff, F. (2013). The transmembrane domain of HIV-1 Vpu is sufficient to confer anti-tetherin activity to SIVcpz and SIVgor Vpu proteins: cytoplasmic determinants of Vpu function. *Retrovirology*, 10:32.
- Kobayashi, T., Ode, H., Yoshida, T., Sato, K., Gee, P., Yamamoto, S. P., Ebina, H., Strebel, K., Sato, H., and Koyanagi, Y. (2011). Identification of amino acids in the human tetherin transmembrane domain responsible for HIV-1 Vpu interaction and susceptibility. *J Virol*, 85(2):932–945.
- Kohlstaedt, L. A., Wang, J., Friedman, J. M., Rice, P. A., and Steitz, T. A. (1992). Crystal structure at 3.5 Å resolution of HIV-1 reverse transcriptase complexed with an inhibitor. *Science*, 256(5065):1783–1790.
- Kozakov, D., Brenke, R., Comeau, S. R., and Vajda, S. (2006). PIPER: an FFT-based protein docking program with pairwise potentials. *Proteins*, 65(2):392–406.

- Krishnan, L., Matreyek, K. A., Oztop, I., Lee, K., Tipper, C. H., Li, X., Dar, M. J., Kevalramani, V. N., and Engelman, A. (2010). The requirement for cellular transportin 3 (TNPO3 or TRN-SR2) during infection maps to human immunodeficiency virus type 1 capsid and not integrase. *J Virol*, 84(1):397–406.
- Krissinel, E. and Henrick, K. (2007). Inference of macromolecular assemblies from crystalline state. *J Mol Biol*, 372(3):774–797.
- Kueck, T. and Neil, S. J. D. (2012). A cytoplasmic tail determinant in HIV-1 Vpu mediates targeting of tetherin for endosomal degradation and counteracts interferon-induced restriction. *PLoS Pathog*, 8(3):e1002609.
- Kühl, A. and Pöhlmann, S. (2012). How Ebola virus counters the interferon system. *Zoonoses Public Health*, 59 Suppl 2:116–131.
- Kupzig, S., Korolchuk, V., Rollason, R., Sugden, A., Wilde, A., and Banting, G. (2003). Bst-2/HM1.24 is a raft-associated apical membrane protein with an unusual topology. *Traffic*, 4(10):694–709.
- Kwong, P. D., Wyatt, R., Robinson, J., Sweet, R. W., Sodroski, J., and Hendrickson, W. A. (1998). Structure of an HIV gp120 envelope glycoprotein in complex with the CD4 receptor and a neutralizing human antibody. *Nature*, 393(6686):648–659.
- Lambert, A. A., Gilbert, C., Richard, M., Beaulieu, A. D., and Tremblay, M. J. (2008). The C-type lectin surface receptor DCIR acts as a new attachment factor for HIV-1 in dendritic cells and contributes to trans- and cis-infection pathways. *Blood*, 112(4):1299–1307.
- Lata, S., Roessle, M., Solomons, J., Jamin, M., Gottlinger, H. G., Svergun, D. I., and Weissenhorn, W. (2008a). Structural basis for autoinhibition of ESCRT-III CHMP3. *J Mol Biol*, 378(4):818–827.
- Lata, S., Schoehn, G., Jain, A., Pires, R., Piehler, J., Gottlinger, H. G., and Weissenhorn, W. (2008b). Helical structures of ESCRT-III are disassembled by VPS4. *Science*, 321(5894):1354–1357.
- Le Grice, S. F. J. (2012). Human immunodeficiency virus reverse transcriptase: 25 years of research, drug discovery, and promise. *J Biol Chem*, 287(49):40850–40857.
- Le Tortorec, A. and Neil, S. J. D. (2009). Antagonism to and intracellular sequestration of human tetherin by the human immunodeficiency virus type 2 envelope glycoprotein. *J Virol*, 83(22):11966–11978.
- Lee, H. K., Lund, J. M., Ramanathan, B., Mizushima, N., and Iwasaki, A. (2007). Autophagy-dependent viral recognition by plasmacytoid dendritic cells. *Science*, 315(5817):1398–1401.

Lee, K., Ambrose, Z., Martin, T. D., Oztop, I., Mulky, A., Julias, J. G., Vandegraaff, N., Baumann, J. G., Wang, R., Yuen, W., Takemura, T., Shelton, K., Taniuchi, I., Li, Y., Sodroski, J., Littman, D. R., Coffin, J. M., Hughes, S. H., Unutmaz, D., Engelman, A., and KewalRamani, V. N. (2010). Flexible use of nuclear import pathways by HIV-1. *Cell Host Microbe*, 7(3):221–233.

Lee, T. H. Y., Mitchell, A., Liu Lau, S., An, H., Rajeaskariah, P., Wasinger, V., Raftery, M., Bryant, K., and Tedla, N. (2013). Glycosylation in a mammalian expression system is critical for the production of functionally active leukocyte immunoglobulin-like receptor A3 protein. *J Biol Chem*, 288(46):32873–32885.

Lehmann, M., Rocha, S., Mangeat, B., Blanchet, F., Uji I, H., Hofkens, J., and Piguet, V. (2011). Quantitative multicolor super-resolution microscopy reveals tetherin HIV-1 interaction. *PLoS Pathog*, 7(12):e1002456.

Lichterfeld, M. and Yu, X. G. (2012). The emerging role of leukocyte immunoglobulin-like receptors (LILRs) in HIV-1 infection. *J Leukoc Biol*, 91(1):27–33.

Lowe, D. M., Aitken, A., Bradley, C., Darby, G. K., Larder, B. A., Powell, K. L., Purifoy, D. J., Tisdale, M., and Stammers, D. K. (1988). HIV-1 reverse transcriptase: crystallization and analysis of domain structure by limited proteolysis. *Biochemistry*, 27(25):8884–8889.

Luban, J., Bossolt, K. L., Franke, E. K., Kalpana, G. V., and Goff, S. P. (1993). Human immunodeficiency virus type 1 Gag protein binds to cyclophilins A and B. *Cell*, 73(6):1067–1078.

Maartens, G., Celum, C., and Lewin, S. R. (2014). HIV infection: epidemiology, pathogenesis, treatment, and prevention. *Lancet*, 384(9939):258–271.

Maldarelli, F., Chen, M. Y., Willey, R. L., and Strebel, K. (1993). Human immunodeficiency virus type 1 Vpu protein is an oligomeric type I integral membrane protein. *J Virol*, 67(8):5056–5061.

Malim, M. H. and Bieniasz, P. D. (2012). HIV Restriction Factors and Mechanisms of Evasion. *Cold Spring Harb Perspect Med*, 2(5):a006940.

Manel, N., Hogstad, B., Wang, Y., Levy, D. E., Unutmaz, D., and Littman, D. R. (2010). A cryptic sensor for HIV-1 activates antiviral innate immunity in dendritic cells. *Nature*, 467(7312):214–217.

Mangeat, B., Gers Huber, G., Lehmann, M., Zufferey, M., Luban, J., and Piguet, V. (2009). HIV-1 Vpu neutralizes the antiviral factor Tetherin/BST-2 by binding it and directing its beta-TrCP2-dependent degradation. *PLoS Pathog*, 5(9):e1000574.

- Margottin, F., Bour, S. P., Durand, H., Selig, L., Benichou, S., Richard, V., Thomas, D., Strebel, K., and Benarous, R. (1998). A novel human WD protein, h-beta TrCp, that interacts with HIV-1 Vpu connects CD4 to the ER degradation pathway through an F-box motif. *Mol Cell*, 1(4):565–574.
- Márquez, J. A. and Cipriani, F. (2014). CrystalDirect™: a novel approach for automated crystal harvesting based on photoablation of thin films. *Methods Mol Biol*, 1091:197–203.
- Martin, B. R., Giepmans, B. N. G., Adams, S. R., and Tsien, R. Y. (2005). Mammalian cell-based optimization of the biarsenical-binding tetracysteine motif for improved fluorescence and affinity. *Nat Biotechnol*, 23(10):1308–1314.
- Masuyama, N., Kuronita, T., Tanaka, R., Muto, T., Hirota, Y., Takigawa, A., Fujita, H., Aso, Y., Amano, J., and Tanaka, Y. (2009). HM1.24 is internalized from lipid rafts by clathrin-mediated endocytosis through interaction with alpha-adaptin. *J Biol Chem*, 284(23):15927–15941.
- Matsuda, A., Suzuki, Y., Honda, G., Muramatsu, S., Matsuzaki, O., Nagano, Y., Doi, T., Shimotohno, K., Harada, T., Nishida, E., Hayashi, H., and Sugano, S. (2003). Large-scale identification and characterization of human genes that activate NF-kappaB and MAPK signaling pathways. *Oncogene*, 22(21):3307–3318.
- Matsumoto, M., Kikkawa, S., Kohase, M., Miyake, K., and Seya, T. (2002). Establishment of a monoclonal antibody against human Toll-like receptor 3 that blocks double-stranded RNA-mediated signaling. *Biochem Biophys Res Commun*, 293(5):1364–1369.
- McNatt, M. W., Zang, T., and Bieniasz, P. D. (2013). Vpu binds directly to tetherin and displaces it from nascent virions. *PLoS Pathog*, 9(4):e1003299.
- Miller, M. D., Farnet, C. M., and Bushman, F. D. (1997). Human immunodeficiency virus type 1 preintegration complexes: studies of organization and composition. *J Virol*, 71(7):5382–5390.
- Mitchell, R. S., Katsura, C., Skasko, M. A., Fitzpatrick, K., Lau, D., Ruiz, A., Stephens, E. B., Margottin Goguet, F., Benarous, R., and Guatelli, J. C. (2009). Vpu antagonizes BST-2-mediated restriction of HIV-1 release via beta-TrCP and endo-lysosomal trafficking. *PLoS Pathog*, 5(5):e1000450.
- Miyakawa, K., Ryo, A., Murakami, T., Ohba, K., Yamaoka, S., Fukuda, M., Guatelli, J., and Yamamoto, N. (2009). BCA2/Rabring7 promotes tetherin-dependent HIV-1 restriction. *PLoS Pathog*, 5(12):e1000700.
- Miyauchi, K., Kim, Y., Latinovic, O., Morozov, V., and Melikyan, G. B. (2009). HIV enters cells via endocytosis and dynamin-dependent fusion with endosomes. *Cell*, 137(3):433–444.

Morita, E., Sandrin, V., McCullough, J., Katsuyama, A., Baci Hamilton, I., and Sundquist, W. I. (2011). ESCRT-III protein requirements for HIV-1 budding. *Cell Host Microbe*, 9(3):235–242.

Muranyi, W., Malkusch, S., Müller, B., Heilemann, M., and Kräusslich, H.-G. (2013). Super-resolution microscopy reveals specific recruitment of HIV-1 envelope proteins to viral assembly sites dependent on the envelope C-terminal tail. *PLoS Pathog*, 9(2):e1003198.

Nazli, A., Kafka, J. K., Ferreira, V. H., Anipindi, V., Mueller, K., Osborne, B. J., Dizzell, S., Chauvin, S., Mian, M. F., Ouellet, M., Tremblay, M. J., Mossman, K. L., Ashkar, A. A., Kovacs, C., Bowdish, D. M. E., Snider, D. P., Kaul, R., and Kaushic, C. (2013). HIV-1 gp120 induces TLR2- and TLR4-mediated innate immune activation in human female genital epithelium. *J Immunol*, 191(8):4246–4258.

Neil, S. J. D., Eastman, S. W., Jouvenet, N., and Bieniasz, P. D. (2006). HIV-1 Vpu promotes release and prevents endocytosis of nascent retrovirus particles from the plasma membrane. *PLoS Pathog*, 2(5):e39.

Neil, S. J. D., Sandrin, V., Sundquist, W. I., and Bieniasz, P. D. (2007). An interferon-alpha-induced tethering mechanism inhibits HIV-1 and Ebola virus particle release but is counteracted by the HIV-1 Vpu protein. *Cell Host Microbe*, 2(3):193–203.

Neil, S. J. D., Zang, T., and Bieniasz, P. D. (2008). Tetherin inhibits retrovirus release and is antagonized by HIV-1 Vpu. *Nature*, 451(7177):425–430.

Nguyen, D. H. and Hildreth, J. E. (2000). Evidence for budding of human immunodeficiency virus type 1 selectively from glycolipid-enriched membrane lipid rafts. *J Virol*, 74(7):3264–3272.

Nityanandam, R. and Serra Moreno, R. (2014). BCA2/Rabring7 targets HIV-1 Gag for lysosomal degradation in a tetherin-independent manner. *PLoS Pathog*, 10(5):e1004151.

Noble, B., Abada, P., Nunez Iglesias, J., and Cannon, P. M. (2006). Recruitment of the adaptor protein 2 complex by the human immunodeficiency virus type 2 envelope protein is necessary for high levels of virus release. *J Virol*, 80(6):2924–2932.

Notredame, C., Higgins, D. G., and Heringa, J. (2000). T-Coffee: A novel method for fast and accurate multiple sequence alignment. *J Mol Biol*, 302(1):205–217.

Obita, T., Saksena, S., Ghazi Tabatabai, S., Gill, D. J., Perisic, O., Emr, S. D., and Williams, R. L. (2007). Structural basis for selective recognition of ESCRT-III by the AAA ATPase Vps4. *Nature*, 449(7163):735–739.

- Ohtomo, T., Sugamata, Y., Ozaki, Y., Ono, K., Yoshimura, Y., Kawai, S., Koishihara, Y., Ozaki, S., Kosaka, M., Hirano, T., and Tsuchiya, M. (1999). Molecular cloning and characterization of a surface antigen preferentially overexpressed on multiple myeloma cells. *Biochem Biophys Res Commun*, 258(3):583–591.
- Pardieu, C., Vigan, R., Wilson, S. J., Calvi, A., Zang, T., Bieniasz, P., Kellam, P., Towers, G. J., and Neil, S. J. D. (2010). The RING-CH ligase K5 antagonizes restriction of KSHV and HIV-1 particle release by mediating ubiquitin-dependent endosomal degradation of tetherin. *PLoS Pathog*, 6(4):e1000843.
- Perez Caballero, D., Hatzioannou, T., Yang, A., Cowan, S., and Bieniasz, P. D. (2005). Human tripartite motif 5alpha domains responsible for retrovirus restriction activity and specificity. *J Virol*, 79(14):8969–8978.
- Perez Caballero, D., Zang, T., Ebrahimi, A., McNatt, M. W., Gregory, D. A., Johnson, M. C., and Bieniasz, P. D. (2009). Tetherin inhibits HIV-1 release by directly tethering virions to cells. *Cell*, 139(3):499–511.
- Petersen, T. N., Brunak, S., von Heijne, G., and Nielsen, H. (2011). SignalP 4.0: discriminating signal peptides from transmembrane regions. *Nat Methods*, 8(10):785–786.
- Pickering, S., Hué, S., Kim, E.-Y., Reddy, S., Wolinsky, S. M., and Neil, S. J. D. (2014). Preservation of tetherin and CD4 counter-activities in circulating Vpu alleles despite extensive sequence variation within HIV-1 infected individuals. *PLoS Pathog*, 10(1):e1003895.
- Piguet, V. and Sattentau, Q. (2004). Dangerous liaisons at the virological synapse. *J Clin Invest*, 114(5):605–610.
- Pires, R., Hartlieb, B., Signor, L., Schoehn, G., Lata, S., Roessle, M., Moriscot, C., Popov, S., Hinz, A., Jamin, M., Boyer, V., Sadoul, R., Forest, E., Svergun, D. I., Göttlinger, H. G., and Weissenhorn, W. (2009). A crescent-shaped ALIX dimer targets ESCRT-III CHMP4 filaments. *Structure*, 17(6):843–856.
- Platanias, L. C. (2005). Mechanisms of type-I- and type-II-interferon-mediated signalling. *Nat Rev Immunol*, 5(5):375–386.
- Pruss, D., Bushman, F. D., and Wolffe, A. P. (1994). Human immunodeficiency virus integrase directs integration to sites of severe DNA distortion within the nucleosome core. *Proc Natl Acad Sci U S A*, 91(13):5913–5917.
- Randall, R. E. and Goodbourn, S. (2008). Interferons and viruses: an interplay between induction, signalling, antiviral responses and virus countermeasures. *J Gen Virol*, 89(Pt 1):1–47.

Rissoan, M.-C., Duhon, T., Bridon, J.-M., Bendriss Vermare, N., Péronne, C., de Saint Vis, B., Brière, F., and Bates, E. E. M. (2002). Subtractive hybridization reveals the expression of immunoglobulin-like transcript 7, Eph-B1, granzyme B, and 3 novel transcripts in human plasmacytoid dendritic cells. *Blood*, 100(9):3295–3303.

Rodriguez, K. R., Bruns, A. M., and Horvath, C. M. (2014). MDA5 and LGP2: accomplices and antagonists of antiviral signal transduction. *J Virol*, 88(15):8194–8200.

Rollason, R., Korolchuk, V., Hamilton, C., Jepson, M., and Banting, G. (2009). A CD317/tetherin-RICH2 complex plays a critical role in the organization of the sub-apical actin cytoskeleton in polarized epithelial cells. *J Cell Biol*, 184(5):721–736.

Rollason, R., Korolchuk, V., Hamilton, C., Schu, P., and Banting, G. (2007). Clathrin-mediated endocytosis of a lipid-raft-associated protein is mediated through a dual tyrosine motif. *J Cell Sci*, 120(Pt 21):3850–3858.

Saulquin, X., Gastinel, L. N., and Vivier, E. (2003). Crystal structure of the human natural killer cell activating receptor KIR2DS2 (CD158j). *J Exp Med*, 197(7):933–938.

Sauter, D. (2014). Counteraction of the multifunctional restriction factor tetherin. *Front Microbiol*, 5:163.

Sauter, D., Schindler, M., Specht, A., Landford, W. N., Münch, J., Kim, K.-A., Votteler, J., Schubert, U., Bibollet Ruche, F., Keele, B. F., Takehisa, J., Ogando, Y., Ochsenbauer, C., Kappes, J. C., Ayoub, A., Peeters, M., Learn, G. H., Shaw, G., Sharp, P. M., Bieniasz, P., Hahn, B. H., Hatzioannou, T., and Kirchhoff, F. (2009). Tetherin-driven adaptation of Vpu and Nef function and the evolution of pandemic and nonpandemic HIV-1 strains. *Cell Host Microbe*, 6(5):409–421.

Sauter, D., Unterwiesing, D., Vogl, M., Usmani, S. M., Heigele, A., Kluge, S. F., Hermkes, E., Moll, M., Barker, E., Peeters, M., Learn, G. H., Bibollet Ruche, F., Fritz, J. V., Fackler, O. T., Hahn, B. H., and Kirchhoff, F. (2012). Human tetherin exerts strong selection pressure on the HIV-1 group N Vpu protein. *PLoS Pathog*, 8(12):e1003093.

Schaller, T., Ocwieja, K. E., Rasaiyaah, J., Price, A. J., Brady, T. L., Roth, S. L., Hué, S., Fletcher, A. J., Lee, K., KewalRamani, V. N., Noursadeghi, M., Jenner, R. G., James, L. C., Bushman, F. D., and Towers, G. J. (2011). HIV-1 capsid-cyclophilin interactions determine nuclear import pathway, integration targeting and replication efficiency. *PLoS Pathog*, 7(12):e1002439.

Schmidt, S., Fritz, J. V., Bitzegeio, J., Fackler, O. T., and Keppler, O. T. (2011). HIV-1 Vpu blocks recycling and biosynthetic transport of the intrinsic immunity factor CD317/tetherin to overcome the virion release restriction. *MBio*, 2(3):e00036–e00011.

- Schubert, H. L., Zhai, Q., Sandrin, V., Eckert, D. M., Garcia Maya, M., Saul, L., Sundquist, W. I., Steiner, R. A., and Hill, C. P. (2010). Structural and functional studies on the extracellular domain of BST2/tetherin in reduced and oxidized conformations. *Proc Natl Acad Sci U S A*, 107(42):17951–17956.
- Schwarzenbacher, R., Godzik, A., Grzechnik, S. K., and Jaroszewski, L. (2004). The importance of alignment accuracy for molecular replacement. *Acta Crystallogr D Biol Crystallogr*, 60(Pt 7):1229–1236.
- Serra Moreno, R., Zimmermann, K., Stern, L. J., and Evans, D. T. (2013). Tetherin/BST-2 antagonism by Nef depends on a direct physical interaction between Nef and tetherin, and on clathrin-mediated endocytosis. *PLoS Pathog*, 9(7):e1003487.
- Sharp, P. M. and Hahn, B. H. (2011). Origins of HIV and the AIDS pandemic. *Cold Spring Harb Perspect Med*, 1(1):a006841.
- Sheehy, A. M., Gaddis, N. C., Choi, J. D., and Malim, M. H. (2002). Isolation of a human gene that inhibits HIV-1 infection and is suppressed by the viral Vif protein. *Nature*, 418(6898):646–650.
- Sheehy, A. M., Gaddis, N. C., and Malim, M. H. (2003). The antiretroviral enzyme APOBEC3G is degraded by the proteasome in response to HIV-1 Vif. *Nat Med*, 9(11):1404–1407.
- Shiroishi, M., Kuroki, K., Rasubala, L., Tsumoto, K., Kumagai, I., Kurimoto, E., Kato, K., Kohda, D., and Maenaka, K. (2006). Structural basis for recognition of the nonclassical MHC molecule HLA-G by the leukocyte Ig-like receptor B2 (LILRB2/LIR2/ILT4/CD85d). *Proc Natl Acad Sci U S A*, 103(44):16412–16417.
- Shiroishi, M., Tsumoto, K., Amano, K., Shirakihara, Y., Colonna, M., Braud, V. M., Allan, D. S. J., Makadzange, A., Rowland Jones, S., Willcox, B., Jones, E. Y., van der Merwe, P. A., Kumagai, I., and Maenaka, K. (2003). Human inhibitory receptors Ig-like transcript 2 (ILT2) and ILT4 compete with CD8 for MHC class I binding and bind preferentially to HLA-G. *Proc Natl Acad Sci U S A*, 100(15):8856–8861.
- Siegfried, N., Muller, M., Deeks, J. J., and Volmink, J. (2009). Male circumcision for prevention of heterosexual acquisition of HIV in men. *Cochrane Database Syst Rev*, (2):CD003362.
- Sievers, F., Wilm, A., Dineen, D., Gibson, T. J., Karplus, K., Li, W., Lopez, R., McWilliam, H., Remmert, M., Söding, J., Thompson, J. D., and Higgins, D. G. (2011). Fast, scalable generation of high-quality protein multiple sequence alignments using Clustal Omega. *Mol Syst Biol*, 7:539.

Sillitoe, I., Cuff, A. L., Dessailly, B. H., Dawson, N. L., Furnham, N., Lee, D., Lees, J. G., Lewis, T. E., Studer, R. A., Rentzsch, R., Yeats, C., Thornton, J. M., and Orengo, C. A. (2013). New functional families (FunFams) in CATH to improve the mapping of conserved functional sites to 3D structures. *Nucleic Acids Res*, 41(Database issue):D490–D498.

Solis, M., Nakhaei, P., Jalalirad, M., Lacoste, J., Douville, R., Arguello, M., Zhao, T., Laughrea, M., Wainberg, M. A., and Hiscott, J. (2011). RIG-I-mediated antiviral signaling is inhibited in HIV-1 infection by a protease-mediated sequestration of RIG-I. *J Virol*, 85(3):1224–1236.

Steenftoft, C., Vakhrushev, S. Y., Joshi, H. J., Kong, Y., Vester Christensen, M. B., Schjoldager, K. T.-B. G., Lavrsen, K., Dabelsteen, S., Pedersen, N. B., Marcos Silva, L., Gupta, R., Bennett, E. P., Mandel, U., Brunak, S., Wandall, H. H., Lavery, S. B., and Clausen, H. (2013). Precision mapping of the human O-GalNAc glycoproteome through SimpleCell technology. *EMBO J*, 32(10):1478–1488.

Stewart, R. S., Drisaldi, B., and Harris, D. A. (2001). A transmembrane form of the prion protein contains an uncleaved signal peptide and is retained in the endoplasmic Reticulum. *Mol Biol Cell*, 12(4):881–889.

Strack, B., Calistri, A., Craig, S., Popova, E., and Göttlinger, H. G. (2003). AIP1/ALIX is a binding partner for HIV-1 p6 and EIAV p9 functioning in virus budding. *Cell*, 114(6):689–699.

Strebel, K., Klimkait, T., Maldarelli, F., and Martin, M. A. (1989). Molecular and biochemical analyses of human immunodeficiency virus type 1 vpu protein. *J Virol*, 63(9):3784–3791.

Strebel, K., Klimkait, T., and Martin, M. A. (1988). A novel gene of HIV-1, vpu, and its 16-kilodalton product. *Science*, 241(4870):1221–1223.

Stremmler, M., Owens, C. M., Perron, M. J., Kiessling, M., Autissier, P., and Sodroski, J. (2004). The cytoplasmic body component TRIM5alpha restricts HIV-1 infection in Old World monkeys. *Nature*, 427(6977):848–853.

Strong, M., Sawaya, M. R., Wang, S., Phillips, M., Cascio, D., and Eisenberg, D. (2006). Toward the structural genomics of complexes: crystal structure of a PE/PPE protein complex from *Mycobacterium tuberculosis*. *Proc Natl Acad Sci U S A*, 103(21):8060–8065.

Stuchell Brereton, M. D., Skalicky, J. J., Kieffer, C., Karren, M. A., Ghaffarian, S., and Sundquist, W. I. (2007). ESCRT-III recognition by VPS4 ATPases. *Nature*, 449(7163):740–744.

- Sun, L., Wu, J., Du, F., Chen, X., and Chen, Z. J. (2013). Cyclic GMP-AMP synthase is a cytosolic DNA sensor that activates the type I interferon pathway. *Science*, 339(6121):786–791.
- Sundquist, W. I. and Kräusslich, H.-G. (2012). HIV-1 assembly, budding, and maturation. *Cold Spring Harb Perspect Med*, 2(7):a006924.
- Swiecki, M., Scheaffer, S. M., Allaire, M., Fremont, D. H., Colonna, M., and Brett, T. J. (2011). Structural and biophysical analysis of BST-2/tetherin ectodomains reveals an evolutionary conserved design to inhibit virus release. *J Biol Chem*, 286(4):2987–2997.
- Takehisa, J., Kraus, M. H., Ayoub, A., Bailes, E., Van Heuverswyn, F., Decker, J. M., Li, Y., Rudicell, R. S., Learn, G. H., Neel, C., Ngole, E. M., Shaw, G. M., Peeters, M., Sharp, P. M., and Hahn, B. H. (2009). Origin and biology of simian immunodeficiency virus in wild-living western gorillas. *J Virol*, 83(4):1635–1648.
- Tavano, B. and Boasso, A. (2014). Effect of immunoglobulin-like transcript 7 cross-linking on plasmacytoid dendritic cells differentiation into antigen-presenting cells. *PLoS One*, 9(2):e89414.
- Tavano, B., Galao, R. P., Graham, D. R., Neil, S. J. D., Aquino, V. N., Fuchs, D., and Boasso, A. (2013). Ig-like transcript 7, but not bone marrow stromal cell antigen 2 (also known as HM1.24, tetherin, or CD317), modulates plasmacytoid dendritic cell function in primary human blood leukocytes. *J Immunol*, 190(6):2622–2630.
- Terwilliger, E. F., Cohen, E. A., Lu, Y. C., Sodroski, J. G., and Haseltine, W. A. (1989). Functional role of human immunodeficiency virus type 1 vpu. *Proc Natl Acad Sci U S A*, 86(13):5163–5167.
- Tokarev, A., Suarez, M., Kwan, W., Fitzpatrick, K., Singh, R., and Guatelli, J. (2013). Stimulation of NF- κ B activity by the HIV restriction factor BST2. *J Virol*, 87(4):2046–2057.
- Trowitzsch, S., Bieniossek, C., Nie, Y., Garzoni, F., and Berger, I. (2010). New baculovirus expression tools for recombinant protein complex production. *J Struct Biol*, 172(1):45–54.
- Turville, S. G., Santos, J. J., Frank, I., Cameron, P. U., Wilkinson, J., Miranda Saksena, M., Dable, J., Stössel, H., Romani, N., Piatak, Jr, M., Lifson, J. D., Pope, M., and Cunningham, A. L. (2004). Immunodeficiency virus uptake, turnover, and 2-phase transfer in human dendritic cells. *Blood*, 103(6):2170–2179.
- Unterholzner, L., Keating, S. E., Baran, M., Horan, K. A., Jensen, S. B., Sharma, S., Sirois, C. M., Jin, T., Latz, E., Xiao, T. S., Fitzgerald, K. A., Paludan, S. R., and Bowie,

A. G. (2010). IFI16 is an innate immune sensor for intracellular DNA. *Nat Immunol*, 11(11):997–1004.

Van Damme, N., Goff, D., Katsura, C., Jorgenson, R. L., Mitchell, R., Johnson, M. C., Stephens, E. B., and Guatelli, J. (2008). The interferon-induced protein BST-2 restricts HIV-1 release and is downregulated from the cell surface by the viral Vpu protein. *Cell Host Microbe*, 3(4):245–252.

Vasiliver Shamis, G., Dustin, M. L., and Hioe, C. E. (2010). HIV-1 Virological Synapse is not Simply a Copycat of the Immunological Synapse. *Viruses*, 2(5):1239–1260.

Venkatesh, S. and Bieniasz, P. D. (2013). Mechanism of HIV-1 virion entrapment by tetherin. *PLoS Pathog*, 9(7):e1003483.

Vigan, R. and Neil, S. J. D. (2010). Determinants of tetherin antagonism in the transmembrane domain of the human immunodeficiency virus type 1 Vpu protein. *J Virol*, 84(24):12958–12970.

Vivian, J. P., Duncan, R. C., Berry, R., O'Connor, G. M., Reid, H. H., Beddoe, T., Gras, S., Saunders, P. M., Olshina, M. A., Widjaja, J. M. L., Harpur, C. M., Lin, J., Maloveste, S. M., Price, D. A., Lafont, B. A. P., McVicar, D. W., Clements, C. S., Brooks, A. G., and Rossjohn, J. (2011). Killer cell immunoglobulin-like receptor 3DL1-mediated recognition of human leukocyte antigen B. *Nature*, 479(7373):401–405.

Wang, Z., Zhao, F., Peng, J., and Xu, J. (2011). Protein 8-class secondary structure prediction using conditional neural fields. *Proteomics*, 11(19):3786–3792.

Weiss, R. A. (2013). Thirty years on: HIV receptor gymnastics and the prevention of infection. *BMC Biol*, 11:57.

Wilkins, M. R., Gasteiger, E., Gooley, A. A., Herbert, B. R., Molloy, M. P., Binz, P. A., Ou, K., Sanchez, J. C., Bairoch, A., Williams, K. L., and Hochstrasser, D. F. (1999). High-throughput mass spectrometric discovery of protein post-translational modifications. *J Mol Biol*, 289(3):645–657.

Willcox, B. E., Thomas, L. M., and Bjorkman, P. J. (2003). Crystal structure of HLA-A2 bound to LIR-1, a host and viral major histocompatibility complex receptor. *Nat Immunol*, 4(9):913–919.

Winn, M. D., Ballard, C. C., Cowtan, K. D., Dodson, E. J., Emsley, P., Evans, P. R., Keegan, R. M., Krissinel, E. B., Leslie, A. G. W., McCoy, A., McNicholas, S. J., Murshudov, G. N., Pannu, N. S., Potterton, E. A., Powell, H. R., Read, R. J., Vagin, A., and Wilson, K. S. (2011). Overview of the CCP4 suite and current developments. *Acta Crystallogr D Biol Crystallogr*, 67(Pt 4):235–242.

- Worobey, M., Telfer, P., Souquière, S., Hunter, M., Coleman, C. A., Metzger, M. J., Reed, P., Makuwa, M., Hearn, G., Honarvar, S., Roques, P., Apetrei, C., Kazanji, M., and Marx, P. A. (2010). Island biogeography reveals the deep history of SIV. *Science*, 329(5998):1487.
- Wu, J., Sun, L., Chen, X., Du, F., Shi, H., Chen, C., and Chen, Z. J. (2013). Cyclic GMP-AMP is an endogenous second messenger in innate immune signaling by cytosolic DNA. *Science*, 339(6121):826–830.
- Wu, X., Anderson, J. L., Campbell, E. M., Joseph, A. M., and Hope, T. J. (2006). Proteasome inhibitors uncouple rhesus TRIM5alpha restriction of HIV-1 reverse transcription and infection. *Proc Natl Acad Sci U S A*, 103(19):7465–7470.
- Wu, X., Li, Y., Crise, B., Burgess, S. M., and Munroe, D. J. (2005). Weak palindromic consensus sequences are a common feature found at the integration target sites of many retroviruses. *J Virol*, 79(8):5211–5214.
- Yang, H., Wang, J., Jia, X., McNatt, M. W., Zang, T., Pan, B., Meng, W., Wang, H.-W., Bieniasz, P. D., and Xiong, Y. (2010). Structural insight into the mechanisms of enveloped virus tethering by tetherin. *Proc Natl Acad Sci U S A*, 107(43):18428–18432.
- Young, N. T., Canavez, F., Uhrberg, M., Shum, B. P., and Parham, P. (2001). Conserved organization of the ILT/LIR gene family within the polymorphic human leukocyte receptor complex. *Immunogenetics*, 53(4):270–278.
- Young, N. T., Waller, E. C. P., Patel, R., Roghanian, A., Austyn, J. M., and Trowsdale, J. (2008). The inhibitory receptor LILRB1 modulates the differentiation and regulatory potential of human dendritic cells. *Blood*, 111(6):3090–3096.
- Yu, X., Yu, Y., Liu, B., Luo, K., Kong, W., Mao, P., and Yu, X.-F. (2003). Induction of APOBEC3G ubiquitination and degradation by an HIV-1 Vif-Cul5-SCF complex. *Science*, 302(5647):1056–1060.
- Zamborlini, A., Usami, Y., Radoshitzky, S. R., Popova, E., Palu, G., and Göttlinger, H. (2006). Release of autoinhibition converts ESCRT-III components into potent inhibitors of HIV-1 budding. *Proc Natl Acad Sci U S A*, 103(50):19140–19145.
- Zenner, H. L., Mauricio, R., Banting, G., and Crump, C. M. (2013). Herpes simplex virus 1 counteracts tetherin restriction via its virion host shutoff activity. *J Virol*, 87(24):13115–13123.
- Zhang, F., Wilson, S. J., Landford, W. C., Virgen, B., Gregory, D., Johnson, M. C., Munch, J., Kirchhoff, F., Bieniasz, P. D., and Hatziioannou, T. (2009). Nef proteins from simian immunodeficiency viruses are tetherin antagonists. *Cell Host Microbe*, 6(1):54–67.

Zheng, Y.-H., Jeang, K.-T., and Tokunaga, K. (2012). Host restriction factors in retroviral infection: promises in virus-host interaction. *Retrovirology*, 9:112.

Appendix A

PCR primer sequences

Construct/Primer	PCR	Sequence (5' → 3')
ILT7#1 + 3		
1	F	AAGAGGATCCGAAAACCTACCCAAACCCATCCTGTGGG
2	R	GAGACCCTCAATCCAGCACAAAAGAAGCCCCGGGCGGCCGCACAC
ILT7#2 + 4		
	F	→ 1
3	R	CTGGTGTCAAGCGTGTCTAGGAAGCCCCGGGCGGCCGCACAC
ILT7#5		
4	F1	ATCTGTCTCGGGCTGAGTCTGGGCCCCAGGACCCGGGTGCAGGCAGAAAACCTACCCAAACCCATCC
5	R1	GTCATCGTCATCCTTGTAAATCTCCCTGAAAATACAGGTTTTCTTCCTAGACACGCCTGACACCAG
6	F2	AAGAGGATCCGCCACCATGACCCCATCCTCACGGTCTGATCTGTCTCGGGCTGAGTCT
7	R2	GTGTTCTAGATTAATGGTGATGGTGATGGTGCTTGTGCATCGTCATCCTTGTAAATCTCCCTG
ILT7#6		
	F1	→ 4
8	R1	GTGCTTGTGCATCGTCATCCTTGTAAATCTCCCTGAAAATACAGGTTTTCTTCCTTTTGTGCTGGATTGAGGGTCTC
	F2	→ 6
	R2	→ 7
ILT7#7		
9	F1	GGTCGTATACATTTCTTACATCTATGCGGATCGAGAAAACCTACCCAAACCCATCC
	R1	→ 5
10	F2	CGGAATTCATGAAATTCTTAGTCAACGTTGCCCTTGTTTTTATGGTCGTATACATTTCTTACATCTATGCCG
	R2	→ 7
ILT7#9		
11	F	AGAGGCCAGCCGGCCATGGCAGAAAACCTACCCAAACCCATCCTGTGGG
12	R	GTGTGAATTCATGATGGTGATGGTGCTTCTAGACACGCCTGACACCAGTAGC
ILT7#10		
13	F	ATATCCATGGGACGCACCCGTGTCC
14	R	ATATAAGCTTATTTACGGCTAACACC
ILT7#11		
15	F	AAGACCATGGCAGGACGCACCCGT
16	R	GTGTGAATTCATGATGGTGATGGTGTTTACGGCTAACACCTGACACCAG
ILT7#12		
	F1a/F2	→ 13
17	R1a	AGGCGATGGTCACCTTCTTCGCACAGGGTAAAACGACCC
18	F1b	ACCATCGCCTGAGTTGGTGTCTGAACTCCCATCAGC
	R1b/R2	→ 14
ILT7#13		
19	F	ATATCATATGGAAAACCTGCCGAAACCGATC

Construct/Primer	PCR	Sequence (5' → 3')
20	R	ATATCTCGAGTTAACCTGACACCAGCAGTTG
ILT7#14 + 15		
	F	→ 19
21	R	ATATCTCGAGACCTGACACCAGCAGTTG
ILT7#16		
	F	→ 19
22	R	ATATCTCGAGTTAGGTAACCACCAGTTCCAGC
ILT7#17		
	F	→ 19
23	R	ATATCTCGAGGGTAACCACCAGTTCCAGC
ILT7#18		
24	F	ATATCCATGGAAAACCTGCCGAAACCGATC
25	R	ATATAAGCTTAGGTAACCACCAGTTCCAGC
ILT7#19		
26	F	ATATGAATTCATGAAATTCCTTGCAACGTCG
27	R	ATATTCTAGATCAAGTCTTGGAATCTGACTTCTTCTGGGCTGGATTCACTG
GST-Tetherin		
32	F	ATATCCATGGCTAAGGCCAACAGCGAGGC
33	R	ATATCTCGAGTCAGTCCTGGGAGCTGGGGTAG
Tetherin(wt)		
34	F	ACACGCTAGCATGGCATCTACTTCGTATGACTATTGC
35	R	ATATGGATCCTCACTGCAGCAGAGCGC
Tetherin-TC155		
	F1a/F2	→ 34
36	R1a	GCAGCAGCCGGGGCAGCAGTAGTACTTCTTGTCGCGATTCTCA
37	F1b	TGCTGCCCCGGCTGCTGCCCCAGCTCCAGGACTCC
	R1b/R2	→ 35
Tetherin-FLN155		
	F1a/F2	→ 34
38	R1a	CTCCATGCAGCAGCCGGGGCAGCAGTTCAGGAAGTAGTACTTCTTGTCGCGATTCTCA
39	F1b	TTCCTGAACTGCTGCCCCGGCTGCTGCATGGAGCCAGCTCCAGGACTCC
	R1b/R2	→ 35

Table A.1 List of PCR primer sequences used for cloning of the constructs described in this work. Construct names refer to Table 2.2 (p. 58).

Appendix B

Structural basis of tetherin function

Review article in *Current HIV Research*, 2012

Structural Basis of Tetherin Function

Winfried Weissenhorn^{*1}, Nolwenn Miguet¹, Nick Aschman¹, Patricia Renesto¹, Yoshiko Usami² and Heinrich G. Gottlinger²

¹Unit of Virus Host Cell Interactions (UVHCI) UMI 3265 Université Joseph Fourier-EMBL-CNRS, 6 rue Jules Horowitz, 38042 Grenoble Cedex 9, France; ²Program in Gene Function and Expression, Program in Molecular Medicine, University of Massachusetts Medical School, Worcester, MA 01605, USA

Abstract: HIV-1 employs its structural proteins to orchestrate assembly and budding at the plasma membrane of host cells, which depends on numerous cellular factors. Although cells evolved interferon inducible restriction factors such as tetherin that act as a first line of defense, enveloped viruses, including HIV-1, developed countermeasures in the form of tetherin antagonists such as Vpu that decrease the effect of tetherin and permits normal viral replication *in vivo*. Here we review recent advances in the understanding of the dynamic structural properties of tetherin that provide the basis to physically retain HIV-1 by bridging plasma and virion membranes after completion of budding.

Keywords: HIV-1, BST2, tetherin, GPI, Vpu, budding, SAXS, coiled coil.

INTRODUCTION

The complex relationship between pathogens and hosts has induced the evolution of a wide range of strategies to establish or combat infection. A first line of immune defense during virus infection evokes a type I interferon response that leads to the production of proteins from interferon-stimulated genes that can counteract infection [1, 2]. Thus, complex co-evolution of viruses and host cell factors has led in many cases to successful virus replication by developing viral countermeasures to nullify or downgrade the effect of the interferon response. During the HIV adaptation process to successfully infect humans, the virus encountered several restriction factors which are in some cases neutralized by viral antagonists. These factors target different stages of the viral life cycle and might slow down viral replication. APOBEC3 (the apolipoprotein B mRNA-editing enzyme catalytic polypeptide-like 3) is a member of the family of cytidine deaminases [3], antagonized by HIV-1 vif [4]. TRIM5 α (the α isoform of the tripartite motif-containing protein 5) restriction is nullified by adaptations in the viral capsid protein [5] and tetherin (known as Bst2 and CD317), the main subject of this review is antagonized by HIV-1 Vpu [6, 7], HIV-2 Env [8] and SIV Nef [9, 10]. The fourth restriction factor, SAMHD1, a deoxynucleoside triphosphate triphosphohydrolase [11] is antagonized by Vpx from HIV-2, as well as Vpr from some primate lentiviruses but not by any HIV-1 factor [12, 13][14].

Notably tetherin-driven adaptation of Vpu and Nef function has been linked to pandemic and non-pandemic HIV-1 strains [15]. Besides HIV, tetherin was shown to restrict replication of a number of enveloped viruses in the absence of viral antagonists (reviewed in [16-20]).

Tetherin is efficiently expressed in plasmacytoid dendritic cells, some cancer cells, differentiated B cells and

bone marrow stromal cells [21-24]. Its expression can be further induced by interferon- α [25], and interferon- α activation leads to HIV-1 retention at the plasma membrane in the absence of Vpu [26]. Induction of interferon expression by HIV-1 involves virion binding to CD4 on plasmacytoid dendritic cells, endocytosis of virions and activation of toll-like receptors 7 and 9 [27]. Furthermore a virus-induced interferon response is required for tetherin function in a mouse model [28]. Tetherin might be regulated *via* its interaction with the immunoglobulin-like transcript 7 (ILT7) present on plasmacytoid dendritic cells, which might provide a negative feedback loop for tetherin expression [29, 30]. However, the importance of interferon-induced expression of tetherin was recently challenged by the transcriptome analyses of human tissues, which detected tetherin in many more cell types and tissues [31]. Because this wide spread tissue distribution might reflect a normal physiological role of tetherin, further work is necessary to place tetherin's function within the framework of interferon-induced innate immune regulators.

TETHERIN HAS AN UNUSUAL TOPOLOGY

BST-2/Tetherin was initially described as a type II transmembrane protein of 180 amino acids [23], which contains a short N-terminal cytoplasmic domain, a transmembrane region, an extracellular domain and a second membrane anchor, a glycosylphosphatidylinositol anchor (Fig. 1A) that targets tetherin to lipid raft microdomains at the cell surface [32] and the trans Golgi network [22, 33, 34]. However, the presence of a GPI anchor was recently challenged, and human tetherin might instead have a second N-terminal transmembrane region [35] (Fig. 1B). Such a topology might be in agreement with difficulties reported to efficiently cleave tetherin's GPI anchor with phosphatidylinositol-specific phospholipase C (PI-PLC)[36, 37]. Alternatively, both forms might coexist. Tetherin forms dimers stabilized by three disulfide bonds, and the presence of at least one disulfide is required for tethering function [23, 38, 39]. Furthermore, two N-linked glycosylation sites contribute to its heterogeneous glycosylation, as evidenced

*Address correspondence to this author at the Unit of Virus Host Cell Interactions (UVHCI) UMI 3265 Université Joseph Fourier-EMBL-CNRS, 6 rue Jules Horowitz, 38042 Grenoble Cedex 9, France; Tel: 33-476-207281; Fax: 33-476-209400; E-mail: weissenhorn@embl.fr

by SDS-PAGE, which reveals molecular weights between 30 and 45 kDa upon tetherin overexpression in HEK cells [40].

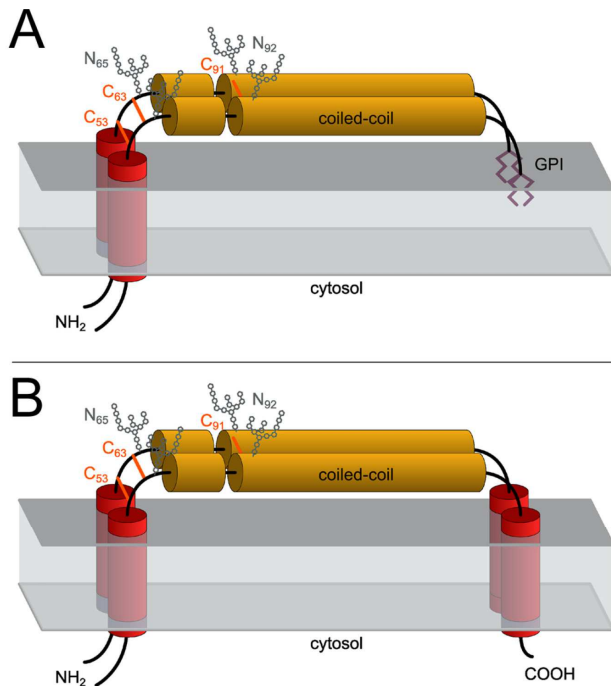


Fig. (1). Schematic topology of tetherin. (A) Tetherin is a type 2 transmembrane protein of 180 amino acids. The short cytoplasmic domain contains the 6-YxY-8 motif for clathrin internalization [22, 80], the Nef recognition motif (14-DDIWK-18) [15, 50] and potential ubiquitination sites such as Lys 18 [89] and the 3-Ser-Thr-Ser-5 sequence motif [70]. Tetherin forms dimers and the extracellular domain is stabilized by 3 interchain disulfide bonds [23, 38, 39, 72], contains 2 glycosylation sites and its C-terminus is anchored by a second membrane anchor, a glycosylphosphatidylinositol anchor [32]. (B) The identity of the second membrane anchor was recently challenged and it was proposed that the C-terminus contains a proper transmembrane region [35]. It is possible that both forms, the TM-GPI and TM-TM form are expressed on the cell surface, because at least some tetherin can be cleaved at the cell surface with PI-PLC treatment.

LENTIVIRAL ANATOGONISTS INTERACT DIRECTLY WITH TETHERIN

The evolution of Vpu function as a tetherin antagonist is highly species-specific [10, 41, 42]. Notably, not all Vpus from HIV-1 such as group P can antagonize tetherin [43] and the tetherin-driven adaptation of Vpu might have contributed to the generation of pandemic and non-pandemic HIV-1 strains [15]. The interaction between Vpu and tetherin requires their respective transmembrane regions [41, 44-46]. Mutations affecting tetherin residues within or bordering the predicted transmembrane domain, such as Ile34, Leu37, Leu41 [47], as well as Thr45, lead to loss of sensitivity to Vpu; however, residues within the cytoplasmic region and within the extracellular domain might play additional roles in species-specific adaptation [44]. Likewise Vpu transmembrane residues Ala14, Ala18 and Trp22 are important for its antagonist function [48], and might thus contribute to the specificity of the anti-parallel helix-helix

interaction suggested by NMR analysis [49]. This interaction involves single faces of each helix: the ¹⁰AXXXAXXXAXXXW²² sequence of Vpu and the ³⁰VXXXLXXLXXXL⁴¹ sequence of tetherin. Notably, the AXXXXXXA motif in Vpu is well conserved among pandemic group M and rare group N HIV-1 isolates, and alanine residues from the transmembrane region of Vpu might fit into ridges formed by large hydrophobic residues within the tetherin transmembrane region [49].

Most SIVs evolved Nef as their tetherin antagonist [9, 10]. The susceptibility of primate tetherins to SIV Nefs is determined by the amino-terminal cytoplasmic region of primate tetherin [15, 50, 51], and myristylation of Nef is important for its antagonist function [9, 10]. Interestingly, mutations in Nef and Vpu that affect CD4 degradation impair anti-tetherin function [9, 52]; this might be due to the fact that these mutations affect the recruitment of adapter proteins (β-TrCP and AP2) that may be required for both, CD4 and tetherin function.

In contrast, HIV-2 and some SIVs such as SIVtan employ Env to antagonize tetherin [8, 53, 54]. It has been shown before that HIV-2 Env can functionally replace HIV-1 Vpu and enhance particle release [55, 56]. The anti-tetherin activity might be mediated by an endocytotic motif within the cytoplasmic domain of gp41 that was shown to interact with AP2, leading to tetherin down regulation [8].

Although quite challenging, it is tempting to propose that drugs that prevent the Vpu-tetherin interaction might have great potential in setting an important immune factor free to help control the infection.

ANTAGONIST INTERACTION LEADS TO DECREASED SURFACE EXPRESSION LEVELS OF TETHERIN.

Vpu interaction with tetherin leads to the down-regulation of tetherin from the plasma membrane [7, 45]. Evidence suggests that this involves the clathrin-mediated endocytic pathway [57]. The well-established interaction of Vpu with β-TrCP (beta transducin repeat-containing protein) might link the pathway to the cellular ubiquitination machinery and direct tetherin towards lysosomal degradation [45, 58-62]. Further Evidence for the involvement of the endo/lysosomal system comes from the requirement of ESCRTs for tetherin downregulation [63], and from the observation that tetherin largely redistributes from the plasma membrane to endosomes upon HIV-1 infection [64].

Vpu trafficking might be important for tetherin down regulation; for instance, Vpu might retain tetherin within endosomal compartments [65, 66] and prevent its recycling after endocytosis [57, 60, 67]. On the other hand, tetherin might be sequestered within the TGN by Vpu [33, 57, 68] or in a perinuclear compartment [34, 61], as an alternative to removal from the plasma membrane [45, 63, 69]. Furthermore the Vpu-dependent polyubiquitination of serine and threonine residues within the cytoplasmic domain of tetherin might play a role in down regulation [70]. However, besides sequestration in intracellular membrane compartments and lysosomal degradation, tetherin proteasome targeting and degradation was also suggested [42, 59]. In addition, Rabring7 might play a role by

facilitating endocytosis of tethered virions and thus enhance tetherin-mediated restriction [71].

STRUCTURE OF THE TETHERIN ECTODOMAIN

The ectodomain of tetherin contains a predicted coiled region, which was confirmed by crystallography [40]. Expression of the extracellular domain of human tetherin comprising residues 47 to 159 leads to the formation of disulfide linked dimers. Notably a shorter fragment identified by proteolysis, (residues 80 to 147) still dimerizes and is stabilized by a disulfide bond formed by Cys91. Although formation of the disulfide bonds is not per se required for dimerization *in vitro*, disulfide bond formation contributes greatly to the thermostability of the ectodomain, because the melting temperature of the ectodomain drops from ~ 61° C to ~ 35° C under reducing conditions [40]. Similar melting temperatures were reported for mouse tetherin [72]. The crystal structure of the shorter fragment revealed a parallel coiled coil as predicted [39, 40]. Intriguingly, along the 90 Å long coiled coil, regular heptad positions with classical knobs-into-holes packing alternate with irregular positions such as stutters at Gly109 and Ala130, as well as with heptad positions that splay the coiled coil apart (Glu105d, Val113, Leu116 and Asn141d) (Fig. 2A). However, coiled coil stabilizing interactions are also present at both ends of the coiled coil [40]. Thus the structure suggests that these coiled coil irregularities contribute to the low thermostability in the absence of the disulfide bond. Notably such coiled coil irregularities, which allow assembly and disassembly of the coiled coil have been described for structures which mediate dynamic processes, such as myosin and tropomyosin or the streptococcal M1 protein [73-75]. The disulfide linkage of tetherin thus guarantees that the coiled coil can form again properly after disassembly. The structural propensity of the labile coiled coil that might be in a dynamic equilibrium between assembly and disassembly thus further explains the necessity for the presence of at least one disulfide bond for tetherin function [23, 38, 39]. The N-terminal part of the ectodomain is linked *via* a protease sensitive region to the coiled coil domain. Together they form an elongated bent 170 Å long rod-like structure as determined by small angle X-ray scattering (SAXS) analysis (Fig. 2B). We speculate that the kink in the structure localizes to the protease cleavage site [40], which is consistent with the proposed hinge at amino acid Ala 88 [76]. The ectodomain structure must lie parallel close to the plasma membrane, because only few residues at both ends are available to link it to the two transmembrane anchors. This in itself is a rather unusual topology for a surface glycoprotein. The extended topology of tetherin was confirmed by the crystal structure of the 145 Å long helical ectodomain of murine tetherin, which is stabilized by three disulfide bonds (Cys58, Cys68 and Cys96, which corresponds to human tetherin Cys91) (Fig. 2D) [72], as predicted for human tetherin [39]. The presence of the three disulfides explains mutagenesis data that indicates that any two of them can be knocked out without loss of function [23, 38, 39]. Notably, the N-terminal fragment forms a continuous helix with the coiled coil domain in the crystal; however, analysis of the structure of the ectodomain in solution by SAXS revealed a similarly bent structure as

observed for human tetherin (Fig. 2C). This thus indicates that the N-terminal fragment is linked flexibly to the coiled coil, and that one potential conformation out of the ensemble of conformations is a continuous helix as shown by the crystal structure [72]. It is thus most likely that this conserved flexible linkage of the N-terminal region to the core coiled coil is important for tetherin function. Alternatively, we cannot exclude the possibility that the presence of both membrane anchors will constrain the ectodomain into one defined conformation. In addition, the coiled coil irregularities are conserved and likely present in all tetherin sequences, highlighting their evolutionarily conserved design [40, 72]. The soluble ectodomain of murine tetherin revealed some degree of self association in solution, and crystal packing showed two potential dimer-dimer interfaces that might be important for function [72]. Furthermore, mapping the sequence conservation of tetherin from different species onto the structure of murine tetherin revealed three major patches, which are close to the glycosylation sites (Asn 70 and Asn 97), as well as within the region of Arg120 to Val128 [72]. Notably, in the case of human tetherin, mutations within the first cluster (Fig. 2E) impair its ability to inhibit HIV-1 release [40]. These regions might be important for tetherin self organization, or may function as binding regions for cellular factors such as human ILT7 [29]. The structure of the ectodomain of human tetherin, was also determined under reducing conditions (Fig. 2F) [76, 77]. Although the biological significance of the reduced structure is as yet unclear, it is interesting to note that the coiled coil conformation of the ectodomain corresponds well to all other structures. However, the N-terminal region that forms a continuous helix with the coiled coil, as in the murine tetherin structure [72], is splayed apart, and the cysteines are too distant to form disulfide bonds (Fig. 2F) [76, 77]. Notably, this N-terminal region is involved in dimerization in the crystal. However, mutations within the dimer-dimer interface had only minor effects on tethering function [76, 77].

A number of mutational analyses provided additional insight into the structure-function relationship. First, as mentioned above, an N-terminal surface patch is important for tethering function [40]. Secondly, the proper formation of the coiled coil is required, because mutations that disrupt coiled coil formation (Fig. 2A) abrogate tethering function [40]. In addition, coiled coil formation is important for subcellular distribution and membrane microdomain clustering, and mutations within the coiled coil affect tetherin endocytosis [78]. Thirdly, although there are 3 disulfide bonds stabilizing the dimer, none of the three is individually required for function [38, 39]. Fourth, the role of intact glycosylation at Asn 65 and Asn 92 is controversial; it might play at best a minor role [38, 40], while others reported that the Asn 92 to Ala mutation markedly impaired activity and the double mutant was almost completely inactive [39]. Fifth, deletion of either membrane anchor showed that both are important for tethering function [39]. Sixth, the general architecture of the ectodomain can be replaced by homologous protein domains. Such an artificial tetherin (art-tetherin), composed of parts of the transferrin receptor ((~20 amino acid residues of its cytoplasmic tail (residues 43-62), the transmembrane domain (residues

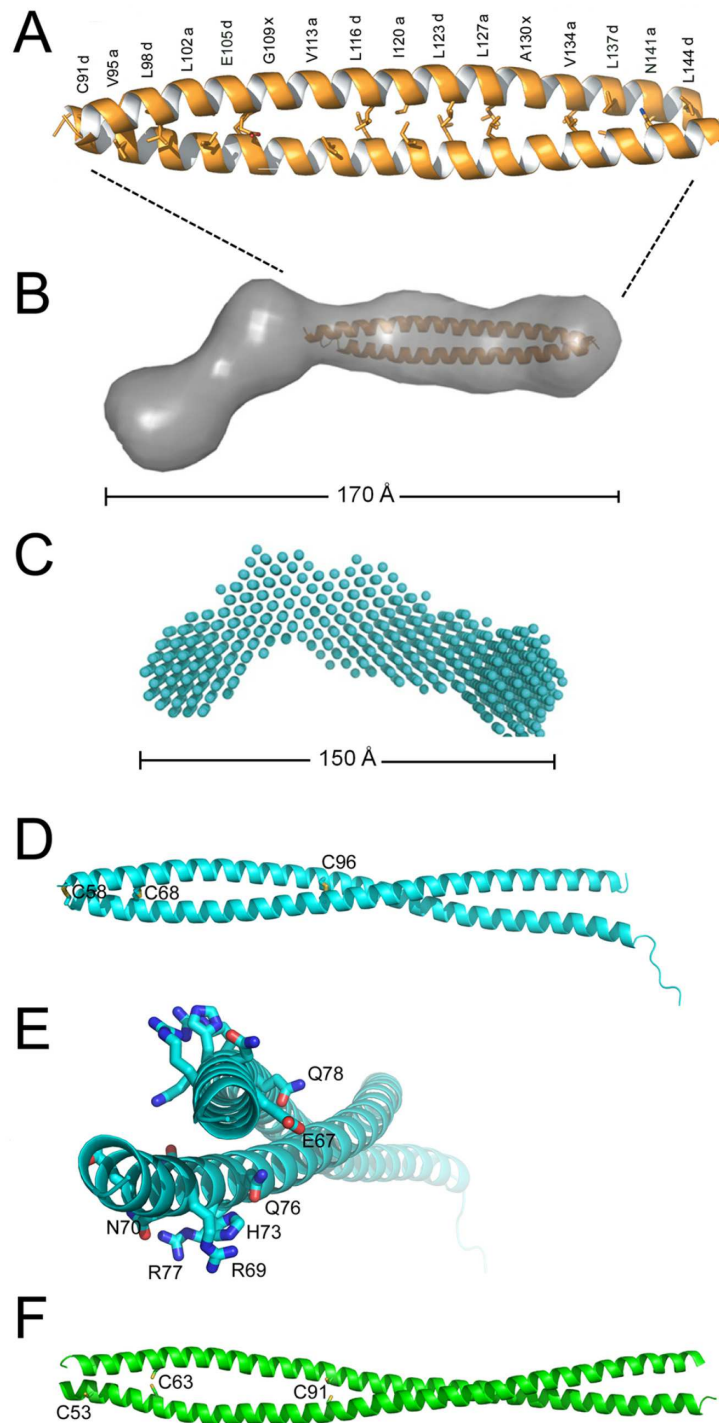


Fig. (2). Structural models of the tetherin ectodomain. (A) Ribbon representation of the 90 Å long parallel coiled coil from the tetherin ectodomain; the residues at heptad positions a and d are shown as sticks. Mutations within the coiled coil designed to destabilize tetherin dimerization (notably two sets of mutations Cys91Gly, Val95Tyr, Leu98Lys, Leu102His and Leu127Lys, Ala130Tyr, Val134Glu, Leu137Glu) render tetherin inactive [40]. (B) Small angle X-ray scattering derived envelope for the complete tetherin ectodomain (residues 47-159) [40]. Maximal protein dimensions were calculated by the distance distribution function. (C) Small angle X-ray scattering derived model for the murine tetherin ectodomain (residues 53-151) [72]. Maximal protein dimensions were calculated by the distance distribution function. (D) X-ray crystal structure of the ectodomain from murine tetherin (residues 53-151). The three cysteines forming disulfide bonds are shown as sticks [72]. (E) A set of mutations that affects tetherin's function maps to the N-terminal domain. The homologous residues of mouse tetherin are shown as sticks (mouse/human: Glu67/62, Arg69/64, Asn70/65, His73/68, Gln76/71, Arg77/Gln72, Glu78/73) [40]. (F) Ribbon diagram of the tetherin ectodomain crystal structure (residues 47 to 152) determined under reducing conditions [76, 77]. The cysteine side chains at positions 53, 63 and 91 are too far apart to form disulfide bonds.

63–88), and part of the extracellular stalk (residues 89–121)) fused to a coiled coil from dystrophin myotonic protein kinase DMPK (~75 residue long coiled coil) and a signal for GPI modification from the urokinase plasminogen activator receptor (uPAR) is still active, albeit at a reduced level [39]. Although full length DMPK forms dimers, the coiled coil region of DMPK forms a trimeric coiled coil in the absence of the kinase domain [79], indicating that it has some conformational flexibility that might substitute for the conformational flexibility of the tetherin coiled coil. Together, these data strongly indicate that the basic tethering function of tetherin is mediated by its overall architecture.

TETHERIN'S TETHERING FUNCTION

The localization of tetherin to plasma membrane microdomains such as lipid rafts [22, 32, 80] provides the ideal condition to interfere with HIV-1 budding from raft-like microdomains [81] and potentially at virological synapses that allow cell-to-cell transfer [82]; although the ability of tetherin to restrict the cell-to-cell transfer of HIV-1 has been challenged [83]. Tetherin enrichment in membrane microdomains was anticipated from its punctuate staining in immunofluorescence images [6, 36, 40]. Tetherin localizes to HIV-1 budding sites [36, 84] and seems to concentrate at such sites, indicating that an enrichment of tetherin might be important for its function [64]. Indeed, super resolution imaging revealed 5–11 tetherin dimers in single 90 nm large clusters in the absence of HIV-1, and 4–7 tetherin dimers associated with HIV-1 budding sites [37]. Tetherin clustering indicates that some form of self association must occur. This view is supported by evidence indicating potential dimerization/multimerization of the tetherin ectodomain [76, 77], which might involve a surface patch within the N-terminal domain [40]. Alternatively, the extent of clustering may be determined by the size of the lipid microdomain that concentrates GPI anchored proteins. The role of clustering was also addressed *via* antibody cross-linking of tetherin that interferes with tethering function, reduces its incorporation into virions, and modifies the distribution of tetherin within membrane raft fractions [85]. Thus, the overall concentration of tetherin at the HIV-1 budding site seems to be important for tetherin function. This is further supported by the fact that even in the presence of Vpu HIV-1 virions incorporate tetherin into their envelope [36] consistent with data indicating that Vpu is not a fully effective antagonist of tetherin [7]. It is therefore plausible that Vpu's reduction of the overall tetherin concentration at the plasma membrane suffices to abrogate tetherin's tethering function.

The original suggestion that tetherin provides a physical link between the plasma membrane and the virus particle [6, 39] is supported by immunogold electron microscopy imaging and by protease experiments that released virions from the plasma membrane [86][36]. In another study, linear filamentous strands that were highly enriched in tetherin bridged the space between some virions [84]. Together these studies provide direct evidence for a physical tetherin linker that retains one set of transmembrane anchors of the parallel rod-like structure in the plasma membrane, while the other set stays anchored in the virion membrane. The average distance between virions and the cell membrane would thus reach up to 17 nm, based on the rod length of the ectodomain

[40]. Inspection of EM images on cell-tethered HIV-1 suggests that such distances are plausible, thus placing the N-terminal or C-terminal membrane anchors either in the plasma membrane or the viral membrane. The alternative mode, which would place one N-terminal transmembrane region and one C-terminal GPI anchor of the dimer in the plasma membrane and the other ones in the viral membrane would align tetherin parallel between the plasma and the virion membrane; this scenario is, however, unlikely, because such close tethering of HIV-1 is not consistent with available EM images of retained virions [6, 36, 39, 64]. Notably, tetherin can physically link one virus to another [6]. This might be explained by a crowded budding site where both sets of membrane anchors end up in two different virions during assembly and budding. This physical linkage of virions by tetherin might also indicate that the directionality of transmembrane anchor insertion might not be important, because both anchors can reside in the viral membrane.

Based on the current data the following model for tetherin activity might apply (Fig. 3). First, the overall length of the rod might serve as a molecular ruler that keeps one set of transmembrane regions outside the budding site while the other set moves into the site of Gag assembly and becomes trapped. We don't know yet whether tetherin is actively recruited and concentrated at the budding site, or whether coincidence of location determines the first contact site. This means that tetherin stays associated with budding virions throughout the budding process including ESCRT-mediated virus release [87]. The dynamic of the coiled coil, evidenced by its propensity to disassemble and assemble and assured by the presence of the disulfide bonds, will guarantee that tetherin will not interfere with the process of virus assembly and budding, thus allowing virion detachment from the plasma membrane [88]. Several tetherin dimers might be required for successful retention of the detached virion, as suggested by tetherin concentrations at budding sites [37, 64]. Retention might require some sort of self assembly that can no longer occur at lower tetherin concentrations induced by Vpu. This is indirectly supported by the observation that HIV-1 virions still incorporate tetherin into their envelope in the presence of Vpu, although tetherin fails to retain virions [36]. However, it should be noted that one dimer could most likely withstand the force exerted by one virion and thus suffice to serve as tether.

CONCLUSIONS

A vast amount of functional and structural data has allowed elucidating the function of tetherin in a relatively short period of time since the discovery of its anti-viral function in 2008, and has led to the emergence of a general model as outlined above and in Fig. (3). However, it still remains an open question how the clustering of tetherin is mediated, and how this affects tetherin's function. What is the regular cellular role of tetherin other than acting as a viral restriction factor? Such a role is strongly supported by the initial discovery that tetherin is implicated in B-cell development and serves as a marker for multiple myeloma cells [22–24]. How is tetherin involved in interferon response control [29]? Furthermore, the fate of tetherin in the presence of Vpu requires further confirmation, and structural work on

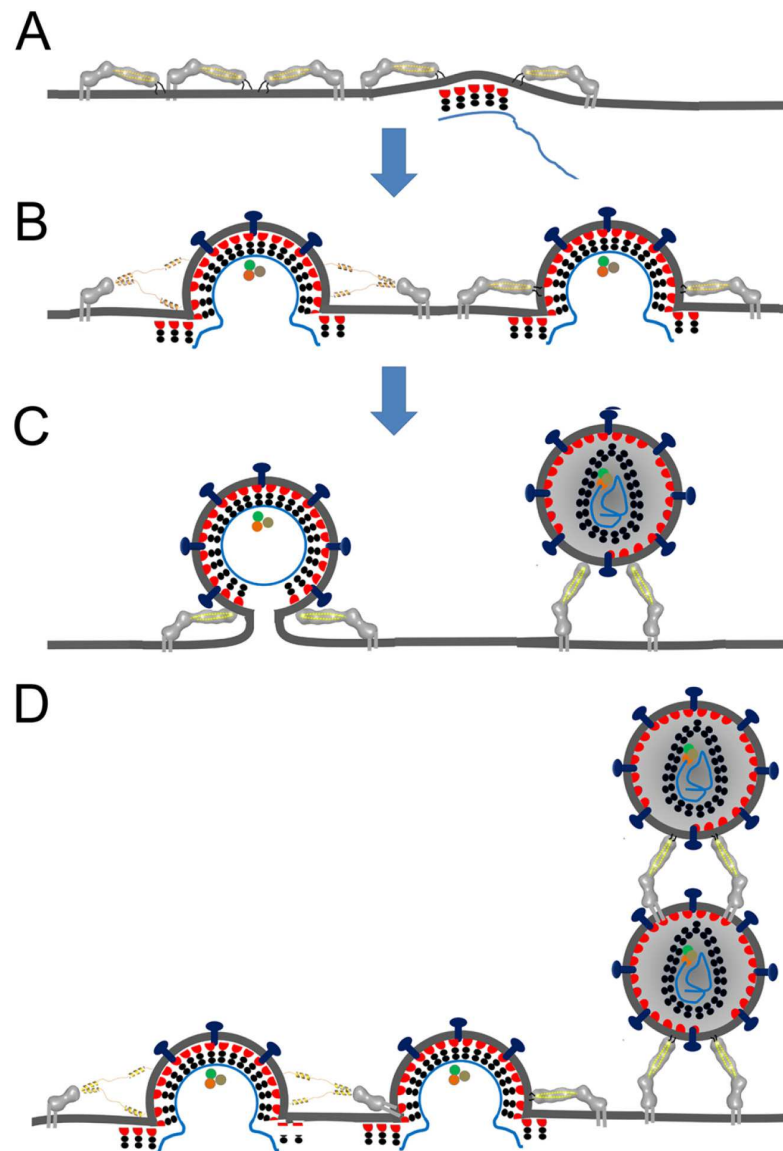


Fig. (3). Model of tetherin function during HIV-1 assembly and budding. (A) Tetherin dimers cluster in lipid microdomains of the plasma membrane, which are sites for virus assembly and budding. Thus tetherin might be present at budding sites by coincidence and could place one membrane anchor within the membrane area that will become the new virus membrane. The kink between the N-terminal region and the core coiled coil observed in the solution structure of the ectodomain might be important for function. (B) The dynamic character of the coiled coil, its opening and closing will not interfere with assembly and budding; in addition the overall length of the extended tetherin ectodomain might act as a molecular ruler keeping the right distance. Notably the length of the coiled coil is important for activity [39]. (C) Thus tetherin might stay associated with budding virions throughout the budding process and retain virions once they are released by ESCRT-driven fission [90]. Because the concentration of tetherin at the budding site seems to be important, it is likely that more than one molecule participates in tethering. Our hypothesis is that some sort of self organization of tetherin might occur around the budding site that renders the tethering process efficient. (D) Crowded budding sites might also lead to tetherin insertion into two budding virions, thus connecting virions after release as supported by the virion clusters observed in EM images [6].

the tetherin-Vpu interaction might form the basis for Vpu inhibitors that prevent the deregulation of tetherin. Thus, the fascinating but rather rare topology of tetherin might capture our attention for some time to come.

ACKNOWLEDGEMENTS

Work in the lab of W.W. is supported by the ANR (Agence Nationale de la Recherche; ANR-08-BLAN-0271-

01), the DFG SPP1175, the ANRS (Agence nationale de recherches sur le sida et les hépatites virales). H.G is supported by the National Institute of Allergy and Infectious Diseases (R37AI029873) and N.A. is supported by a PhD fellowship from the Fond National de la Recherche du Luxembourg.

CONFLICT OF INTEREST

Declared none.

REFERENCES

- [1] Neil, SP Bieniasz. Human immunodeficiency virus, restriction factors, and interferon. *J Interferon Cytokine Res* 2009; 9(29): 569-80.
- [2] Sauter, D, A SpechtF Kirchoff. Tetherin: holding on and letting go. *Cell* 2010; 141(3): 392-8.
- [3] Malim, MH, APOBEC proteins and intrinsic resistance to HIV-1 infection. *Philos Trans R Soc Lond B Biol Sci* 2009; 364(1517): 675-87.
- [4] Sheehy, AM, NC Gaddis, JD ChoiMH Malim. Isolation of a human gene that inhibits HIV-1 infection and is suppressed by the viral Vif protein. *Nature* 2002; 418(6898): 646-50.
- [5] Sastri, JE Campbell. Recent insights into the mechanism and consequences of TRIM5? retroviral restriction. *AIDS Res Hum Retroviruses* 2011; 27(3): 231-8.
- [6] Neil, SJ, T ZangPD Bieniasz. Tetherin inhibits retrovirus release and is antagonized by HIV-1 Vpu. *Nature* 2008; 451(7177): 425-30.
- [7] Van Damme, N, D Goff, C Katsura, *et al.* The interferon-induced protein BST-2 restricts HIV-1 release and is downregulated from the cell surface by the viral Vpu protein. *Cell Host Microbe* 2008; 3(4): 245-52.
- [8] Le Tortorec, ASJ Neil. Antagonism to and intracellular sequestration of human tetherin by the human immunodeficiency virus type 2 envelope glycoprotein. *J Virol* 2009; 83(22): 11966-78.
- [9] Zhang, F, SJ Wilson, WC Landford, *et al.* Nef proteins from simian immunodeficiency viruses are tetherin antagonists. *Cell Host Microbe* 2009; 6(1): 54-67.
- [10] Jia, B, R Serra-Moreno, W Neidermyer, *et al.* Species-specific activity of SIV Nef and HIV-1 Vpu in overcoming restriction by tetherin/BST2. *PLoS Pathog* 2009; 5(5): e1000429.
- [11] Goldstone, DC, V Ennis-Adeniran, JJ Hedden, *et al.* HIV-1 restriction factor SAMHD1 is a deoxynucleoside triphosphate triphosphohydrolase. *Nature* 2011; 480(7377): 379-82.
- [12] Laguette, N, B Sobhian, N Casartelli, *et al.* SAMHD1 is the dendritic- and myeloid-cell-specific HIV-1 restriction factor counteracted by Vpx. *Nature* 2011; 474(7353): 654-7.
- [13] Hrecka, K, C Hao, M Gierszewska, *et al.* Vpx relieves inhibition of HIV-1 infection of macrophages mediated by the SAMHD1 protein. *Nature* 2011; 474(7353): 658-61.
- [14] Lim, ES, OI Fregoso, CO McCoy, *et al.* The Ability of Primate Lentiviruses to Degrade the Monocyte Restriction Factor SAMHD1 Preceded the Birth of the Viral Accessory Protein Vpx. *Cell Host Microbe* 2012; 11(2): 194-204.
- [15] Sauter, D, M Schindler, A Specht, *et al.* Tetherin-Driven Adaptation of Vpu and Nef Function and the Evolution of Pandemic and Nonpandemic HIV-1 Strains. *Cell Host Microbe* 2009; 6(5): 409-421.
- [16] Martin-Serrano, JSJ Neil. Host factors involved in retroviral budding and release. *Nat Rev Microbiol* 2010; 9(7): 519-31.
- [17] Arias, JF, Y IwabuK Tokunaga. Structural basis for the antiviral activity of BST-2/tetherin and its viral antagonism. *Front Microbiol* 2011; 2: 250.
- [18] Andrew, AK Strebel. The interferon-inducible host factor bone marrow stromal antigen 2/tetherin restricts virion release, but is it actually a viral restriction factor? *J Interferon Cytokine Res* 2011; 31(1): 137-44.
- [19] Evans, DT, R Serra-Moreno, RK SinghJC Guatelli. BST-2/tetherin: a new component of the innate immune response to enveloped viruses. *Trends Microbiol* 2010; 18(9): 388-96.
- [20] Douglas, JL, JK Gustin, K Viswanathan, *et al.* The great escape: viral strategies to counter BST-2/tetherin. *PLoS Pathog* 2010; 6(5): e1000913.
- [21] Blasius, AL, E Giuriso, M Cella, *et al.* Bone marrow stromal cell antigen 2 is a specific marker of type I IFN-producing cells in the naive mouse, but a promiscuous cell surface antigen following IFN stimulation. *J Immunol* 2006; 177(5): 3260-5.
- [22] Masuyama, N, T Kuronita, R Tanaka, *et al.* HM1.24 is internalized from lipid rafts by clathrin-mediated endocytosis through interaction with alpha-adaptin. *J Biol Chem* 2009; 284(23): 15927-41.
- [23] Ohtomo, T, Y Sugamata, Y Ozaki, *et al.* Molecular cloning and characterization of a surface antigen preferentially overexpressed on multiple myeloma cells. *Biochem Biophys Res Commun* 1999; 258(3): 583-91.
- [24] Goto, T, SJ Kennel, M Abe, *et al.* A novel membrane antigen selectively expressed on terminally differentiated human B cells. *Blood* 1994; 84(6): 1922-30.
- [25] Kawai, S, Y Azuma, E Fujii, *et al.* Interferon-alpha enhances CD317 expression and the antitumor activity of anti-CD317 monoclonal antibody in renal cell carcinoma xenograft models. *Cancer Sci* 2008; 99(12): 2461-6.
- [26] Neil, SJ, V Sandrin, WI Sundquist, PD Bieniasz. An interferon-alpha-induced tethering mechanism inhibits HIV-1 and Ebola virus particle release but is counteracted by the HIV-1 Vpu protein. *Cell Host Microbe* 2007; 2(3): 193-203.
- [27] Lepelley, A, S Louis, M Sourisseau, *et al.* Innate Sensing of HIV-Infected Cells. *PLoS Pathog* 2011; 7(2): e1001284.
- [28] Liberatore, RA, PD Bieniasz. Tetherin is a key effector of the antiretroviral activity of type I interferon *in vitro* and *in vivo*. *Proc Natl Acad Sci U S A* 2011; 108(44): 18097-101.
- [29] Cao, W, L Bover, M Cho, *et al.* Regulation of TLR7/9 responses in plasmacytoid dendritic cells by BST2 and ILT7 receptor interaction. *J Exp Med* 2009; 206(7): 1603-14.
- [30] Cao, WL Bover. Signaling and ligand interaction of ILT7: receptor-mediated regulatory mechanisms for plasmacytoid dendritic cells. *Immunol Rev* 2010; 234(1): 163-76.
- [31] Erikson, E, T Adam, S Schmidt, *et al.* *In vivo* expression profile of the antiviral restriction factor and tumor-targeting antigen CD317/BST-2/HM1.24/tetherin in humans. *Proc Natl Acad Sci U S A* 2011; 108(33): 13688-93.
- [32] Kupzig, S, V Korolchuk, R Rollason, *et al.* Bst-2/HM1.24 is a raft-associated apical membrane protein with an unusual topology. *Traffic* 2003; 4(10): 694-709.
- [33] Dube, M, BB Roy, P Guiot-Guillain, *et al.* Suppression of Tetherin-restricting activity upon human immunodeficiency virus type 1 particle release correlates with localization of Vpu in the trans-Golgi network. *J Virol* 2009; 83(9): 4574-90.
- [34] Hauser, H, LA Lopez, SJ Yang, *et al.* HIV-1 Vpu and HIV-2 Env counteract BST-2/tetherin by sequestration in a perinuclear compartment. *Retrovirology* 2010; 7: 51.
- [35] Andrew, AJ, S KaoK Strebel. C-terminal hydrophobic region in human bone marrow stromal cell antigen 2 (BST-2)/tetherin protein functions as second transmembrane motif. *J Biol Chem* 2011; 286(46): 39967-81.
- [36] Fitzpatrick, K, M Skasko, TJ Deerinck, *et al.* Direct Restriction of Virus Release and Incorporation of the Interferon-Induced Protein BST-2 into HIV-1 Particles. *PLoS Pathog* 2010; 6(3): e1000701.
- [37] Lehmann, M, S Rocha, B Mangeat, *et al.* Quantitative Multicolor Super-Resolution Microscopy Reveals Tetherin HIV-1 Interaction. *PLoS Pathog* 2011; 7(12): e1002456.
- [38] Andrew, A, E Miyagi, S Kao, K Strebel. The formation of cysteine-linked dimers of BST-2/tetherin is important for inhibition of HIV-1 virus release but not for sensitivity to Vpu. *Retrovirology* 2009; 6(1): 80.
- [39] Perez-Caballero, D, T Zang, A Ebrahimi, *et al.* Tetherin inhibits HIV-1 release by directly tethering virions to cells. *Cell* 2009; 139(3): 499-511.
- [40] Hinz, A, N Miguet, G Natrajan, *et al.* Structural basis of HIV-1 tethering to membranes by the BST-2/tetherin ectodomain. *Cell Host Microbe* 2010; 7(4): 314-23.
- [41] McNatt, MW, T Zang, T Hatziioannou, *et al.* Species-specific activity of HIV-1 Vpu and positive selection of tetherin transmembrane domain variants. *PLoS Pathog* 2009; 5(2): e1000300.

- [42] Goffinet, C, I Allespach, S Homann, *et al.* HIV-1 antagonism of CD317 is species specific and involves Vpu-mediated proteasomal degradation of the restriction factor. *Cell Host Microbe* 2009; 5(3): 285-97.
- [43] Sauter, D, S Hue, SJ Petit, *et al.* HIV-1 Group P is unable to antagonize human tetherin by Vpu, Env or Nef. *Retrovirology* 2011; 8(1): 103.
- [44] Gupta, RK, S Hue, T Schaller, *et al.* Mutation of a single residue renders human tetherin resistant to HIV-1 Vpu-mediated depletion. *PLoS Pathog* 2009; 5(5): e1000443.
- [45] Iwabu, Y, H Fujita, M Kinomoto, *et al.* HIV-1 accessory protein Vpu internalizes cell-surface BST-2/tetherin through transmembrane interactions leading to lysosomes. *J Biol Chem* 2009; 284(50): 35060-72.
- [46] Rong, L, J Zhang, J Lu, *et al.* The transmembrane domain of BST-2 determines its sensitivity to down-modulation by human immunodeficiency virus type 1 Vpu. *J Virol* 2009; 83(15): 7536-46.
- [47] Kobayashi, T, H Ode, T Yoshida, *et al.* Identification of amino acids in the human tetherin transmembrane domain responsible for HIV-1 Vpu interaction and susceptibility. *J Virol* 2011; 85(2): 932-45.
- [48] Vigan, R, SJ Neil. Determinants of tetherin antagonism in the transmembrane domain of the human immunodeficiency virus type 1 Vpu protein. *J Virol* 2010; 84(24): 12958-70.
- [49] Skasko, M, Y Wang, Y Tian, *et al.* HIV-1 Vpu Protein Antagonizes Innate Restriction Factor BST-2 via Lipid-embedded Helix-Helix Interactions. *J Biol Chem* 2012; 287(1): 58-67.
- [50] Lim, ES, HS Malik, M Emerman. Ancient adaptive evolution of tetherin shaped the functions of Vpu and Nef in human immunodeficiency virus and primate lentiviruses. *J Virol* 2010; 84(14): 7124-34.
- [51] Yang, SJ, LA Lopez, H Hauser, *et al.* Anti-tetherin activities in Vpu-expressing primate lentiviruses. *Retrovirology* 2010; 7: 13.
- [52] Schindler, M, D Rajan, C Banning, *et al.* Vpu serine 52 dependent counteraction of tetherin is required for HIV-1 replication in macrophages, but not in ex vivo human lymphoid tissue. *Retrovirology* 2010; 7: 1.
- [53] Gupta, RK, P Mlcochova, A Pelchen-Matthews, *et al.* Simian immunodeficiency virus envelope glycoprotein counteracts tetherin/BST-2/CD317 by intracellular sequestration. *Proc Natl Acad Sci USA* 2009; 106(49): 20889-94.
- [54] Serra-Moreno, R, B Jia, M Breed, *et al.* Compensatory changes in the cytoplasmic tail of gp41 confer resistance to tetherin/BST-2 in a pathogenic nef-deleted SIV. *Cell Host Microbe* 2011; 9(1): 46-57.
- [55] Bour, S, K Strebel. The human immunodeficiency virus (HIV) type 2 envelope protein is a functional complement to HIV type 1 Vpu that enhances particle release of heterologous retroviruses. *J Virol* 1996; 70(12): 8285-300.
- [56] Abada, P, B Noble, PM Cannon. Functional domains within the human immunodeficiency virus type 2 envelope protein required to enhance virus production. *J Virol* 2005; 79(6): 3627-38.
- [57] Lau, D, W Kwan, J Guatelli. Role of the endocytic pathway in the counteraction of BST-2 by human lentiviral pathogens. *J Virol* 2011; 85(19): 9834-46.
- [58] Douglas, JL, K Viswanathan, MN McCarroll, *et al.* Vpu directs the degradation of the human immunodeficiency virus restriction factor BST-2/Tetherin via a β -TrCP-dependent mechanism. *J Virol* 2009; 83(16): 7931-47.
- [59] Mangeat, B, G Gers-Huber, M Lehmann, *et al.* HIV-1 Vpu neutralizes the antiviral factor Tetherin/BST-2 by binding it and directing its β -TrCP2-dependent degradation. *PLoS Pathog* 2009; 5(9): e1000574.
- [60] Mitchell, RS, C Katsura, MA Skasko, *et al.* Vpu antagonizes BST-2-mediated restriction of HIV-1 release via β -TrCP and endo-lysosomal trafficking. *PLoS Pathog* 2009; 5(5): e1000450.
- [61] Dube, M, BB Roy, P Guiot-Guillain, *et al.* Antagonism of tetherin restriction of HIV-1 release by Vpu involves binding and sequestration of the restriction factor in a perinuclear compartment. *PLoS Pathog* 2010; 6(4): e1000856.
- [62] Tervo, HM, S Homann, I Ambiel, *et al.* β -TrCP is dispensable for Vpu's ability to overcome the CD317/Tetherin-imposed restriction to HIV-1 release. *Retrovirology* 2011; 8: 9.
- [63] Janvier, K, A Pelchen-Matthews, JB Renaud, *et al.* The ESCRT-0 component HRS is required for HIV-1 Vpu-mediated BST-2/tetherin down-regulation. *PLoS Pathog* 2011; 7(2): e1001265.
- [64] Habermann, A, J Krijnse Locker, H Oberwinkler, *et al.* CD317/Tetherin is enriched in the HIV-1 envelope 1 and downregulated from the plasma membrane upon virus infection. *J Virol* 2010; 84(9): 4646-58.
- [65] Gupta, RK, P Mlcochova, A Pelchen-Matthews, *et al.* Simian immunodeficiency virus envelope glycoprotein counteracts tetherin/BST-2/CD317 by intracellular sequestration. *Proc Natl Acad Sci U S A* 2009; 106(49): 20889-94.
- [66] Goffinet, C, S Homann, I Ambiel, *et al.* Antagonism of CD317 restriction of human immunodeficiency virus type 1 (HIV-1) particle release and depletion of CD317 are separable activities of HIV-1 Vpu. *J Virol* 2010; 84(8): 4089-94.
- [67] Schmidt, S, JV Fritz, J Bitzegeio, *et al.* HIV-1 Vpu blocks recycling and biosynthetic transport of the intrinsic immunity factor CD317/tetherin to overcome the virion release restriction. *M Bio* 2011; 2(3): e00036-11.
- [68] Andrew, AJ, E Miyagi, K Strebel. Differential effects of human immunodeficiency virus type 1 Vpu on the stability of BST-2/tetherin. *J Virol* 2011; 85(6): 2611-9.
- [69] Skasko, M, A Tokarev, CC Chen, *et al.* BST-2 is rapidly down-regulated from the cell surface by the HIV-1 protein Vpu: evidence for a post-ER mechanism of Vpu-action. *Virology* 2011; 411(1): 65-77.
- [70] Tokarev, AA, J Munguia, JC Guatelli. Serine-threonine ubiquitination mediates downregulation of BST-2/tetherin and relief of restricted virion release by HIV-1 Vpu. *J Virol* 2011; 85(1): 51-63.
- [71] Miyakawa, K, A Ryo, T Murakami, *et al.* BCA2/Rabring7 promotes tetherin-dependent HIV-1 restriction. *PLoS Pathog* 2009; 5(12): e1000700.
- [72] Swiecki, M, SM Scheaffer, M Allaire, *et al.* Structural and biophysical analysis of BST-2/tetherin ectodomains reveals an evolutionary conserved design to inhibit virus release. *J Biol Chem* 2010; 286(4): 2987-97.
- [73] Blankenfeldt, W, NH Thoma, JS Wray, *et al.* Crystal structures of human cardiac beta-myosin II S2-Delta provide insight into the functional role of the S2 subfragment. *Proc Natl Acad Sci U S A* 2006; 103(47): 17713-7.
- [74] Li, Y, JH Brown, L Reshetnikova, *et al.* Visualization of an unstable coiled coil from the scallop myosin rod. *Nature* 2003; 424(6946): 341-345.
- [75] McNamara, C, AS Zinkernagel, P Macheboeuf, *et al.* Coiled-coil irregularities and instabilities in group A Streptococcus M1 are required for virulence. *Science* 2008; 319(5868): 1405-8.
- [76] Yang, H, J Wang, X Jia, *et al.* Structural insight into the mechanisms of enveloped virus tethering by tetherin. *Proc Natl Acad Sci U S A* 2010; 107(43): 18428-32.
- [77] Schubert, HL, Q Zhai, V Sandrin, *et al.* Structural and functional studies on the extracellular domain of BST2/tetherin in reduced and oxidized conformations. *Proc Natl Acad Sci U S A* 2010; 107(42): 17951-6.
- [78] Hammonds, J, L Ding, H Chu, *et al.* The Tetherin/BST-2 Coiled-Coil Ectodomain Mediates Plasma Membrane Microdomain Localization and Restriction of Particle Release. *J Virol* 2011.
- [79] Garcia, P, Z Ucurum, R Bucher, *et al.* Molecular insights into the self-assembly mechanism of dystrophin myotonic kinase. *Faseb J* 2006; 20(8): 1142-51.
- [80] Rollason, R, V Korolchuk, C Hamilton, *et al.* Clathrin-mediated endocytosis of a lipid-raft-associated protein is mediated through a dual tyrosine motif. *J Cell Sci* 2007; 120(Pt 21): 3850-8.
- [81] Waheed, AA, EO Freed. The Role of Lipids in Retrovirus Replication. *Viruses* 2010; 2(5): 1146-80.
- [82] Casartelli, N, M Sourisseau, J Feldmann, *et al.* Tetherin restricts productive HIV-1 cell-to-cell transmission. *PLoS Pathog* 2010; 6(6): e1000955.
- [83] Jolly, C, NJ Booth, SJ Neil. Cell-cell spread of human immunodeficiency virus type 1 overcomes tetherin/BST-2-mediated restriction in T cells. *J Virol* 2010; 84(23): 12185-99.

- [84] Hammonds, J, JJ Wang, H Yi, P Spearman. Immunoelectron microscopic evidence for Tetherin/BST2 as the physical bridge between HIV-1 virions and the plasma membrane. *PLoS Pathog* 2010; 6(2): e1000749.
- [85] Miyagi, E, A Andrew, S Kao, *et al.* Antibody-mediated enhancement of HIV-1 and HIV-2 production from BST-2/tetherin-positive cells. *J Virol* 2011; 85(22): 11981-94.
- [86] Neil, SJ, SW Eastman, N Jouvenet, PD Bieniasz. HIV-1 Vpu promotes release and prevents endocytosis of nascent retrovirus particles from the plasma membrane. *PLoS Pathog* 2006; 2(5): e39.
- [87] Usami, Y, S Popov, E Popova, *et al.* The ESCRT pathway and HIV-1 budding. *Biochem Soc Trans* 2009; 37(Pt 1): 181-4.
- [88] Dordor, A, E Poudevigne, H Gottlinger, W Weissenhorn. Essential and supporting host cell factors for HIV-1 budding. *Future Microbiol* 2011; 6(10): 1159-70.
- [89] Mansouri, M, K Viswanathan, JL Douglas, *et al.* Molecular mechanism of BST2/Tetherin downregulation by K5/MIR2 of Kaposi's sarcoma herpesvirus. *J Virol* 2009.
- [90] Peel, S, P Macheboeuf, N Martinelli, W Weissenhorn. Divergent pathways lead to ESCRT-III-catalyzed membrane fission. *Trends Biochem Sci* 2011; 36(4): 199-210.

Received: January 19, 2012

Revised: March 1, 2012

Accepted: March 4, 2012

Appendix C

La tétherine, dernière amarre du HIV

Review article in *Virologie*, 2012

La tétherine, dernière amarre du VIH

Nicolas Aschman
Winfried Weissenhorn
Patricia Renesto

Unit of Virus Host Cell Interactions
(UVHCI)-UMI 3265,
université Joseph-Fourier-EMBL-CNRS,
6, rue Jules-Horowitz,
38042 Grenoble,
France
<prenesto@embl.fr>

Résumé. La tétherine est une glycoprotéine originale qui utilise ses extrémités N- et C-terminales pour s'ancrer dans les membranes. Chez certains types cellulaires, l'expression de cette protéine est induite par l'interféron, ce qui conduit à l'inhibition de la réplication du VIH-1, en l'absence de son antagoniste viral, la protéine Vpu. Cette revue présente les progrès récents relatifs à la compréhension des mécanismes moléculaires impliqués dans la rétention, par la tétherine, des virus enveloppés, dont le VIH-1. La régulation négative de la tétherine par divers antagonistes viraux est également discutée. Les données structurales récentes ont mis en évidence une structure allongée de l'ectodomaine de la tétherine, qui est vraisemblablement orienté parallèlement à la membrane cellulaire. L'interprétation de ces données structurales est abordée par rapport à la capacité de la tétherine à retenir physiquement les virions au niveau de la membrane plasmique.

Mots clés : VIH-1, tétherine, BST-2, Vpu, Nef

Abstract. Tetherin is an unusual surface glycoprotein that employs an N-terminal and a C-terminal region to anchor the protein into membranes. Structural analyses revealed an elongated structure for the ectodomain that is probably oriented parallel to cellular membranes. Expression of tetherin can be induced by interferon in selected cell types, which leads to the restriction of HIV-1 replication in the absence of the viral antagonist Vpu. This review focuses on recent progress on the understanding of the molecular mechanisms of tetherin function during HIV and other enveloped virus budding processes. We discuss the role of diverse viral antagonists in tetherin down regulation and place the structural information on the ectodomain into the context of tetherin's ability to physically link virions such as HIV-1 to the plasma membrane after completion of budding.

Key words: HIV-1, tetherin, BST-2, Vpu, Nef

Introduction

La tétherine est une protéine cellulaire initialement clonée en 1995 à partir d'une lignée synoviale dérivée d'un patient atteint de polyarthrite rhumatoïde et exprimée par les cellules stromales de la moelle osseuse d'où son appellation *bone marrow stromal cell antigen 2* (BST-2) [1]. Ce n'est qu'une décennie plus tard que son rôle majeur dans la réponse immunitaire de l'hôte en réponse à une infection virale a été évoqué. En 2008, cette protéine (aussi appelée CD317 ou HM1.24) fut en effet caractérisée comme un facteur de restriction cellulaire induit par l'interféron α (IFN α)

[2], et capable de bloquer la libération de virus enveloppés, dont le VIH-1, qui restent alors ancrés à la surface de la cellule hôte, d'où sa désignation tétherine, du verbe *to tether*, attacher [3, 4]. Deux autres familles de facteurs de restriction induits par une réponse interféron et capables d'inhiber la réplication du VIH-1 ont été antérieurement décrites, soit APOBEC qui sont des cytidines déaminases, enzymes de modification de l'ARN et/ou de l'ADN [5] et *tripartite motif 5 alpha* (TRIM5 α) [6]. Dans les deux cas, il a été montré que le virus disposait d'une stratégie spécifique pour contrer l'activité inhibitrice de ces facteurs de restriction [7]. En plus, des protéines structurales Gag, Env et Pol, le génome du VIH-1 code pour deux protéines régulatrices Tat et Rev qui interviennent dans le contrôle de la réplication virale, ainsi que pour quatre protéines, dites accessoires

Tirés à part : P. Renesto

qui sont Vif, Vpu, Nef et Vpr et qui jouent un rôle clé dans la pathogénicité du VIH-1 [8]. Ainsi, c'est la protéine virale Vif qui empêche l'activité de la protéine *apolipoprotein B mRNA-editing enzyme, catalytic polypeptide-like G3* (APOBEC3G) en induisant sa poly-ubiquitinylation, ce qui conduit à sa dégradation par la voie du protéasome et empêche son encapsidation [9]. C'est une autre protéine accessoire, en l'occurrence la protéine Vpu, qui assure la neutralisation de la tétherine [3, 4]. Il est intéressant de souligner que, loin d'être spécifique, l'activité de la tétherine affecte le relargage de plusieurs rétrovirus ainsi que d'un certain nombre de virus enveloppés d'autres familles comprenant les *Filoviridae*, les *Arenaviridae* et les *Herpesviridae* [10]. De fait, il est maintenant clairement établi que ce mode d'action ubiquitaire de la tétherine résulte de sa capacité à cibler une composante commune à l'infection cellulaire par différents virus, en l'occurrence la bicouche lipidique dérivée de la cellule hôte.

La découverte de l'activité antivirale de la tétherine a suscité un grand intérêt dans la communauté scientifique dans la mesure où l'interaction tétherine/Vpu représente une cible thérapeutique potentielle pour lutter contre le VIH-1. Bloquer l'effet de Vpu par de petites molécules pourrait en effet promouvoir l'exposition des particules virales à la tétherine et empêcher la sortie du virus de la cellule. Cette revue fait le point sur l'état des connaissances actuelles sur ce sujet, et en particulier les caractéristiques moléculaires de la tétherine, les mécanismes par lesquels ce facteur de restriction exerce son activité antivirale, ainsi que les stratégies mises en place par la protéine Vpu du VIH-1 pour neutraliser cet effet. La capacité de protéines d'autres virus à contrer l'effet de la tétherine humaine sera également abordée.

Qu'est-ce que la tétherine ?

Régulation transcriptionnelle et localisation sub-cellulaire

La tétherine est codée par le gène *bst-2* composé de quatre exons et présent en une seule copie dans le génome humain [1]. Alors que le polymorphisme de ce gène est quasi nul chez l'homme, les orthologues présents dans les génomes d'autres mammifères montrent des variations de séquence significatives. Cette protéine est constitutivement exprimée par les cellules stromales de la moelle osseuse, les cellules B matures, certaines lignées cancéreuses, les macrophages dérivés de monocytes ainsi que par les cellules dendritiques plasmacytoïdes (pDCs) [7, 11]. L'expression de la tétherine peut également être induite par l'IFN α , comme c'est le cas concernant les lignées de cellules T cancéreuses classiquement utilisées en laboratoire pour les études d'infection par le VIH. Cette surexpression met en jeu le facteur de

transcription Stat3 pour lequel il existe un site de liaison dans la région promotrice de *bst-2*. Outre sa capacité à interagir avec Vpu, la tétherine est aussi un ligand du récepteur *immunoglobulin-like transcript 7* (ILT7) exprimé à la surface des pDCs. Étant donné que cette voie de signalisation inhibe la production de l'interféron et de cytokines pro-inflammatoires par les pDCs, la tétherine pourrait par conséquent exercer un rétro-contrôle négatif de sa sécrétion [12]. Il faut souligner que des analyses transcriptomiques récentes, réalisées à partir de tissus humains prélevés sur différents organes sains, indiquent que la tétherine est exprimée dans beaucoup plus de tissus qu'on ne le pensait et que son expression pourrait ne pas être essentiellement IFN α -dépendante [13].

Des analyses en immuno-microscopie électronique ont montré que la tétherine endogène était localisée sur la membrane plasmique, le réseau trans-Golgi et le compartiment endosomal [14]. Suite à l'infection des cellules par les particules virales, l'on assiste à une redistribution de la tétherine au niveau des endosomes, effet partiellement contrebalancé par Vpu. Au sein de la membrane cellulaire, la tétherine est plus spécifiquement concentrée au niveau des radeaux lipidiques riches en cholestérol. L'imagerie par fluorescence montre d'ailleurs une distribution ponctuelle en grappe de la protéine [15, 16]. C'est aussi au niveau de ces microdomaines qu'intervient l'assemblage des sous-unités Gag de VIH-1 et le bourgeonnement viral [17]. Une colocalisation de la tétherine et de Gag a d'ailleurs été mise en évidence à la surface de cellules infectées [3, 4].

Topologie de la tétherine

La tétherine a initialement été décrite comme une protéine transmembranaire de type II caractérisée par la présence d'un court domaine N-terminal cytoplasmique et d'un domaine C-terminal exposé dans l'espace extracellulaire (*figure 1*) [7, 18, 19]. Le domaine N-terminal de la tétherine humaine possède le motif conservé YXY impliqué dans l'endocytose clathrine-dépendante de la tétherine *via* le recrutement préalable de complexes adaptateurs AP-1 et AP-2 [20]. Ce domaine cytoplasmique peut également interagir indirectement avec le réseau d'actine sous-cortical, la connexion étant assurée par des protéines ezrine, radixine, moésine (ERM) [21]. À ce jour, aucun lien entre cette interaction et le rôle exercé par la tétherine comme facteur de restriction n'a toutefois été établi.

Le domaine extracellulaire présente une conformation *coiled coil* ou faisceau d'hélices dont les deux extrémités sont amarrées à la membrane plasmique. L'ancrage dans la bicouche lipidique est assuré par une hélice α du côté N-terminal et l'extrémité du domaine C-terminal est modifiée par un groupement *glycosyl-phosphatidylinositol* (GPI)

Toutefois, sans remettre complètement en question le postulat initial, ces auteurs évoquent un problème d'accessibilité de ces liaisons par les agents réducteurs, dû au repliement de la protéine. Si la corrélation entre l'organisation dimérique et l'activité de la tétherine vis-à-vis du VIH-1 a pu être établie par la mutation des trois résidus cystéine extracellulaires (C53A C63A C91A) [24, 25], il faut souligner que ces mutations n'ont aucune conséquence sur la rétention d'arénavirus (virus de Lassa) ou de Marburgvirus [26]. Par ailleurs, il a été montré que la glycosylation de la tétherine (N65 et N92) n'interfère pas avec son activité de rétention virale [25]. L'ensemble de ces travaux plaide en faveur d'un rôle direct de la tétherine qui ne nécessiterait pas le recrutement de cofacteurs.

Données cristallographiques

Si la conformation de la tétherine lors du bourgeonnement viral reste inconnue, des études cristallographiques et biophysiques récentes du domaine extracellulaire des protéines humaines et murines ont permis d'élucider les bases structurales de l'attachement des virions naissants à la membrane plasmique. Plusieurs structures cristallographiques de l'ectodomaine de la tétherine ont été publiées au cours de l'année 2010. La première de ces structures, publiée par notre laboratoire [15], décrit le faisceau d'hélices disposées de façon antiparallèle et qui forme un domaine *coiled coil* de 90 Å de long (figure 2A). Les mesures de thermostabilité de cette région *coiled coil*, par rapport à l'ectodomaine dans sa globalité, ont démontré

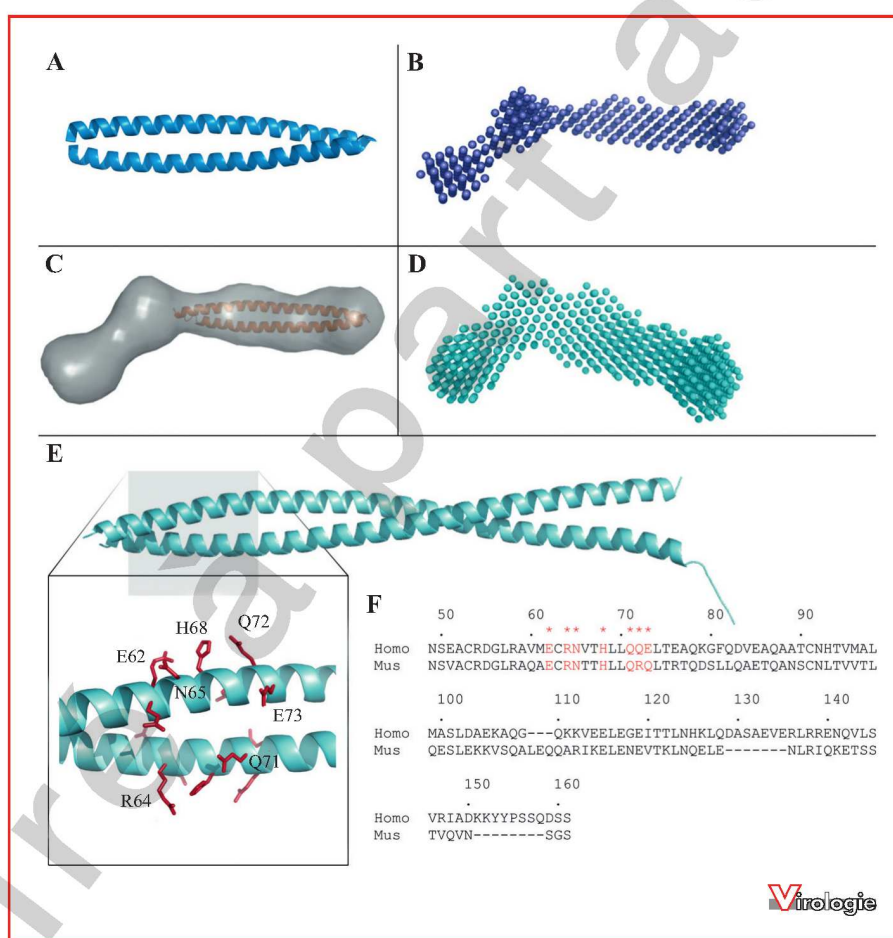


Figure 2. Structure cristallographique de la tétherine.

A) Structure cristallographique de la tétherine humaine (80-147). **B)** Modélisation de la tétherine humaine (47-159) par diffusion aux petits angles des rayons X en solution (SAXS). **C)** Superposition de la structure cristallographique de la tétherine humaine dans le modèle dérivé des données SAXS. **D)** Modélisation de données SAXS et **E)** structure cristallographique de la tétherine murine (53-151). Projection, sur la structure murine, des résidus de la tétherine humaine impliqués dans la rétention du VIH-1 [15]. **F)** Alignements des séquences protéines des protéines humaines et murines. Les résidus montrés en E sont indiqués par une étoile.

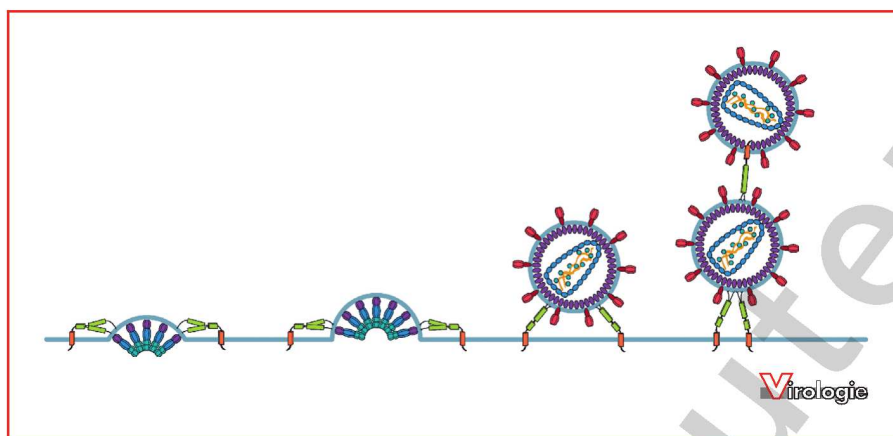


Figure 3. Représentation schématique de la rétention virale exercée par la tétherine.

La tétherine insère l'une de ses extrémités dans les nouveaux virions au cours du processus de bourgeonnement. Plusieurs molécules de tétherine pourraient être recrutées simultanément, cordonnées par une interaction du domaine N-terminal. Cette étape est facilitée par la flexibilité conformationnelle de cette protéine qui permet l'assemblage et le désassemblage du domaine *coiled coil*, grâce à la présence de ponts disulfures. Ainsi, la flexibilité conformationnelle de la tétherine permet son association avec les virions naissants tout au long du processus dynamique de bourgeonnement. Lorsque ceux-ci sont libérés *via* un processus ESCRT-dépendant [72], la tétherine conserve la capacité de retenir les virions par un lien physique.

En effet, la tétherine est non seulement localisée entre la membrane plasmique des cellules infectées et les particules virales, mais également entre les particules virales elles-mêmes [3]. Lorsque des cellules adhérentes exprimant la tétherine sont infectées avec des virions VIH-1 déficients en Vpu (delVpu), la proportion de particules retenues à la surface cellulaire est significativement supérieure à celle observée avec la souche sauvage (WT) du virus. Dans ces conditions, des virions VIH-1 (delVpu) matures sont aussi fréquemment retrouvés dans le compartiment intracellulaire des cellules infectées. Les particules virales retenues par la tétherine peuvent en effet être internalisées par endocytose Rab5a-dépendante et s'accumuler dans les endosomes tardifs CD63⁺ [3]. Une étude récente a montré que l'interaction entre *breast cancer associated gene 2* ([BCA2] aussi connu sous le nom de Rabring7 ou RFN115) et la tétherine favorisait l'endocytose des particules VIH-1 retenues à la surface plasmique et leur ciblage vers leur destination lysosomale [31]. Inversement, une déplétion de la protéine BCA2 endogène se traduit par une diminution significative de l'accumulation des particules virales intracellulaires et une augmentation de virions à la surface de la cellule infectée. Bien que la protéine BCA2 soit exprimée dans de nombreux types cellulaires, son activité antivirale n'est observée que dans les cellules exprimant la tétherine. Compte tenu de son activité antivirale potentielle, cette protéine produite par la cellule hôte pourrait représenter une nouvelle cible thérapeutique dans le traitement des infections VIH. Les mécanismes moléculaires mis en jeu restent à élucider, mais les effets conjoints de BCA2 et de Rab7 sur le trafic vésiculaire a été évoqué. Le domaine de BCA2 qui

interagit avec la tétherine est distinct de son site de liaison à Rab7, ce qui indique que BCA2 pourrait assurer le lien entre les différents partenaires. Enfin, il a été montré que la surexpression de Vpu, l'antagoniste viral de la tétherine, contrecarrait l'activité de BCA2. La capacité de la tétherine à réduire la transmission des particules VIH-1 de cellules à cellules a aussi été rapportée [32], mais des données contradictoires décrivant le phénomène inverse ont également été publiées [33].

Mécanismes d'échappement à la tétherine

La première ligne de défense immunitaire contre une infection virale est la réponse innée, en partie composée de cytokines appelées IFN de type I (α/β). Une des stratégies communément développées par un certain nombre de virus (voire tous) pour neutraliser ces processus de défense antivirale est de réprimer la synthèse de ces cytokines qui jouent un rôle crucial dans la défense de l'organisme [34]. Cela se traduit par une diminution de l'expression de la tétherine ainsi que d'autres facteurs dont la transcription est IFN-dépendante. Dans la plupart des cas, les virus disposent également d'antagonistes de la tétherine comme la protéine Vpu pour VIH-1 [35].

Un antagoniste de la tétherine : la protéine Vpu du VIH-1 (viral protein U)

Le gène *vpu* est exclusif au génome du VIH-1 et à certains isolats de *simian immunodeficiency virus* (SIV) alors

La manière dont la tétherine est exprimée *in vitro* (protéine endogène ou recombinante) pourrait expliquer cette divergence de résultats [10] dans la mesure où il a été observé que l'expression de la protéine recombinante taggée provoque souvent l'accumulation de tétherine non mature dans le réticulum endoplasmique [25].

Séquestration intracellulaire de la tétherine par Vpu

Il est aujourd'hui acquis que, si Vpu peut induire la dégradation de la tétherine dans la plupart des modèles cellulaires étudiés, cette activité ne peut cependant pas rendre compte, à elle seule, de la neutralisation de la tétherine. Un certain nombre de données expérimentales (dégradation de la tétherine présente à la surface cellulaire vs tétherine totale ; mutation dans le site de reconnaissance de β -TrCP ; comparaison des cinétiques de dégradation de la tétherine et de CD4) suggèrent en effet que la neutralisation de la tétherine fait appel un mécanisme plus complexe [18]. En fait, la diminution de la tétherine à la surface cellulaire, qui accompagne l'effet neutralisateur de Vpu, n'est pas impérativement associée à la dégradation de ce facteur de restriction. En effet, la séquestration intracellulaire de la tétherine, au niveau des compartiments endosomaux [48, 52, 53] ou dans les compartiments périmoléculaires [54, 55], suffit à assurer son élimination de son site d'action membranaire.

La polyubiquitination Vpu-dépendante des résidus sérine et thréonine du domaine cytoplasmique de la tétherine semble jouer un rôle critique dans la neutralisation sans avoir de conséquences sur la stabilité de ce facteur de restriction, ce qui indique que ces deux événements sont indépendants [56].

Rôle ubiquitaire exercé par la tétherine sur la rétention d'autres virus et stratégies de défenses déployées

Ainsi que nous l'avons évoqué antérieurement, le fait que la tétherine n'ait pas pour cible une protéine virale, mais une structure d'origine cellulaire, en l'occurrence la membrane lipidique, lui confère un rôle ubiquitaire. Ainsi, l'activité antivirale de la tétherine s'exerce sur un large spectre de virus enveloppés dont les *Spumavirus* (ou virus *foamy*) et les bétarétrovirus qui ont un mode de répllication particulier [57, 58]. La capacité de la tétherine à bloquer la sécrétion de certains virus à ARN (filovirus, arénavirus et rhabdovirus) et d'un herpesvirus a également été démontrée [7]. Des expériences récentes suggèrent que c'est aussi le cas pour les virus influenza [59]. Ces virus sont tous capables de

neutraliser l'activité antivirale de la tétherine humaine en mettant en jeu des mécanismes originaux. À l'exception du virus Ebola [60], un point commun à ces inhibiteurs viraux de l'activité tétherine est leur capacité d'induire une diminution significative de l'expression de la tétherine à la surface cellulaire [11, 16].

La protéine Env du VIH-2

Le VIH-2 ne code pas de protéine Vpu. La capacité de la glycoprotéine (GP) d'enveloppe Env de certains de ces isolats à promouvoir la libération cellulaire de particules VIH-1 déficientes en Vpu est connue depuis longtemps [61]. Toutefois, ce n'est que récemment qu'un lien a été établi entre cette activité de la protéine Env de VIH-2 et sa capacité à neutraliser la tétherine [55, 62]. Il a été décrit que cet antagonisme était dépendant du type cellulaire, dans la mesure où la tétherine endogène des cellules HeLa peut être neutralisée, contrairement à la protéine exprimée par des cellules 293T transfectées [62]. Cette activité de neutralisation, dont sont dépourvues les protéines Env des virus VIH-1 et de certains VIS, semble mettre en jeu non seulement un, mais plusieurs mécanismes, dont la séquestration intracellulaire au niveau du réseau trans-Golgi et la dégradation de la tétherine [55, 62]. La délétion du motif GYxx θ (partenaire de AP-2), présent dans la queue cytoplasmique de cette GP, a démontré son implication dans la libération des particules virales et dans la *down-regulation* de la tétherine de la surface cellulaire, suggérant que le transfert de Env à la surface cellulaire soit requis pour neutraliser la tétherine [62]. Ce motif, qui est conservé au sein de protéines d'enveloppe de *Lentivirus* de primates, n'assure pas la spécificité de la protéine Env du VIH-2 vis-à-vis de la tétherine humaine qui est apportée par un déterminant extracellulaire.

La protéine Nef du virus de l'Immunodéficience simienne

La plupart des souches du VIS ne codent pas de protéines homologues de Vpu, à l'exception de celles affectant les gorilles (VISgor), les chimpanzés (VIScpz), les singes hocheurs (VISgsn), les moustacs (VISmus) et les singes de Mona (VISmon) [11]. Alors que les protéines Vpu exprimées par les souches VISgsn/mus/mon sont capables de neutraliser la tétherine, ce n'est pas le cas en ce qui concerne les souches VISgor et VIScpz, précurseur direct du VIH-1 [63]. De fait, les *Lentivirus* simiens ont développé une troisième arme contre la tétherine : la protéine Nef. Les protéines Nef codées par différents virus dont VISmac, VISagm et VISsmm ont la capacité de neutraliser la tétherine de leurs hôtes respectifs (macaque rhésus, singe vert, mangabey enfumé), mais pas la tétherine humaine [64, 65]. Avec une efficacité moindre que la protéine Nef du VIS, les protéines Nef des virus VIH-1 et VIH-2 sont elles aussi

et les hépatites virales (ANRS) pour leur soutien financier. N. Aschman perçoit un financement du Fonds national de la recherche du Luxembourg.

Conflits d'intérêts : aucun.

Références

- Ishikawa J, Kaisho T, Tomizawa H, *et al.* Molecular cloning and chromosomal mapping of a bone marrow stromal cell surface gene, *BST2*, that may be involved in pre-B-cell growth. *Genomics* 1995 ; 26 : 527-34.
- Kawai S, Azuma Y, Fujii E, *et al.* Interferon-alpha enhances CD317 expression and the antitumor activity of anti-CD317 monoclonal antibody in renal cell carcinoma xenograft models. *Cancer Sci* 2008 ; 99 : 2461-6.
- Neil SJ, Zang T, Bieniasz PD. Tetherin inhibits retrovirus release and is antagonized by HIV-1 Vpu. *Nature* 2008 ; 451 : 425-30.
- Van Damme N, Goff D, Katsura C, *et al.* The interferon-induced protein BST-2 restricts HIV-1 release and is downregulated from the cell surface by the viral Vpu protein. *Cell Host Microbe* 2008 ; 3 : 245-52.
- Sheehy AM, Gaddis NC, Choi JD, Malim MH. Isolation of a human gene that inhibits HIV-1 infection and is suppressed by the viral Vif protein. *Nature* 2002 ; 418 : 646-50.
- Stremlau M, Owens CM, Perron MJ, *et al.* The cytoplasmic body component TRIM5alpha restricts HIV-1 infection in Old World monkeys. *Nature* 2004 ; 427 : 848-53.
- Evans DT, Serra-Moreno R, Singh RK, Guatelli JC. BST-2/tetherin: a new component of the innate immune response to enveloped viruses. *Trends Microbiol* 2010 ; 18 : 388-96.
- Malim MH, Emerman M. HIV-1 accessory proteins – ensuring viral survival in a hostile environment. *Cell Host Microbe* 2008 ; 3 : 388-98.
- Harris RS, Sheehy AM, Craig HM, Malim MH, Neuberger MS. DNA deamination: not just a trigger for antibody diversification but also a mechanism for defense against retroviruses. *Nat Immunol* 2003 ; 4 : 641-3.
- Douglas JL, Gustin JK, Viswanathan K, *et al.* The great escape: viral strategies to counter BST-2/tetherin. *PLoS Pathog* 2010 ; 6 : e1000913.
- Kuhl BD, Cheng V, Wainberg MA, Liang C. Tetherin and its viral antagonists. *J Neuroimmune Pharmacol* 2011 ; 6 : 188-201.
- Cao W, Bover L, Cho M, *et al.* Regulation of TLR7/9 responses in plasmacytoid dendritic cells by BST2 and ILT7 receptor interaction. *J Exp Med* 2009 ; 206 : 1603-14.
- Erikson E, Adam T, Schmidt S, *et al.* *In vivo* expression profile of the antiviral restriction factor and tumor-targeting antigen CD317/BST-2/HM1.24/tetherin in humans. *Proc Natl Acad Sci U S A* 2011 ; 108 : 13688-93.
- Habermann A, Krijnse-Locker J, Oberwinkler H, *et al.* CD317/tetherin is enriched in the HIV-1 envelope and downregulated from the plasma membrane upon virus infection. *J Virol* 2010 ; 84 : 4646-58.
- Hinz A, Miguet N, Natrajan G, *et al.* Structural basis of HIV-1 tethering to membranes by the BST-2/tetherin ectodomain. *Cell Host Microbe* 2010 ; 7 : 314-23.
- Fitzpatrick K, Skasko M, Deerinck TJ, *et al.* Direct restriction of virus release and incorporation of the interferon-induced protein BST-2 into HIV-1 particles. *PLoS Pathog* 2010 ; 6 : e1000701.
- Waheed AA, Freed EO. Lipids and membrane microdomains in HIV-1 replication. *Virus Res* 2009 ; 143 : 162-76.
- Dube M, Bego MG, Paquay C, Cohen EA. Modulation of HIV-1-host interaction: role of the Vpu accessory protein. *Retrovirology* 2010 ; 7 : 114.
- Kupzig S, Korolchuk V, Rollason R, *et al.* Bst-2/HM1.24 is a raft-associated apical membrane protein with an unusual topology. *Traffic* 2003 ; 4 : 694-709.
- Rollason R, Korolchuk V, Hamilton C, Schu P, Banting G. Clathrin-mediated endocytosis of a lipid-raft-associated protein is mediated through a dual tyrosine motif. *J Cell Sci* 2007 ; 120 : 3850-8.
- Rollason R, Korolchuk V, Hamilton C, Jepson M, Banting G. A CD317/tetherin-RICH2 complex plays a critical role in the organization of the subapical actin cytoskeleton in polarized epithelial cells. *J Cell Biol* 2009 ; 184 : 721-36.
- Hegde RS, Mastrianni JA, Scott MR, *et al.* A transmembrane form of the prion protein in neurodegenerative disease. *Science* 1998 ; 279 : 827-34.
- Andrew AJ, Kao S, Strebel K. The C-terminal hydrophobic region in human BST-2/tetherin functions as a second transmembrane motif. *J Biol Chem* 2011 ; 286 : 39967-81.
- Perez-Caballero D, Zang T, Ebrahimi A, *et al.* Tetherin inhibits HIV-1 release by directly tethering virions to cells. *Cell* 2009 ; 139 : 499-511.
- Andrew AJ, Miyagi E, Kao S, Strebel K. The formation of cysteine-linked dimers of BST-2/tetherin is important for inhibition of HIV-1 virus release but not for sensitivity to Vpu. *Retrovirology* 2009 ; 6 : 80.
- Sakuma T, Sakurai A, Yasuda J. Dimerization of tetherin is not essential for its antiviral activity against Lassa and Marburg viruses. *PLoS One* 2009 ; 4 : e6934.
- Swiecki M, Scheaffer SM, Allaire M, *et al.* Structural and biophysical analysis of BST-2/tetherin ectodomains reveals an evolutionary conserved design to inhibit virus release. *J Biol Chem* 2010 ; 286 : 2987-97.
- Schubert HL, Zhai Q, Sandrin V, *et al.* Structural and functional studies on the extracellular domain of BST2/tetherin in reduced and oxidized conformations. *Proc Natl Acad Sci U S A* 2010 ; 107 : 17951-6.
- Yang H, Wang J, Jia X, *et al.* Structural insight into the mechanisms of enveloped virus tethering by tetherin. *Proc Natl Acad Sci U S A* 2010 ; 107 : 18428-32.
- Hammonds J, Wang JJ, Yi H, Spearman P. Immunoelectron microscopic evidence for Tetherin/BST2 as the physical bridge between HIV-1 virions and the plasma membrane. *PLoS Pathog* 2010 ; 6 : e1000749.
- Miyakawa K, Ryo A, Murakami T, *et al.* BCA2/Rabring7 promotes tetherin-dependent HIV-1 restriction. *PLoS Pathog* 2009 ; 5 : e1000700.
- Casartelli N, Sourisseau M, Feldmann J, *et al.* Tetherin restricts productive HIV-1 cell-to-cell transmission. *PLoS Pathog* 2010 ; 6 : e1000955.
- Jolly C, Booth NJ, Neil SJ. Cell-cell spread of human immunodeficiency virus type 1 overcomes tetherin/BST-2-mediated restriction in T cells. *J Virol* 2010 ; 84 : 12185-99.
- Versteeg GA, Garcia-Sastre A. Viral tricks to grid-lock the type I interferon system. *Curr Opin Microbiol* 2010 ; 13 : 508-16.
- Martin-Serrano J, Neil SJ. Host factors involved in retroviral budding and release. *Nat Rev Microbiol* 2011 ; 9 : 519-31.
- Aiken C, Konner J, Landau NR, Lenburg ME, Trono D. Nef induces CD4 endocytosis: requirement for a critical dileucine motif in the membrane-proximal CD4 cytoplasmic domain. *Cell* 1994 ; 76 : 853-64.
- Chaudhuri R, Lindwasser OW, Smith WJ, Hurley JH, Bonifacino JS. Downregulation of CD4 by human immunodeficiency virus type 1 Nef is dependent on clathrin and involves direct interaction of Nef with the AP2 clathrin adaptor. *J Virol* 2007 ; 81 : 3877-90.
- Miyagi E, Andrew AJ, Kao S, Strebel K. Vpu enhances HIV-1 virus release in the absence of Bst-2 cell surface down-modulation and intracellular depletion. *Proc Natl Acad Sci U S A* 2009 ; 106 : 2868-73.
- Ruiz A, Hill MS, Schmitt K, Stephens EB. Membrane raft association of the Vpu protein of human immunodeficiency virus type 1 correlates with enhanced virus release. *Virology* 2010 ; 408 : 89-102.
- Kobayashi T, Ode H, Yoshida T, *et al.* Identification of amino acids in the human tetherin transmembrane domain responsible for HIV-1 Vpu interaction and susceptibility. *J Virol* 2011 ; 85 : 932-45.

